

# **Synthesis and Self-assembly Studies of Amphiphilic Stimuli-Responsive Linear-Dendritic Block Copolymers**

Thesis Submitted to AcSIR for the Award of the  
Degree of

**DOCTOR OF PHILOSOPHY**

**In Chemical Sciences**



*By*

**Nagendra Kalva**

Registration Number: 10CC11J26019

Under the Guidance of  
**Dr. Ashootosh V. Ambade**

CSIR-National Chemical Laboratory,  
Pune - 411008, India

**March 2016**



# सीएसआईआर - राष्ट्रीय रासायनिक प्रयोगशाला

(वैज्ञानिक तथा औद्योगिक अनुसंधान परिषद)

डॉ. होमी भाभा मार्ग, पुणे - 411 008. भारत



## CSIR - NATIONAL CHEMICAL LABORATORY

(Council of Scientific & Industrial Research)

Dr. Homi Bhabha Road, Pune - 411 008, India

### CERTIFICATE

This is to certify that the work incorporated in the thesis entitled, “**Synthesis and Self-assembly Studies of Amphiphilic Stimuli-Responsive Linear-Dendritic Block Copolymers**” submitted by **Mr. Nagendra Kalva**, to Academy of Scientific and Innovative Research (AcSIR) in fulfilment of the requirements for the award of the Degree of **Doctor of Philosophy in Chemical Sciences**, embodies original research work under my supervision. I further certify that this work has not been submitted to any other University or Institution in part or full for the award of any degree or diploma. Research material obtained from other sources has been duly acknowledged in the thesis. Any text, illustration, table etc. used in the thesis from other sources, have been duly cited and acknowledged.

Nagendra Kalva

Research Student

Dr. Ashootosh V. Ambade

(Research Guide)

#### Communication Channels

NCL Level DID : 2590  
NCL Board No. : +91-20-2590 2000  
EPABX : +91-20-2589 3300  
: +91-20-2589 3400



#### FAX

Director's Office : +91-20-2590 2601  
COA's Office : +91-20-2590 2660  
COS&P's Office : +91-20-2590 2664

#### WEBSITE

[www.ncl-india.org](http://www.ncl-india.org)

# DECLARATION

I, hereby declare that all the experiments in this thesis entitled, “**Synthesis and Self-assembly Studies of Amphiphilic Stimuli-Responsive Linear-Dendritic Block Copolymers**” submitted for the degree of **Doctor of Philosophy in Chemical Sciences** to the Academy of Scientific & Innovative Research (AcSIR), has been carried out by me at the Polymer Science and Engineering Division of CSIR-National Chemical Laboratory, Pune, India under the guidance of **Dr. Ashootosh V. Ambade**. Research material obtained from other sources has been duly cited and acknowledged in the thesis. The work is original and has not been submitted in part or full by me for any other degree or diploma to other University.

Date: 02-03-2016

**Nagendra Kalva**

Polymer Science and Engineering Division

CSIR-National Chemical Laboratory,

Pune-411 008, India.

*Dedicated to.....  
my loving parents*



# Acknowledgement

*I wish to express my sincere gratitude to all those peoples that have contributed and supported with their professional and personal support to the successful completion of my thesis.*

*It gives me immense pleasure to express my enormous gratitude to my research supervisor **Dr. Ashootosh V. Ambade** for his excellent guidance, encouragement and patience in achieving this entire endeavour. At all times he has been open to discussions and I am grateful to him for sharing his scientific knowledge and experience. I greatly appreciate his confidence in me and the freedom he gave me to follow my ideas. Working with him was really a great pleasure and fetched me a lot of learning experience.*

*I sincerely thank the University Grants Commission (UGC) for their funding support. I would also like to express my gratitude to Dr. Sourav Pal and Dr. Sivaram (former Directors, CSIR-NCL), present director Dr. Vijayamohanan, Dr. M. G. Kulkarni, Dr. A. J. Varma (former Heads of the Polymer Science and Engineering Division), Dr. Ashish Lele (Head of the Polymer Science and Engineering Division) for providing the infrastructure and advanced facilities for research and giving me an opportunity to work at CSIR-NCL.*

*It gives me immense pleasure to thank Dr. K. Krishnamoorthy, for giving opportunity to join in CSIR-NCL and his support and help during the initial stage of my research. I also thank Dr. J. Nithyanandhan, Dr. K. Guruswamy and Dr. Sayam Sen Gupta for their helpful discussions and suggestions on any scientific problem.*

*I am indebted to my Doctoral Advisory Committee (DAC) members Dr. T. Raja, Dr. J. Nithyanandhan, and Dr. C. P. Vinod for their valuable suggestions, advice and fruitful discussions during the DAC meetings. Their judicious suggestions have helped me to improve my research work.*

*I would like to say my sincere thanks to Dr. V. K. Aswal and his group for their kind help in doing SANS studies that were carried out at BARC, Mumbai.*

*I admire and appreciate Student Academic Office (SAO) staff initially led by Dr. C. G. Suresh and now by Dr. M. S. Shashidhar for their kind help and co-operation, through this journey.*

*I would like to thank and give my acknowledgements to entire NMR especially Dr. P. R. Rajamohanan and microscopic analysis group from CMC. My sincere thanks to the library staff, members of Glassblowing, Stores and Purchase, Workshop, Account and Bill section and other office staffs for their timely help.*

*I extend my gratitude towards Dr. P. P. Wadgaonkar, Dr. B. L. V. Prasad, Dr. Suresh Bhat, Dr. C. V. Avadhani, Dr. S. K. Asha, Dr. M. V. Badiger, Dr. Samir Chikkali, Dr. B. B. Idage, Dr. S. B. Idage Mr. Anandrao Patil, Mr. Shamal menon, Dr. Nilakshi Sadavarte, Dr. Nimisha Parekh, Mrs. Deepa Dhoble for their valuable guidance and help.*

*It gives me immense pleasure to thank Sri S. V. Subba Reddy garu (Ex. MLA) and Sri. S. Ramachandra Reddy garu and his wife Smt. S. Nagaratnamma for their kind help for my education. I would like to thank all my teachers in my entire academic journey from Z. P. Boys' High School, Junior and Degree College from Pattikonda for their inspirational teaching, ethics and discipline. I sincerely thank Dr. Sreenivas, lecturer in chemistry in Warangal, for his inspirational teaching towards chemical sciences and his constant guidance.*

*I deeply acknowledge my friends and seniors Dr. Prakash Sane, Dr. Debasis Pati, Dr. Bhausahab Tawade, Dr. Chinmay, Dr. Nagesh Kolhe, Dr. Nisha, Dr. Koushal Kumar and Dr. Senthil Kumar, Dr. Pradeep Pachfule, Dr. Tamas, Dr. Arijit, and Dr. Subhadeep Saha.*

*I owe deeply to my ever-trustful friends and labmates, Naganath G. patil and Nitin Basutkar, Indravadan Parmar, Sachin Patil, Sachin Kuhire, Samadhan, Deepak Maher, Deepshikha, Kavita Garg, Vikas Garg, Sachin Basutkar, Dr. Shambho, Dr. Murugesan, Ashwini, Uday, Shradha Chatre, Sayali Saligram, Rupali, Bharat Shrimant, Amol Ichake, Abhijeet, Dr. Aarti and Durgaprasad for their kind help, support and cheerful environment in the lab. I would like to thank to my labmates from Dr. Krishnamoorthy's group, Rajashree Mahale, Mrinmoy Chinni, Satej Dharmapurikar, Manik Bhosale, Arul Kashmir, Soumya Singh, Chayanika Das, Bhanu Prakash, Chitravel, Sudhakar and Kumar for their affection, warm help and support. I also wish to thank my colleagues Saibal Bhaumik, Prajitha Thampam,*

*Sarabjot, Bapu surnar, Rajendra, Narasimha, Swapnil, Shekhar, Soumen Das, Vinita Dhavare, Praveen, Neeta, Rajesh, and Manik.*

*I cannot forget the assistance and helpful suggestions from GJ hostel friends Dr. Seenivasulu, Dr. Rajanna, Dr. Venu, Dr. Ramesh, Dr. Ravi Dharbha, Dr. Yadagiri, Dr. B. Narasimha Reddy, Dr. Narasimha Kanna, Dr. Chandra babu, Dr. Manoj Kumar, Dr. Rambabu, Dr. Suneel Chopuri, Balanagulu, Shiva kumar burugu, Rami Reddy, Suresh babu, Devadutta, Shanthi Vardan, Ravi, Narendra, Srikanth Dama, Sreekanth Reddy, Hanuman Prasad, Seenu, Lakshmi Prasad, Innaiah Kumar, Trinadh, Chaitanya Kamaja, Kashinath, Satheesh, Satheesh Bhattu, Tarun and Sagar. I also wish to thank my childhood friends (Leos) Mohammad Zilani (zill), Satheesh Kumar (sathya), Chandra Sekhar Naidu (badri), Ali P. M.D. (trusty), Ali J. M. D (captain), Mastan, Ram (Gemini), Akbar, Iqbal (IQ), Mallikarjuna (VRO), A. Seenu, Dr. Chandra sekhar (espent) and Dr. Madhusudhan Rao.*

*No word would suffice to express my gratitude and love to my amma Sanjamma Kalva and nanna Lakshminarasaiiah Kalva (late) and my sisters (Narayanamma Kalva and Eswaramma Kalva) for their continuous showering of boundless affection on me whatever my choice. Precious thanks to their sacrifices, adjustments and support throughout my PhD research work. They are the one who became my strength and motivation in all kinds of situations. Very warm thanks for their patience, love, support and for believing in my dreams.*

*I wish to express my gratitude and love towards “God-almighty”, who gave me the strength and courage to fulfill my dreams and showered upon me his choicest blessings.*

.....**Nagendra Kalva**

## List of Abbreviations

Abbreviation	Expansion
ATRP	Atom Transfer Radical Polymerization
CMC	Critical Micelle Concentration
CuAAC	Copper-catalyzed Azide-Alkyne Cycloaddition
$D_h$	Hydrodynamic diameter
DLS	Dynamic Light Scattering
DCM	Dichloromethane
DMF	N,N-Dimethyl formamide
DOX	Doxorubicin
DCC	Dicyclohexyl Carbodiimide
DMAP	4-(N,N-dimethylamino)pyridine
DMSO	Dimethyl sulfoxide
FT-IR	Fourier Transform-Infrared
GSH	Glutathione
GPC	Gel Permeation Chromatography
Hz	Hertz
LCST	Lower Critical Solution Temperature

LDBC	Linear-Dendritic Block Copolymer
MALDI-TOF	Matrix Assisted Laser Desorption/Ionization-Time of Flight
$M_n$	Number Average Molecular Weight
$M_w$	Weight Average Molecular Weight
Me <sub>6</sub> TREN	Tris[2-(dimethylamino)ethyl]amine
NIR	Near Infrared
NaH	Sodium Hydride
nm	nanometer
NMR	Nuclear Magnetic Resonance
ONB	<i>o</i> -Nitrobenzyl
PCL	poly( $\epsilon$ -caprolactone)
PMMA	poly(methyl methacrylate)
PDMAEMA	Poly(N,N-dimethylaminoethyl methacrylate)
PBS	Phosphate Buffer Solution
PVDF	Polyvinylidene Fluoride
PEO	Poly(ethylene oxide)
PEG	Poly(ethylene glycol)
PDI	Polydispersity Index

PNIPAM	Poly(N-isopropyl acrylamide)
PMDETA	N,N,N',N'',N''-Pentamethyldiethylenetriamine
SEM	Scanning Electron Microscopy
SANS	Small Angle Neutron Scattering
TEM	Transmission Electron Microscopy
THF	Tetrahydrofuran
TLC	Thin Layer Chromatography
TMS	Tetramethylsilane
TEA	Triethylamine
UV-vis	Ultraviolet-visible

**Instrumentation**

NMR spectra were recorded on Bruker spectrometer (200 MHz or 400 MHz). FT-IR spectra were recorded on Perkin Elmer FT-IR spectrum GX instrument by making KBr pellets. Matrix-assisted laser desorption/ionization time-of-flight (MALDI-TOF) spectra were recorded on an ABSCIEX TOF/TOF 5800 mass spectrometer using dithranol as matrix. UV-vis spectra were recorded on Specord 210 plus Analytikjena spectrophotometer. TEM images were taken on FEI Technai T20 instrument operating at 200kV.

## Table of Contents

Abstract.....	1
---------------	---

### Chapter 1

#### Linear and Linear-Dendritic Block Copolymers: Self-assembly and Stimuli-responsive Behaviour

1.1 Self-assembly of block copolymers and its significance.....	5
1.2 Polymer architectures.....	7
1.2.1 Polymer architectures based on linear blocks.....	7
1.2.2 Dendrimers.....	8
1.2.3 Linear-dendritic block copolymers.....	11
1.4 Efficient coupling reactions.....	13
1.4.1 Copper-catalyzed azide-alkyne cycloaddition (CuAAC) reaction.....	14
1.4.2 Diels-Alder reaction.....	16
1.5 Self-assembly of block copolymers in solution.....	17
1.5.1 Stimuli-responsive block copolymers.....	19
1.6 Self-assembly of linear-dendritic block copolymers in bulk.....	25
1.7 Self-assembly of linear-dendritic block copolymers in solution.....	27
1.7.1 Self-assembly studied without application of stimuli.....	27
1.7.2 Stimuli-responsive self-assembly studies.....	30
1.8 Scope and objectives of the present work.....	38
1.9 References.....	39

### Chapter 2

#### Effect of Branching Pattern of Hydrophobic Dendrons on the Linear-Dendritic Block Copolymer Micelle Structure

2.1 Introduction.....	50
2.2 Experimental Section.....	51
2.2.1 Materials.....	51
2.2.2 Instrumentation.....	52



2.2.3 Synthetic procedures and characterization data.....	52
2.2.4 Preparation of aqueous solutions.....	55
2.2.5 cmc measurements.....	56
2.2.6 Dye encapsulation.....	56
2.2.7 SANS measurements and analysis.....	56
2.3 Results and Discussion.....	57
2.3.1 Synthesis.....	57
2.3.2 Determination of cmc and dye encapsulation study.....	60
2.3.3 SANS Study.....	63
2.3.3.1 At 30 °C and Fixed Solvent Composition.....	63
2.3.3.2 Effect of Solvent Composition.....	68
2.3.3.3 Effect of Temperature.....	70
2.3.4 Self-assembly into reverse micelles.....	71
2.3.5 Organogels.....	72
2.4 Summary.....	73
2.5 References.....	74

### Chapter 3

#### Tuning Micellar Core Properties of Linear-Dendritic Block Copolymers using Photoresponsive Dendron

3.1 Introduction.....	78
3.2 Experimental section.....	79
3.2.1 Materials.....	79
3.2.2 Instrumentation.....	79
3.2.3 Synthetic procedures and characterization data.....	80
3.2.4 Preparation of polymer aqueous solution and Nile red encapsulation.....	85
3.2.5 Nile red encapsulation capacity experiment.....	85
3.3 Results and discussion.....	85
3.3.1 Synthesis.....	85
3.3.2 Self-assembly in water.....	88
3.3.3 Azobenzene isomerization in micelles.....	90
3.3.4 Dye encapsulation and release.....	94

3.4 Summary.....	100
3.5 References.....	101

## Chapter 4

### Controlled Micellar Disassembly of Photo- and pH-cleavable Linear-Dendritic Block Copolymers

4.1 Introduction.....	104
4.2 Experimental section.....	105
4.2.1 Materials.....	105
4.2.2 Instrumentation.....	105
4.2.3 Synthetic procedures and characterization data.....	105
4.2.4 Preparation and characterisation of aqueous solution of polymer.....	108
4.2.5 Encapsulation of DOX in micelles.....	109
4.2.6 Cell viability assay .....	109
4.2.7 Cellular uptake and intra-cellular release of DOX .....	110
4.3 Results and Discussion.....	111
4.3.1 Synthesis.....	111
4.3.2 Self-assembly.....	113
4.4 Summary.....	121
4.5 References.....	121

## Chapter 5

### Effect of dendron periphery on thermoresponsive properties of bis-MPA dendron- azobenzene-PNIPAM copolymer assemblies

5.1 Introduction.....	125
5.2 Experimental Section.....	128
5.2.1 Materials.....	128
5.2.2 Instrumentation.....	128
5.2.3 Synthesis.....	128
5.2.4 Preparation of aqueous solution of polymer and Nile red encapsulation.....	131
5.3 Results and discussion.....	131
5.3.1 Synthesis.....	131
5.3.2 Temperature-responsive self-assembly .....	133

5.3.3 Photo-responsive behaviour.....	139
5.3.4 Temperature-induced dye release.....	140
5.4 Summary.....	143
5.5 References.....	143

## **Chapter 6**

### Summary and Future Directions

6.1 Summary.....	146
6.2 Future directions.....	148
6.3 References.....	149

## **Appendix**

Appendix I.....	150
Appendix II.....	157
Appendix III.....	166
Appendix IV.....	172
List of publications.....	176

## Abstract

Amphiphilic linear-dendritic block copolymers is a promising class of polymers for design of smart materials owing to the advantages offered by perfectly branched dendron and mechanical stability of the linear segment. A pre-determined number of multiple kinds of functionalities can be introduced in a controlled manner due to stepwise synthesis of dendrons while the stability and hydrophilic/lipophilic balance can be controlled by the chain length of linear polymer. Towards development of better and improved building blocks for tomorrow's advanced materials it is imperative to carry out detailed structure-property relationship studies on stimuli-responsive LDBC. The research work presented in this thesis is an attempt to gain insight into and better understanding of the micellar properties of stimuli-responsive linear-dendritic copolymers. There is little work in literature on introducing more than one functionality in this polymer architecture hence one of the goals is also to design and study multi-stimuli-responsive LDBC. All the polymers studied in this work are synthesized using Cu-catalyzed azide-alkyne cycloaddition (CuAAC) reaction to couple dendron and linear parts. Their self-assembly in dilute aqueous solution is characterized by TEM, DLS techniques, and UV-vis and fluorescence spectroscopy. The polymers contain one or more of photo-, pH- and temperature-responsive groups in various locations along the polymer backbone.

Chapter 1 gives a detailed literature report on the synthesis and self-assembly of linear-dendritic copolymers and put it in relation with linear block copolymers. Firstly, the significance of block copolymer self-assembly is described and the concept of polymer architecture is introduced followed by synthetic methods for dendrimers and linear-dendritic copolymers. Self-assembly of stimuli-responsive linear block copolymers is discussed briefly with introduction to various stimuli-responsive groups. Literature reports on self-assembly of stimuli-responsive linear-dendritic copolymers are then covered extensively with emphasis on structure-property relationship studies. Finally, scope and objectives of the present work in light of the reported literature are described.

Chapter 2 describes the effect of the branching pattern of hydrophobic dendrons on the core structure of LDBC micelles. This chapter deals with study of the micellar properties of a series of polymers with only small increase in size of dendron and number of peripheral groups in contrast to literature reports that study the properties as a function

of dendron generation. Hydrophobic dendrons based on 3,5-di- and 3,4,5-trisubstituted phenyl rings that consist of the benzyl ether backbone but exhibit different sizes, shapes, and hydrophobic densities, were synthesized and attached to PEG of constant chain length. Properties of the micellar core were investigated in THF/water mixtures by SANS technique. The aggregation numbers for 3,4,5-based dendron copolymers were found to be lower, with more THF molecules of solvation compared with the 3,5-based dendron copolymer due to higher hydrophobic density at the same generation. The difference was greater at higher generations due to different molecular shapes. The micellar core size increased in small steps so that dye encapsulation could be tuned. Two polymers with intermediate hydrophobicity were also studied further with variations in the solvent composition and temperature. Effect of thermoresponsive nature of PEG was evident on micelle size.

Chapter 3 deals with LDBC containing dendrons with azobenzene in the internal layers in order to fine-tune the dye release behaviour of micelles induced by *trans-cis-trans* isomerization of azobenzene. PEG of constant chain length is used as linear polymer. Hydrophobic groups on dendron periphery and number and position of azobenzene units is varied during the stepwise dendron synthesis. Effect of photoirradiation on self-assembly in aqueous solution was studied and it showed a clear dependence of dye encapsulation and photo-induced release properties on the dendron structure, that is, position and number of azobenzene units as well as different groups (dodecyl or benzyl) on the dendron periphery. Dye release was also influenced depending on whether *cis-trans* isomerization was carried out using visible light or by storing the sample in dark. Photoisomerization of azobenzene in the micellar assembly was studied in detail and rate constant of thermal *cis-trans* isomerization was calculated for each polymer. The self-assembly was also characterized by DLS and TEM techniques.

Chapter 4 deals with synthesis and self-assembly of linear-dendritic copolymer with both photo- and pH-cleavable linkages at the junction between the hydrophobic dendron and hydrophilic linear polymer. The photocleavable *o*-nitro-benzyl group attached to alkyne was introduced at the focal point of polyester bis-MPA dendron and acid-degradable linear acetal with terminal azide was introduced at one end of linear PEG. The copolymer was found to self-assemble into micellar aggregates in 0.1 wt% aqueous

solution. Stimuli-responsive disassembly of the aggregates was studied by monitoring fluorescence emission of the encapsulated hydrophobic dye (Nile red) and DLS technique. Products of acetal cleavage at acidic pH were analyzed by NMR spectroscopy and GPC. Photo and pH stimuli were applied separately as well as simultaneously to study the rate of dye release. Synergistic effect of the two stimuli on dye release was demonstrated and the non-cytotoxic nature of the polymer was shown using the MTT assay. Cell uptake of DOX-loaded micelles and photo-induced release of the drug resulting in significantly higher cytotoxicity than by free DOX was demonstrated using MDA-MB-231 cells.

Chapter 5 deals with temperature-responsive linear-dendritic copolymer wherein polarity of dendron periphery is varied. In this chapter, bis-MPA dendron with pH-cleavable acetonide units (cyclic acetal) on the periphery was connected to PNIPAM of varied chain lengths *via* azobenzene linker. Acetonide groups were deprotected to obtain polymers with a polar dendron periphery. A total of four polymers - two with acetonide and two with hydroxy groups were synthesized. Polymers with less polar acetonide dendron showed complete but irreversible change in morphology above LCST whereas those with hydroxylated dendron showed morphology only above LCST. Change in morphologies was observed for polymers with different PNIPAM chain lengths. Dye release from polymeric micelles containing acetonide dendron after multiple heating-cooling cycles was only 9% whereas change in microenvironment of the dye was observed upon photoisomerization without any release. Micelles containing polar dendron showed dye encapsulation on increasing the temperature and dye release with decreasing temperature.

Chapter 6 summarizes important results from all chapters with respect to design and synthesis of dendron building blocks, placement of stimuli-responsive groups and pH- or photo- or temperature-induced micellar reorganization and disassembly. Latter part of the chapter outlines future directions arising out of the results of this work in particular as well as for the field of linear-dendritic copolymers in general.

## **Chapter 1**

# **Linear and Linear-Dendritic Block Copolymers: Self-assembly and Stimuli-Responsive Behaviour**

### 1.1 Self-assembly of block copolymers and its significance

Block copolymers are defined as two or more homopolymers of different chemical structures covalently or non-covalently attached together, where each homopolymer part is called a 'block'.<sup>1</sup> Since the blocks are attached to each other macrophase separation due to incompatibility is not possible however, they individually segregate into nanoscale domains - a phenomenon known as microphase separation.<sup>2</sup> This property of phase separation in block copolymers, either in bulk or solution, has been exploited for many promising applications.<sup>3</sup> This is illustrated by a few examples below.

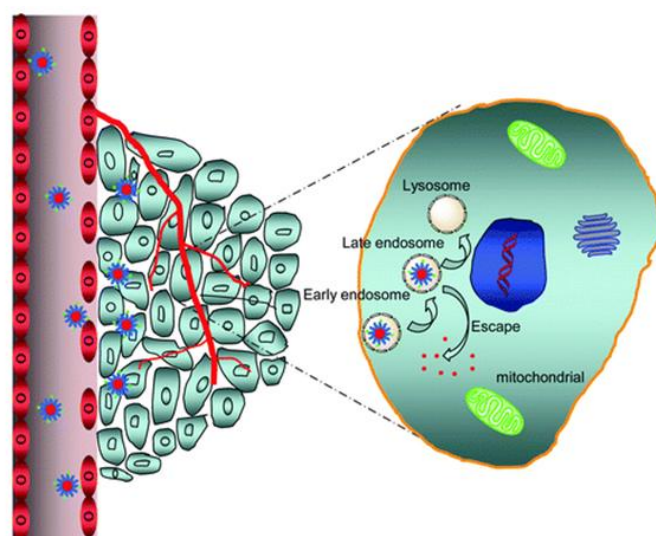


**Figure 1.1** Schematic representation for entry of polymer nanocarrier into tumor tissue via EPR effect. (Reproduced by permission from The Royal Society of Chemistry)

A major problem in chemotherapy for cancer treatment is the difficulty in directing the cytotoxicity to tumour cells selectively since many anticancer drugs also kill normal cells in the process that leads to severe side effects. An additional problem is poor solubility of hydrophobic drugs in water. A promising approach to circumvent these obstacles is to employ nanoscale drug delivery vehicles such as polymeric micelles. Block copolymers can self-assemble into well-defined micelles on the nanometer scale in aqueous solution by virtue of hydrophobic and hydrophilic blocks. These nanocarriers offer the advantages of improved drug solubility and higher accumulation in tumours *via* enhanced permeation and retention (EPR) effect (Figure 1.1).<sup>4,5</sup> Moreover, various stimuli-responsive functionalities can be introduced into the polymeric structure so that drug can be released specifically at the tumor site by taking advantage of differential environment of the cancer



cells such as difference in pH and temperature. In addition to this, size of the drug delivery vehicles plays an important role in determining its circulation time. For example, it has been found that particles with size less than 200 nm overcome renal clearance while particles with diameter larger than 100 nm are found to accumulate mostly in liver and spleen.<sup>6</sup> With block copolymers as building blocks, it is possible to control the size of micelles and even the type of morphology that is, it is possible to selectively obtain vesicles to entrap both hydrophilic and hydrophobic drugs or cylindrical micelles that possess longer circulation times.<sup>7</sup>

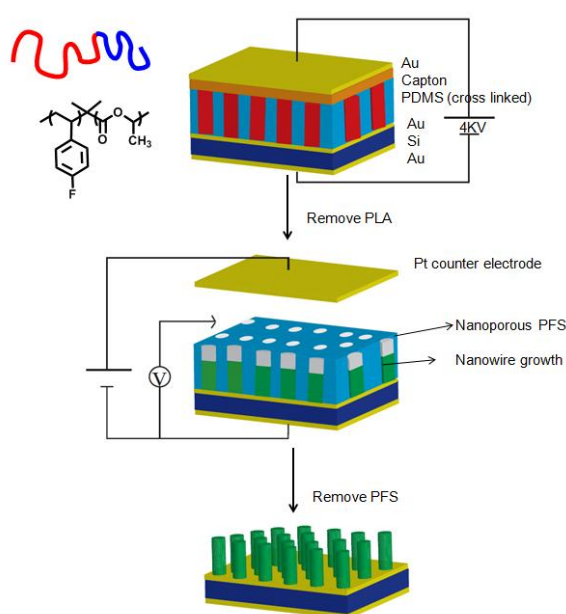


**Figure 1.2** Schematic representation of formation of free-standing nanowires using block copolymer thin film.

Self-assembly of block copolymers in bulk is attractive for fabrication of nanostructures for applications in nanoelectronics such as more efficient computer chips and solar cells as well as catalytic surfaces.<sup>8,9</sup> Using a template-assisted approach, it is possible to control the dimensions and shape of the microdomains, which can then act as templates for silicon-based materials.<sup>10-12</sup> Block copolymer microdomains with dimensions below 10 nm have been achieved that goes below the limit of photolithography. In the example shown above (Figure 1.2), block copolymer thin films with cylindrical morphology were used as templates for generating ZnO nanowires of uniform diameter.<sup>13</sup>

## 1.2 Polymer architectures

### 1.2.1 Polymer architectures based on linear blocks

Polymer architecture or topology that is the connectivity of constituent blocks with each other is an important factor in determining the phase separation and the properties that depend on the morphology and hence various polymer architectures have been explored.<sup>14,15</sup> Block copolymers classified into different architectures are shown in Figure 1.3.

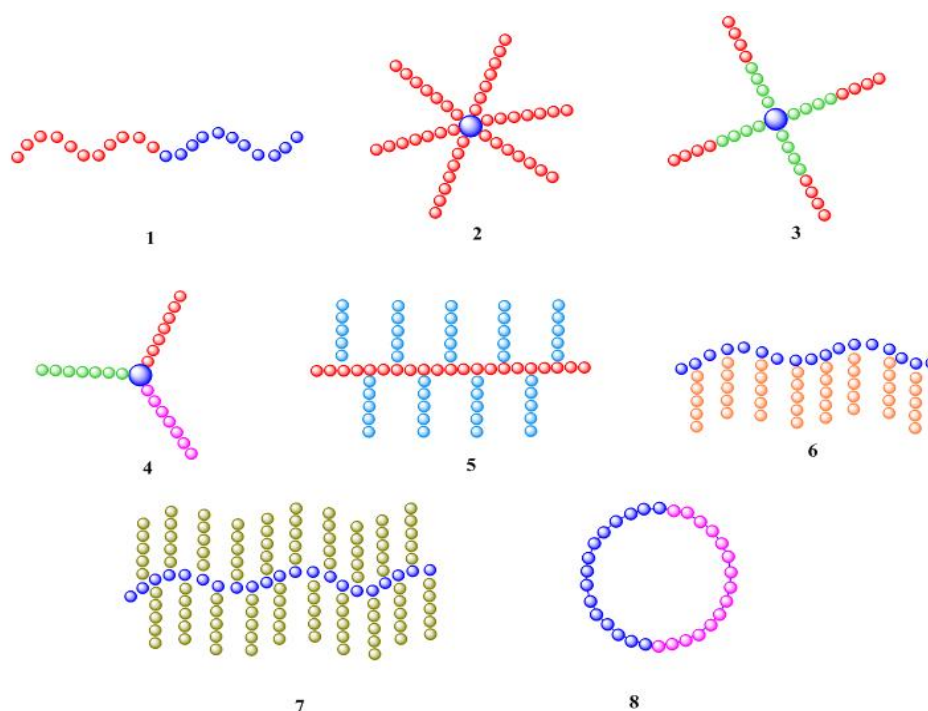


**Figure 1.3** Schematic representation of various polymer architectures.

Linear block copolymers (1) contain two or more polymer chains attached end-to-end in a linear fashion. Star copolymers are composed of more than two linear polymer chains (arms) attached at a common branch point (core).<sup>16</sup> The arms can either be homopolymers (2) or block copolymers (3). When three chemically distinct homopolymers are attached to the core these are called mikto-arm star copolymers (4).<sup>17</sup> Mikto-arm star polymers form interesting nanostructures called ‘multi-compartment micelles’ in solution that can be used to carry multiple types of guest molecules.<sup>18-20</sup> Side-chain branched polymers comprise a linear main chain from which more than one polymeric side chain emanates. Depending on

the density of side chains there are sub-classes such as comb polymers<sup>21</sup> with high density of polymeric side-chains (6) and graft polymers<sup>22</sup> where the density of side chains is typically much lower (5). Another sub-class of side-chain branched polymers is brush polymers<sup>23-25</sup> in which the branching points are separated along the main chain by a few atoms, and acquire the shape of a brush (7). Bottle-brush polymers exhibit side-chains on each and every repeat unit.<sup>26,27</sup> Cyclic polymers are ring-shaped polymers without chain ends (8) and hence show dramatically different behaviour in certain properties when compared to linear polymers.<sup>28-30</sup> Cyclic polymers can be produced either by intramolecular cyclization of homotelechelic or heterotelechelic polymers or by coupling both ends of two different polymer chains. This gives rise to blocky structure in a cyclic architecture.<sup>31,32</sup>

### 1.2.2 Dendrimers

Dendritic polymers is a class of polymer architecture that are highly branched and possess dense molecular structure. Dendritic polymers are further divided into two sub-classes based on polydispersity, which are closely related to each other, 1) monodisperse and 2) polydisperse. Dendrimers come under monodisperse dendritic polymers and show PDI values between 1.01 to 1.05 while hyperbranched polymers, dendrigrafts, dendronized polymers and linear-dendritic copolymers are polydisperse and show PDI values from 1.5 to 10.<sup>33-37</sup> Schematic structures for these dendritic polymers are shown in Figure 1.4.

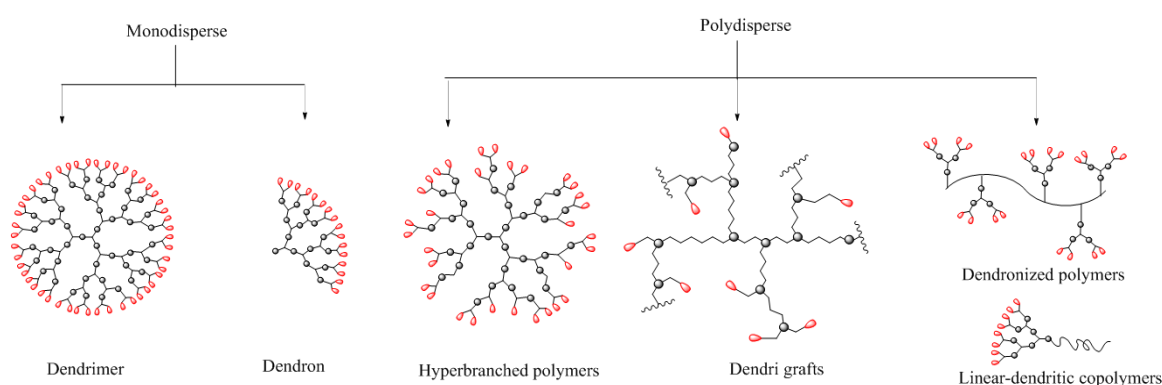


**Figure 1.4** Schematic representation of various types of dendritic polymers.

In contrast to other dendritic polymers, dendrimers are perfectly branched macromolecules, and display a defined number of chain ends.<sup>38-43</sup> The first dendritic wedge was reported by the Vögtle et al in 1978.<sup>44</sup> In 1979, Tomalia and his group proposed the name “dendrimers”, coined from Greek words *dendr* = tree and *meros* part. Thus, ‘dendrimer’ means tree-like polymer and reflects the highly branched nature of dendritic polymers. Dendrimer synthesis requires multiple repetitive synthetic steps, time consuming activation/protection steps and purification steps to remove the excess of reactants and by-products to get pure final products. The layer added after every coupling step is called a ‘generation’ and is represented by ‘Gn’, which translates to ‘n<sup>th</sup> generation. Number of terminal groups on the periphery increases exponentially at each generation. A dendrimer comprises three distinct structural features *viz.* core, interior and periphery. Wedge-like segment of the dendrimer is called a ‘dendron’ that can be synthesized separately and attached to a multi-functional molecule to obtain a dendrimer. Core of a dendron is called a ‘focal point’, which is functional and can be used to attach it to a multi-functional molecule or a telechelic polymer. Dendrimers are multivalent macromolecules on account of a large number of peripheral groups that can be modified to afford polymers with desired properties. Solubility of dendrimers is dictated by polarity of peripheral groups. Physical properties of dendrimers like viscosity and thermal properties also differ significantly from their linear analogues. This has led to these polymers being exploited in different areas like supramolecular chemistry, templates for nanomaterials and biomedical applications.<sup>45-48</sup>

The iterative synthesis of dendrimers is categorized into two synthetic strategies, the divergent approach and the convergent approach.

**a) Divergent approach:** Divergent approach was introduced by the teams of Tomalia and Newkome.<sup>49,50</sup> In this approach the dendrimer grows from the core by successive attachment of the branching units and continues outward towards periphery by the repetition of coupling and activation steps (Figure 1.5). The number of coupling reactions increases with increasing generation number since reactions are carried out on the periphery and after a certain generation, incomplete functionalization of the periphery of the dendrimer results. Thus, excess of reagent and complete functionalization of periphery is needed to afford a perfectly branched dendrimer or dendron.

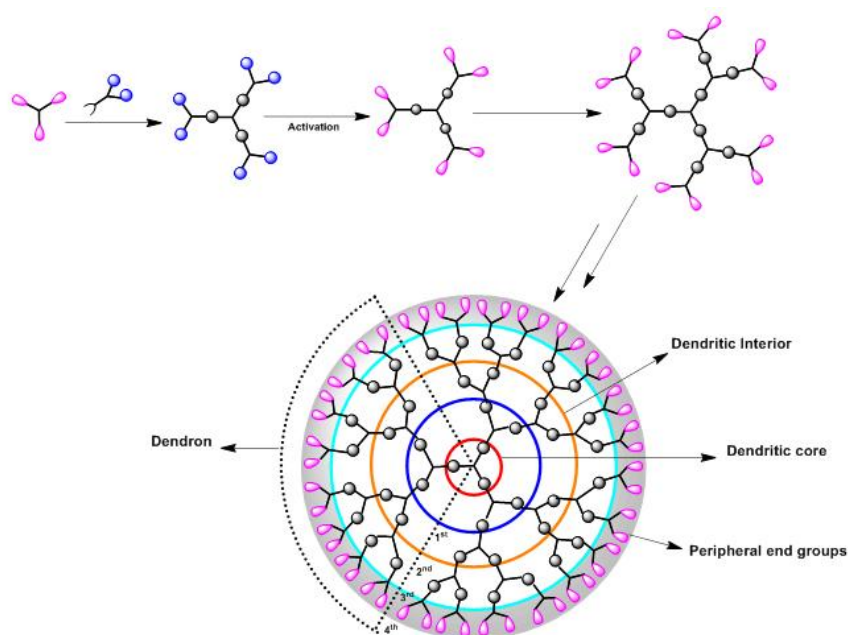


**Figure 1.5** Divergent synthesis approach for dendrimers.

A dendron is obtained by using a monofunctional molecule at the first step in ‘divergent approach’. Poly(amidoamine) (PAMAM) dendrimers were the first to be synthesized by this method.<sup>51</sup> Other dendrimers synthesized by this approach are poly(propylene imine) (PPI)<sup>52</sup> and 2,2-bis(methylol) propionic acid (bis-MPA dendrimers).<sup>53</sup> PAMAM and PPI dendrimers have been commercialized.

**b) Convergent Approach:** This approach was first introduced by Hawker and Fréchet in 1990.<sup>54,55</sup> In this approach, first the dendron is synthesized and then attached to the poly functional core to obtain perfectly branched dendrimer. Dendrons were synthesized by the repetitive multistep synthesis by inward coupling of the end groups to each branch of the monomer that is, dendron is synthesized from periphery to focal point. After desired generation was reached, dendrons were coupled to the core molecule (Figure 1.6). This approach requires less number of coupling reactions so that the excess of reactants can be removed by purification due to the large difference in their molar mass and polarity. In fact, large excess of reagents are more often unnecessary. This approach affords dendrimers with more regular structure than divergent approach. However, at higher generations coupling reactions are challenging due to steric hindrance at the focal point, which results in less regular structure. Number of generations achieved by convergent

approach are typically less than by divergent approach. Furthermore, this approach is less attractive for large scale preparation due to its rigorous purification steps.

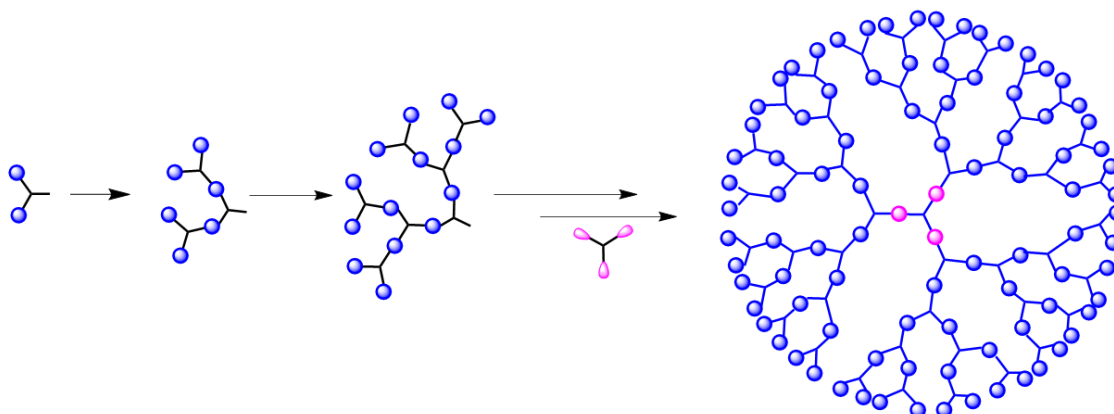


**Figure 1.6** Convergent synthesis approach for dendrimers.

Aromatic poly(benzyl ether) a well known type of dendrimers (Fréchet-type) were synthesized by this approach.<sup>55</sup> Convergent approach is the method of choice for functional dendrimers.

### 1.2.3 Linear-dendritic block copolymers

Tedious synthetic methods as well as symmetrical structure limit the applications of dendrimers. Researchers have attempted to improve upon the properties of dendrimers and linear block copolymers by synthesizing a new macromolecular architecture known as, Linear-dendritic block copolymers (LDBC) considered as a sub-class of dendritic copolymers. LDBC are block copolymers obtained by attachment of a single linear chain to the focal point of dendron. These polymers combine the features of constituent blocks - the perfectly branched, multivalent architecture of dendron and mechanical strength of linear polymer.<sup>56</sup> First such polymer was described and synthesized by Gitsov and Fréchet in 1992.<sup>54</sup> They synthesized AB dendritic-linear and ABA dendritic-linear-dendritic type structures. Poly(benzyl ether) dendron with bromobenzyl group at the focal point synthesized by the convergent method up to 4<sup>th</sup> generation was reacted with hydroxy mono- and di-telechelic linear PEO under Williamson etherification conditions.

Generally, LDBCs are synthesized *via* three different strategies. These are 1) chain first strategy 2) dendron first strategy and 3) coupling strategy. The different strategies are schematically shown in Figure 1.7.

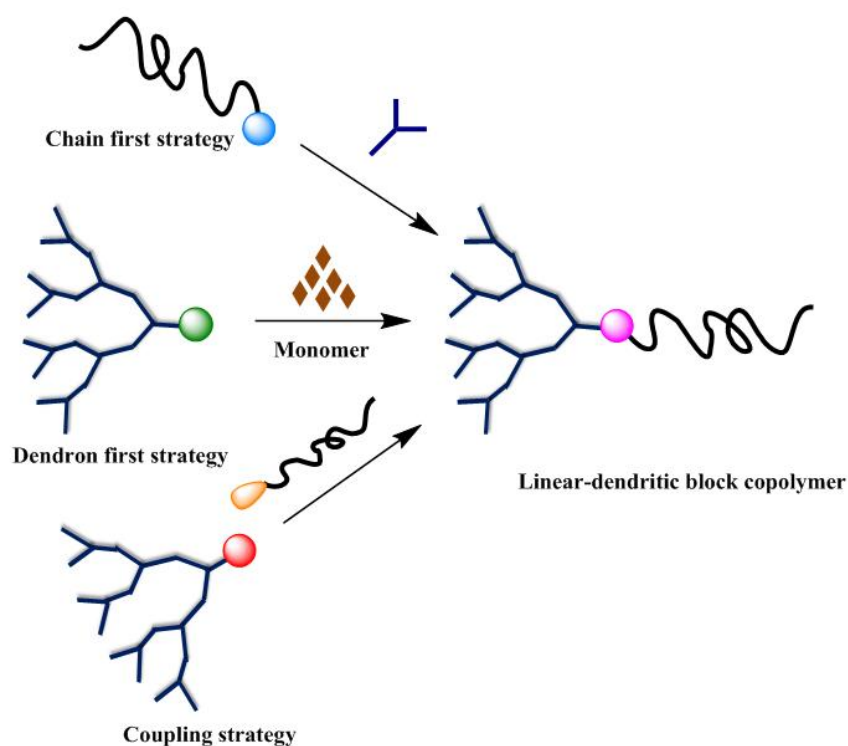


**Figure 1.7** Schematic representation of different approaches for the synthesis of linear-dendritic block copolymers.

**a) Chain first strategy:** In this strategy, functional chain end of a linear polymer is used to construct dendron by divergent approach. Efforts in synthesis of LDBCs by this strategy were led by several research groups.<sup>57-62</sup> However, this synthetic strategy suffers from the drawback of dendron synthesis being carried out in divergent manner in the presence of polymeric starting material that becomes more difficult at higher generation<sup>63</sup> and results in lack of control over purity.

**b) Dendron first strategy:** This strategy was developed by the groups of Matyjaszewski and Fréchet jointly and involves synthesis of dendron that carries initiator group for controlled polymerization at the focal point.<sup>64</sup> This dendron is then used as initiator for the synthesis of linear polymer so that dendron and linear blocks are attached covalently.<sup>65-69</sup>

Most of the LDBC's prepared by this method are based on poly(benzyl ether) dendrons. The dendron is functionalized with initiators such as 2,2,6,6-tetramethyl-1-piperidinyloxy (TEMPO) group and alkyl halide such as isobutyryl bromide for nitroxide-mediated polymerization (NMP) atom transfer radical polymerization (ATRP), respectively.<sup>70,71</sup> Ring opening polymerisation initiated by the dendron has also been explored by several other groups.<sup>72</sup> Gitsov et al. reported<sup>73</sup> the first asymmetric ABC copolymers, where A and C blocks are two different dendrons. Anionic polymerization of ethylene oxide initiated by poly(benzyl ether) dendron alkoxide afforded AB linear-dendritic copolymers with narrow polydispersities. Living chain ends of this polymer were reacted with another dendron with reactive group at focal point to get the dendritic-linear-dendritic copolymers.

**c) Coupling strategy:** In this strategy, the dendritic segment and linear polymer segment with complementary functional groups present at the focal point and chain end, respectively, are prepared first and then the fragments are coupled. This method was first reported by Fréchet and coworkers<sup>54,74,75</sup> by reacting dendritic bromides with one or both hydroxyl groups at chain ends of PEG or with living chain ends of anionically synthesized polystyrene. This technique offers an advantage in that it is possible to fully characterize both linear polymer and dendron segments prior to coupling. Dong and coworkers synthesized<sup>76-78</sup> alkyne-functionalised PAMAM dendron and azide-terminated linear polymers and coupled the two segments using click chemistry. PAMAM dendrons with peripheral poly( $\epsilon$ -caprolactone) chains were coupled to azide-terminated PEG. The group synthesized<sup>79-82</sup> library of linear-dendritic AB and dendritic-linear-dendritic ABA copolymers using efficient coupling reaction between linear PEG or PCL and PAMAM dendrons with PCL or polypeptide chains on the periphery.

#### 1.4 Efficient coupling reactions

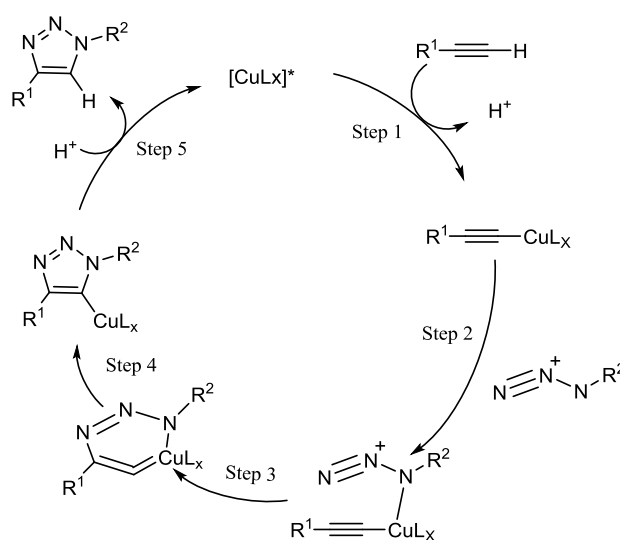
The key to generation of novel polymeric architectures based on block copolymers is an efficient coupling of the constituent blocks. Until recently, polymeric building blocks were connected to each other using traditional coupling reactions such as esterification and amidation that give low yields and require long reaction times for polymers. With the advancement in synthetic organic chemistry a set of reactions called 'click chemistry' has been introduced that has proved to be a boon for synthetic polymer chemists. Click



chemistry are a set of well-known reactions in organic chemistry modified to afford efficient coupling of small molecules as well as polymers. Click chemistry was first described by Sharpless and group.<sup>83,84</sup> The concept of click reactions for polymers was defined as a reaction that is modular, tolerant to many functional groups, wide in scope, is stoichiometric and gives high yield under mild conditions with no by-products so that desired products can be purified without column chromatography.<sup>85</sup> Some examples of such reactions used in polymer chemistry are discussed below.

### 1.4.1 Copper-catalyzed azide-alkyne cycloaddition (CuAAC) reaction

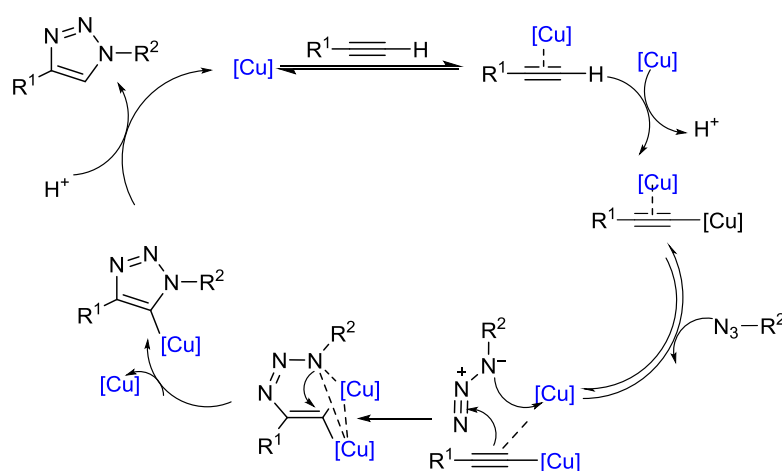
1,3-dipolar cycloaddition reaction of azide and alkyne was first introduced about 50 years ago by Huisgen,<sup>86,87</sup> in which aliphatic alkyne and azide cyclize into 1,4- and 1,5-substituted regioisomers of 1,2,3-triazole at 150 °C. In 2002, Meldal and Sharpless independently introduced Cu(I)-catalyzed Huisgen's 1,3 dipolar cycloaddition reaction.<sup>84,88</sup> This reaction selectively gives only 1,4-substituted 1,2,3-triazole. This reaction fulfills most of the conditions for click reactions, is named as copper-catalyzed azide-alkyne cycloaddition (CuAAC) and is the most widely used reaction in click chemistry.



**Scheme 1.1** Mechanism for CuAAC as proposed in 2007.

CuBr is the most common source for Cu(I) ion. To facilitate the reaction, Cu(I) concentration must be kept at its maximum. Cu(I) catalyst also can be generated by Cu(II)

pre-catalyst along with reducing agent, Cu(I) catalyst complex with a base or amine ligand and Cu wire surface which forms the Cu(I) catalyst. The reaction mechanism was proposed by Fokin and Finn in 2007 and is shown in Scheme 1.1.<sup>89</sup> Despite the widespread use of CuAAC reaction it was a challenging task to establish the mechanism due to the involvement of multiple equilibria between several reaction intermediates. Recently, Worrel et. al investigated<sup>90</sup> the detailed mechanism by using heat-flow reaction calorimetry and isotope crossover experiments. Their studies show that dinuclear copper complex is the key intermediate in CuAAC as shown in Scheme 1.2.



**Scheme 1.2** Two-copper-atom mechanism of azide-alkyne cycloaddition reaction.

Among the group of click reactions, CuAAC has emerged as useful tool for the synthesis of well defined and complex macromolecular polymeric architectures.<sup>91</sup> CuAAC has been successfully used in the synthesis of LDBC. As mentioned above Dong and coworkers.<sup>78,82</sup> described the synthesis of biocompatible dendritic star copolymers comprising PCL chains at the periphery of PAMAM dendron with alkyne functionality at the focal point that was coupled to azide-terminated PEG. Later, groups of Oriol and Sanchez coupled several generations of polyester dendrons with azobenzene at the periphery and alkyne at focal point with azide-terminated PEG by using CuAAC to afford photoresponsive LDBC.<sup>92,93</sup> Thayumanavan and coworkers synthesized<sup>94</sup> dendritic-rod-coil architecture to combine light harvesting and charge transfer properties of dendron with the intermolecular charge transport properties of the linear polymers. Alkyne-functionalised poly(benzyl ether) dendron with diarylaminopyrene groups as hole

transporting moieties was connected to electron carrying rod-coil linear polymer by using CuAAC reaction.

### 1.4.2 Diels-Alder reaction

Diels-Alder reaction is a widely used organic reaction invented by Otto Diels and Kurt Alder (Nobel Prize 1950).<sup>95,96</sup> Diels-Alder reaction is a [4+2] cycloaddition reaction between electron rich conjugated diene and electron poor dienophile to afford a stable 6-membered structure as shown in Figure 1.8. These reactions are thermally reversible and decomposition reaction of cyclic adduct is temperature-controlled. The advantage is that these can proceed in the absence of metal catalyst.

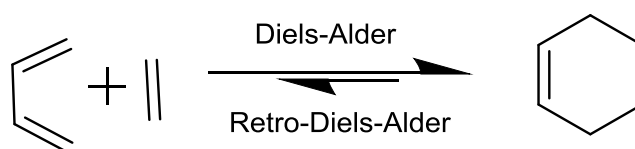
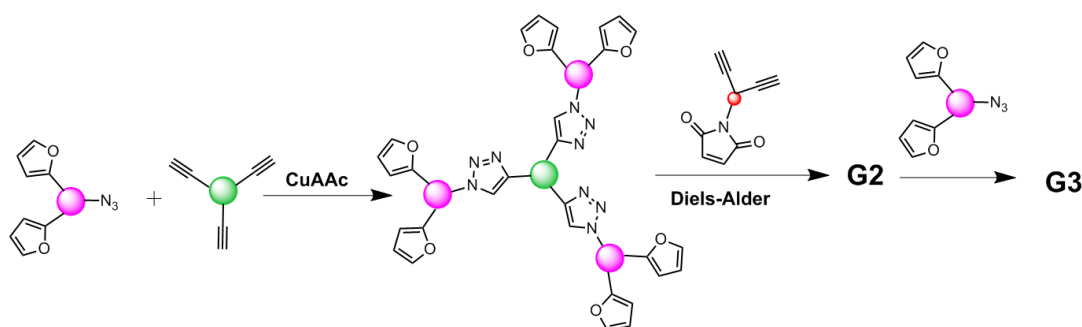


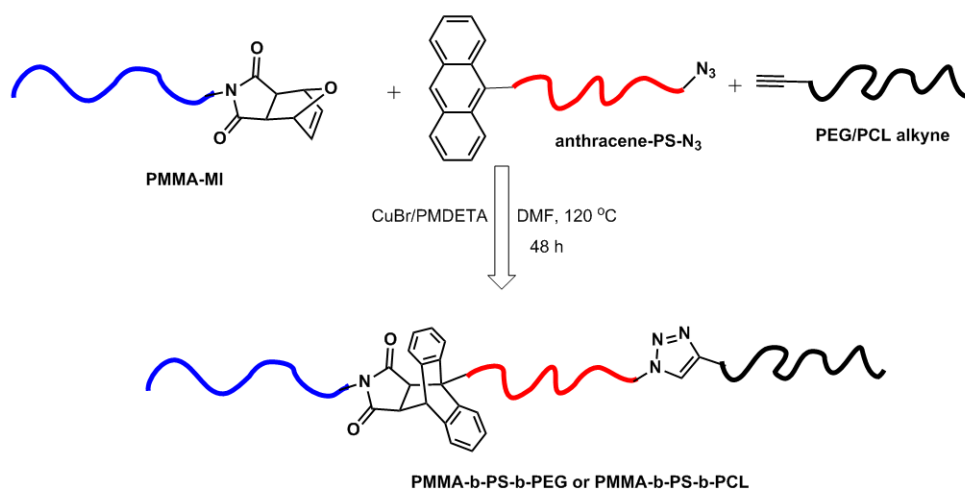
**Figure 1.8** An example of Diels-Alder/retro-Diels-Alder reaction.

The diene/dienophile pairs commonly utilized in polymer synthesis are anthracene/maleimide, furan/maleimide and butadiene/electron-deficient dithioesters. The anthracene/maleimide cycloaddition reaction takes place at high temperature of 110 °C. Furan/maleimide cycloaddition reactions are usually conducted at lower temperatures but the product is unstable above 100 °C. Polymer chemists have employed Diels-Alder reactions for synthesis of various macromolecular architectures like block copolymers, star polymers, dendrimers and dendronized polymers.



**Scheme 1.3** Synthesis of dendrimer using CuAAC and Diels-Alder reactions.

Kakkar and coworkers synthesized<sup>97</sup> thermally reversible dendrimers up to third generation by Azide-alkyne and furan-maleimide Diels-Alder click reactions by using divergent approach as shown in Scheme 1.3. A bisfuran azide functionalised molecule was reacted with tris-alkyne functional molecule to get G1 dendrimer, which was then subjected to Diels-Alder reaction with bis-maleimide alkyne linker to yield G2 dendrimer. Repetition of these reactions afforded higher generations dendrimers. Tunca and coworkers synthesized<sup>98</sup> ABC linear triblock copolymer by combining CuAAC and Diels-Alder reaction in one pot. In this report they have synthesized PEG-*b*-PS-PMMA triblock copolymers by furan-protected maleimide end-functionalised PMMA,  $\alpha$ -anthracene and  $\omega$ -azide end-functionalized PS, and PEG/PCL functionalized with alkyne at one end were reacted in one pot (Scheme 1.4).



**Scheme 1.4** Triblock copolymer synthesized by Diels-Alder reaction.

Later, the same group reported<sup>99</sup> synthesis of three-arm star copolymer by employing double-click strategy in one-pot reaction.

### 1.5 Self-assembly of linear block copolymers in solution

Block copolymers self-assemble into more complex morphologies in solution than in bulk.<sup>19,100-102</sup> In solution, the interaction between polymer and solvent plays an important role in determining the thermodynamically favoured nanostructure. For self-assembly in water, the main driving force is the hydrophobic effect that is aggregation of non-polar

block in order to decrease the unfavourable interaction with water molecules. Micellization of block copolymers in aqueous solution is exothermic process which involves negative change in the  $\Delta H^{\circ}_{\text{mic}}$ . However, micellization is entropically unfavourable because polymer chains are in a frozen state in the micellar aggregation. Eisenberg and his group have done pioneering work on block copolymer self-assembly in solution.<sup>101,103-107</sup> According to Eisenberg, the self-assembly in solution is governed by three factors a) interaction between hydrophobic blocks in the core, b) interaction between hydrophobic core and solvent at the interface and c) repulsive interactions between hydrophilic chains in the corona.<sup>108</sup>

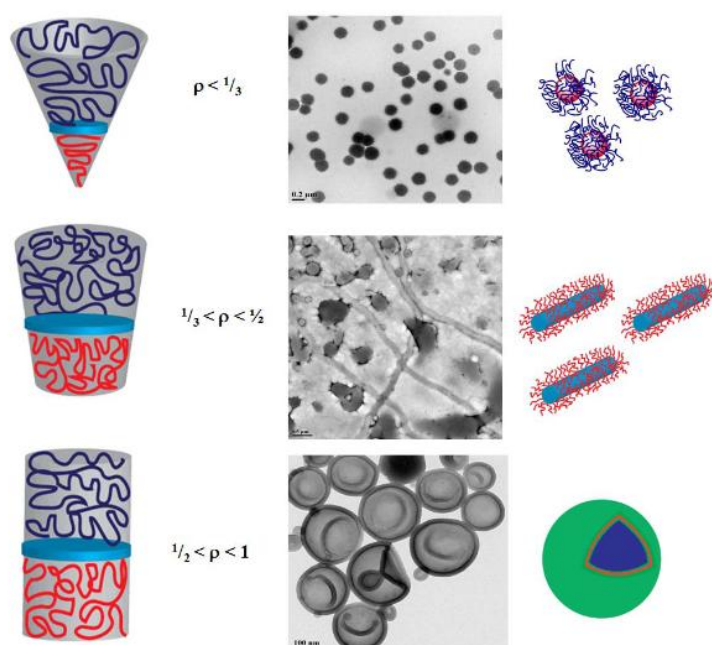


**Figure 1.9** Schematic representation of self-assembly of diblock copolymers into micelles, cylindrical micelles and vesicles according to packing parameter concept.  $W_{\text{philic}}$  decreases from top to bottom.

Amphiphilic block copolymers tend to self-assemble in aqueous solution into morphologies such as spherical micelles, cylindrical micelles and vesicles. Morphologies of block copolymers in solution strongly depend on geometry of each block and can be predicted to an extent by the packing parameter. Packing parameter<sup>109</sup> ( $\rho$ ) was developed

for small-molecule surfactants and then applied for block copolymer self-assembly (Equation 1).

$$\rho = V/a_0 \cdot l \quad (1)$$

where,  $V$  is volume of the hydrophobic block,  $l$  is length of hydrophobic block and  $a_0$  is surface area occupied by the hydrophilic block. The packing parameter determines the geometry of the aggregates. Approximate relationship between  $\rho$  and aggregate geometry is shown in Figure 1.9. Since the packing parameter concept cannot be directly applied to the complex assembly process due to wider range of possible chemical structures in block copolymers, Discher and Eisenberg proposed a general rule for predicting the morphology by relative content of the hydrophilic block termed as, hydrophilic weight fraction of the block copolymer ( $W_{philic}$ ).<sup>110,111</sup>  $W_{philic}$  is considered to be more suitable for predicting the geometry of the aggregates than packing parameter. According to this theory, spherical micelles are formed when  $W_{philic} > 40-50\%$  and rod like micelles are formed when  $W_{philic} > 50\%$ , vesicles are formed when  $W_{philic} \sim 35\%$  where as  $W_{philic} < 25\%$  inverse structures or crew-cut micelles are formed. However, this rule has no universal validity; the complex self-assembly of block copolymers in solution is not yet fully understood.

Amphiphilic block copolymers associate into micellar aggregates even at very low concentration and are more stable when compared with small molecule surfactant micelles. The morphology of the polymeric aggregates mostly depends on molecular as well as solution parameters. The molecular parameters are mainly influenced by the chemical structure, overall molecular weight, chain length ratio and architecture of the block copolymer.<sup>105</sup> The solution parameters mostly depend on solvent used for the preparation of micelles, ratio of solvent/non-solvent, polymer concentration, salt impurities, pH, temperature and preparation method.<sup>112,113</sup> When morphology is influenced by solution parameters, it is said to be 'kinetically controlled'. Many novel morphologies have been obtained from block copolymer assembly by using kinetic control.<sup>114</sup>

### 1.5.1 Stimuli-responsive block copolymers

Stimuli-responsive polymers are a class of materials wherein it is possible to reversibly alter solubility, volume, conformation and configuration by the external stimuli like pH,

temperature, ionic strength, light, redox, enzymes, ultrasound and others.<sup>115-119</sup> Stimuli-responsive polymeric systems allow for fabricating smart functional materials and may find use in applications such as controlled drug delivery, catalysis, smart interfaces, diagnostics and biosensors among others.<sup>120-123</sup> Selected examples of stimuli-responsive linear block copolymer self-assembly are discussed below.

Temperature-responsive polymers are among the most studied stimuli-responsive materials due to their ability to reversibly change their solubility, conformation, volume and hydrophilic-hydrophobic balance. Generally, these polymers form hydrogen-bonds with water molecules and become soluble in aqueous solution below LCST. However, above the LCST intra/intermolecular hydrophobic interaction is favoured over solvation by water molecules. The polymer changes its conformation from coil to globule and undergoes phase separation (Figure 1.10).

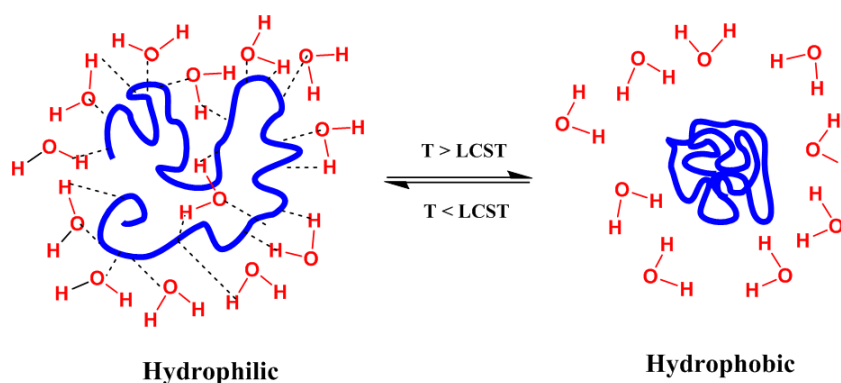


**Figure 1.10** Schematic showing the mechanism for change in conformation of a temperature-responsive polymer.

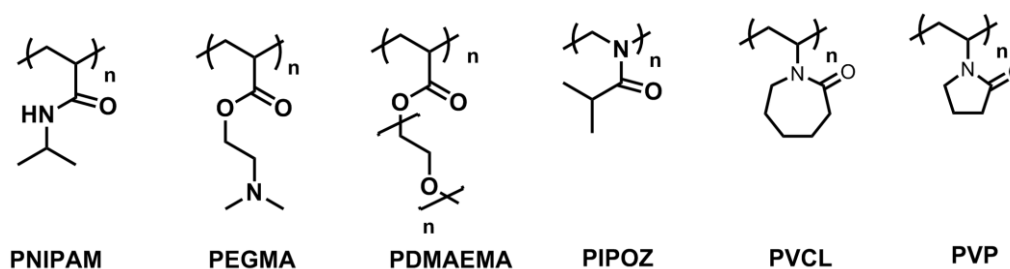


**Chart 1.1** Chemical structures of some of the temperature-responsive polymers.

Poly(N-isopropyl acrylamide) (PNIPAM), poly(N-vinylcaprolactam) (PVCA), poly(ethylene glycol) methyl ether methacrylate (PEGMA) and poly(oxazoline) N-substituted polyamides, poly(ethers), poly(oxazolines) and poly(vinylcaprolactones) are

some examples of temperature-responsive polymers (Chart 1.1). PNIPAM is a widely studied temperature-responsive polymer because it shows LCST around 32 °C, a temperature that is close to that of the human body. These polymers can be used in thermoresponsive membranes, which can shrink due to the hydrogen-bonding below the LCST temperature, resulting in pore “opening” while above the LCST breakage of hydrogen-bonds occurs and leads to pore “closing”.<sup>124</sup> By cycling the temperature below and above the LCST temperature these membranes can be used for separation of mixture of solutes with identical molecular sizes. Temperature-responsive polymers are potential candidates for targeted delivery of anticancer drugs as well.<sup>125</sup>

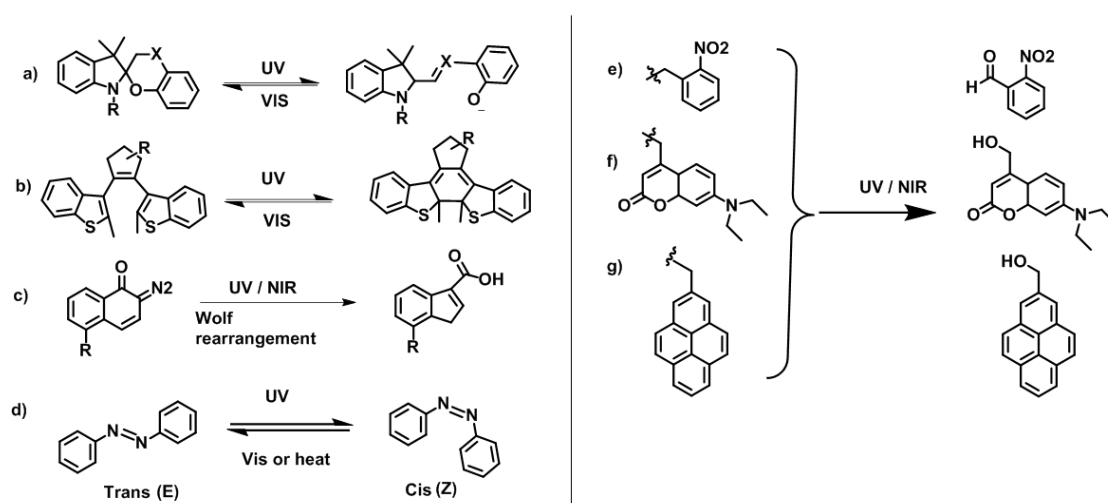


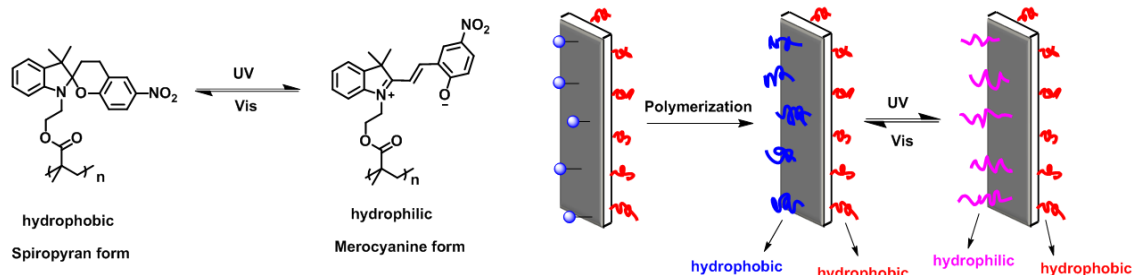
**Chart 1.2** Chemical structures of photoresponsive molecules. a) spiropyran, b) dithienylethene, c) diazonaphthoquinone, d) azobenzene, e) o-nitrobenzyl ester, f) coumarinyl ester, g) pyrenylmethyl ester.

Photoresponsive polymers are an important class of smart materials due to their potential applications in wide ranging fields such as liquid crystal displays, optical data storage, drug delivery, gene delivery, microreactors and photodynamic therapeutics.<sup>125-133</sup> Light responsive groups are of three types that undergo 1) geometrical isomerisation, 2) ring-opening/closing and 3) reversible or irreversible rearrangements when exposed to light of specific wavelength. Many chromophores undergo these processes rapidly and induce imbalance in the hydrophilic/hydrophobic ratio of the polymer since there is a change in polarity upon photoirradiation. This can cause complete disruption or change in



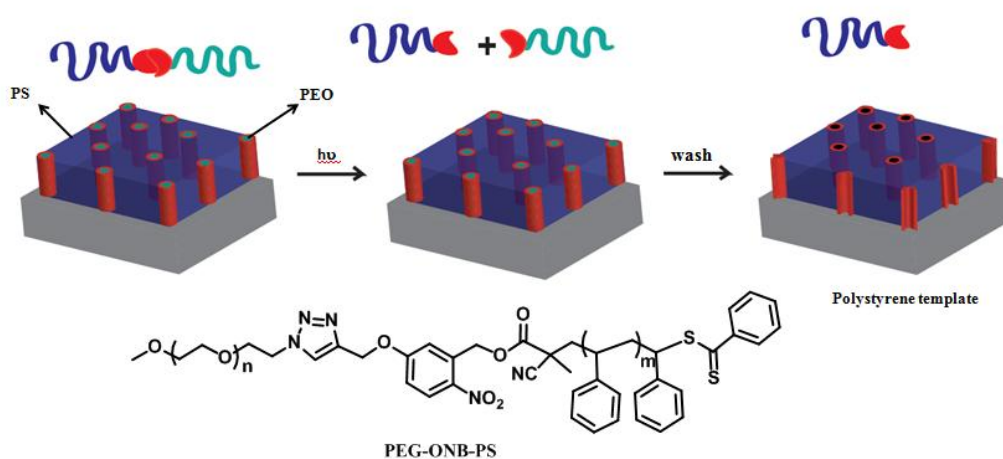
the morphology. Chemical structures of some of the photoresponsive organic molecules are shown in Chart 1.2 including examples of each type.

Recently, Yang et al.<sup>128</sup> synthesized light triggered Janus silica nanosheets grafted with spiropyran polymer brushes by using ATRP. They have shown reversible transformation in the hydrophobicity of nanosheets by irradiating with UV and visible light caused by conversion of hydrophobic spiropyran to hydrophilic zwitterionic merocyanine form (Figure 1.11). The Janus composite nanosheets can be used as light triggered solid emulsifiers.



**Figure 1.11** Surfaces with switchable hydrophobicity using photoresponsive brushes.

Zhao et al. reported<sup>134</sup> an amphiphilic block copolymer comprising PEO and hydrophobic poly(2-nitrobenzyl methacrylate) (PNBM). They demonstrated self-assembly of the block copolymer into micelles that dissociated upon irradiation with either one photon UV or two photon NIR absorption by the 2-nitrobenzyl moieties.

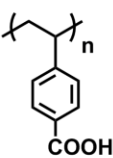
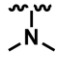
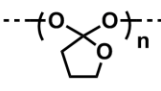
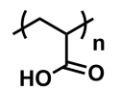
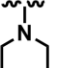
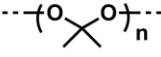
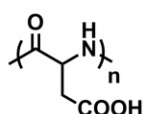
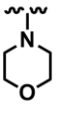
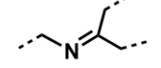
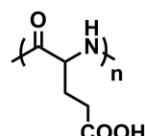
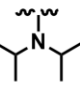
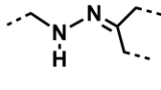


**Figure 1.12** Highly ordered nanoporous PS thin films, prepared from block copolymer with ONB at the junction, as templates for SiO<sub>2</sub> nanodots.

Theato and coworkers reported the first example of nanoporous thin films derived from photo-cleavable block copolymer for template applications.<sup>135</sup> They synthesized a block copolymer, *viz.* poly(styrene-*b*-ethylene oxide) with an *o*-nitrobenzyl ester photo-cleavable junction using reversible addition fragmentation chain-transfer (RAFT) polymerization and CuAAC. These ordered films were exposed to UV, the PEO domains were washed out with water and nanoporous PS films with pore diameter 15-20 nm were obtained (Figure 1.12).

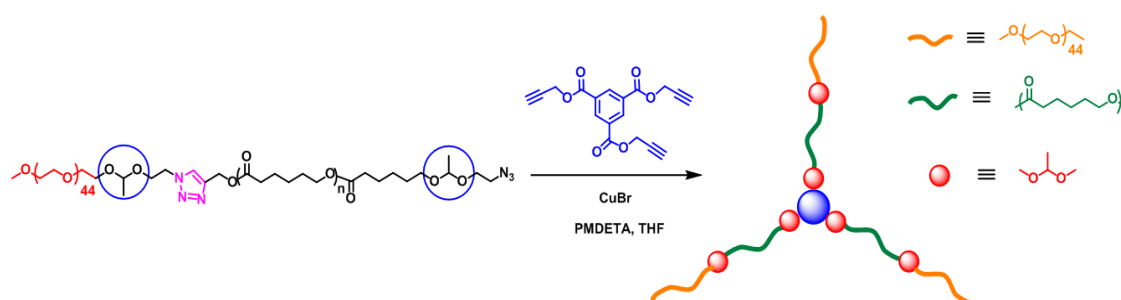
pH-responsive polymers can be broadly divided into two classes. One of the classes is polyelectrolytes that bear weak acidic or basic groups along the polymer chain, which can in respond to changes in the surrounding pH by receiving or losing protons. Protonation or deprotonation of these polymers causes change in the water solubility of these polymers due to the variation in the pKa value. For example, polyacrylic acid contains pendant acid groups that accept proton at low pH and release proton above its pKa (4.8). Hence, the polymer exhibits a collapsed conformation at low pH and expanded coil state at high pH. Among the stimuli-responsive polymers, this class of polymers is widely studied for drug delivery applications.<sup>118,136,137</sup> Indeed, it has been shown that pH gradient exists between intra and extracellular milieu of cancer cells, which can be exploited to target drugs to tumor tissue selectively using pH-responsive polymer assemblies. The other class of pH-responsive polymers is the polymers containing pH-cleavable groups. Many types of acid-cleavable bonds such as acetal, ketal, hydrazone, and  $\beta$ -thioester that can rupture under mild acidic conditions have been introduced in polymers. Chemical structures of pH-responsive groups are given in Chart 1.3. Some examples of pH-responsive block copolymer assemblies are discussed here.

Ni et al. synthesized<sup>138</sup> a series of star polymers composed of PEO-*b*-PCL with acid-cleavable acetal group at the block junction by using ring-opening polymerization and CuAAC (Scheme 1.4). Assemblies of these polymers in water were shown to be disrupted at mild acidic conditions. Further, pH-triggered release of anticancer drug doxorubicin DOX and cell uptake of DOX into nuclei was shown.

	$pK_a$		$pK_a$	
 PVBA	7.1	 PDMAEMA	7.4	 Orthoester
 PMMA	5.6	 PDEAEMA	7.3	 Acetal / ketal
 PGlu	4.3	 PMEMA	4.9	 Imine
 PASP	4.9	 PDPA	6.3	 Hydrazone

**Chart 1.3** Chemical structures of pH-responsive groups commonly used in polymers.

Hawker et al.<sup>139</sup> synthesized linear diblock copolymer (PEO-*acetal*-PS) with acid-cleavable acetal group at the middle of the diblock and derived nanoporous thin films by cleavage of acetal linker and subsequent selective removal of PEO domains. The nanoporous films further could be functionalized with primary alcohols at the interior of the pores.



**Scheme 1.4** Synthesis of acetal-containing star copolymer with PEO-*b*-PCL as arms.

## 1.6 Self-assembly of linear-dendritic block copolymers in bulk

To minimise the interfacial area with the incompatible block and to lower the total interfacial energy block copolymers undergo microphase separation.<sup>2</sup> The enthalpic contribution to this process is the interfacial energy between the two blocks while chain stretching is the entropic contribution. In the bulk, the microphase separation leads to variety of morphologies such as spheres, cylinders, bicontinuous gyroids and lamellae. As the number of blocks increases the number of possible morphologies increases as well. It has been shown that the phase separation in diblock copolymers mainly depends on three parameters, *viz.* 1) volume fraction of the two blocks A and B ( $f_A + f_B = 1$ ), 2) degree of polymerization of each block and 3) Flory-Huggins interaction parameter ( $\chi_{AB}$ ).<sup>140</sup> The  $\chi$  parameter refers to the degree of incompatibility between A and B blocks. The degree of microphase separation is determined by the factor  $\chi N$ , where  $N$  is the molecular weight of the block copolymer. It should be noted that with increasing temperature, the incompatibility between the blocks decreases and entropy increases, which results in order to disorder transition (ODT) and order to order transition (OOT).

Similar to other amphiphilic block copolymer architectures, LDBC's spontaneously self-assemble in both solid and solution state. The hydrophilic/hydrophobic balance can be tuned by the chain length of linear polymer and dendron generation. Early work was carried out by Weisner and coworkers who synthesized<sup>141</sup> amphiphilic third generation dendron attached with hydrophilic PEO chain at focal point. The copolymers exhibited phase separation in bulk into mesophases like micellar, hexagonal columnar, continuous cubic and lamellar, and were shown to be potentially useful for charge transport applications. Later, the same group synthesized<sup>142</sup> amphiphilic dumbbell-shaped triblock LDBC containing second and third generation dendrons attached to PEO as the middle block. The second generation dendron polymer phase separated into 2D-hexagonal columnar mesophases and third generation dendron polymer into micellar cubic mesophases in bulk. These results demonstrated that the LDBC self-assembly can fine tuned when compared to linear polymers and change in molecular shape with dendron generation is a parameter that can be tuned independently to manipulate solid-state morphologies. Lee et al. reported<sup>143</sup> amphiphilic LDBC's of aliphatic third generation polyether dendron with peripheral tetradecyl chains and hydrophilic linear PEO chains of

different chain lengths. Crystallinity of these polymers was shown to depend on the linear polymer chain length by thermal and X-ray scattering analysis. Similarly, the self-assembly in bulk into different mesophases depended on the linear polymer chain length. Photoresponsive LDBC's composed of PEG and four generations of polyester bis-MPA dendrons functionalized with mesogenic and photochromic 4-cyanoazobenzene groups on the periphery were reported by del Barrio et al.<sup>144</sup> These copolymers self-assembled into liquid crystalline lamella mesophases as demonstrated by using X-ray diffraction and TEM analysis. The photo-induced orientation properties of polymer with dendron containing sixteen azobenzene groups were studied under irradiation with 488 nm linearly polarized light. Later, to improve the film properties, the same group<sup>145</sup> synthesized a series of polymers with linear amorphous PMMA coupled to dendron (G2-G4) containing 4-cyanoazobenzene on the periphery connected through flexible spacer (5 and 10 carbons). They studied photo-induced anisotropy in detail by irradiating with polarised light at 488 nm and higher order parameter for the 10 carbon spacer with G4-dendron polymer was achieved. In another report<sup>146</sup> the influence of various linear polymers such as PMMA, poly(ethyl methacrylate) (PEMA) and polystyrene was studied and lower photoinduced anisotropic parameters were observed for PMMA and PEMA. Malkoch and coworkers fabricated a library of micrometer-sized honeycomb structures from amphiphilic LDBC's comprising PCL or poly(L-lactic acid) (PLA) hydrophobic blocks on polyester based third generation dendron periphery and hydrophilic PEG at dendron focal point. These polymers produced well-ordered honeycomb films with hundreds of micrometer size.<sup>147</sup>

A series of azobenzene-containing LDBC's with linear PEG and PAMAM dendron of different generations G0 to G3 were synthesized<sup>148</sup> (Figure 1.13). The dendron was grown from amine-terminated PEG precursor by the divergent approach. Dendron periphery was functionalized with azobenzene bearing octyloxy tails and flexible decamethylene spacers by Michael addition with corresponding acrylate mesogen units. In the solid state self-assembly study well defined lamellar structures were shown by G0, G1 and G2 with spacing between the layers from 12.2 nm and 13 nm wherein G0 exhibited simple lamellar structure whereas G1 and G2 showed hierarchical structures such as tetragonal within lamellar and lamellar within lamellar structures, respectively.

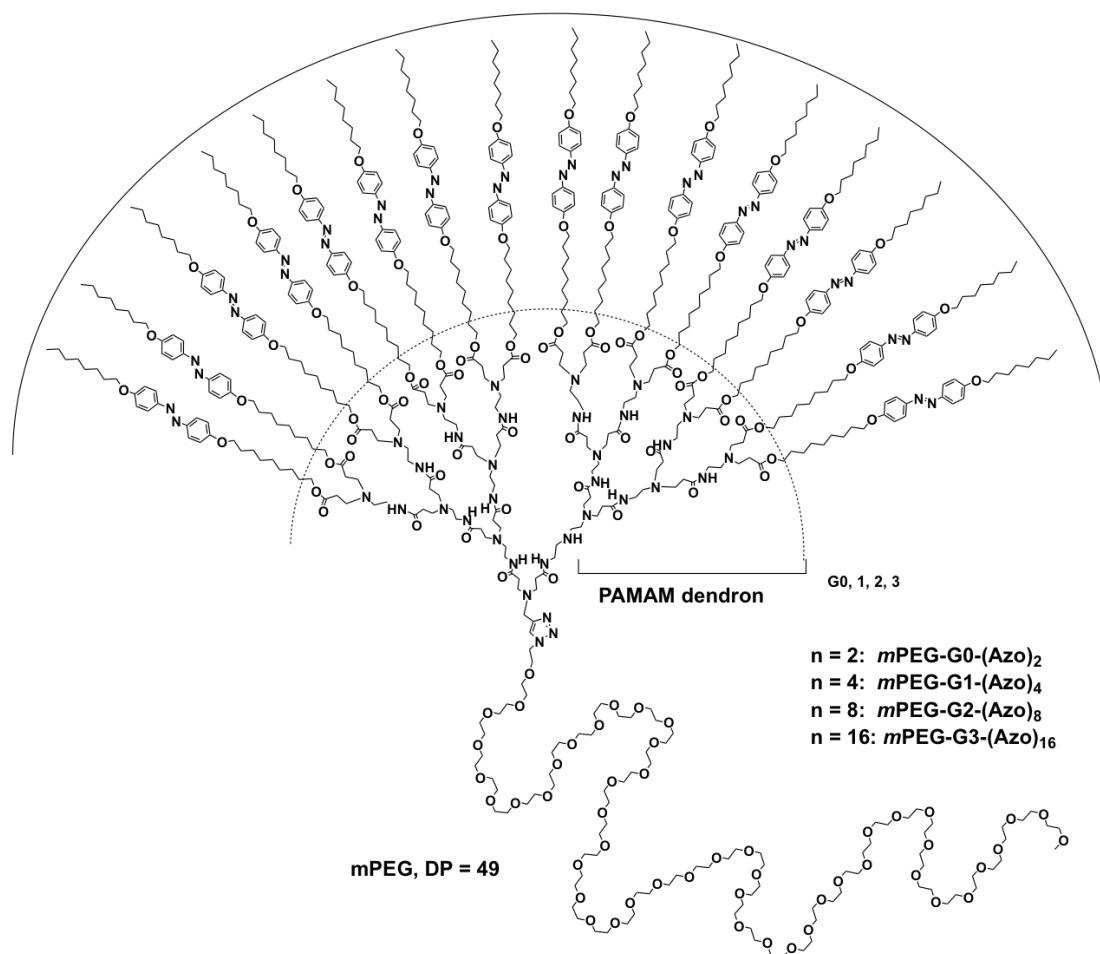


**Figure 1.13** Azobenzene-containing PAMAM-PEG copolymers studied for self-assembly in bulk.

For G3 the morphology changed significantly from lamellar to rectangular columnar structure. Incorporation of photoresponsive groups into the nanosized domains rendered these materials useful for applications like liquid crystal displays and optical data storage, similar to azobenzene-containing linear block copolymers that have been explored for holographic data storage applications.<sup>149,150</sup>

## 1.7 Self-assembly of linear-dendritic block copolymers in solution

### 1.7.1 Self-assembly studied without application of stimuli

Initially, self-assembly of linear-dendritic block copolymers in solution was studied without application of any stimuli. Extensive work has been carried out on synthesis and self-assembly of linear-dendritic block copolymers in solution by Fréchet and coworkers.

In their first report<sup>54</sup> in 1992, synthesis of LDBC's comprising poly(benzyl ether) dendron attached to linear PEG was described. Self-assembly of these polymers was studied in different solvents and formation of micelles was shown in solvents in which, one block is soluble or both the blocks have low solubility. In the subsequent report,<sup>151</sup> self-assembly of these polymers was studied in different solvents by varying the dendron generation and linear polymer chain length. It was shown that the polymers self-assembled into uni- and multimolecular micelles in methanol/water mixture, which is good for the linear polymer whereas only unimolecular micelles were observed in THF, which is good solvent for dendrons. Kim and coworkers reported<sup>58</sup> LDBC's based on carbosilane dendron and linear PEG synthesized by using divergent method from the allyl-terminated PEG chain. Self-assembly of these polymers in water showed that G1 and G2 polymers formed micelles. The cmc of these polymers was calculated by using pyrene as fluorescence probe and hydrodynamic sizes of these aggregates were measured by using DLS technique. Gitsov et al. synthesized<sup>152</sup> polymers composed of first and second generation poly(benzyl ether) dendrons and linear PEG of two different molecular weights (5000 and 11000 g/mol). These polymers self-assembled into micelles in water and environment of micellar core was investigated by using pyrene as fluorescence probe. Encapsulation of aromatic compounds with fused rings like anthracene, perylene and fullerene in the micelles was studied. Jiang et al. reported<sup>153</sup> copolymers comprising Fréchet-type dendrons and linear PMMA polymer synthesized from dendritic benzyl chloride macroinitiators by using ATRP with CuCl/bipy catalyst system. Self-assembly of these polymers in THF/H<sub>2</sub>O mixture showed formation of micellar assemblies. In 1998 Hammond and coworkers reported<sup>154</sup> synthesis and self-assembly of copolymers comprising linear PEG of molecular weight 2000 and 5000 g/mol and PAMAM dendron. The aqueous self-assembly behaviour was studied by using intrinsic viscosity and GPC techniques and the influence of chain length of PEG and functionality on the dendron periphery was observed. The longer PEG containing copolymers self-assembled into unimolecular micelles. Gitsov et al. described<sup>155</sup> nanoreactors formed by adsorption of amphiphilic linear-dendritic AB and ABA copolymers onto glycoprotein laccase. These polymer-enzyme complexes showed improved reactivity of the oxidative enzyme laccase at elevated temperatures and were able to oxidize phenolic compounds and polyaromatic hydrocarbons in aqueous medium.

Later, these researchers reported<sup>156</sup> similar assemblies for Diels-Alder reaction between fullerene (C<sub>60</sub>) and polycyclic aromatic hydrocarbons in water at room temperature, which are considered 'green chemistry' conditions. These polymer assemblies were shown to possess lower microviscosity, stability and higher binding capacity than similar linear analogues. Recently, Kim and coworkers reported<sup>157</sup> LDBC's comprising Fréchet-type dendrons with six PEG chains on periphery and hydrophobic linear polystyrene at focal point that self-assembled into polymer cubosomes with internal inverse bicontinuous cubic phase in aqueous solution. Later, they described<sup>158</sup> a scalable method for the mesoporous monoliths with large-sized pore networks (>25 nm diameter) in the crystalline lattices. The surface functional groups on the pores were shown to accommodate large molecules such as proteins and these monoliths were also demonstrated to act as templates for self-supporting skeletal structures of inorganic oxides such as titania and silica. Moon et al. synthesized linear-dendritic copolymers comprising hydrophilic dendron and hydrophobic linear polymer having fixed molecular weight but different number of peripheral groups without changing the hydrophilic/hydrophobic block ratio, which is the deciding factor for change in the morphology.<sup>159</sup> These polymers showed different morphologies from cylindrical micelles to toroid and lasso micelles. This example shows that control over morphology of polymeric micelles can be achieved through polymeric architecture of the building blocks of the block copolymer. Cai et al. reported a series of amphiphilic rod-coil LDBC's composed of a Percec-type dendrons (G1–G3, based on gallic acid) functionalised with hydrophilic PEG chains and rod-like liquid crystalline linear polymer poly{2,5-bis[4'-methoxy-phenyl]oxycarbonyl] styrene} (PMPCS).<sup>160</sup> These polymers were shown to form vesicles, large compound vesicles (LCVs) and cylindrical micelles depending on dendron generation. Dhar and coworkers recently reported<sup>161</sup> a novel biodegradable dendritic-linear-dendritic triblock copolymer for combination therapeutics. These polymers were synthesized by incorporating different generations of bis(MPA) polyester dendrons functionalized with anti-inflammatory drug aspirin and anti-cancer drug cisplatin. The blending of the final polymer with poly(lactide-co-glycolide)-*b*-PEG-OH resulted in a cocktail containing both the drugs in pre-defined concentration. These polymer nanoparticles were demonstrated as model drug carriers for prostate cancer and cisplatin-resistant cancer.



## 1.7.2 Stimuli-responsive self-assembly studies

### a) pH-responsive linear-dendritic block copolymers

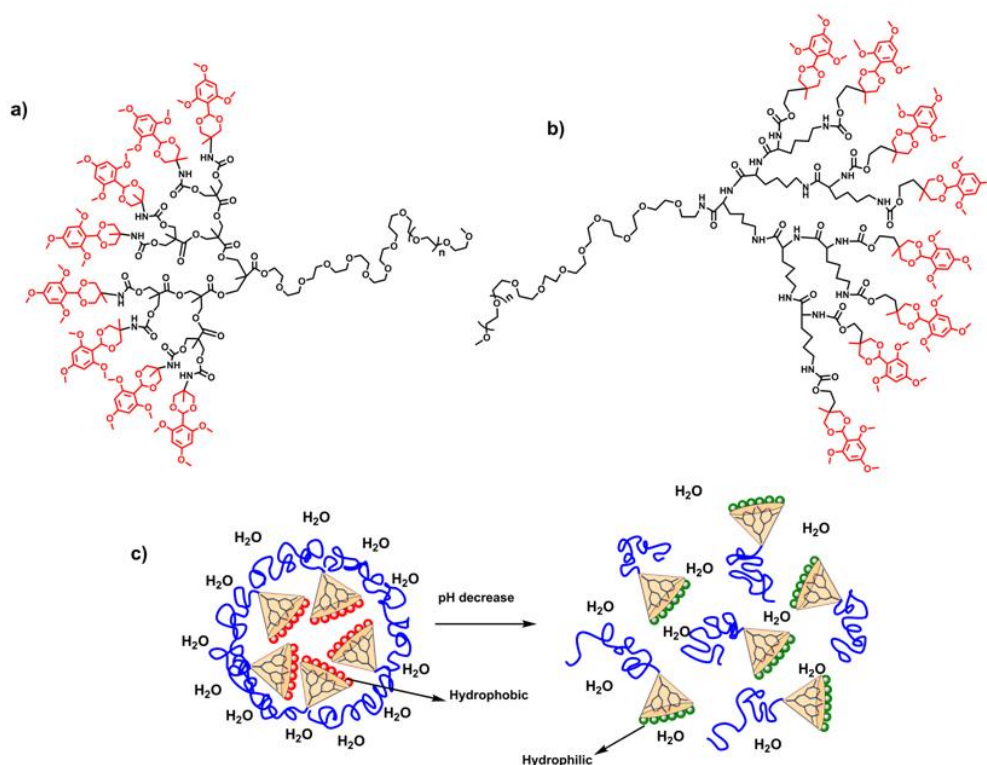


**Figure 1.14** Chemical structure of LDBCs containing a) polyester bis-MPA dendron with acetal on periphery and b) poly(L-lysine) dendron with acetal on periphery and c) schematic representation of disruption of corresponding pH-responsive micelles.

As discussed above, pH is an attractive stimulus to cause change in the morphology or the disassembly of micelles of block copolymers at mild acidic conditions and is attractive for targeted drug delivery to cancer cells among other applications. First report on the synthesis of pH-responsive LDBCs came from Meijer and coworkers.<sup>162</sup> A series of polymers comprising polystyrene attached to poly(propylene imine) dendron with number of acid groups on dendron periphery increasing exponentially from 2 to 32 were synthesized. Their pH-dependent self-assembly at the toluene/water interface was shown. Gillies et al. synthesized hydrophobic polyester and polylysine dendrons with pH-responsive cyclic acetals at the periphery attached to hydrophilic linear PEG at the focal point (Figure 1.14).<sup>163</sup> Effect of different chain lengths of PEG and dendron generations on cmc, micelle size and release of cargo under mild acidic conditions was explored. In the next report, they studied the polyester dendron-PEG conjugates for pH-responsive release

of anti-cancer drug DOX in the pH range of 4.0 to 7.4 and their cytotoxicity was determined and compared with free DOX.<sup>164</sup>

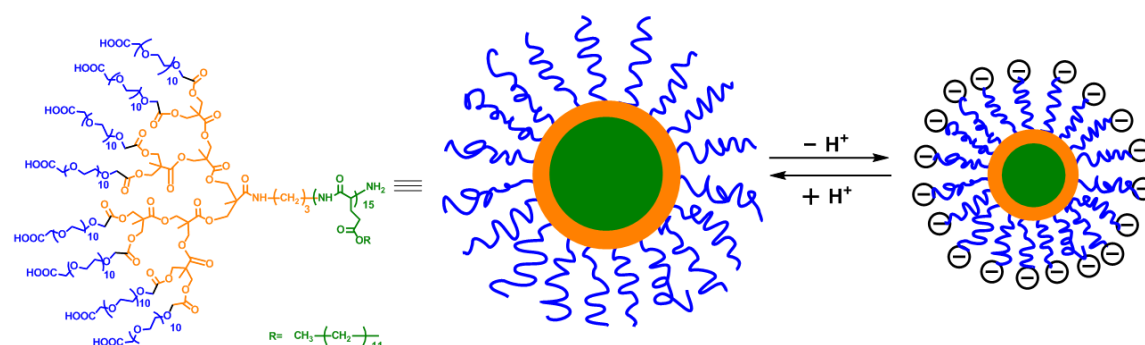


**Figure 1.15** Chemical structure of pH-responsive bis-MPA dendron-*b*-poly( $\gamma$ -*n*-dodecyl-L-glutamate) LDBC and schematic representation of pH-responsive changes in micellar assembly.

Dendritic-linear-dendritic triblock copolymers with PAMAM dendron and linear poly(propylene oxide) were reported by Hammond group.<sup>165</sup> Micellar properties of these triblock copolymers were studied by varying dendron generation, ionic strength and pH; smaller aggregates were observed with increasing dendron generation. It was found that the cmc was at pH 5.2 was higher than at pH 2 in presence of salts in the buffer. Encapsulation and release properties of the polymers by using model hydrophobic drugs were investigated. Later, group synthesized LDBCs containing bis-MPA based dendron displaying PEG-COOH on periphery and comb-like poly( $\gamma$ -*n*-dodecyl-L-glutamate) as hydrophobic linear block (Figure 1.15). The polymers self-assembled into core-shell type spherical micelles with comb block in the core.<sup>166</sup> The pH-dependant change in size of these aggregates due to carboxylic groups at the micellar surface was demonstrated. Dong and coworkers described<sup>80</sup> copolymers comprising linear PEG and 3<sup>rd</sup> generation PAMAM dendron with poly(L-glutamic acid) (PGA) on the periphery (Figure 1.16). At neutral pH or acidic conditions due to inter-molecular hydrogen-bonding between PGA chains micellization occurred. At pH above 8, the micelles disassembled into individual polymer chains due to ionization of carboxylic groups on PGA chains, however self-assembly into reverse micelle was observed at alkaline conditions due to guest-host complexation between  $\alpha$ -cyclodextrin and PEG. Release and uptake of DOX controlled by pH was demonstrated.

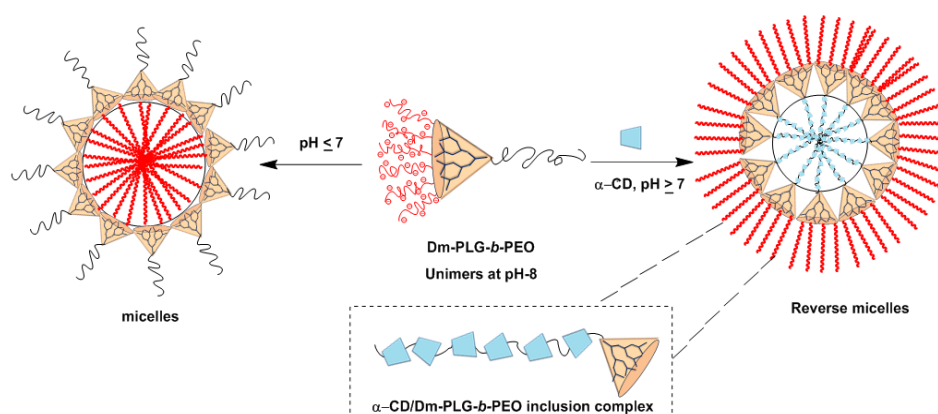


**Figure 1.16** Schematic representation of pH-responsive polypeptide based LDBC.

Chen and coworkers reported<sup>167</sup> synthesis of LDBC conjugated with DOX by hydrazone formation at the periphery of dendron and camptothecin was encapsulated in the assembly with high loading efficiency (Figure 1.17). Thus, more than one drug was sequestered in a single nanocarrier.

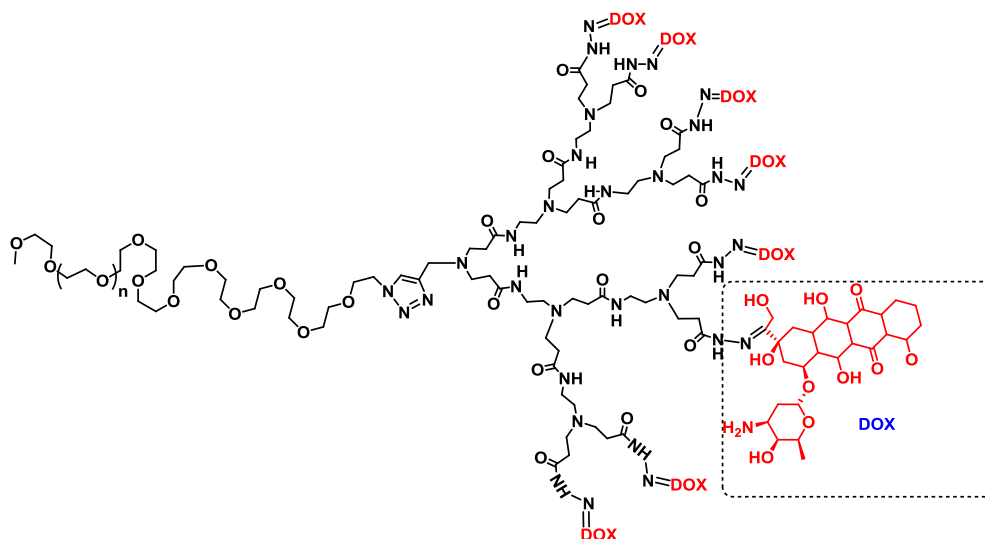


**Figure 1.17** Dox conjugated pH-responsive linear-dendritic block copolymer.

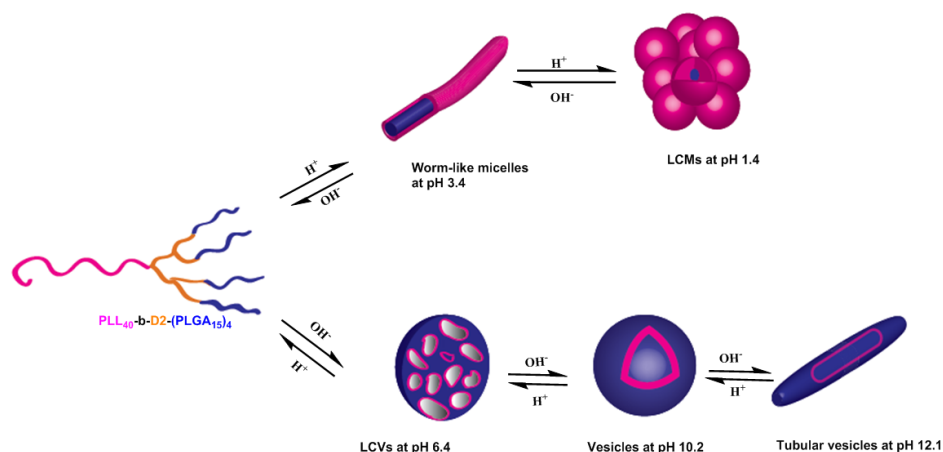


**Figure 1.18** Schematic representation of pH-dependent assembly of linear-dendritic block copolymers.

Linear-dendritic polyelectrolyte block copolymers *viz.* poly(L-lysine)-*b*-D2-poly(L-glutamic acid) synthesized by ring-opening polymerization and click chemistry, where D2 stands for second generation PAMAM dendron were reported<sup>79</sup> (Figure 1.18). In this system, both the linear segment and dendron segments were pH-responsive. The linear polymer poly(L-lysine) contains cationic amino groups and dendron peripheral poly(L-glutamic acid) chains contain anionic carboxylic groups and their hydrophilic/hydrophobic balance can be tuned depending on degree of ionization of carboxylic and amine groups. The reversible pH-responsive behaviour of these copolymers has been investigated in detail and a various morphologies were observed depending on pH of the solution. Recently, Chen and coworkers synthesized pH and redox-responsive PEG-PAMAM linear-dendritic copolymers. The dendron periphery was conjugated with lipoic acid and DOX *via* acid-labile hydrazone linkage and the polymer micelles were cross-linked using dithiothreitol (DTT). These polymers self-assembled into nanosized spherical micelles as determined by the TEM and DLS techniques. Controlled release of DOX at mild acidic conditions and by adding GSH to the micellar aggregates was shown and biocompatibility of polymers was determined by using cytotoxicity assay.<sup>168</sup>

### b) Temperature-responsive linear-dendritic block copolymers

Early example of temperature-responsive LDBC was reported by Zhu et al. who synthesized PNIPAM from the focal point of second generation poly(benzyl ether)

dendron *via* ATRP (Figure 1.19).<sup>69</sup> Self-assembly studies showed change in morphology from spherical micelles to entangled nanotubules above the LCST of PNIPAM.

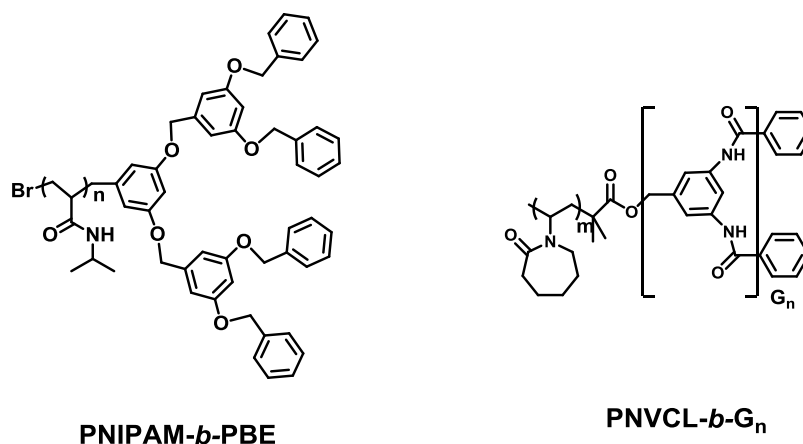


**Figure 1.19** Temperature-responsive linear-dendritic copolymers.

Liu and coworkers reported LDBC's synthesized by using poly(benzyl ether) (PBE) dendron focal point functionalized with chain-transfer agent to polymerize PNIPAM as well as pyrene-labelled PNIPAM.<sup>65</sup> Two stage collapse of PNIPAM chains well before LCST temperature was studied by using pyrene as fluorescence probe. Bi et al. synthesized LDBC's with dendritic aromatic polyamide as hydrophobic block and thermoresponsive poly(N-vinyl caprolactam) (PNVCL) as hydrophilic block using similar strategy (Figure 1.19).<sup>169</sup> The reversible temperature-responsive behaviour was studied at LCST range of 36–46 °C. The block copolymers self-assembled in aqueous solution into spherical micelles that were reversible upon heating and cooling. Drug loading content and efficiency for the model hydrophobic drug, indomethacin, was found to be dependent on dendron generation. Release of drug was achieved by heating above the LCST. Hammond and coworkers reported PEG-functionalized hydrophilic bis-MPA dendron attached to temperature-responsive poly(2-(2'-methoxyethoxy) ethyl methacrylate).<sup>170</sup> Below the LCST these polymers were in the form of unimers due to double hydrophilic nature of both the blocks. Upon heating above the LCST temperature (50 °C) for 2 h the polymer formed spherical micelles 43 nm in diameter. After cooling to 25 °C that is, below the LCST the micelles disassembled into unimers and were regenerated by heating to 50 °C (Figure 1.20).

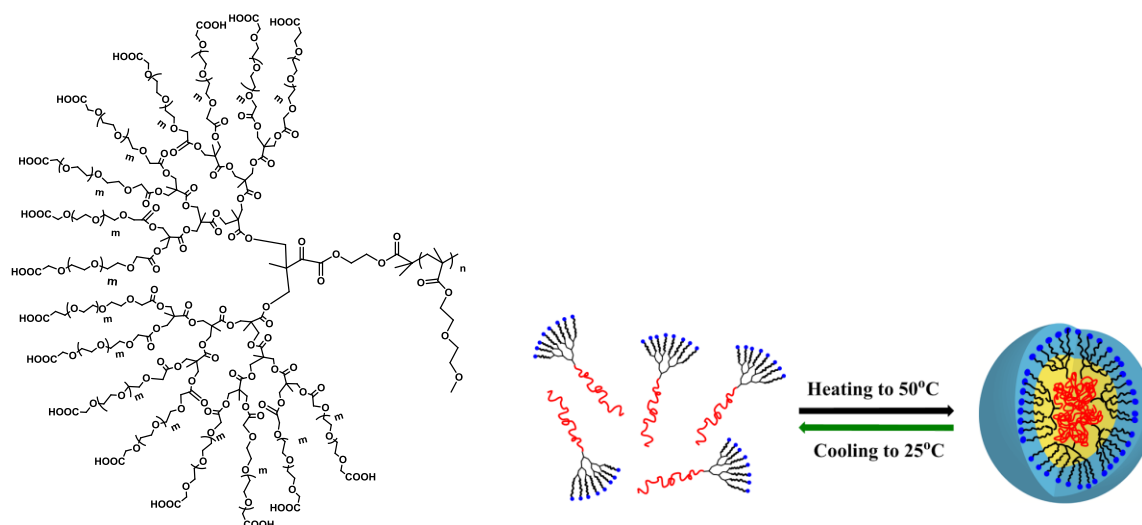


**Figure 1.20** Chemical structure of temperature-responsive double hydrophilic block copolymer and schematic representation of temperature-induced morphology change.

Kim et al. reported the synthesis of biodegradable LDBC with third generation polylysine dendron and PNIPAM grafted with poly-lactide linear polymer. They have synthesized these polymers by DCC coupling reaction between third generation dendron and PNIPAM chains. Temperature-responsive behaviour of these polymers was studied by using UV-vis spectroscopy and DLS techniques and biodegradability was studied by using FT-IR analysis.<sup>171</sup> Zou et al. reported synthesis of dual-stimuli responsive linear-dendritic hybrids *via* guest-host complexation between  $\beta$ -cyclodextrin ( $\beta$ -CD) end-functionalized linear PNIPAM chains and poly(benzyl ether) dendrons with an azobenzene at the focal point. These polymers self-assembled into vesicles in water at room temperature and reversibility of self-assembly and disassembly upon irradiation with UV and visible light was shown.<sup>172</sup> Recently, Kim et al. reported<sup>173</sup> dual-stimuli-responsive LDBC comprising pH-responsive poly(benzyl ether) dendrons with carboxylic acid groups at the periphery and poly(2-isopropyl 2-oxazoline) (PiPrOx) as the temperature-responsive linear polymer. LCST variation depended on the dendron generation at different pH values. These copolymers underwent change in the morphology under different pH and temperature conditions. Hoogenboom and coworkers reported copolymers comprising bis-MPA dendron with pH-cleavable acetonide groups at periphery of dendron and temperature-responsive linear poly(2-ethyl-2-oxazoline).<sup>174</sup> The polymers were synthesized in one pot by using CuAAC and Diels-Alder double click reaction method. Self-assembly of these

polymers in aqueous solution and pH-responsive behaviour at neutral and mild acidic conditions were studied.

### c) Photoresponsive linear-dendritic block copolymers

As discussed above, imparting photosensitivity to polymer assemblies provides the opportunity to release the cargo upon photoirradiation in solution. Compared to linear block copolymers light-responsive LDBC are less explored. Well defined morphologies in solution from azobenzene containing LDBC were first reported by Oriol, Sanchez and coworkers.<sup>92</sup> The polymer shown in Figure 1.21 that was earlier used for solid state studies was employed. In aqueous solution, the polymer was observed to form morphologies such as micelles, nanofibers, vesicles and lamellae, selectively depending on dendron generation.

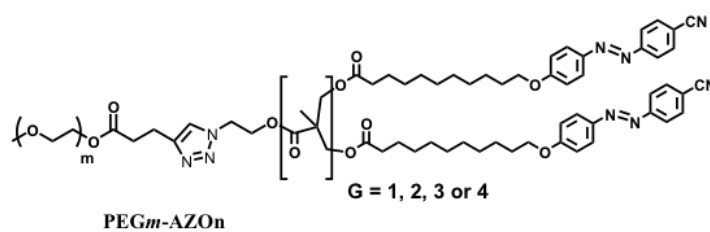


**Figure 1.21** Chemical structure of copolymers with azobenzene on dendron periphery that form defined morphologies in solution.

Recently, Sheng and coworkers supported this shape change and polarity change associated with *trans* to *cis* isomerization by the simulation studies.<sup>175</sup> Subsequent work done by this group<sup>93</sup> focused on the 4<sup>th</sup> generation dendron bearing sixteen 4-isobutyloxyazobenzene peripheral groups that show lower aggregation tendency than the cyano-derivative. 4-isobutyloxyazobenzene also shows larger photoinduced change in the dipole moment than with 4-cyanoazobenzene, which made disruption of the vesicles with low intensity UV light possible. Later, LDBC with decreasing azobenzene content (75 mol%, 50 mol% and 25 mol%) were designed<sup>176</sup> by random replacement of peripheral azobenzene units with hydrocarbon chain to tune photoresponsiveness of the inner membrane. The self-assembly was not altered but disruption in the membrane was significantly enhanced at 50 mol% azobenzene content; no change in the morphology was observed at 25 mol%. Encapsulation of hydrophilic and hydrophobic fluorescent dyes as

model drugs and their photoinduced release was demonstrated with variable azobenzene content. UV radiation shows less penetration into tissues and long exposure may result in damage to surrounding cells that limits their biological applications.<sup>177</sup> NIR radiation (750-1000 nm) is attractive due to its higher tissue penetration and causes less harm to the tissue. Fréchet and coworkers developed photodegradable LDBC by introducing hydrophobic 2-diazo-1,2-naphthoquinone (DNQ) at the periphery of the dendron (Figure 1.22).<sup>178</sup> The DNQ moiety undergoes light induced Wolff rearrangement to 3-indenecarboxylate accompanied with polarity change. This rearrangement can be achieved either by one photon absorption or two photon NIR (750 nm) light. These polymers self-assembled into micelles in water and showed NIR triggered Nile red release.

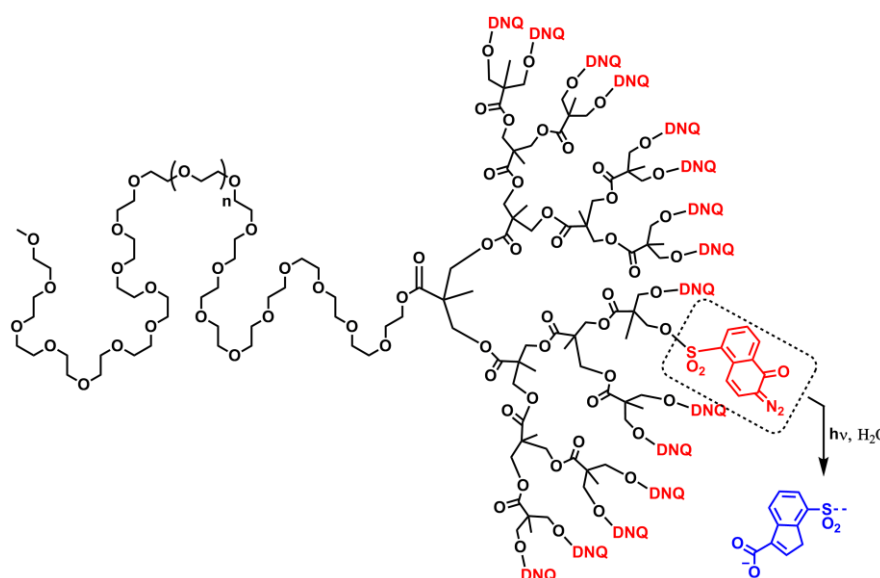


**Figure 1.22** Chemical structure of NIR-degradable linear-dendritic copolymer.

Recently, a similar design was reported by Dong and coworkers who synthesized third-generation PAMAM dendron decorated with DNQ moieties coupled to the hydrophilic linear polymer PEG.<sup>179</sup> Release of DOX encapsulated in the micelles upon irradiation at 808 nm NIR light was demonstrated.

#### **d) Enzyme-responsive linear-dendritic block copolymers**

Enzyme-responsive micellar carriers are potential candidates for drug delivery due to their high selectivity. Amir group reported<sup>180</sup> a series of LDBC composed of PEG of different



molecular weights and enzyme-responsive hydrophobic dendron with phenyl acetamide groups on periphery, which can be hydrolyzed by an enzyme *viz.* penicillin G amidase.

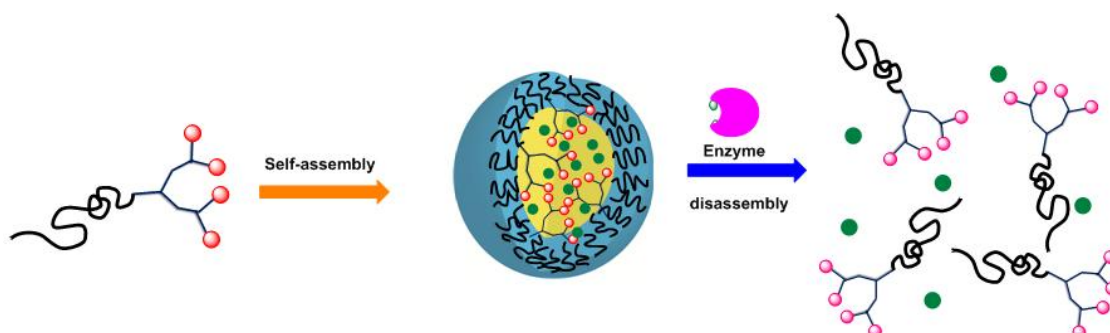


**Figure 1.23** Schematic representation of enzyme-responsive micellar disassembly of LDBC.

These amphiphilic polymers self-assembled into micelles with diameter less than 20 nm and the release rates could be tuned by PEG chain length. The enzymatic disassembly of micellar aggregates was demonstrated by release of Nile red (Figure 1.23). In a subsequent report by the same group the enzyme-responsive encapsulation and release of the drugs by two different pathways was investigated.<sup>181</sup>

### 1.8 Scope and objectives of the present work

The extensive literature survey presented above shows that block copolymers self-assemble into various morphologies, either in bulk or solution and the self-assembly can be exploited for many promising applications. Moreover, through the many examples discussed here, it is clear that research on fundamental as well as applied aspects of stimuli-responsive LDBC has been carried out by researchers in this field over the last two decades. Various types of stimuli-responsive groups such as photoresponsive, pH-responsive, temperature-responsive and enzyme-responsive have been incorporated into LDBC. Although the important feature of dendritic architecture that is, multiple functionalities in a compact perfectly branched molecule has been exploited, detailed structure-property relationship study is lacking in many examples. There is wide scope for installing stimuli-responsive groups in various locations along the linear-dendritic architecture - examples in literature only rely on functionalities on the periphery of dendron. Further, to achieve multi-functional and tunable assemblies it is necessary to incorporate multiple types of stimuli-responsive groups in the same LDBC. This is

particularly important towards realizing the true potential of this class of copolymers mainly in the area of drug delivery and also in designing nanomaterials for other applications. Installing more than one type of stimuli-responsive groups in a LDBC will also help establish the corresponding structure-property relationships.

In view of the above observations, in the present work I have focused on the synthesis of amphiphilic stimuli-responsive linear-dendritic block copolymers and studies of their self-assembly behaviour with the following objectives.

- 1) To synthesize LDBCs containing dendrons of different generations displaying stimuli-responsive moieties at various positions along the dendritic backbone that is on dendron periphery as well as in the dendron interior.
- 2) To install stimuli-responsive groups at the junction of linear and dendritic blocks by synthesizing dendron with desired group at the focal point or by preparing the linear polymer with the stimuli-responsive group at one end. To synthesize a stimuli-responsive hydrophilic linear polymer.
- 3) To incorporate stimuli-responsive groups such pH-, temperature- and light-responsive groups of both cleavable and non-cleavable nature.
- 4) To synthesize the copolymers using a high-yield coupling reaction such as CuAAC to connect the dendron to the pre-formed linear polymer. To synthesize dendrons and telechelic linear polymers or modify commercially available polymers with appropriate functionalities, such as azide and alkyne for the coupling.
- 5) To characterize the self-assembly of the LDBCs in aqueous solution using light scattering, electron microscopy, UV and fluorescence spectroscopy techniques.
- 6) To investigate the effect of dendron generation, linear block length and location of stimuli-responsive groups on the self-assembly using external stimuli such as light, pH and temperature towards a systematic structure-property relationship study.

## 1.9 References

- 1) Mai, Y.; Eisenberg, A. *Chem. Soc. Rev.* **2012**, *41*, 5969.

- 2) Bates, F. S. *Science* **1991**, *251*, 898.
- 3) Schacher, F. H.; Rugar, P. A.; Manners, I. *Angew. Chem. Int. Ed.* **2012**, *51*, 7898.
- 4) Gheybi, H.; Adeli, M. *Polym. Chem.* **2015**, *6*, 2580.
- 5) Fox, M. E.; Szoka, F. C.; Frechet, J. M. J. *Acc. Chem. Res.* **2009**, *42*, 1141.
- 6) Yuan, F.; Dellian, M.; Fukumura, D.; Leunig, M.; Berk, D. A.; Torchilin, V. P.; Jain, R. K. *Cancer Res.* **1999**, *55*, 3752.
- 7) Geng, Y.; Dalhaimer, P.; Cai, S.; Tsai, R.; Tewari, M.; Minko, T.; Discher, D. E. *Nat. Nanotechnol.* **2007**, *2*, 249.
- 8) Hamley, I. W. *Nanotechnology.* **2003**, *14*, R39.
- 9) Hu, H.; Gopinadhan, M.; Osuji, C. O. *Soft matter* **2014**, *10*, 3861.
- 10) Parka, C.; Yoonb, J.; Thomas, E. L. *Polymer* **2003**, *44*, 6725.
- 11) Kim, S. O.; Solak, H. K.; Stoykovich, M. P.; Ferrier, N. J.; de Pablo, J. J.; Nealey, P. F. *Nature* **2003**, *424*, 411.
- 12) Cheng, J. Y.; Ross, C. A.; Smith, H. I.; Thomas, E. L. *Adv. Mater.* **2006**, *18*, 2505.
- 13) Crossland, E. J. W.; Ludwigs, S.; Hillmyer, M. A.; Steiner, U. *Soft Matter* **2007**, *3*, 94.
- 14) Ge, Z.; Liu, S. *Macromol. Rapid Commun.* **2009**, *30*, 1523-1532.
- 15) Kujawa, P.; Winnik, F. M. *Langmuir* **2013**, *29*, 7354-7361.
- 16) Hadjichristidis, N.; Pispas, S.; Pitsikalis, M.; Hermis, L.; Costas, V. *Adv. Polym. Sci.* **1999**, *142*, 71.
- 17) Khanna, K.; Varshney, S.; Kakkar, A. *Polym. Chem.* **2010**, *1*, 1171.
- 18) Groschel, A. H.; Schacher, F. H.; Schmalz, H.; Borisov, O. V.; Zhulina, E. B.; Walther, A.; Muller, A. H. E. *Nat Commun.* **2012**, *3*, 710.
- 19) Li, Z.; Kesselman, E.; Talmon, Y.; Hillmyer, M. A.; Lodge, T. P. *Science* **2004**, *306*, 98.
- 20) Moughton, A. O.; Hillmyer, M. A.; Lodge, T. P. *Macromolecules* **2012**, *45*, 2-19.
- 21) Ostmark, E.; Harrison, S.; Wooley, K. L.; Malmstrom, E. E. *Biomacromolecules* **2007**, *8*, 1138.
- 22) Feng, C.; Li, Y.; Yang, D.; Hu, J.; Zhang, X.; Huang, X. *Chem. Soc. Rev.* **2011**, *40*, 1282.
- 23) Granville, A. M.; Brittain, W. J. In *Polymer Brushes*; Wiley-VCH Verlag GmbH & Co. KGaA: **2005**, p 33.

- 24) Husseman, M.; Malmstrom, E. E.; McNamara, M.; Mate, M.; Mecerreyes, D.; Benoit, D. G.; Hedrick, J. L.; Mansky, P.; Huang, E.; Russell, T. P.; Hawker, C. J. *Macromolecules* **1999**, *32*, 1424.
- 25) Qiao, Y.; Islam, M. S.; Yin, X.; Han, K.; Yan, Y.; Zhang, J.; Wang, Q.; Ploehn, H. J.; Tang, C. *Polymer* **2015**, *72*, 428.
- 26) Dalsin, S. J.; Rions-Maehren, T. G.; Beam, M. D.; Bates, F. S.; Hillmyer, M. A.; Matsen, M. W. *ACS Nano* **2015**, *9*, 12233.
- 27) Verduzco, R.; Li, X.; Pesek, S. L.; Stein, G. E. *Chem. Soc. Rev.* **2015**, *44*, 2405.
- 28) Laurent, B. A.; Grayson, S. M. *Chem. Soc. Rev.* **2009**, *38*, 2202.
- 29) Williams, R. J.; Dove, A. P.; O'Reilly, R. K. *Polym. Chem.* **2015**, *6*, 2998-3008.
- 30) Zhu, Y.; Hosmane, N. S. *ChemistryOpen* **2015**, *4*, 408.
- 31) Durmaz, H.; Dag, A.; Hizal, G.; Tunca, U. *J. Polym. Sci., Part A: Polym. Chem.* **2010**, *48*, 5083-5091.
- 32) Eugene, D. M.; Grayson, S. M. *Macromolecules* **2008**, *41*, 5082.
- 33) Jiang, W.; Zhou, Y.; Yan, D. *Chem. Soc. Rev.* **2015**, *44*, 3874.
- 34) Liu, Y.; Yu, C.; Jin, H.; Jiang, B.; Zhu, X.; Zhou, Y.; Lu, Z.; Yan, D. *J. Am. Chem. Soc.* **2013**, *135*, 4765.
- 35) Schlüter, A. D.; Rabe, J. P. *Angew. Chem. Int. Ed.* **2000**, *39*, 864.
- 36) Tonga, M.; Yesilbag Tonga, G.; Seber, G.; Gok, O.; Sanyal, A. *J. Polym. Sci., Part A: Polym. Chem.* **2013**, *51*, 5029.
- 37) Zhou, Y.; Yan, D. *Angew. Chem. Int. Ed.* **2004**, *43*, 4896.
- 38) Astruc, D.; Chardac, F. *Chem. Rev.* **2001**, *101*, 2991.
- 39) Park, C.; Lee, J.; Kim, C. *Chem. Commun.* **2011**, *47*, 12042.
- 40) Bosman, A. W.; Janssen, H. M.; Meijer, E. W. *Chem. Rev.* **1999**, *99*, 1665.
- 41) Fischer, M.; Vögtle, F. *Angew. Chem. Int. Ed.* **1999**, *38*, 884.
- 42) Tomalia, D. A.; Fréchet, J. M. J. *J. Polym. Sci., Part A: Polym. Chem.* **2002**, *40*, 2719.
- 43) Zeng, F.; Zimmerman, S. C. *Chem. Rev.* **1997**, *97*, 1681.
- 44) Buhleier, E. W.; Wehner, W.; Voigt, F. *Synthesis* **1978**, 155.
- 45) Lee, C. C.; MacKay, J. A.; Frechet, J. M. J.; Szoka, F. C. *Nat. Biotechnol.* **2005**, *23*, 1517.
- 46) Tekade, R. K.; Kumar, P. V.; Jain, N. K. *Chem. Rev.* **2009**, *109*, 49.

- 47) Wu, L.-p.; Ficker, M.; Christensen, J. r. B.; Trohopoulos, P. N.; Moghimi, S. M. *Bioconjugate Chem.* **2015**, *26*, 1198.
- 48) Percec, V.; Glodde, M.; Bera, T. K.; Miura, Y.; Shiyanovskaya, I.; Singer, K. D.; Balagurusamy, V. S. K.; Heiney, P. A.; Schnell, I.; Rapp, A.; Spiess, H. W.; Hudson, S. D.; Duan, H. *Nature* **2002**, *417*, 384.
- 49) Tomalia, D. A.; Baker, H.; Dewald, J.; Hall, M.; Kallos, G.; Martin, S.; Roeck, J.; Ryder, J.; Smith, P. *Polym. J.* **1985**, *17*, 117.
- 50) Newkome, G. R.; Yao, Z.; Baker, G. R.; Gupta, V. K. *J. Org. Chem.* **1985**, *50*, 2003.
- 51) Tomalia, D. A.; Baker, H.; Dewald, J.; Hall, M.; Kallos, G.; Martin, S.; Roeck, J.; Ryder, J.; Smith, P. *Macromolecules* **1986**, *19*, 2466.
- 52) de Brabander-van den Berg, E. M. M.; Meijer, E. W. *Angew. Chem. Int. Ed.* **1993**, *32*, 1308
- 53) Ihre, H.; Hult, A.; Soderlind, E. *J. Am. Chem. Soc.* **1996**, *118*, 6388.
- 54) Gitsov, I.; Wooley, K. L.; Fréchet, J. M. J. *Angew. Chem. Int. Ed.* **1992**, *31*, 1200.
- 55) Hawker, C. J.; Frechet, J. M. J. *J. Am. Chem. Soc.* **1990**, *112*, 7638.
- 56) Gitsov, I. *J. Polym. Sci., Part A: Polym. Chem.* **2008**, *46*, 5295.
- 57) Chang, Y.; Kim, C. *J. Polym. Sci., Part A: Polym. Chem.* **2001**, *39*, 918.
- 58) Chang, Y.; Kwon, Y. C.; Lee, S. C.; Kim, C. *Macromolecules* **2000**, *33*, 4496.
- 59) Chapman, T. M.; Hillyer, G. L.; Mahan, E. J.; Shaffer, K. A. *J. Am. Chem. Soc.* **1994**, *116*, 11195.
- 60) Iyer, J.; Fleming, K.; Hammond, P. T. *Macromolecules* **1998**, *31*, 8757.
- 61) Lambrych, K. R.; Gitsov, I. *Macromolecules* **2003**, *36*, 1068.
- 62) van Hest, J. C. M.; Delnoye, D. A. P.; Baars, M. W. P. L.; Elissen-Román, C.; van Genderen, M. H. P.; Meijer, E. W. *Chem. Eur. J.* **1996**, *2*, 1616.
- 63) Fréchet J. M. J; Tomalia, D. *Dendrimers and other dendritic polymers.*; New York: John Wiley & Sons;, 2005.
- 64) Matyjaszewski, K.; Shigemoto, T.; Frechet, J. M. J.; Leduc, M. *Macromolecules* **1996**, *29*, 4167.
- 65) Ge, Z.; Luo, S.; Liu, S. *J. Polym. Sci., Part A: Polym. Chem.* **2006**, *44*, 1357.
- 66) Pyun, J.; Tang, C.; Kowalewski, T.; Frechet, J. M. J.; Hawker, C. J. *Macromolecules* **2005**, *38*, 2674.

- 67) Sill, K.; Emrick, T. *J. Polym. Sci., Part A: Polym. Chem.* **2005**, *43*, 5429.
- 68) Zhu, L.; Tong, X.; Li, M.; Wang, E. *J. Polym. Sci., Part A: Polym. Chem.* **2000**, *38*, 4282.
- 69) Zhu, L.; Zhu, G.; Li, M.; Wang, E.; Zhu, R.; Qi, X. *Eur. Polym. J.* **2002**, *38*, 2503.
- 70) Emrick, T.; Hayes, W.; Fréchet, J. M. J. *J. Polym. Sci., Part A: Polym. Chem.* **1999**, *37*, 3748.
- 71) Leduc, M. R.; Hayes, W.; Fréchet, J. M. J. *J. Polym. Sci., Part A: Polym. Chem.* **1998**, *36*, 1.
- 72) Mecerreyes, D.; Dubois, P.; Jérôme, R.; Hedrick, J. L.; Hawker, C. J. *J. Polym. Sci., Part A: Polym. Chem.* **1999**, *37*, 1923.
- 73) Gitsov, I.; Simonyan, A.; Vladimirov, N. G. *J. Polym. Sci., Part A: Polym. Chem.* **2007**, *45*, 5136.
- 74) Gitsov, I.; Frechet, J. M. J. *Macromolecules* **1994**, *27*, 7309.
- 75) Malenfant, P. R. L.; Groenendaal, L.; Frechet, J. M. J. *J. Am. Chem. Soc.* **1998**, *120*, 10990.
- 76) Hua, C.; Peng, S.-M.; Dong, C.-M. *Macromolecules* **2008**, *41*, 6686.
- 77) Peng, S.-M.; Chen, Y.; Hua, C.; Dong, C.-M. *Macromolecules* **2009**, *42*, 104.
- 78) Yang, Y.; Hua, C.; Dong, C.-M. *Biomacromolecules* **2009**, *10*, 2310.
- 79) Chen, L.; Chen, T.; Fang, W.; Wen, Y.; Lin, S.; Lin, J.; Cai, C. *Biomacromolecules* **2013**, *14*, 4320.
- 80) Chen, Y.; Dong, C.-M. *J. Phys. Chem. B.* **2010**, *114*, 7461.
- 81) Xu, Y.-C.; Dong, C.-M. *J Polym Sci Part A: Polym. Chem.* **2012**, *50*, 1216.
- 82) You, Y.; Chen, Y.; Hua, C.; Dong, C.-M. *J. Polym. Sci., Part A: Polym. Chem.*, *48*, 709.
- 83) Demko, Z. P.; Sharpless, K. B. *Angew. Chem. Int. Ed.* **2002**, *41*, 2113.
- 84) Kolb, H. C.; Finn, M. G.; Sharpless, K. B. *Angew. Chem. Int. Ed.* **2001**, *40*, 2004.
- 85) Iha, R. K.; Wooley, K. L.; Nystrom, A. M.; Burke, D. J.; Kade, M. J.; Hawker, C. J. *Chem. Rev.* **2009**, *109*, 5620.
- 86) Huisgen, R. *Proc. Chem. Soc.* **1961**, 357.
- 87) Huisgen, R.; Szeimies, G.; Möbius, L. *Chem. Ber.* **1967**, *100*, 2494.
- 88) Tornadoe, C. W.; Christensen, C.; Meldal, M. *J. Org. Chem.* **2002**, *67*, 3057.

- 89) Rodionov, V. O.; Presolski, S. I.; Diaz Diaz, D.; Fokin, V. V.; Finn, M. G. *J. Am. Chem. Soc.* **2007**, *129*, 12705.
- 90) Hein, J. E.; Fokin, V. V. *Chem. Soc. Rev.* **2010**, *39*, 1302.
- 91) Binder, W. H.; Sachsenhofer, R. *Macromol. Rapid. Commun.* **2008**, *29*, 952.
- 92) del Barrio, J.; Oriol, L.; Sanchez, C.; Serrano, J. L.; Di Cicco, A.; Keller, P.; Li, M.-H. *J. Am. Chem. Soc.* **2010**, *132*, 3762.
- 93) Blasco, E.; del Barrio, J.; Sánchez-Somolinos, S.; Piñola, M.; Oriol, L. *Polym. Chem.* **2013**, *4*, 2246.
- 94) Nantalaksakul, A.; Mueller, A.; Klaikherd, A.; Bardeen, C. J.; Thayumanavan, S. *J. Am. Chem. Soc.* **2009**, *131*, 2727-2738.
- 95) Diels, O.; Alder, K. *Ber.* **1929**, *62*, 2087.
- 96) Kwart, H.; King, K. *Chem. Rev.* **1968**, *68*, 415.
- 97) Vieyres, A.; Lam, T.; Gillet, R.; Franc, G.; Castonguay, A.; Kakkar, A. *Chem. Commun.*, *46*, 1875.
- 98) Durmaz, H.; Dag, A.; Altintas, O.; Erdogan, T.; Hizal, G.; Tunca, U. *Macromolecules* **2007**, *40*, 191.
- 99) Durmaz, H.; Dag, A.; Hizal, A.; Hizal, G.; Tunca, U. *J. Polym. Sci., Part A: Polym. Chem.* **2008**, *46*, 7091.
- 100) Harada, A.; Kataoka, K. *Prog. Polym. Sci.* **2006**, *31*, 949.
- 101) Zhang, L.; Eisenberg, A. *Macromolecules* **1996**, *29*, 8805.
- 102) Zhong, S.; Cui, H.; Chen, Z.; Wooley, K. L.; Pochan, D. J. *Soft Matter* **2008**, *4*, 90.
- 103) Desbaumes, L.; Eisenberg, A. *Langmuir* **1999**, *15*, 36.
- 104) Gao, Z.; Eisenberg, A. *Macromolecules* **1993**, *26*, 7353.
- 105) Mai, Y.; Eisenberg, A. *Macromolecules* **2011**, *44*, 3179.
- 106) Yu, K.; Eisenberg, A. *Macromolecules* **1996**, *29*, 6359.
- 107) Yu, K.; Eisenberg, A. *Macromolecules* **1998**, *31*, 3509.
- 108) Cameron, N. S.; Corbierre, M. K.; Eisenberg, A. *Can. J. Chem.* **1999**, *77*, 1311.
- 109) Israelachvili, J. N. In *Intermolecular and Surface Forces (Third Edition)*; Academic Press: Boston, 2008.
- 110) Discher, D. E.; Eisenberg, A. *Science* **2002**, *297*, 967.

- 111) Discher, D. E.; Ortiz, V.; Srinivas, G.; Klein, M. L.; Kim, Y.; Christian, D.; Cai, S.; Photos, P.; Ahmed, F. *Prog. Polym. Sci.* **2007**, *32*, 838.
- 112) Hayward, R. C.; Pochan, D. J. *Macromolecules* **2010**, *43*, 3577.
- 113) Zhu, J.; Hayward, R. C. *Macromolecules* **2008**, *41*, 7794.
- 114) Cui, H.; Chen, Z.; Zhong, S.; Wooley, K. L.; Pochan, D. J. *Science* **2007**, *317*, 647.
- 115) Mura, S.; Nicolas, J.; Couvreur, P. *Nat. Mater.* **2013**, *12*, 991.
- (116) Binauld, S.; Stenzel, M. H. *Chem. Soc. Rev.* **2013**, *49*, 2082.
- 117) Cheng, R.; Meng, F.; Deng, C.; Klok, H.-A.; Zhong, Z. *Biomaterials* **2013**, *34*, 3647.
- 118) Ge, Z.; Liu, S. *Chem. Soc. Rev.* **2013**, *42*, 7289.
- 119) Wei, H.; Zhuo, R.-X.; Zhang, X.-Z. *Prog. Polym. Sci.* **2013**, *38*, 503.
- 120) Stuart, M. A. C.; Huck, W. T. S.; Genzer, J.; Muller, M.; Ober, C.; Stamm, M.; Sukhorukov, G. B.; Szleifer, I.; Tsukruk, V. V.; Urban, M.; Winnik, F.; Zauscher, S.; Luzinov, I.; Minko, S. *Nat. Mater.* **2010**, *9*, 101.
- 121) Lee, S.-M.; Nguyen, S. T. *Macromolecules* **2013**, *46*, 9169.
- 122) Mendes, P. M. *Chem. Soc. Rev.* **2008**, *37*, 2512.
- 123) Park, C.; Yoon, J.; Thomas, E. L. *Polymer* **2003**, *44*, 6725.
- 124) Luo, F.; Xie, R.; Liu, Z.; Ju, X.-J.; Wang, W.; Lin, S.; Chu, L.-Y. *Nature* **2015**, *5*, 14708.
- 125) Gohy, J.-F.; Zhao, Y. *Chem. Soc. Rev.* **2013**, *42*, 7117.
- 126) Bai, S.; Zhao, Y. *Macromolecules* **2001**, *34*, 9032.
- 127) Schattling, P.; Jochum, F. D.; Theato, P. *Polym. Chem.* **2014**, *5*, 25.
- 128) Cao, Z.; Wang, G.; Chen, Y.; Liang, F.; Yang, Z. *Macromolecules* **2015**, *48*, 7256.
- 129) Dai, S.; Ravi, P.; Tam, K. C. *Soft Matter* **2009**, *5*, 2513.
- 130) Ganta, S.; Devalapally, H.; Shahiwala, A.; Amiji, M. *J. Controlled Release.* **2008**, *126*, 187.
- 131) Huang, Y.; Dong, R.; Zhu, X.; Yan, D. *Soft Matter* **2014**, *10*, 6121.
- 132) Sévigny, S.; Bouchard, L.; Motallebi, S.; Zhao, Y. *Macromolecules* **2003**, *36*, 9033.
- 133) Zhao, Y.; Tong, X. *Adv. Mater.* **2003**, *15*, 1431.
- 134) Jiang, J.; Tong, X.; Morris, D.; Zhao, Y. *Macromolecules* **2006**, *39*, 4633.
- 135) Zhao, H.; Gu, W.; Sterner, E.; Russell, T. P.; Coughlin, E. B.; Theato, P. *Macromolecules* **2011**, *44*, 6433.



- 136) Dai, S.; Ravi, P.; Tam, K. C. *Soft Matter* **2008**, *4*, 435.
- 137) Liu, Y.; Wang, W.; Yang, J.; Zhou, C.; Sun, J. *Asian J. Pharm. Sci.* **2013**, *8*, 159.
- 138) Hu, J.; He, J.; Zhang, M.; Ni, P. *Polym. Chem.* **2015**, *6*, 1553.
- 139) Satoh, K.; Poelma, J. E.; Campos, L. M.; Stahl, B.; Hawker, C. J. *Polym. Chem.* **2012**, *3*, 1890.
- 140) Bates, F. S.; Fredrickson, G. H. *Phys. Today.* **1999**, *52*, 32.
- 141) Cho, B. K.; Jain, A.; Gruner, S. M.; Wiesner, U. *Science* **2004**, *305*, 1598.
- 142) Cho, B.-K.; Jain, A.; Gruner, S. M.; Wiesner, U. *Chem. Commun.* **2005**, 2143.
- 143) Lee, E.; Lee, B.-I.; Kim, S.-H.; Lee, J.-K.; Zin, W.-C.; Cho, B.-K. *Macromolecules* **2009**, *42*, 4134.
- 144) del Barrio, J.; Oriol, L.; Alcalá, R.; Sanchez, C. *Macromolecules* **2009**, *42*, 5752.
- 145) del Barrio, J.; Oriol, L.; Alcalá, R.; Sanchez, C. *J. Polym. Sci., Part A: Polym. Chem.* **2010**, *48*, 1538.
- 146) Blasco, E.; Barrio, J. d.; Pinol, M.; Oriol, L.; Berges, C.; Sanchez, C.; Alcalá, R. *Polymer* **2012**, *53*, 4604.
- 147) Walter, M. V.; Lundberg, P.; Hult, D.; Hult, A.; Malkoch, M. *Polym. Chem.* **2013**, *4*, 2680.
- 148) Shi, Z.; Chen, D.; Lu, H.; Wu, B.; Ma, J.; Cheng, R.; Fang, J.; Chen, X. *Soft Matter* **2012**, *8*, 6174.
- 149) Wu, Y.; Kanazawa, A.; Shiono, T.; Ikeda, T.; Zhang, Q. *Polymer* **1999**, *40*, 4787.
- 150) Breiner, T.; Kreger, K.; Hagen, R.; Hackel, M.; Kador, L.; Muller, A. H. E.; Kramer, E. J.; Schmidt, H.-W. *Macromolecules* **2007**, *40*, 2100.
- 151) Gitsov, I.; Frechet, J. M. J. *Macromolecules* **1993**, *26*, 6536.
- 152) Gitsov, I.; Lambrych, K. R.; Remnant, V. A.; Pracitto, R. *J. Polym. Sci., Part A: Polym. Chem.* **2000**, *38*, 2711.
- 153) Jiang, G.; Wang, L.; Chen, T.; Yu, H. *Polymer* **2005**, *46*, 81.
- 154) Iyer, J.; Fleming, K.; Hammond, P. T. *Macromolecules* **1998**, *31*, 8757.-8765.
- 155) Gitsov, I.; Hamzik, J.; Ryan, J.; Simonyan, A.; Nakas, J. P.; Omori, S.; Krastanov, A.; Cohen, T.; Tanenbaum, S. W. *Biomacromolecules* **2008**, *9*, 804.
- 156) Simonyan, A.; Gitsov, I. *Langmuir* **2008**, *24*, 11431.

- 157) La, Y.; Park, C.; Shin, T. J.; Joo, S. H.; Kang, S.; Kim, K. T. *Nat. Chem.* **2013**, *6*, 534.
- 158) Park, C.; La, Y.; An, T. H.; Jeong, H. Y.; Kang, S.; Joo, S. H.; Ahn, H.; Shin, T. J.; Kim, K. T. *Nat Commun.* **2014**, *6*, 6392.
- 159) Jeong, M. G.; van Hest, J. C. M.; Kim, K. T. *Chem. Commun.* **2012**, *48*, 3590.
- 160) Cai, H.; Jiang, G.; Chen, C.; Li, Z.; Shen, Z.; Fan, X. *Macromolecules* **2014**, *47*, 146.
- 161) Pathak, R. K.; Dhar, S. *J. Am. Chem. Soc.* **2015**, *137*, 8324.
- 162) van Hest, J. C. M.; Baars, M. W. P. L.; Elissen-Roman, C.; van Genderen, M. H. P.; Meijer, E. W. *Macromolecules* **1995**, *28*, 6689.
- 163) Gillies, E. R.; Jonsson, T. B.; Frechet, J. M. J. *J. Am. Chem. Soc.* **2004**, *126*, 11936.
- 164) Gillies, E. R.; Frechet, J. M. J. *Bioconjugate Chem.* **2005**, *16*, 361.
- 165) Nguyen, P. M.; Hammond, P. T. *Langmuir* **2006**, *22*, 7825.
- 166) Tian, L.; Hammond, P. T. *Chem. Mater.* **2006**, *18*, 3976.
- 167) Zhang, Y.; Xiao, C.; Li, M.; Chen, J.; Ding, J.; He, C.; Zhuang, X.; Chen, X. *Macromol. Biosci.* **2013**, *13*, 584.
- 168) Zhang, Y.; Xiao, C.; Li, M.; Ding, J.; He, C.; Zhuang, X.; Chen, X. *Polym. Chem.* **2014**, *5*, 2801.
- 169) Bi, Y.; Yan, C.; Shao, L.; Wang, Y.; Ma, Y.; Tang, G. *J. Polym. Sci., Part A: Polym. Chem.* **2013**, *51*, 3240.
- 170) Lee, H.-i.; Ah Lee, J.; Poon, Z.; Hammond, P. T. *Chem. Commun.* **2008**, 3726.
- 171) Kim, Y. S.; Gil, E. S.; Lowe, T. L. *Macromolecules* **2006**, *39*, 7805.
- 172) Zou, J.; Guan, B.; Liao, X.; Jiang, M.; Tao, F. *Macromolecules* **2009**, *42*, 7465.
- 173) Kim, J.-H.; Lee, E.; Park, J.-S.; Kataoka, K.; Jang, W.-D. *Chem. Commun.* **2012**, *48*, 3662.
- 174) Kempe, K.; Onbulak, S.; Schubert, U. S.; Sanyal, A.; Hoogenboom, R. *Polym. Chem.* **2013**, *4*, 3236.
- 175) Lin, Y.-L.; Chang, H.-Y.; Sheng, Y.-J.; Tsao, H.-K. *Macromolecules* **2012**, *45*, 7143.
- 176) Blasco, E.; Serrano, J. L.; Pinol, M.; Oriol, L. *Macromolecules* **2013**, *46*, 5951.
- 177) Young, A. R. *J. Photochem. Photobiol., B.* **1990**, *6*, 237.
- 178) Mynar, J. L.; Goodwin, A. P.; Cohen, J. A.; Ma, Y.; Fleming, G. R.; Frechet, J. M. J. *Chem. Commun.* **2007**, 2081.

179) Sun, L.; Zhu, B.; Su, Y.; Dong, C.-M. *Polym. Chem.* **2014**, *5*, 1605.

180) Harnoy, A. J.; Rosenbaum, I.; Tirosh, E.; Ebenstein, Y.; Shaharabani, R.; Beck, R.; Amir, R. J. *J. Am. Chem. Soc.* **2014**, *136*, 7531.

181) Rosenbaum, I.; Harnoy, A. J.; Tirosh, E.; Buzhor, M.; Segal, M.; Frid, L.; Shaharabani, R.; Avinery, R.; Beck, R.; Amir, R. J. *J. Am. Chem. Soc.* **2015**, *137*, 2276.

## Chapter 2

### **Effect of Branching Pattern of Hydrophobic Dendrons on the Linear-Dendritic Block Copolymer Micelle Structure**

This chapter is adapted from “Kalva, N.; Aswal, V. K.; Ambade, A. V. *Macromol. Chem. Phys.* **2014**, *215*, 1456-1465. DOI: 10.1002/macp.201400150”.

## 2.1 Introduction

Tuning the macromolecular architecture to study its effect on the morphology and aggregation behavior is an important theme in study of self-assembly of amphiphilic polymers in solution<sup>1</sup> because architecture is one of the factors that govern self-assembly. Amphiphilic copolymers of various architectures have attracted great interest recently due to their potential of generating novel morphologies in solution, the size and stability of which can be tuned in response to various stimuli. Dendritic polymers, in particular, have been explored in this direction due to their unusual architecture.<sup>2</sup> Linear-dendritic block copolymers (LDBC), a class of dendritic macromolecules have emerged as promising candidates for controlled generation of supramolecular aggregates in solution with potential for various applications including drug delivery.<sup>3-8</sup> LDBCs have been studied towards realization of functional assemblies in solution, either by connecting hydrophobic dendron with hydrophilic linear chain<sup>9-11</sup> or by joining hydrophilic dendron to hydrophobic linear chain.<sup>12-14</sup> Typically, micellar behavior and morphology of these LDBCs has been studied with reference to dendron generation.<sup>15-18</sup> For example, it has been shown that cmc of PAMAM-PEG LDBCs decreased with increasing generation in keeping with increasing hydrophobicity of the dendrons.<sup>19,20</sup> Morphology of an azobenzene-dendron-PEG copolymer changed with increasing dendron generation from nanofibers to micelles and then to vesicles.<sup>21</sup> However, hydrophobic fraction in these polymers increases rapidly with dendron generation because of exponential increase in the number of terminal groups accompanied by large increase in dendron size. On this background, it is a worthy goal to investigate the solution behavior of LDBCs where the hydrophobicity of dendrons increases in small steps within a group of closely related structures. Such an investigation would afford an insight into the structural parameters that influence the self-assembly in solution of these polymers.

LDBCs are excellent candidates for carrying out systematic variation in molecular structure of amphiphilic polymers. Because of the stepwise synthesis it is possible to precisely control the number and functionality of peripheral groups in a dendron while keeping the same backbone structure<sup>22</sup> so that their size and polarity can be manipulated. Here the hypothesis is that dendrons with slight structural variation attached to a hydrophilic chain of fixed length would afford a set of amphiphilic copolymers suitable for the study to provide an insight into the influence of molecular mass and shape of

hydrophobic dendron on micellar behavior of amphiphilic LDBC. The design relies on dendrons synthesized from similar building blocks with different number of substituents *viz.* 3,5-dialkoxy benzyl ether and 3,4,5-trialkoxy benzyl ether. The series of dendrons obtained from both the units will possess the same backbone but display different branching patterns. This will impart the polymers with useful molecular features such as, the number of alkyl chains on dendron periphery will increase linearly and the hydrophobic fraction across the series will change gradually in contrast to dendrons from a single building block. Moreover, one subset of polymers from each building block will be obtained that would possess differential density of hydrophobic groups within same generation when the complete set is considered. At higher generations, this difference would be significant due to difference in shape of dendrons from the two building blocks. This variation in molecular parameters of the hydrophobic dendrons is likely to affect their interaction with the polar solvent during micellization, which in turn may affect the aggregation number and encapsulation ability of the micellar assemblies. Thus, it would provide a handle to tune the properties of micellar core of the designed LDBC. Moreover, PEG is selected as the hydrophilic block in order to take advantage of its temperature-responsive behaviour and study the effect of temperature on micellar behaviour of the LDBC.

## 2.2 Experimental Section

### 2.2.1 Materials

3,5-dihydroxy benzoic acid, gallic acid, potassium carbonate, potassium iodide, thionyl chloride, sodium hydride, triphenyl phosphine, carbon tetrabromide, copper sulphate monohydrate, sodium ascorbate, 18-crown-6, methanesulfonyl chloride, sodium azide were obtained from Avra Chemicals, India and Loba Chemicals, India. Methoxy-PEG ( $M_n = 2000$  g/mol, PDI = 1.1), dodecyl bromide, propargyl bromide, lithium aluminum hydride, Nile red and pyrene, anhydrous N,N-dimethylformamide were purchased from Aldrich Chemicals Co. Tetrahydrofuran was passed through alumina and distilled over Na/benzophenone ketyl immediately before use. DCM was distilled over  $CaH_2$ ; acetone was stirred over  $K_2CO_3$  and distilled. All solvents were stored in Schlenk flasks. All compounds were purified using column chromatography on silica gel (mesh size 60-120).

### 2.2.2 Instrumentation

GPC analysis was performed on Viscotek PL-GPC-220 with  $\text{CHCl}_3$  as eluent. DLS experiments were performed on 90 Plus particle size analyser by Brookhaven Instruments Corporation at an angle of  $90^\circ$  equipped with laser beam of 633 nm wavelength. Fluorescence emission spectra were recorded on CARY Eclipse spectrometer. Neutron-scattering experiments were performed using a SANS diffractometer at the Dhruva reactor, Bhabha Atomic Research Centre (BARC), Mumbai.

### 2.2.3 Synthetic procedures and characterization data

- a) Synthesis of the 3,4,5-trialkoxy benzyl ether based dendrons with alkyne functionality was carried out as reported previously.<sup>23,30</sup>
- b) Synthesis of the 3,5-dialkoxy benzyl ether based dendrons with alkyne functionality at the focal point was carried out by following similar procedure to that for 3,4,5-trialkoxy benzyl ether based dendrons.

**3,5G1:**  $^1\text{H}$  NMR (200.13MHz,  $\text{CDCl}_3$   $\delta$ ): 0.88(t, 6H,  $J=6\text{Hz}$ ;  $-\text{CH}_3$ ), 1.26-1.45(overlapped peaks, 36H;  $-\text{CH}_2$ ), 1.70(m, 4H;  $-\text{CH}_2$ ), 2.46(t, 1H; alkyne H), 3.93(t, 4H,  $J=6.2\text{Hz}$ ;  $-\text{OCH}_2$ ), 4.17(d, 2H,  $J=6.4\text{Hz}$ ;  $-\text{OCH}_2$ ), 4.54(s, 2H;  $-\text{OCH}_2$ ), 6.38(t, 1H,  $J=4\text{Hz}$ ; Ar H), 6.48(d, 2H,  $J=2\text{Hz}$ ; Ar H). Yield 85%.

**3,5G2:**  $^1\text{H}$  NMR (200.13MHz,  $\text{CDCl}_3$   $\delta$ ): 0.88(t, 12H,  $J=6\text{Hz}$ ;  $-\text{CH}_3$ ), 1.26-1.45(overlapped peaks, 72H;  $-\text{CH}_2$ ), 1.70(m, 8H,  $\text{CH}_2$ ), 2.46(t, alkyne -H, 1H), 3.93(t, 8H,  $J=6.2\text{Hz}$ ;  $-\text{OCH}_2$ ), 4.17(d, 2H,  $J=6.4$ ;  $-\text{OCH}_2$ ), 4.55(s, 2H;  $-\text{OCH}_2$ ), 4.95(s, 4H;  $-\text{OCH}_2$ ), 6.40(t, 2H,  $J=2\text{Hz}$ ; Ar H), 6.54-6.6(overlapped peaks, 7H,  $J=2\text{Hz}$ ; Ar H). Yield 87%.

**3,5G3:**  $^1\text{H}$  NMR (200.13MHz,  $\text{CDCl}_3$ ,  $\delta$ ): 0.88(t, 24H,  $J=7\text{Hz}$ ;  $-\text{CH}_3$ ), 1.26-1.45(overlapped peaks, 144H;  $-\text{CH}_2$ ), 1.76(m, 16H;  $-\text{CH}_2$ ), 2.46(t, 1H,  $J=4\text{Hz}$ ; alkyne H), 3.93(t, 16H,  $J=6\text{Hz}$ ;  $-\text{OCH}_2$ ), 4.17(d, 2H,  $J=2\text{Hz}$ ;  $-\text{OCH}_2$ ), 4.55(d, 2H,  $J=6\text{Hz}$ ;  $-\text{OCH}_2$ ), 4.94-4.96(overlapped peaks, 12H,  $-\text{OCH}_2$ ), 6.41(t, 4H,  $J=2\text{Hz}$ ; Ar H), 6.55-6.68(overlapped peaks, Ar, 17H). Yield 75%.

**(3,4,5)3,5G2:**  $^1\text{H}$  NMR (200.13MHz,  $\text{CDCl}_3$ ,  $\delta$ ): 0.88(t, 18H, 6Hz;  $-\text{CH}_3$ ), 1.26-1.46(overlapped peaks, 108H;  $-\text{CH}_2$ ) 1.76(m, 12H;  $-\text{CH}_2$ ), 2.46(t, 1H, 4Hz; alkyne H),

3.97(q, 12H, 6Hz; -OCH<sub>2</sub>), 4.16(d, 2H; -OCH<sub>2</sub>), 4.56(s, 2H; -OCH<sub>2</sub>), 4.91(s, , 4H; -OCH<sub>2</sub>) 6.56-6.61(m, 7H; Ar H). Yield 82%

### ***Synthesis of PEG-Azide***

PEG-Azide was synthesized by the modification of the reported procedure.<sup>24</sup> MeO-PEG-OH ( $M_n = 2000$  g/mol) was dried by heating at 80 °C overnight under vacuum. The PEG monomethyl ether was dissolved in anhydrous CH<sub>2</sub>Cl<sub>2</sub> and triethylamine (3eq) was added to it. The mixture was cooled to 0 °C, and methanesulfonyl chloride (2eq) was added dropwise over 15 min with stirring. Upon addition of all the reagent, the mixture was stirred at same temperature for additional 15 min, then at room temperature for 3.5 h. After completion of the reaction, the mixture was filtered through Whatman filter paper and residue was washed with additional CH<sub>2</sub>Cl<sub>2</sub>. Filtrate was concentrated, and the oily residue was precipitated into cold diethyl ether to get the PEG mesylate as white solid. The obtained PEG mesylate was dissolved in dimethylformamide and 10 eq of the sodium azide was added. The reaction mixture was stirred at 70 °C for 24h. The solvent was evaporated under reduced pressure, the residue was washed with water and extracted with CH<sub>2</sub>Cl<sub>2</sub>. The organic layer was dried on anhydrous sodium sulphate and solvent was evaporated on rotary evaporator under reduced pressure and precipitated into cold diethyl ether. The obtained white solid was dried under high vacuum. Yield 75%.

<sup>1</sup>H NMR (200.13 MHz, CDCl<sub>3</sub>)  $\delta$  ppm 3.32 (m, 5H, -OCH<sub>3</sub>, -CH<sub>2</sub>N<sub>3</sub>), 3.58 (m, 174H, -OCH<sub>2</sub>). FT-IR (KBr, cm<sup>-1</sup>): 2908, 2762, 2679, 2118, 2068, 1471, 1354, 1293, 1284, 1150, 1085, 960, 847.

### ***General procedure for CuAAC reaction between alkyne-functionalized dendrons and azide-functionalized PEG.***

To a solution of alkyne-functionalized dendron (1.2 eq) in THF/methanol/water (2:1:0.2) azide-functionalized PEG (1 eq) was added and the resultant mixture was degassed for half an hour. CuSO<sub>4</sub> (0.2 eq), and sodium ascorbate (0.4 eq) were then added and allowed to stir for 24 h under argon atmosphere. The progress of the reaction was monitored by the disappearance of the azide stretching frequency at 2115 cm<sup>-1</sup>. After completion of the reaction, the reaction mixture was extracted with dichloromethane and washed with water. Organic layer was concentrated under reduced pressure. Crude product was purified by



eluting through a short plug of silica gel with dichloromethane. The obtained solid was dried under high vacuum. Yield 50-55%.

**P-3,4,5G1:**  $^1\text{H}$  NMR (400.13MHz,  $\text{CDCl}_3$   $\delta$ ): 0.89 (t, 9H,  $J=8\text{Hz}$ ;  $-\text{CH}_3$ ), 1.27-1.46 (overlapped peaks, 54H;  $-\text{CH}_2$ ), 1.79(m, 6H;  $-\text{CH}_2$ ), 3.39(s, 3H;  $-\text{OCH}_3$ ), 3.65(m, 172H;  $-\text{OCH}_2$ ), 3.93(t, 4H,  $J=6.2\text{Hz}$ ;  $-\text{OCH}_2$ ), 3.97(m, 8H;  $-\text{OCH}_2$ ), 4.50-4.55 (overlapped peaks, 4H;  $-\text{OCH}_2$ ), 4.67(s, 2H;  $-\text{NCH}_2$ ), 6.58(s, 2H; Ar H), 6.71(s, 1H; Ar H), 7.76(s, 1H; Trz H) ppm.  $^{13}\text{C}$  NMR (100MHz,  $\text{CDCl}_3$   $\delta$ ) 14.0, 22.56, 26.01, 29.52, 31.80, 50.11, 58.90, 63.39, 70.44, 106.34, 123.73, 132.76, 137.61, 153.03. FT-IR (KBr,  $\text{cm}^{-1}$ ): 847, 960, 1120, 1147, 1290, 1286, 1352, 1469, 1599, 1658, 2003, 2895, 2928. MALDI-TOF MS Calcd. 2727.09. Found 2727.06.

**P-3,4,5G2:**  $^1\text{H}$  NMR (400.13MHz,  $\text{CDCl}_3$   $\delta$ ): 0.85(t, 27H,  $J=8\text{Hz}$ ;  $-\text{CH}_3$ ), 1.23-1.37(overlapped peaks, 162H;  $-\text{CH}_2$ ), 1.71(m, 18H;  $-\text{CH}_2$ ), 3.36(s, 3H;  $-\text{OCH}_3$ ), 3.62(m, 172H;  $-\text{OCH}_2$ ), 3.72(t, 4H,  $J=6.2\text{Hz}$ ;  $-\text{OCH}_2$ ), 3.84(m, 14H;  $-\text{OCH}_2$ ), 4.48(s, 2H;  $-\text{OCH}_2$ ), 4.53(t, 2H,  $-\text{OCH}_2$ ,  $J=4\text{Hz}$ ), 4.62(s, 2H;  $-\text{NCH}_2$ ), 4.92(s, 2H;  $-\text{OCH}_2$ ), 4.98(s, 4H;  $-\text{OCH}_2$ ), 6.60(s, 6H; Ar H), 6.67(s, 2H; Ar H), 7.72(s, 1H; Trz H) ppm.  $^{13}\text{C}$  NMR ( $\text{CDCl}_3$ , 100MHz,  $\delta$ ) 13.91, 22.48, 25.97, 29.48, 31.73, 58.8, 68.79, 70.34, 73.14, 105.36, 131.98, 137.43, 152.99. FT-IR (KBr,  $\text{cm}^{-1}$ ): 648, 811, 939, 1106, 1235, 1328, 1436, 1586, 1606, 1871, 2850, 2995. MALDI-TOF MS: Calcd. 4149.37 Found 4151.60.

**P-3,5G1:**  $^1\text{H}$  NMR (400.13MHz,  $\text{CDCl}_3$   $\delta$ ): 0.86 (t, 6H,  $J=7\text{Hz}$ ;  $-\text{CH}_3$ ), 1.24-1.39(overlapped peaks, 36H;  $-\text{CH}_2$ ), 1.71(m, 4H;  $-\text{CH}_2$ ), 3.36(s, 3H;  $-\text{OCH}_3$ ), 3.60(m, 172H;  $-\text{OCH}_2$ ), 3.85(t, 2H,  $J=4\text{Hz}$ ;  $-\text{OCH}_2$ ), 3.90(t, 4H,  $J=4\text{Hz}$ ;  $-\text{OCH}_2$ ), 4.50(s, 2H;  $-\text{OCH}_2$ ), 4.52(t, 2H,  $J=4\text{Hz}$ ;  $-\text{OCH}_2$ ), 4.64(s, 2H;  $-\text{NCH}_2$ ), 6.34(t, 1H,  $J=4\text{Hz}$ ; Ar H), 6.47(d, 2H,  $J=4\text{Hz}$ ; Ar H), 7.73(s, 1H; Trz H) ppm.  $^{13}\text{C}$  NMR ( $\text{CDCl}_3$   $\delta$ ): 13.94, 22.49, 25.87, 29.40, 31.72, 50.05, 58.84, 67.84, 70.40, 100.45, 105.89, 123.60, 139.93, 144.78, 160.22. FT-IR (KBr,  $\text{cm}^{-1}$ ): 850, 957, 1123, 1280, 1294, 1355, 1466, 1605, 1746, 1997, 2890, 2931. MALDI-TOF MS: Calcd. 2542.78 Found 2572.84.

**P-3,5G2:**  $^1\text{H}$  NMR (400.13MHz,  $\text{CDCl}_3$   $\delta$ ): 0.88(t, 12H,  $J=7\text{Hz}$ ;  $-\text{CH}_3$ ), 1.26-1.45(overlapped peaks, 72H;  $-\text{CH}_2$ ), 1.70(m, 8H;  $-\text{CH}_2$ ), 3.36(s, 3H;  $-\text{OCH}_3$ ), 3.60(m, 172H;  $-\text{OCH}_2$ ), 3.86(t, 2H,  $J=4\text{Hz}$ ;  $-\text{OCH}_2$ ), 3.91(t, 8H,  $J=4\text{Hz}$ ;  $-\text{OCH}_2$ ), 4.52(overlapped

peaks, 4H; -OCH<sub>2</sub>), 4.66(s, 2H; -NCH<sub>2</sub>), 4.92(s, 4H; -OCH<sub>2</sub>), 6.38(t, 2H, J=4Hz; Ar H), 6.53 (overlapped peaks, 5H, Ar H), 6.60(d, 2H, J=4Hz; Ar H), 7.73(s, 1H; Trz H) ppm. <sup>13</sup>C NMR (100 MHz, CDCl<sub>3</sub> δ): 14.04, 22.58, 25.95, 29.52, 31.81, 50.12, 58.94, 63.50, 67.95, 70.46, 100.67, 105.61, 123.73, 138.86, 144.76, 160.37. FT-IR (KBr, cm<sup>-1</sup>): 857, 954, 1120, 1148, 1292, 1304, 1358, 1466, 1603, 1773, 2007, 2871, 2929. MALDI-TOF MS: Calcd. 3123.66, Found 3152.57.

**P-3,5G3:** <sup>1</sup>H NMR (400.13MHz, CDCl<sub>3</sub> ) δ: 0.85(t, 24H, J=7Hz; -CH<sub>3</sub>), 1.24-1.41(overlapped peaks, 144H; -CH<sub>2</sub>), 1.74(m, 16H; -CH<sub>2</sub>), 3.36(s, 3H; -OCH<sub>3</sub>), 3.63(m, 172H; -OCH<sub>2</sub>), 3.84(t, 2H, J=4Hz; -OCH<sub>2</sub>), 3.91(t, 16H, J=4Hz; -OCH<sub>2</sub>), 4.51-4.53(overlapped peaks, 4H; -OCH<sub>2</sub>), 4.66(s, 2H; -NCH<sub>2</sub>), 4.92(s, 8H; -OCH<sub>2</sub>), 4.94(s, 4H; -OCH<sub>2</sub>), 6.38(t, 4H, J=4Hz; Ar H), 6.53 (m, 11H; Ar H) , 6.61(d, 2H, 4Hz; Ar H), 6.66(d, 4H; ArH), 7.73 (s, 1Hz; Trz H) ppm. <sup>13</sup>C NMR (100 MHz, CDCl<sub>3</sub> δ): 14.06, 22.61, 25.98, 29.28, 31.84, 50.14, 58.95, 67.98, 70.45, 100.73, 105.68, 138.80, 160.41. FT-IR (KBr, cm<sup>-1</sup>): 845, 959, 1112, 1156, 1279, 1340, 1352, 1462, 1603, 2025, 2863, 2928. MALDI-TOF MS: Calcd. 4284.42, Found 4314.57.

**P-(3,4,5)3,5G2:** <sup>1</sup>H NMR (200.13MHz,CDCl<sub>3</sub>) δ: 0.80 (t, 3H, J=8Hz; -CH<sub>3</sub>), 1.19-1.39 (overlapped peaks, 12H; -CH<sub>2</sub>), 1.79(m, 12H; -CH<sub>2</sub>), 3.31(s, 3H; -OCH<sub>3</sub>), 3.57(m, 172H; -OCH<sub>2</sub>), 3.81(t, 2H, J=6Hz; -OCH<sub>2</sub>), 3.90(t, 12H, J=6Hz; -OCH<sub>2</sub>), 4.48(t, 4H, J=6Hz; -OCH<sub>2</sub>), 4.60(s, 2H; -NCH<sub>2</sub>), 4.83(s, 4H; -OCH<sub>2</sub>), 6.47(t, 1H, J=2Hz; ArH), 6.54-6.55(overlapped peaks, 5H; ArH), 7.71(s, 1H; Trz H) ppm. <sup>13</sup>C NMR (100 MHz, CDCl<sub>3</sub> δ): 14.39, 22.95, 26.38, 29.92, 32.18, 50.48, 59.28, 63.79, 69.36, 70.77, 106.49, 124.17, 131.93, 138.15, 138.15, 140.56, 153.52, 160.33. FT-IR (KBr, cm<sup>-1</sup>): 847, 945, 1115, 1267, 1340, 1349, 1461, 1605, 2019, 2862, 2927. MALDI-TOF MS: Calcd. 3490.32, Found: 3495.05.

#### 2.2.4 Preparation of aqueous solutions

To the weighed amount of polymer taken in a sample vial was added THF and shaken to get a clear solution. To this solution, water was added in one portion to obtain the required solvent composition (5, 10 or 20% THF v/v) and polymer concentration (1, 0.1 or 0.05 wt%). The resulting solution was stirred for 5 h to allow for complete micellization and used directly for analysis. For SANS measurements, D<sub>2</sub>O was used instead of H<sub>2</sub>O.

### 2.2.5 cmc measurements

A stock solution of Nile red in THF ( $5 \times 10^{-6}$  M) was added to the polymer in a sample vial followed by addition of water to reach desired polymer concentration (0.1wt%) and solvent composition (THF/H<sub>2</sub>O = 10/90 v/v). This solution was diluted by addition of THF/H<sub>2</sub>O (10/90 v/v) to obtain a series of concentrations and fluorescence emission spectra were recorded. A curve of intensity versus log(conc.) was plotted. cmc was determined to be the point where tangents to the curve crossed.

### 2.2.6 Dye encapsulation

Pyrene (5mg) was added to the solution of polymer in THF/H<sub>2</sub>O and stirred for 4h. This suspension was filtered through 0.45 $\mu$ m filter and UV-vis spectra were recorded.

### 2.2.7 SANS measurements and analysis

The neutron-scattering diffractometer uses a polycrystalline BeO filter as a monochromator with a Bragg cutoff at 4.7 Å. The mean wavelength of the incident neutron beam is 5.2 Å with a wavelength resolution ( $\Delta\lambda/\lambda$ ) of approximately 15%. The angular divergence of the incident beam is  $\pm 0.5^\circ$ , and the beam size at the sample position is 1.5 cm  $\times$  1.0 cm. The sample-to-detector distance is 1.85m. The angular distribution of the scattered neutrons was recorded by a linear 100-cm-long, 3.8-cm-diameter He<sup>3</sup> position-sensitive detector (PSD). The data were recorded in the  $Q$  range of 0.017-0.35 Å<sup>-1</sup>. The solutions were held in a quartz cell of 0.5 cm thickness with tight-fitting Teflon stoppers. The measured SANS distributions were corrected for the background, empty cell, and solvent contribution, and the data were normalized to the cross-sectional unit using standard procedures.<sup>25</sup>

In SANS experiments, one measures the coherent differential scattering cross-section per unit volume ( $d\Sigma/d\Omega$ ) as a function of  $Q$ . In the case of micellar solution, it can be written as<sup>26,27</sup>

$$\frac{d\Sigma}{d\Omega}(Q) = nV^2 (\rho_p - \rho_s)^2 P(Q)S(Q) + B \quad (1)$$

where  $n$  is the number density and  $V$  is micellar volume.  $\rho_p$  and  $\rho_s$  are scattering length densities of micelle and solvent, respectively.  $P(Q)$  is intraparticle structure factor and  $S(Q)$  is interparticle structure factor.  $B$  is a constant term representing incoherent background.

$P(Q)$  accounts for the scattering from a single particle and hence depends on shape and size of the particle. It is the square of single particle form factor  $F(Q)$  as given by

$$P(Q) = \langle |F(Q)|^2 \rangle \quad (2)$$

For a spherical particle of radius  $R$ ,  $F(Q)$  is given by

$$F(Q) = \frac{3\{\sin(QR) - (QR)\cos(QR)\}}{(QR)^3} \quad (3)$$

$S(Q)$  correlates particles present in the system and is the Fourier transform of the radial distribution function  $g(r)$  for the mass centers of the particle. For diluted samples,  $S(Q) \sim 1$ .

For polydisperse systems,  $d\Sigma/d\Omega$  in equation (1) is modified as

$$\frac{d\Sigma}{d\Omega}(Q) = \int \frac{d\Sigma}{d\Omega}(Q, R) f(R) dR + B \quad (4)$$

where  $f(R)$  is the size distribution and usually accounted by log normal distribution as given by

$$f(R) = \frac{1}{R\sigma\sqrt{\pi}} \exp\left[-\frac{\left(\ln R/R_{med}\right)^2}{2\sigma^2}\right] \quad (5)$$

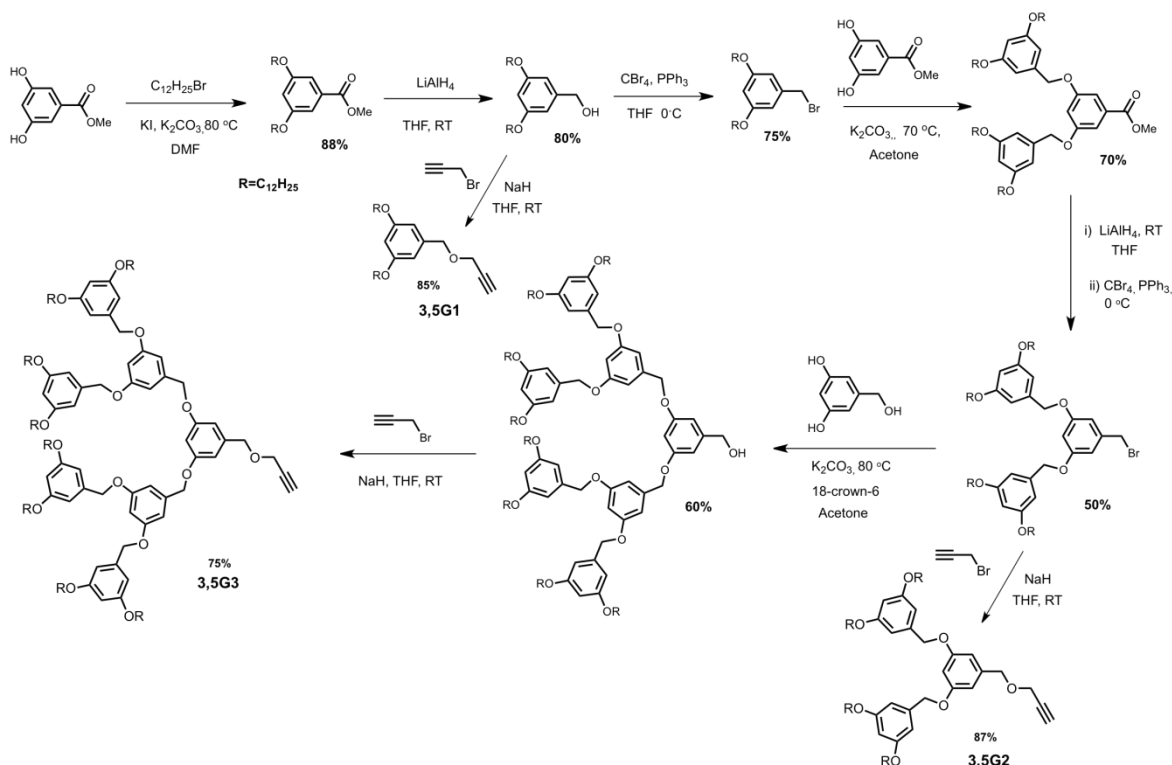
where  $R_{med}$  and  $\sigma$  are the median value and standard deviation respectively. The mean and median values are related as  $R_m = R_{med} \exp(\sigma^2/2)$ .

Throughout the data analysis corrections were made for instrumental smearing. Calculated scattering profiles were smeared by the appropriate resolution function to compare with the measured data. The parameters in the analysis were optimized by means of nonlinear least-square fitting program.<sup>28</sup> The micellar core dimension, aggregation number and the composition have been derived from the analysis.

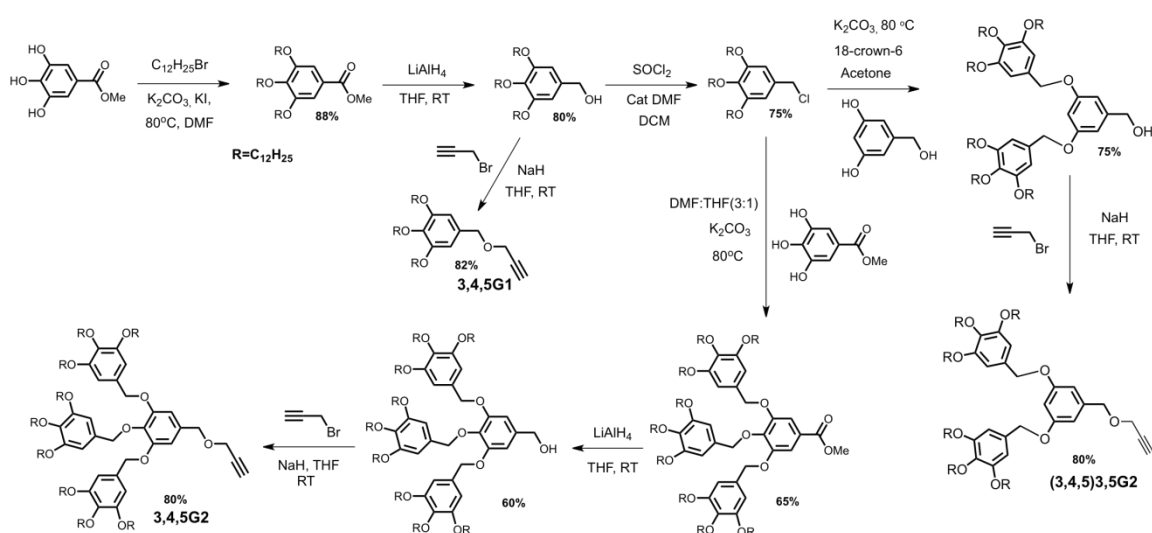
## 2.3 Results and Discussion

### 2.3.1 Synthesis

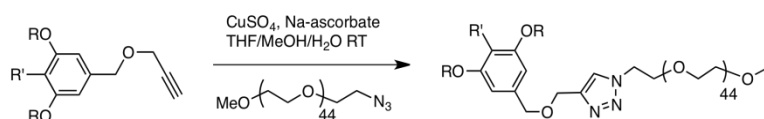
Hydrophobic benzyl ether dendrons were synthesized from *viz.* 3,5-dihydroxy benzoic acid and 3,4,5-trihydroxy benzoic acid (gallic acid) - compounds with different number of hydroxyl groups on the phenyl ring, as starting materials using established protocols in the convergent approach. Dendrons up to third generation with benzyl alcohol at the focal point were synthesized from the former building block (3,5G1-G3) as shown in Scheme 2.1.<sup>29</sup> Dendrons up to second generation (3,4,5G1-G2) were synthesized from the latter building block as shown in Scheme 2.2.<sup>30</sup> Dodecyl chains were installed on dendron periphery to aid the self-assembly and the propargyloxy group was introduced at focal point. These five dendrons together make up a series with 2, 3, 4, 8 and 9 dodecyl chains on the periphery. One more dendron ((3,4,5)3,5-G2) was synthesized using both the building blocks to obtain an intermediate number of dodecyl chains (six) on the periphery (Scheme 2.2).<sup>31</sup> These alkynylated dendrons were coupled with azide terminated PEG (PEG-N<sub>3</sub>) using CuAAC reaction.<sup>32,33</sup> The crude products were purified by passing through a short plug of silica gel to obtain the targeted LDBC. The polymers are labeled as **P-x,y,zGn**, where x,y,z indicates branching pattern that is, 3,5-dialkoxy or 3,4,5-trialkoxy benzyl ether and Gn is the dendron generation.



**Scheme 2.1** Synthesis of 3,5-dialkoxy benzyl ether dendrons with alkyne functionality.



**Scheme 2.2** Synthesis of 3,4,5-trialkoxy benzyl ether dendrons and (3,4,5)3,5G2 dendron with alkyne functionality.



**Scheme 2.3** General synthetic scheme for LDBC by CuAAC reaction.

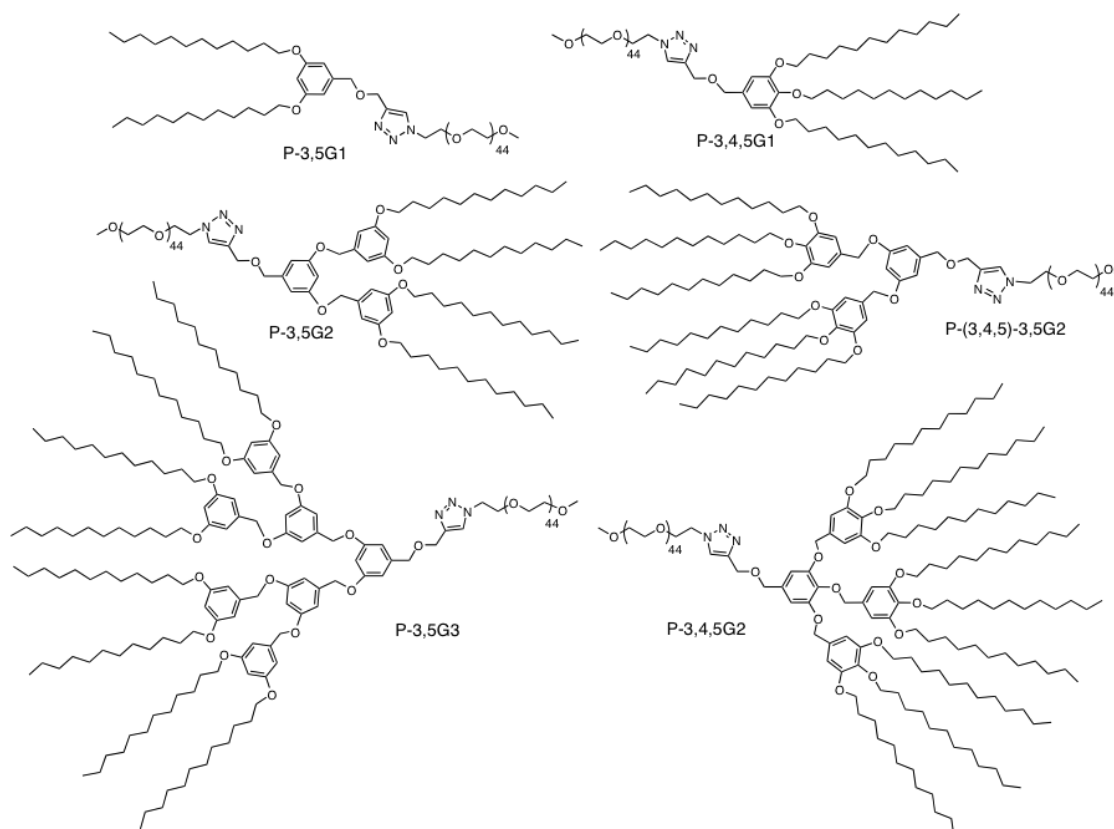


**Chart 2.1** Chemical structures of synthesized copolymers.

Chemical structures of all synthesized LDBC are shown in Chart 2.1. The copolymers were characterized by  $^1\text{H}$ ,  $^{13}\text{C}$  NMR spectroscopy and MALDI-TOF analysis (see Appendix I). Disappearance of band at  $2100\text{ cm}^{-1}$  confirmed the absence of PEG-azide in the product (Figure 2.1) and absence of alkyne protons in  $^1\text{H}$  NMR spectrum confirmed formation of product. Purity of the polymers was confirmed by GPC analysis (Figure 2.2).

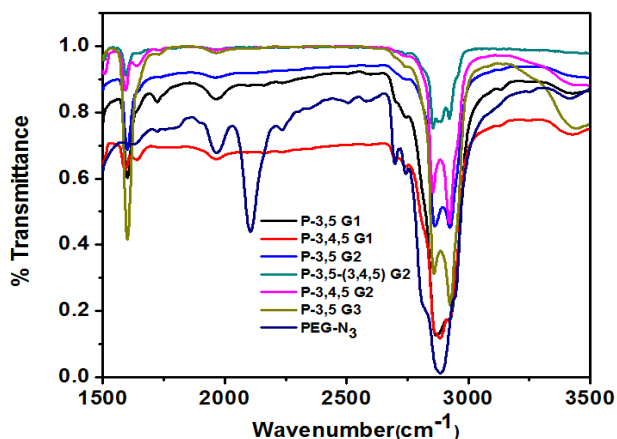


**Figure 2.1.** FT-IR spectra of PEG azide and LDBC after CuAAC reaction.

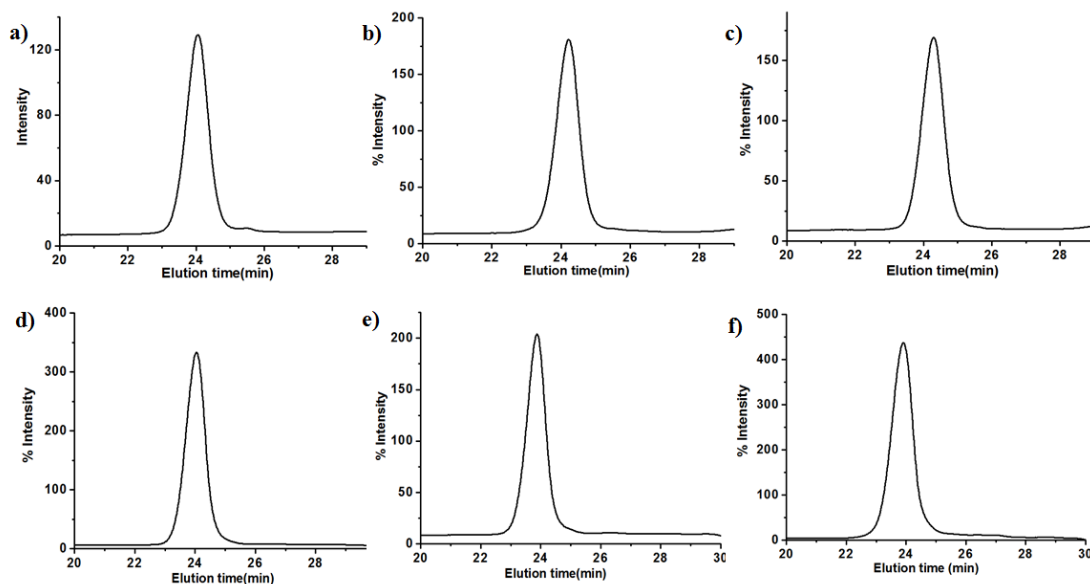


**Figure 2.2** GPC chromatograms for (a) **P3,5G1** (b) **P-3,4,5G1** (c) **P-3,5G2** (d) **P-(3,4,5)3,5G2** (e) **P-3,4,5G2** (f) **P-3,5G3**.

### 2.3.2 Determination of cmc and dye encapsulation study

Self-assembly of the copolymers was studied in THF and water mixture as solvent. This was done for two purposes. Firstly, we were interested in using SANS technique to gain better insight into properties of micellar core. Solutions for this experiment with required concentration and stability could be easily prepared in THF/D<sub>2</sub>O mixtures without need of dialysis. For preparation of solutions in pure water dialysis was found to be necessary. Secondly, the self-assembly behaviour could be studied as a function of the solvent composition.

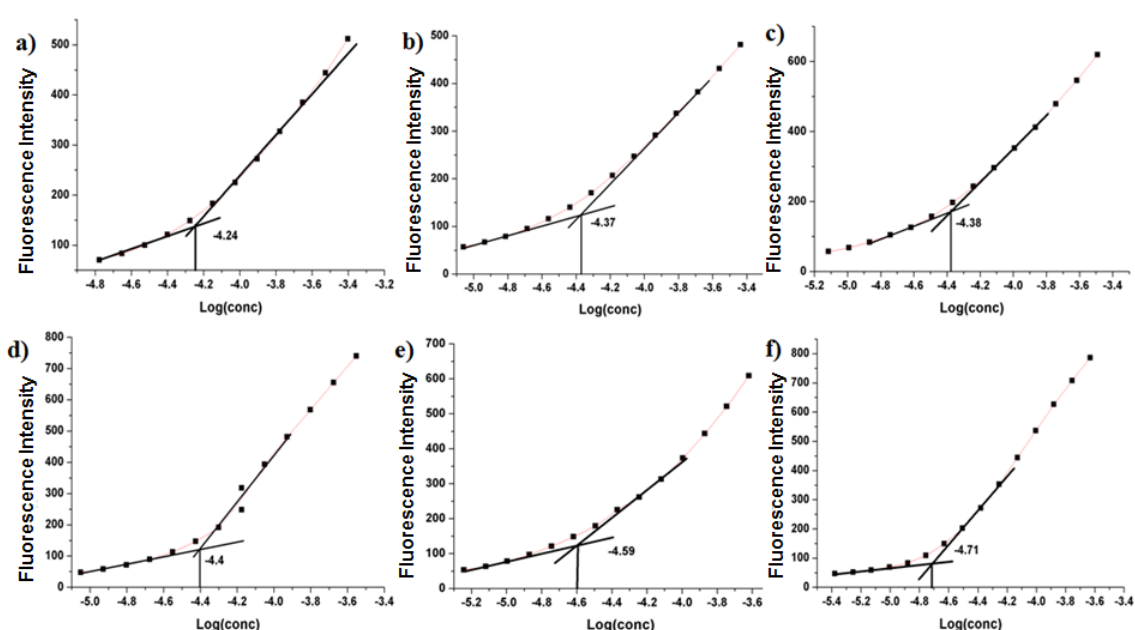


**Figure 2.3** Plots of intensity versus log(conc.) for (a) P-3,5G1 (b) P-3,4,5G1 (c) P-3,5G2 (d) P-(3,4,5)3,5G2 (e) P-3,4,5G2 (f) P-3,5G3 in using Nile red in THF/H<sub>2</sub>O (10/90).

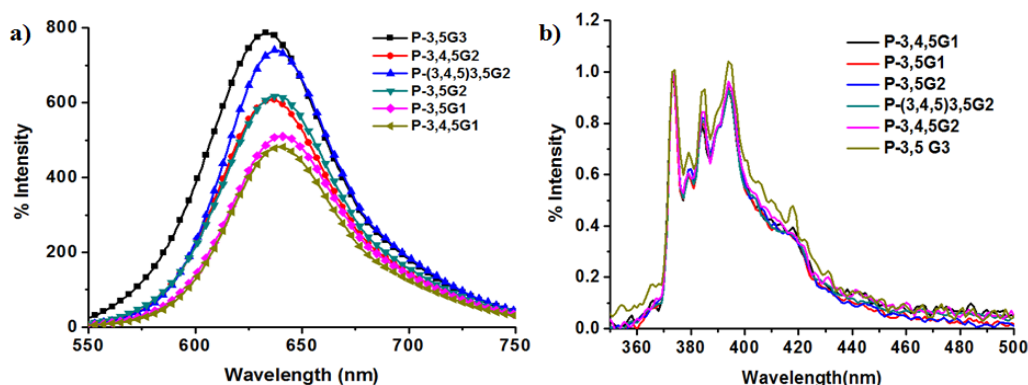
Nile red was used as a solvatochromic probe for determination of cmc values of the copolymers. Fluorescence emission spectra were recorded above 550 nm by exciting the Nile red encapsulated copolymer solutions at 530 nm. Upon dilution of the solutions, a red shift in  $\lambda_{em}$  that is characteristic of the dye in polar medium was observed. The cmc values determined from the plot of fluorescence intensity versus log (conc.) (Figure 2.3) were in the range of  $1.94\text{--}5.75 \times 10^{-5}$  M and decreased with increasing hydrophobic weight fraction of the copolymer (Table 2.1). Shape of this plot was typical of a cmc curve.



**Table 2.1.** Hydrophobic weight fraction for LDBC and their cmc,  $D_h$  values in THF/H<sub>2</sub>O (10/90) solution.

Polymer	Hydrophobic weight fraction [ $W_{\text{phobic}}$ ]	cmc [M]	$D_h^\dagger$ (nm)
<b>P-3,5G1</b>	0.2044	$5.75 \times 10^{-5}$	18.6
<b>P-3,4,5G1</b>	0.2588	$4.26 \times 10^{-5}$	14.2
<b>P-3,5G2</b>	0.3538	$4.16 \times 10^{-5}$	37.7
<b>P-(3,4,5)3,5G2</b>	0.4245	$3.98 \times 10^{-5}$	41.6
<b>P-3,4,5G2</b>	0.5174	$2.57 \times 10^{-5}$	201.5
<b>P-3,5G3</b>	0.5302	$1.94 \times 10^{-5}$	152.2

$^\dagger$  at 1wt% conc.

**Figure 2.4** Overlay of fluorescence emission spectra of (a) Nile red and (b) pyrene in 0.1 wt% aqueous solution of LDBC.

Polarity of the microenvironment of the micellar core was then explored using fluorescence emission spectroscopy solvatochromic dyes *viz.* Nile red and pyrene. Similar to the observation in cmc experiments,  $\lambda_{\text{em}}$  of Nile red was around 636 nm suggesting that polarity of the core was similar to that of 60% THF in water, which is less polar environment than the bulk solvent (10% THF in water). With increasing hydrophobicity of the dendron the emission wavelength showed a gradual shift, decreasing from 642 nm for **P-3,5G1** to 632 nm for **P-3,5G3** (Figure 2.4a). The  $I_1/I_3$  value obtained from fluorescence emission spectrum of pyrene is indicative of the polarity of the surrounding medium. Hence, pyrene was also used for this study. Value of  $I_1/I_3$  for the bulk solvent was 1.34, however it was 1.26 for **P-3,5G1** and then decreased to 1.11 for **P-3,5G3** (Figure 2.4b). It is to be noted that **P-3,5G1** and **P-3,5G3** are copolymers with the least and the highest

hydrophobic weight fraction, respectively (Table 2.1). Although, hydrophobic weight fractions of **P-3,4,5G2** and **P-3,5G3** are close, effect of  $\pi$ - $\pi$  stacking apparently plays a role for  $I_1/I_3$  value being lower in case of the latter. The range of  $I_1/I_3$  values indicates a non-polar environment of the core and the value of 1.11 is comparable to that in toluene.<sup>34</sup>

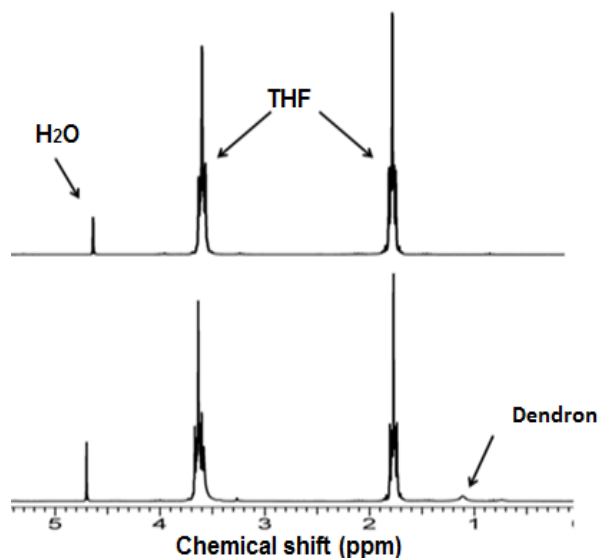


**Figure 2.5**  $^1\text{H}$  NMR spectra of the solvent mixture (THF/ $\text{D}_2\text{O}$  = 10/90) in the absence (above) and presence (below) of 0.1 wt% **P-3,5G2**.

It is possible that since the copolymers are not directly soluble in water, aggregation of the LDBC's in THF/ $\text{H}_2\text{O}$  mixture is most likely aided by solvation of dendrons by THF. This may lead to formation of micelles with THF in the hydrophobic core. To test this possibility,  $^1\text{H}$  NMR spectra of the solvent mixture used (THF/ $\text{D}_2\text{O}$  = 10/90) were recorded in the presence and absence of LDBC. The intensity of signals for THF protons decreased in relation to the intensity of peak for  $\text{H}_2\text{O}$  in the presence of **P-3,5G2** suggesting that THF gets partitioned to the core (Figure 2.5). Since amount of THF in the core may depend on extent of hydrophobicity of the dendron this observation has important consequences on properties of the micellar core.

### 2.3.3 SANS Study

#### 2.3.3.1 At 30 °C and Fixed Solvent Composition

SANS is a highly valuable technique employed to understand the polymeric micellar behaviour and polymer conformations.<sup>35-38</sup> However, it has been relatively less explored

to study LDBC aggregates in solution.<sup>39,40</sup> To investigate the influence of dendron structure on properties of micellar core of the LDBCs studied here, SANS measurements were carried out on 1wt% solution in THF/D<sub>2</sub>O (10/90) at 30 °C.

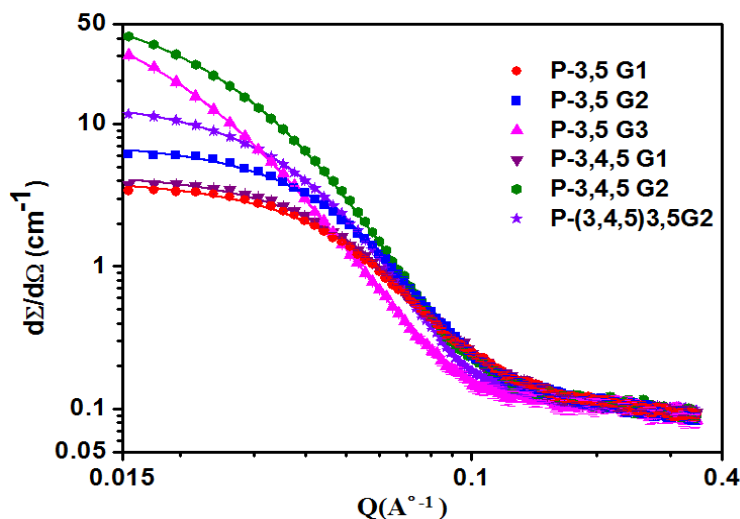


**Figure 2.6** SANS profiles of 1wt% solutions of LDBCs in THF/D<sub>2</sub>O (10/90) measured at 30 °C.

**Table 2.2** Fitted micellar parameters of 1 wt% solutions of LDBCs in THF/D<sub>2</sub>O (10/90) at 30°C.

Polymer	Mean Core Radius R [Å]	Aggregation Number N	Polydispersity $\sigma$	THF molecules/ dendron n
P-3,5G1	40.7	113	0.22	12
P-3,4,5G1	41.0	72	0.23	21
P-3,5G2	43.6	47	0.23	42
P-(3,4,5)3,5G2	50.3	37	0.29	89
P-3,4,5G2	64.2	19	0.43	407
P-3,5G3	78.9	45	0.50	312

The scattering curves shown in Figure 2.6 (solid lines represent the theoretical fits and the points represent the experimental data) could be fitted to a spherical model indicating spherical nature of all copolymer aggregates. Mean core radius of micellar assemblies increased gradually across the series with increasing size of the dendron (Table 2.2). For

example, **P-3,5G2** that has four dodecyl chains forms a micelle with smaller core radius than that of **P-(3,4,5)3,5G2**, which has six dodecyl chains on periphery. It is noteworthy that both the dendrons have same number of phenyl rings.

**Table 2.3** Molecular volume of dendrons calculated using mass/density = volume

Dendron	Mol. wt. [g/mol]	volume [nm <sup>3</sup> ]
3,5G1	514.84	0.86
3,4,5G1	675.12	1.13
3,5G2	1071.68	1.79
(3,4,5)3,5G2	1440.32	2.41
3,4,5G2	2099.40	3.52
3,5G3	2233.44	3.74

Aggregation numbers (N) of the micelles as calculated from dendron volumes (Table 2.3; based on) revealed an interesting trend. The density of dendrons was assumed to be 0.99g/cm<sup>3</sup> based on a literature report for this calculation.<sup>30</sup> The ‘N’ values for **P-3,4,5G2** and **P-3,5G3** are very different even though hydrophobic weight fractions (shown in Table 2.1) are very similar. There is also a significant difference in core radius (~15 Å) for respective micelles. The dendrons in these two copolymers are based on different branching patterns - trisubstituted versus disubstituted benzyl ether, so that the copolymers possess different hydrophobic group density. Dendron 3,4,5G2 was suggested by molecular modeling to be conical-shaped due to restricted rotation of phenyl rings on account of alkyl substitution at 3,4,5 positions.<sup>30</sup> The 3,5-dialkoxy benzyl ether dendrons are thought to possess extended (flat) shape up to 3<sup>rd</sup> generation, however tend to be globular at 4<sup>th</sup> and higher generation.<sup>41</sup> Moreover, 3,4,5G2 dendron has only four phenyl rings and nine dodecyl chains whereas 3,5G3 dendron has seven phenyl rings and eight dodecyl chains. It is reasonable to assume that the differences in chemical structure and molecular shape, lead to greater hydrophobic density in 3,4,5G2 dendron than in 3,5G3 dendron. This assumption is supported by the fact that due to presence of multiple hydrophobic groups in a smaller volume gallate-based benzyl ether dendrons have been widely employed in the field of macromolecular self-assembly.<sup>43,44</sup>

As discussed earlier, micellization is assisted by solvation of dendrons with THF during addition of water to solution of the copolymer in THF. If a dendron has greater density of

dodecyl chains then more THF molecules will solvate the core during micellization. To confirm this, number of THF molecules associated with each dendron during micelle formation was calculated from SANS data. It revealed that higher number of THF molecules was indeed present per 3,4,5G2 dendron than that for 3,5G3 dendron (Table 2.2). Due to this **P-3,4,5G2** shows significantly lower aggregation number because fewer copolymer molecules are then needed to fill the space in micellar core. Difficulty in packing of cone-shaped dendrons in the spherical core may be another reason for lower aggregation number. is the two other pairs of copolymers *viz.* **P-(3,4,5)3,5G2** versus **P-3,5G2** and **P-3,4,5G1** versus **P-3,5G1** also seem to be follow this trend whereas it is exactly opposite for micelles formed by copolymers containing 3,5-dialkoxy benzyl ether dendron, that is higher aggregation number with few THF molecules. This mechanism of micellization influenced by hydrophobic density is shown schematically in Figure 2.7 by taking **P-3,4,5G2** and **P-3,5G3** as examples.

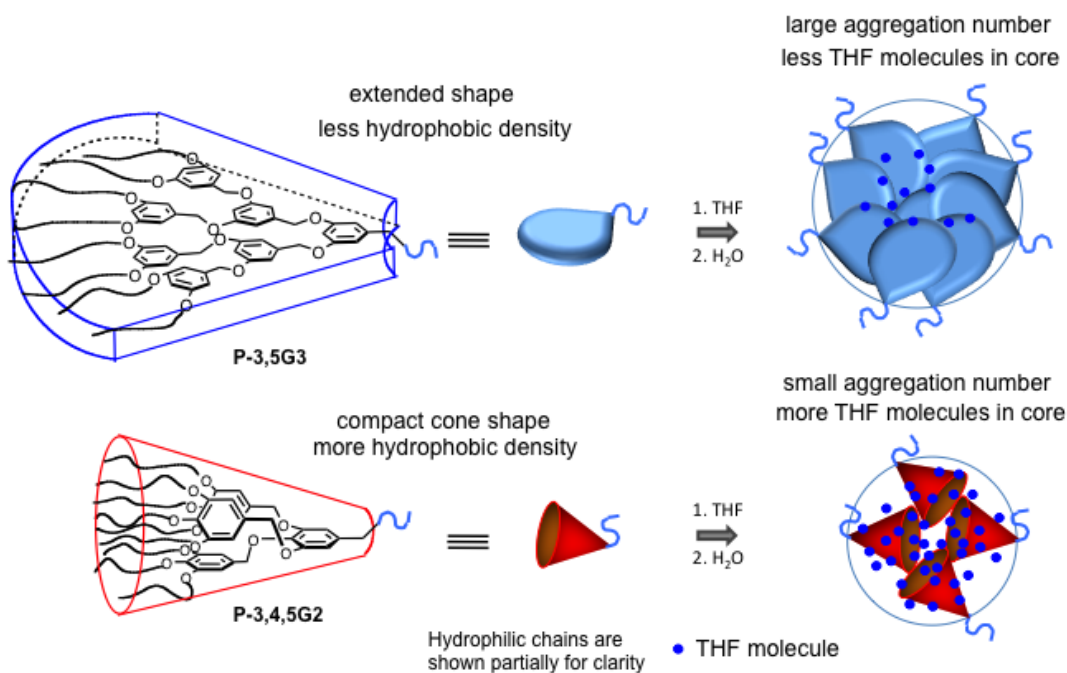


**Figure 2.7** Schematic representation of the possible mechanism for self-assembly of LDBC.

It was observed that hydrodynamic size ( $D_h$ ) of the micelles as obtained from DLS analysis and size in terms of mean core radius as obtained from SANS analysis differ widely. To understand this phenomenon, DLS analysis of one of the polymers, **P-(3,4,5)3,5G2**, was carried out at different concentrations in THF:water (10/90). It was

found that  $D_h$  value varied with concentration as given in Table 2.4. This suggested a dynamic nature for the assemblies and probable presence of multi-micellar aggregates.

**Table 2.4** DLS data for **P-(3,4,5)3,5G2** at different concentrations.

Concentration	0.1 wt%	0.5 wt%	1 wt%
$D_h$ (nm)/PDI	136 (0.36)	57.9 (0.37)	41.6 (0.37)

Size of the micellar core gives an indication of its encapsulation capacity for a hydrophobic dye. To study whether the core sizes obtained from SANS measurements correlate with the amount of dye taken, pyrene was sequestered in 0.05 wt% copolymer solution in THF/H<sub>2</sub>O (10/90). The concentration of 0.05wt% is  $\sim 10^{-4}$  M and hence higher than cmc. Lower concentration of the polymer than that in earlier experiments was used to limit the absorbance of pyrene below 1.5 units for accurate estimation of encapsulation. Amount of pyrene in the micellar core was calculated using Beer-Lambert law. Molar extinction coefficient of pyrene in THF was determined to be  $63917 \text{ L mol}^{-1} \text{ cm}^{-1}$  (Figure 2.8).

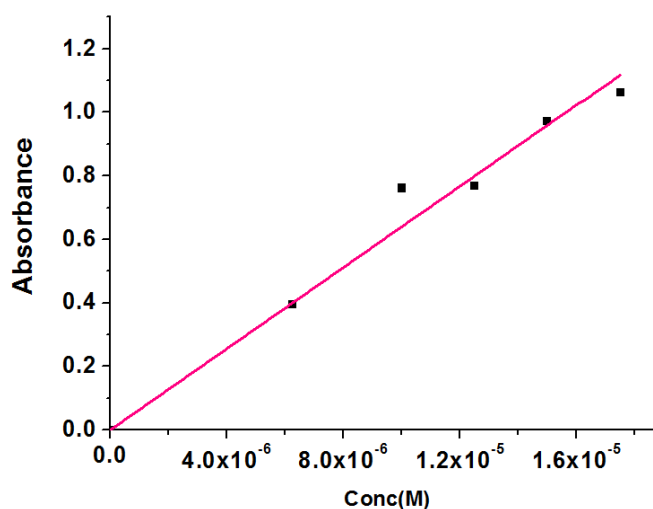


**Figure 2.8** Plot of absorbance vs. concentration for pyrene in THF for determination of molar extinction coefficient.

Overlay of UV-vis spectra of pyrene encapsulated in LDBC micelles showed that amount of encapsulated pyrene increases with the the mean core size and maximum amount was taken up by **P-3,5G3** (Figure 2.9a). Generally, uptake of hydrophobic dye increases at higher generation of dendrons,<sup>45,46</sup> however with systematic variation in

hydrophobicity of dendrons studied here, it was possible to tune the dye uptake by micelles in small increments. Figure 2.9b clearly shows the dependence of amount of encapsulated pyrene on the molecular structure of dendron, which is expressed as a function of hydrophobic weight fraction ( $W_{\text{phobic}}$ ) and molecular volume of the dendron. **P-3,5G3** with its larger and extended dendron captured more dye molecules than **P-3,4,5G2**. Similarly **P-(3,4,5)3,5G2** showed higher encapsulation capacity than **P-3,5G2**.

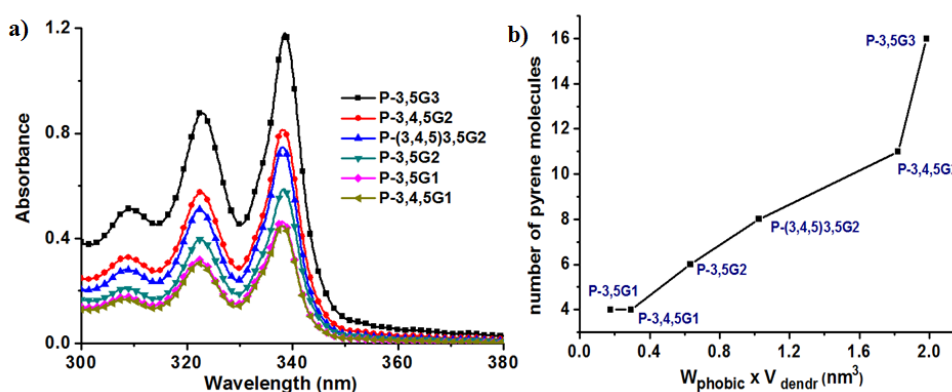


**Figure 2.9** (a) Absorption spectra of pyrene and (b) number of pyrene molecules per dendron encapsulated in 0.05wt% LDBC in THF/H<sub>2</sub>O (10/90).

**2.3.3.2 Effect of Solvent Composition:** Two LDBC *viz.* **P-3,5G2** and **P-(3,4,5)3,5G2**, were selected to further understand the relationship between branching pattern of dendron and micellar properties of the copolymer. As mentioned above, these dendrons differ in number of dodecyl chains and their hydrophobicity is intermediate in the series. Solvation of hydrophobic block is an important thermodynamic parameter for the process.<sup>47</sup> Therefore, micellization of an amphiphilic block copolymer in aqueous solution from a water-miscible solvent depends on polarity of that solvent. To explore this phenomenon in case of micellization of copolymers studied here, percentage of THF in the solvent mixture was varied. Two different solutions with 5% and 20% THF in D<sub>2</sub>O were prepared as described before and SANS measurements were carried out for the two copolymers. The results with data from 10% THF included for comparison are shown in Table 2.5 and the corresponding SANS curves are shown in Figure 2.10. The scattering curves could be fitted to a spherical model.

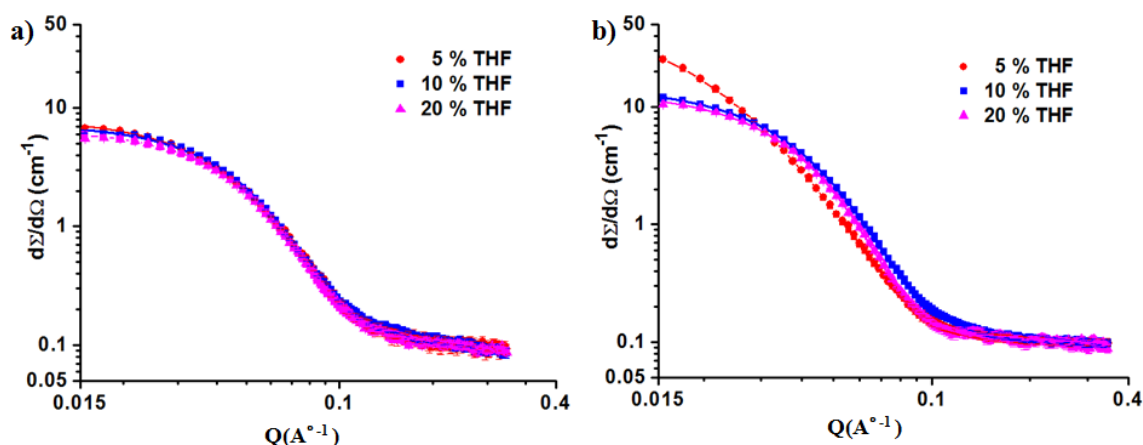


**Figure 2.10** SANS profiles for 1wt% solutions of (a) **P-3,5G2** and (b) **P-(3,4,5)3,5G2** in varying THF/D<sub>2</sub>O ratios at 30 °C.

Effect of THF concentration on the core size of P-3,5G2 micelles was observed to be negligible. However, in case of P-(3,4,5)3,5G2 micelles decrease percentage of THF led to increase in the mean core size. This is because of the decrease in solvent quality for the gallate-based dendron, which has higher hydrophobic density than 3,5G2 dendron. Understandably, this was accompanied with large increase in aggregation number for P-(3,4,5)3,5G2 micelles.

**Table 2.5** Fitted micellar parameters from SANS measurements of 1wt% LDBC at different THF concentrations at 30°C.

THF [%]	Mean Core Radius (Å)	Aggregation Number N	Polydispersity $\sigma$
<i>P-3,5G2</i>			
5	42.0	42	0.23
10	43.6	47	0.23
20	42.5	44	0.24
<i>P-(3,4,5)3,5G2</i>			
5	73.0	113	0.48
10	50.3	37	0.29
20	53.2	44	0.25



**2.3.3.3 Effect of Temperature:** Block copolymers with PEG as the hydrophilic block exhibit lower critical solution temperature (LCST) behavior in aqueous solutions.<sup>48,49</sup> Since the LDBCs also contain PEG chain, the effect of temperature on micellar size of **P-3,5G2** and **P-(3,4,5)3,5G2** was investigated by SANS measurements, and the results are shown in Table 2.6. The neutron scattering curves fitted to a spherical model are shown in Figure 2.11. Two temperature values higher than room temperature, 45 and 60 °C, were chosen. Solvent composition and polymer concentration were kept same as that in room temperature experiments. Both the copolymer micelles showed an increase in mean core size with temperature. From 30 °C to 60 °C, that is, over a temperature range of 30 degrees, **P-3,5G2** showed overall increase of 22% in core size whereas for **P-(3,4,5)3,5G2** the increase was 38%. Change in size for both copolymer micelles was larger for the 45 °C to 60 °C step than for temperature change from 30 °C to 45 °C. However, turbidity was not observed at 60 °C in both the samples.

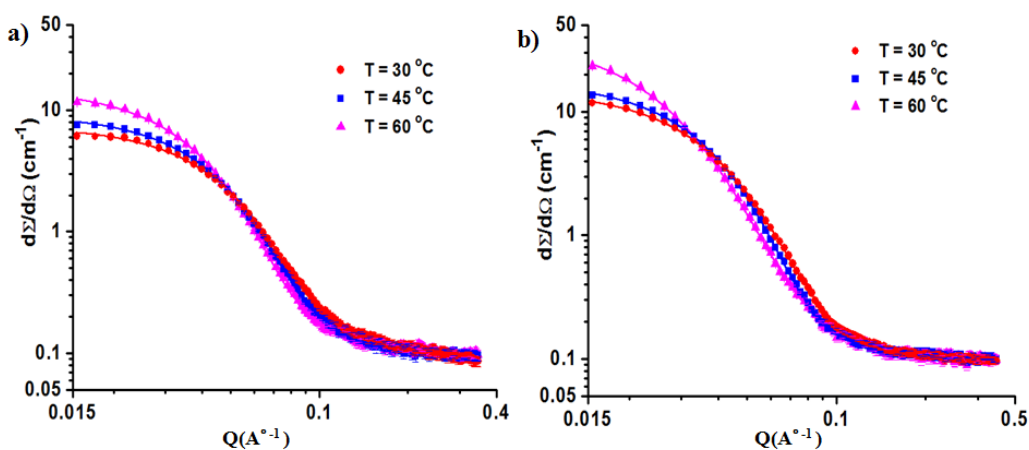


**Figure 2.11** SANS profiles for 1wt% solutions of (a) P-3,5G2 and (b) P-(3,4,5)3,5G2 in THF/D<sub>2</sub>O (10/90) at variable temperature.

Although LCST of PEG is around 100 °C, it has been reported that its solubility in water begins to decrease with increasing temperature at temperatures far lower than 100 °C.<sup>50</sup> Furthermore, temperature-responsive polymers are known to show LCST behavior in mixed solvent systems.<sup>51,52</sup> The PEG chains in the shell of micellar aggregates are in a water-rich environment and may follow the same behavior above 45 °C. As dehydration of PEG chains starts with increasing temperature, the interfacial area between hydrophobic dendron and bulk aqueous solvent increases since PEG is unable to shield the dendron. To counter this, the polymer tries to decrease the interfacial area by increasing the aggregation

number.<sup>53</sup> The increase was significantly higher in case of the polymer with more hydrophobic (3,4,5)3,5G2 dendron and consequently mean core radius of the micellar aggregate also increased.

**Table 2.6.** Fitted micellar parameters from SANS measurements of 1wt% LDBC's at different temperatures.

Temperature [°C]	Mean Core Radius [Å]	Aggregation Number N	Polydispersity $\sigma$
<i>P-3,5G2</i>			
30	43.6	47	0.23
45	46.6	57	0.24
60	53.5	87	0.25
<i>P-(3,4,5)3,5G2</i>			
30	50.3	37	0.29
45	56.9	54	0.30
60	69.5	98	0.35

### 2.3.4 Self-assembly into reverse micelles

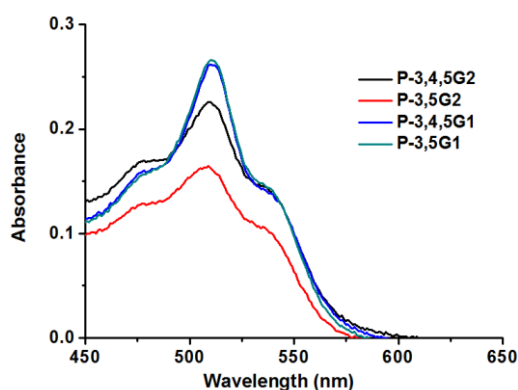


**Figure 2.12** UV-vis spectra of Rhodamine in 0.1 wt% solution of LDBC's in toluene.

Amphiphilic polymers tend to assemble in polar as well as non-polar solvents. The assemblies in non-polar solvents wherein the hydrophobic groups are in the corona and hydrophilic groups are in the core are termed as reverse micelles. LDBC's studied in this

chapter were tested for their ability to form reverse micelles. Polymers with lower generation of dendron were first studied by dissolving in toluene at 0.1 wt% and adding 5  $\mu\text{L}$  of water to solvate the PEG chains to drive them into core. Rhodamine, a hydrophilic dye was added to the solutions and UV-vis spectra were recorded after filtration. The solutions did show absorption for Rhodamine suggesting presence of reverse micelles, however the absorbance decreased with increasing generation (Figure 2.12), that is, from G1 to G2 suggesting that higher generations would limit formation of reverse micelles due to steric hindrance. Hence, the **P-3,5G3** was not studied.

### 2.3.5 Organogels

Gelation of a polymer in a solvent depends on strong solvophobic interactions that lead to physical crosslinking of polymer chains and entrapment of solvent within the network. It was thought that the difference in hydrophobic density of 3,4,5-substituted and 3,5-substituted dendrons can be utilized to test their gelation property using **P-3,4,5G2** and **P-3,5G3**. Further, to study the effect of PEG chain length, two polymers in addition to **P-3,4,5G2** were synthesized from 3,4,5G2 dendron, *viz.* **P-3,4,5G2-1K** and **P-3,4,5G2-500** containing PEG of molecular weight 1000 and 500 g/mol, respectively. To investigate the capacity of these copolymers to gel polar and non-polar solvents, solutions of **P-3,4,5G2**, **P-3,4,5G2-1K** and **P-3,4,5G2-500** were prepared in triethylene glycol (polar solvent) and in hexane (non-polar solvent) at 0.7wt% concentration. It was observed that the solution in hexane turned into a non-flowing gel at 0 °C (Figure 2.13 insets). The gels were dried and examined by scanning electron microscopy (SEM) that showed a fibrillar network like-structure for all gels (Figure 2.13).

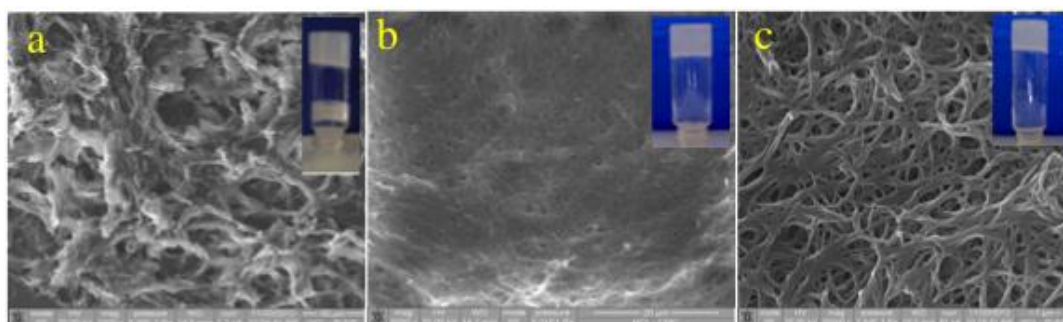


**Figure 2.13** Pictures of gels in hexane at 0.7wt% and 0°C of (a) **P-3,4,5G2**, (b) **P-3,4,5G2-1K** and (c) **P-3,4,5G2-500** and corresponding SEM images of dried gels in the insets.

Solutions of the three polymers in triethylene glycol also formed gels at room temperature that did not flow on inverting the vial (Figure 2.14).

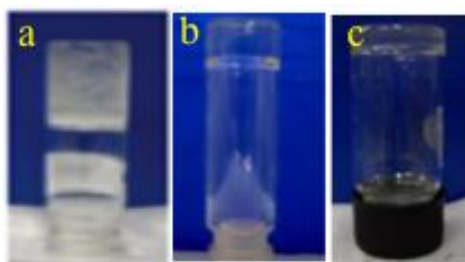


**Figure 2.14** Pictures of gels in triethylene glycol of (a) **P-3,4,5G2**, (b) **P-3,4,5G2-1K** and (c) **P-3,4,5G2-500** at 0.7wt% at room temperature.

## 2.4 Summary

A systematic study of the micellar properties of LDBC was carried out in order to elucidate the effect of hydrophobic density on the aggregation number and core size. The aim was to demonstrate that attributes of LDBC micelle core could be tuned by incorporating minor structural changes in the dendron. Dendrons with same backbone but based on two different branching patterns *viz.* 3,5-dialkoxy and 3,4,5-trialkoxy benzyl ether were synthesized and attached to PEG of fixed chain length using click chemistry. There was linear increase in number of dodecyl chains on periphery but hydrophobic density varied across the series in contrast to conventional series of dendrons prepared from a single building block. The aggregation number of the copolymer micelles number of THF molecules associated during micellization as determined from SANS measurements on solutions in THF/H<sub>2</sub>O were correlated with branching pattern of dendron that determines hydrophobic density.

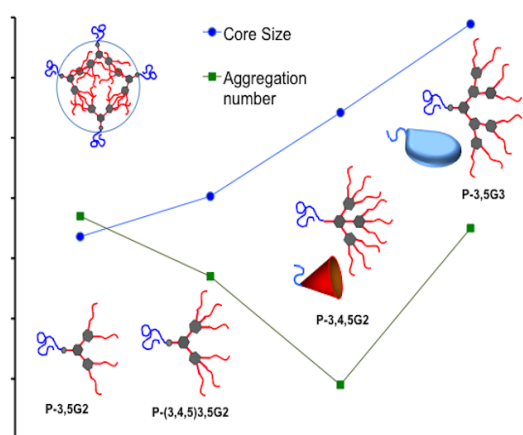


**Figure 2.15** Trend in core size and aggregation number of LDBC micelles.

The 3,4,5-dendron based copolymers showed lower aggregation numbers and higher THF molecules of solvation than 3,5-dendron based copolymers as summarized in Figure 2.15. However, micellar core size increased gradually across the series according to the dendron size. Thus, in contrast to large changes in the dye encapsulation ability of the micelles as a function of dendron generation typically seen in literature, it was shown to vary in small increments across the series of copolymers studied here. Effect of solvent on core size of **P-3,4,5(3,5)G2** and **P-3,5G2** was not prominent, however for both the copolymers core size increased with temperature. This was attributed to temperature-sensitive behavior of PEG chains. The effect of hydrophobic density was also evident in the formation of organogels where **P-3,4,5G2** formed organogels in triethylene glycol and hexane, polar and non-polar solvent, respectively, whereas **P-3,5G3** did not gel in these solvents.

## 2.5 References

- 1) Ge, Z.; Liu, S. *Macromol. Rapid Commun.* **2009**, *30*, 1523.
- 2) Peterca, M.; Percec, V.; Leowanawat, P.; Bertin, A. *J. Am. Chem. Soc.* **2011**, *133*, 20507.
- 3) Wurm, F.; Frey, H. *Prog. Polym. Sci.* **2011**, *36*, 1.
- 4) Gitsov, I. *J. Polym. Sci., Part A: Polym. Chem.* **2008**, *46*, 5295.
- 5) Jeong, M. G.; van Hest, J. C. M.; Kim, K. T.; *Chem. Commun.* **2012**, *48*, 3590.
- 6) Dong, C. M.; Liu, G. *Polym. Chem.* **2013**, *4*, 46.
- 7) Zhou, Z.; Ma, X.; Jin, E.; Tang, J.; Sui, M.; Shen, Y.; van Kirk, E. A.; Murdoch, W. J.; Radosz, M. *Biomaterials* **2013**, *34*, 5722.
- 8) Hed, Y.; Zhang, Y.; Andr n, O. C. J.; Zeng, X.; Nystr m, A. M.; Malkoch, M. *J. Polym. Sci., Part A: Polym. Chem.* **2013**, *51*, 3992.
- 9) Gillies, E. R.; Jonsson, T. B.; Fr chet, J. M. J. *J. Am. Chem. Soc.* **2004**, *126*, 11936.
- 10) Gitsov, I.; Simonyan, A.; Vladimirov, N.G. *J. Polym. Sci., Part A: Polym. Chem.* **2007**, *45*, 5136.
- 11) Chang, Y.; Kwon, Y. C.; Lee, S. C.; Kim, C. *Macromolecules* **2000**, *33*, 4496.
- 12) Kim, Y. S.; Gil, E. S.; Lowe, T. L. *Macromolecules* **2006**, *39*, 7805.
- 13) Tian, L.; Hammond, P.T. *Chem. Mater.* **2006**, *18*, 3976.

- 14) van Hest, J. C. M.; Delnoye, D. A. P.; Baars, M.W. P. L.; van Genderen, M. H. P.; Meijer, E. W. *Science* **1995**, *268*, 1592.
- 15) Gitsov, I.; Lambrych, K.R.; Remnant, V.A.; Pracitto, R. *J. Polym. Sci., Part A: Polym. Chem.* **2000**, *38*, 2711.
- 16) Lin, Y.-L.; Chang, H.-Y.; Sheng, Y.-J.; Tsao, H.-K. *Macromolecules* **2012**, *45*, 7143.
- 17) Ge, Z.; Luo, S.; Liu, S. *J. Polym. Sci., Part A: Polym. Chem.* **2006**, *44*, 1357.
- 18) Cai, H.; Jiang, G.; Chen, C.; Shen, Z.; Li, Z.; Fan, X. *Macromolecules* **2014**, *47*, 146.
- 19) Iyer, J.; Fleming, K.; Hammond, P. T. *Macromolecules* **1998**, *31*, 8757.
- 20) Nguyen, P. M.; Hammond, P. T. *Langmuir* **2006**, *22*, 7825.
- 21) Del Barrio, J.; Oriol, V.; Sánchez, C.; Serrano, J. L.; Di Cicco, A.; Keller, P.; Li, M.-H. *J. Am. Chem. Soc.* **2010**, *132*, 3762.
- 22) Röglin, L.; Lempens, E. H. M.; Meijer, E. W. *Angew. Chem., Int. Ed.* **2011**, *50*, 102.
- 23) Pati, D.; Kalva, N.; Das, S.; Kumaraswamy, G.; Sen Gupta, S.; Ambade, A. V. *J. Am. Chem. Soc.* **2012**, *134*, 7796.
- 24) Jolck, R. I.; Berg, R. H.; Anderson, T. L. *Bioconjugate Chem.* **2010**, *21*, 807.
- 25) Aswal, V. K.; Goyal, P.S. *Curr. Sci.* **2000**, *79*, 947.
- 26) Chen, S. H.; Sheu, E. Y.; Kalus, J.; Hoffmann, H. *J. Appl. Crystallogr.* **1988**, *21*, 751.
- 27) Hayter, J. B.; Penfold, J. *Colloid Polym. Sci.* **1983**, *261*, 1022.
- 28) Pedersen, J. S. *Adv. Colloid Interface Sci.* **1997**, *70*, 171.
- 29) Venicio, V. A.; Nava, B. J.; Carrion-Castro, M. P.; Rivera, E.; Mendez, I. A.; Acosta-Huerta, A.; Nava, M. G. *Polymer* **2008**, *49*, 3911.
- 30) Balagurusamy, V. S. K.; Ungar G.; Percec, V.; Johannson, G. *J. Am. Chem. Soc.* **1997**, *119*, 1539.
- 31) Zeng, X.; Ungar, G.; Liu, Y.; Percec, V.; Dulcey, A. E.; Hobbs, J. K. *Nature* **2004**, *428*, 157.
- 32) Meldal, M.; Tornøe, C. W. *Chem. Rev.* **2008**, *108*, 2952.
- 33) Kolb, H. C.; Finn, M. G.; Sharpless, K. B. *Angew. Chem., Int. Ed.* **2001**, *40*, 2004.
- 34) Kalyanasundaram, K.; Thomas, J. K. *J. Am. Chem. Soc.* **1977**, *99*, 2039.
- 35) Lejeune, E.; Drechsler, M.; Jestin, J.; Muller, A. H. E.; Chassenieux, C.; Colombani, O. *Macromolecules* **2010**, *43*, 2667.
- 36) Kelley, E. G.; X Smart, E. G.; Jackson, A. J.; Sullivan, M. O.; Epps, T. H. *Soft Matter* **2011**, *7*, 7094.

- 37) Cristobal, G.; Berret, J.-F.; Chevallier, C.; Talingting-Pabalan, R.; Joanicot, M.; Grillo, I. *Macromolecules* **2008**, *41*, 1872.
- 38) Yun, S. I.; Lai, K.-C.; Briber, R. M.; Teertstra, S. J.; Gauthier, M.; Bauer, B. J. *Macromolecules* **2008**, *41*, 175.
- 39) Aoi, K.; Motoda, A.; Okada, M. *Macromol. Rapid Commun.* **1997**, *18*, 945.
- 40) Passeno, L. M.; Mackay, M. E.; Baker, G. L.; Vestberg, R.; Hawker, C. J. *Macromolecules* **2006**, *39*, 740.
- 41) Hawker, C. J.; Wooley, K. L.; Frechet, J. M. J. *J. Am. Chem. Soc.* **1993**, *115*, 4375.
- 42) Kim, K.T.; Park, C.; Kim, C.; Winnik, M. A.; Manners, I. *Chem. Commun.* **2006**, 1372.
- 43) Abbel, R.; van der Weegen, R.; Pisula, W.; Surin, M.; Leclere, P.; Lazzaroni, R.; Meijer, E. W.; Schenning, A. P. H. J. *Chem. Eur. J.* **2009**, *15*, 9737.
- 44) Molla, M. R.; Das, A.; Ghosh, S. *Chem. Eur. J.* **2010**, *16*, 10084.
- 45) Aathimanikandan, S. V.; Savariar, E. N.; Thayumanavan, S. *J. Am. Chem. Soc.* **2005**, *127*, 14922.
- 46) Smith, D. K. *Chem. Commun.* **1999**, 1685.
- 47) Yu, Y.; Zhang, L.; Eisenberg, A. *Macromolecules* **1998**, *31*, 1144.
- 48) Kim, M. S.; Hyun, H.; Seo, K. S.; Cho, Y. H.; Lee, J. W.; Lee, C. R.; Khang, G.; Lee, H. B. *J. Polym. Sci., Part A: Polym. Chem.* **2006**, *44*, 5413.
- 49) Hocine, S.; Cui, D.; Rager, M.-N.; Di Cicco, A.; Liu, J. M.; Wdzieczak-Bakala, J.; Brûlet, A.; Li, M.-H. *Langmuir* **2013**, *29*, 1356.
- 50) Hocine, S.; Li, M.-H. *Soft Matter* **2013**, *9*, 5839.
- 51) Hao, J.; Cheng, H.; Butler, P.; Zhang, L.; Han, C. C. *J. Chem. Phys.* **2010**, *132*, 154902.
- 52) Yamauchi, H.; Maeda, Y. *J Phys. Chem. B.* **2007**, *111*, 12964.
- 53) Zhang, L.; Eisenberg, A. *Macromolecules* **1996**, *29*, 8805.

## **Chapter 3**

### **Tuning Micellar Core Properties of Linear-Dendritic Block Copolymers using Photoresponsive Dendron**



### 3.1 Introduction

Photoresponsive polymers are an important class of functional materials due to their potential applications in various fields such as liquid crystal displays,<sup>1-3</sup> optical data storage,<sup>4-5</sup> and drug delivery systems.<sup>6-9</sup> Light as a stimulus can be triggered at a specific position easily and precisely at the desired time that allows the properties of photoresponsive polymers such as conformation and polarity to be reversibly altered. This is achieved through incorporation of chromophores such as azobenzene that shows geometrical isomerism or dithienyl ethene and spiropyran that switch between ring opening and closing.<sup>10</sup> The change in polarity or conformation of the polymer may cause release of the encapsulated guest molecule. Hence, photoresponsive polymer assemblies are being explored as controlled release systems.

Azobenzene is one of the most widely studied chromophore by polymer chemists due to its fast and reversible photoisomerisation.<sup>11</sup> The *trans* isomer is converted to *cis* isomer upon exposure to UV light and the process is reversed upon illumination with visible light or thermally by storage in the dark. *Cis*-isomer of azobenzene is more polar due to higher dipole moment and hence the photoisomerisation leads to imbalance in hydrophilic/hydrophobic ratio of the polymer. This can be exploited to cause complete disruption or morphology changes in polymer assemblies.<sup>12</sup> The *trans-cis* conversion may also lead to change in polarity of micellar core without disruption and the encapsulated guest is released. However, some of the released dye may re-enter the micellar core during isomerisation of *cis* to *trans* form due to reversal of polarity and affect the net dye release. This *cis-trans* isomerisation has been carried out by either photoirradiation<sup>13</sup> or thermal<sup>6, 14, 24</sup> pathway to study the net dye release. Recently, micelles from a dendronized polymer with azobenzene in the side chain were subjected to a series of *trans-cis-trans* photocycles with intermittent thermal restoration and it was shown that amount of dye released could be controlled by varying the time of restoration.<sup>15</sup>

Incorporation of light-responsive moieties has been less explored in LDBC's compared to other architectures. Azobenzene-containing amphiphilic LDBC's with 4-cyanoazobenzene on dendron periphery were shown to self-assemble in water into morphologies such as cylindrical micelles, sheet like micelles, tubular micelles and polymersomes with increasing dendron generation.<sup>16</sup> Later, similar polymers with 4-isobutyloxyazobenzene on periphery were shown to form stable vesicles in water and significant membrane

deformation and subsequent dye release upon UV light irradiation was investigated.<sup>17</sup> Dye release could be tuned by varying the content of 4-isobutyloxyazobenzene on periphery.<sup>18</sup> In these reports, *cis*-to-*trans* isomerization was effected by incubating the sample in dark.

In all of the above reports, the photoresponsive LDBC's contain azobenzene unit at the periphery of the dendron. It was hypothesized that incorporation of azobenzene units in the dendron interior at the desired position would afford micellar assemblies wherein polarity of the micellar core could be tuned in a controlled manner using photoirradiation. By varying the position and number of azobenzenes it may be possible to exert fine control over the dye release. In this chapter, amphiphilic LDBC's were designed and synthesized with variation in position of azobenzene in the dendron structure. Towards a systematic structure-property relationship study, different hydrophobic groups were installed on the dendron periphery. Photoinduced dye release from copolymer micelles was found to depend on number of azobenzene units as well as the nature of hydrophobic groups. *Cis*-*trans* isomerization in the photoisomerization cycle was carried out by photo as well as thermal pathway and the extent of dye release in the respective photocycle was compared.

## 3.2 Experimental section

### 3.2.1 Materials

3,5 dihydroxy benzyl alcohol, 4-aminobenzyl alcohol, Methoxy-PEG ( $M_n = 2000 \text{ g mol}^{-1}$ , PDI = 1.1), dodecyl bromide, Copper (I) bromide, PMDETA, propargyl bromide, lithium aluminium hydride and Nile red were purchased from Aldrich Chemicals Co. benzyl bromide, triphenyl phosphine, carbon tetrabromide, 18-crown-6 ether, phenol, sodium azide, potassium carbonate and triethylamine were purchased from Avra Chemicals, Spectrochem and Merck Chemicals, India. Dichloromethane was dried over  $\text{CaH}_2$  and acetone was dried over  $\text{K}_2\text{CO}_3$ , distilled and stored in a Schlenk flask. THF was passed through alumina, dried on sodium wire and freshly distilled. All compounds were purified using column chromatography on silica gel (mesh size 60–120 and 220–440).

### 3.2.2 Instrumentation

GPC analysis was performed using Viscotek instrument comprising VE 1122 pump, VE 3580 RI detector, and VE 3210 UV-vis detector in THF using polystyrene as standards. Fluorescence emission spectra were recorded on CARY Eclipse spectrometer. Philips

TUV 8W lamp and Naava LT 6W T5 lamp were used for 365 nm and 450 nm irradiation, respectively. For dye release studies, a 100W UV lamp equipped with 365 nm filter (intensity  $21000 \mu\text{W cm}^{-2}$ ) was used. DLS experiments were performed on (Zetasizer Nano ZS, Malvern) instrument equipped with a 633nm He-Ne laser.

### 3.2.3 Synthetic procedures and characterization data

Precursors to dendron with benzyl ether on periphery were synthesized by reported procedure.<sup>19</sup> Procedures and data for compounds with dodecyloxy group are given below. 3,5-didodecyloxybenzyl alcohol was synthesized using our earlier method.<sup>20</sup>

**Compound 1:** 3,5-didodecyloxybenzyl alcohol (1 g, 2.1 mmol) was dissolved in dry THF and triphenyl phosphine (0.82 g, 3.1 mmol),  $\text{CBr}_4$  (1.04 g, 3.1 mmol) was added and stirred at  $0^\circ\text{C}$  for 30 min. The reaction was monitored by the TLC. After completion of the reaction, evaporated the solvent under reduced pressure washed with water and extracted with dichloromethane and dried over anhydrous sodium sulfate. Solvent was evaporated on rotary evaporator under reduced pressure. The crude product was purified by flash column chromatography by eluting with 10% ethyl acetate and pet ether. This compound was used for the next step without characterization. Yield: 80%.

**Compound 2:** Compound 1 (2.67 g, 11.7 mmol) (5.4 g, 14 mmol) were dissolved in 50 mL dry acetone, added the  $\text{K}_2\text{CO}_3$  (3.74 g, 28 mmol) and 18-Crown-6 ether (0.6 g, 2.3 mmol) reflux for 24 h. After completion of the reaction solvent was removed under the reduced pressure and extract the product in ethyl acetate. Organic layer was dried over sodium sulfate and solvent was evaporated under reduced pressure. The crude product was purified by column chromatography in 20% ethyl acetate and pet ether. Yield 80%.  $^1\text{H}$  NMR (200.13 MHz,  $\text{CDCl}_3$ )  $\delta$ : 0.89(s, 6H,  $-\text{CH}_2$ ), 1.27(s, 36H,  $-\text{CH}_2$ ), 1.77(m, 4H), 3.95(t, 4H,  $J=6\text{Hz}$ ), 4.78(d, 2H,  $J=2\text{Hz}$ ), 5.08(s, 2H), 6.43(s, 1H), 6.58(s, 2H), 7.06(d, 2H,  $J=10\text{Hz}$ ), 7.53-(d, 2H,  $J=10\text{Hz}$ ), 7.87-7.94(t, 4H,  $J=6\text{Hz}$ ) ppm.  $^{13}\text{C}$  NMR ( $\text{CDCl}_3$ , 50.32 MHz): 14.16, 22.73, 26.08, 29.64, 31.96, 64.98, 68.13, 70.31, 100.87, 105.67, 115.16, 122.82, 124.76, 127.47, 138.61, 143.19, 147.13, 152.25, 160.61, 161.23 ppm.

**Compound 3:** Compound **2** (5 g, 7.2 mmol) was dissolved in dry THF and triphenyl phosphine (2.86 g, 10.9 mmol), CBr<sub>4</sub> (3.61 g, 10.9 mmol) was added and stirred at 0 °C for 30 min. The reaction was monitored by TLC. After completion of the reaction, the solvent was evaporated under reduced pressure, product was washed with water, extracted with dichloromethane and dried over anhydrous sodium sulfate. Solvent was evaporated on rotary evaporator under reduced pressure. The crude product was purified by flash column chromatography by eluting with 20% ethyl acetate and pet ether. This compound was further used for the next step. Yield 70 %.

**Compound 4:** Compound **3** (3.7 g, 4.9 mmol), 3,5 dihydroxy benzyl alcohol (0.314 g, 2.2 mmol) were dissolved in 50 mL of dry acetone-THF (1:1) mixture, K<sub>2</sub>CO<sub>3</sub> (1.24 g, 8.9 mmol) and 18-Crown-6 ether (0.118 g, 0.4 mmol) were added and refluxed for 24 h. After completion of the reaction solvent was removed under reduced pressure and the product was extracted in dichloromethane. Organic layer was dried over sodium sulfate and solvent was evaporated under reduced pressure. The crude product was purified by flash column chromatography in 20% ethyl acetate and pet ether. Yield 75%. <sup>1</sup>H NMR (200.13 MHz, CDCl<sub>3</sub>) δ: 0.89(s, 12H, -CH<sub>2</sub>), 1.27(s, 72H, -CH<sub>2</sub>), 1.75(m, 8H), 3.95(t, 8H, J=6Hz), 4.64(d, 2H, J=8Hz), 5.08(m, 8H), 6.43(s, 2H), 6.59-6.66(m, 7H, Ar-H), 7.06(d, 4H, J=10Hz), 7.53(d, 4H, J=10Hz), 7.88-7.94(m, 8H) ppm. <sup>13</sup>C NMR (CDCl<sub>3</sub>, 50.32 MHz) δ: 14.17, 22.74, 26.09, 29.68, 31.96, 68.13, 70.32, 100.88, 101.42, 105.67, 115.16, 122.85, 124.81, 127.97, 138.60, 147.13, 152.44, 160.04, 160.61, 161.29 ppm.

**Compound 5:** 4-(4'-hydroxy phenylazo) benzyl alcohol (2 g, 8.7 mmol), dodecyl bromide (2.61 g, 10.5 mmol) were dissolved in 50 mL of dry acetone:THF mixture (1:1), K<sub>2</sub>CO<sub>3</sub> (4.8 g, 28 mmol) and catalytic amount of KI were added and refluxed for 24 h. After completion of the reaction solvent was removed under reduced pressure, product was extracted in ethyl acetate. Organic layer was dried over sodium sulphate and solvent was evaporated under reduced pressure. The crude product was purified by column chromatography in 10% ethyl acetate and pet ether. Yield 80%. <sup>1</sup>H NMR (200.13 MHz, CDCl<sub>3</sub>) δ: 0.89(s, 3H,-CH<sub>2</sub>), 1.28(m, 18H, -CH<sub>2</sub>), 1.78(m, 4H), 4.05(t, 2H, J=6Hz), 4.77(d, 2H, J=2Hz), 6.99(d, 2H, J=8Hz), 7.48(d, 2H, J=8Hz), 7.86( t, 4H, J=8Hz) ppm. <sup>13</sup>C NMR

(CDCl<sub>3</sub>, 50.32 MHz): 14.16, 22.73, 26.04, 29.67, 31.95, 65.00, 68.41, 114.73, 122.78, 124.78, 127.48, 143.06, 146.84, 152.3, 161.77 ppm.

**Compound 6:** Compound 5 (1.8 g, 4.5 mmol) was dissolved in dry THF and triphenyl phosphine (1.78 g, 6.6 mmol), CBr<sub>4</sub> (2.2 g, 6.6 mmol) was added and stirred at 0 °C for 30 min. After completion of the reaction as indicated by TLC, solvent was evaporated under reduced pressure, crude product was washed with water and extracted with DCM. Organic layer was dried over anhydrous sodium sulfate. Solvent was evaporated on rotary evaporator under reduced pressure. The crude product was purified by flash column chromatography by eluting with 20% ethyl acetate and pet ether. Yield 70 %. Product was directly used for next step.

**Compound 7:** Compound 6 (1.5 g, 3.2 mmol), 3,5 dihydroxy benzyl alcohol (0.207 g, 1.4 mmol) were dissolved in 40 mL dry acetone:THF mixture (1:1). K<sub>2</sub>CO<sub>3</sub> (0.82 g, 5.8 mmol) and 18-Crown-6 ether (0.072 g, 0.2 mmol) were added and refluxed for 24 h. solvent was removed under reduced pressure and product was extracted in dichloromethane. Organic layer was dried over sodium sulphate and solvent was evaporated on rotary evaporator. Crude product was purified by flash column chromatography in 20% ethyl acetate and pet ether. <sup>1</sup>H NMR (200.13 MHz, CDCl<sub>3</sub>) δ: : 0.89(s, 6H, -CH<sub>2</sub>), 1.28(bs, 36H, -CH<sub>2</sub>), 1.83(m, 4H), 4.05(t, 4H, J=6Hz), 4.67(d, 2H, J=4Hz), 5.13(s, 4H), 6.57(s, 1H), 6.66(d, 2H, J=2Hz), 6.99(d, 4H, J=8Hz), 7.53(d, 4H, J=8Hz), 7.88-7.94( m, 8H) ppm. <sup>13</sup>C NMR (CDCl<sub>3</sub>, 50.32 MHz): 14.15, 22.72, 26.04, 29.67, 31.95, 64.61, 68.41, 69.68, 105.92, 114.73, 122.80, 124.81, 127.96, 143.59, 146.85, 152.49, 160.04, 161.82 ppm. Yield 75%.

**Compound 8:** Synthesis was carried out by following same procedure as for compound 6. Yield 65%.

**Compound 9:** Compound 7 (2 g, 2.08 mmol), 3,5 dihydroxy benzyl alcohol (0.132 g, 0.9 mmol) were dissolved in 60 mL of dry acetone:THF mixture (1:1), K<sub>2</sub>CO<sub>3</sub> (0.527 g, 3.7 mmol) and 18-Crown-6 ether (0.049 g, 0.18 mmol) were added reflux for 24 h. <sup>1</sup>H NMR (200.13 MHz, CDCl<sub>3</sub>) δ: 0.89(t, 12H, J=6Hz), 1.28(bs, 72H, -CH<sub>2</sub>), 1.82(m, 8H), 4.03(t,

8H, J=6Hz), 4.58(d, 2H, J=4Hz), 4.98(s, 4H), 5.11(s, 8H), 6.53-6.67(m, 9H), 6.97(d, 2H, J=2Hz), 6.99(d, 8H, J=8Hz), 7.50(d, 8H, J=8Hz), 7.88-7.93(t, 16H, J=8Hz) ppm.  $^{13}\text{C}$  NMR ( $\text{CDCl}_3$ , 50.32 MHz): 14.15, 22.72, 26.04, 29.67, 31.95, 61.9, 63.36, 65.27, 68.41, 69.69, 101.78, 105.93, 114.73, 122.80, 124.81, 127.96, 143.59, 146.85, 152.49, 160.04, 161.82 ppm. Yield 79%.

### ***General procedure for synthesis of alkyne-azo-dendrons***

In a dry three-necked round bottom flask NaH (1.2mol, 60% suspension in mineral oil) was taken and washed with hexanes under argon. Dry THF followed by dendron with benzyl alcohol at the focal point (1 mol) were added and stirred for 10 min followed by addition of propargyl bromide (1.1mol). The reaction mixture was stirred for 12h and poured in water and extracted with dichloromethane, organic layer was washed with water, brine and dried over anhydrous sodium sulphate before concentrating on rotary evaporator. The crude product was purified by precipitating it in cold diethyl ether.

**Dendron D1:**  $^1\text{H}$  NMR (200 MHz,  $\text{CDCl}_3$ )  $\delta$ : 2.48(t, 1H, J=2Hz), 4.1(d, 2H, J=4Hz), 4.58(s, 2H,  $-\text{CH}_2$ ), 5.06-5.14(m, 16H,  $-\text{CH}_2$ ), 6.61-6.71(m, 9H, Ar H), 7.05(d, 4H, J=8Hz), 7.36-7.42(m, 20H, Ar H), 7.54(d, 4H, J=8Hz), 7.89-7.93(m, 8H, Ar H) ppm.  $^{13}\text{C}$  NMR ( $\text{CDCl}_3$ , 50.32 MHz) : 57.17, 69.71, 70.20, 71.41, 74.78, 101.77, 106.41, 107.14, 115.20, 122.85, 124.83, 127.57, 128.64, 136.78, 138.94, 139.22, 147.23, 152.48, 159.99, 160.29, 161.19 ppm. MALDI-TOF MS: Calcd. 1203.41 Found 1203.39 for  $[\text{M}^+]$ . Yield 80%.

**Dendron D2:**  $^1\text{H}$  NMR (200 MHz,  $\text{CDCl}_3$ )  $\delta$ : 0.89(t, 12H, J=6Hz), 1.27(bs, 72H), 1.78(m, 8H), 2.48(t, 1H, J=2Hz), 3.95(t, 8H, J=6Hz), 4.19(t, 2H, J=2Hz), 4.58(s, 2H), 5.08-5.13(m, 8H,  $-\text{ArCH}_2$ ), 6.43(s, 2H, Ar H), 6.59-6.65(m, 7H), 7.06(d, 4H, J=10Hz), 7.54(d, 4H, J=8Hz), 7.88-7.92(m, 8H, Ar H) ppm.  $^{13}\text{C}$  NMR ( $\text{CDCl}_3$ , 50.32 MHz): 14.17, 22.74, 26.09, 29.29, 29.64, 31.96, 57.14, 62.96, 68.15, 70.34, 74.78, 100.91, 105.69, 107.09, 115.18, 122.85, 124.82, 128.03, 138.63, 138.63, 139.17, 147.16, 152.46, 159.98, 160.63, 161.30 ppm. MALDI-TOF MS: Calcd. 1516.20 Found 1538.85 for  $[\text{M}^+ + \text{Na}^+]$ . Yield 78%.

**Dendron D3:**  $^1\text{H}$  NMR (200 MHz,  $\text{CDCl}_3$ )  $\delta$ : 0.89(t, 12H, J=6Hz), 1.27(bs, 72H), 1.78(m, 8H), 2.46(t, 1H, J=2Hz), 4.04(t, 8H, J=6Hz), 4.16(d, 2H, J=2Hz), 4.55(s, 2H), 4.99(s, 4H),

5.12(s, 8H, -ArCH<sub>2</sub>), 6.60-6.70(m, 9H), 6.98(d, 8H, J=8Hz), 7.52(d, 8H, J=8Hz), 7.87-7.93(m, 16H, Ar-H) ppm. <sup>13</sup>C NMR (CDCl<sub>3</sub>, 125.76 MHz): 14.51, 23.09, 26.43, 29.61, 30.07, 32.33, 57.52, 68.80, 70.31, 71.82, 75.11, 80.02, 102.18, 106.90, 107.43, 111.53, 115.12, 123.18, 125.19, 128.36, 139.41, 139.88, 147.27, 152.87, 160.44, 162.19 ppm. MALDI-TOF MS: Calcd. 1936.11 Found 1958.92 for [M<sup>+</sup> + Na<sup>+</sup>]. Yield 82%.

***General procedure for CuAAC reaction between alkyne-azo-dendron and azide-functionalised PEG***

To a solution of alkyne functionalised dendron (1.2 eq) in a mixture of THF and MeOH (8:2) was added the azide-PEG<sub>2K</sub> and resultant mixture was degassed for 15 min. CuBr (1 eq) and PMDETA (1 eq) were then added and allowed to stir for 24 hr under argon atmosphere. The progress of the reaction was monitored by the disappearance of azide stretching frequency at 2105 cm<sup>-1</sup>. Organic layer was concentrated under reduced pressure. Copper salts were removed by passing through neutral alumina. Crude product was purified by precipitating in cold diethyl ether. The obtained orange-coloured solid was dried under high vacuum. Yield 65%.

**Polymer P1:** <sup>1</sup>H NMR (400.13 MHz, CDCl<sub>3</sub>) δ: 3.38(s, 3H), 3.64(bs, 174H), 4.52-4.55(m, 4H), 4.68(s, 2H, -CH<sub>2</sub>), 5.04-5.12(m, 16H, -CH<sub>2</sub>), 6.58-6.70(m, 9H, Ar H), 7.04(d, 4H, J=12Hz), 7.30-7.42(m, 20H, Ar H), 7.53(d, 4H, J=8Hz), 7.74(s, 1H, Triazole), 7.88-7.91(m, 8H, Ar H) ppm. <sup>13</sup>C NMR (CDCl<sub>3</sub>, 50.32 MHz) : 50.32, 59.11, 63.76, 69.55, 69.74, 70.24, 70.66, 72.04, 72.31, 101.61, 106.44, 106.99, 114.78, 115.24, 122.89, 123.90, 124.86, 127.61, 128.68, 136.82, 138.98, 139.33, 140.69, 144.94, 147.25, 152.49, 160.02, 160.33, 161.23 ppm. Yield 80%. MALDI-TOF MS: Calcd. 1515.05 Found 1538.86 for [M<sup>+</sup> + Na<sup>+</sup>].

**Polymer P2:** <sup>1</sup>H NMR (400.13 MHz, CDCl<sub>3</sub>) δ: 0.88(t, 12H, J=8Hz), 1.26(bs, 72H), 1.77(m, 8H), 3.38(s, 8H), 3.64(bs, 172H), 3.96(t, 8H, J=8Hz), 4.55(m, 4H), 4.68(s, 2H, -ArCH<sub>2</sub>), 5.07-5.12(m, 8H), 6.42(s, 2H, Ar H), 6.58-6.66(m, 7H), 7.07(d, 4H, J=8Hz), 7.54(d, 4H, J=8Hz), 7.75(s, 1H, Triazole), 7.88-7.92(m, 8H, Ar H) ppm. <sup>13</sup>C NMR (CDCl<sub>3</sub>, 50.32 MHz): 14.23, 22.78, 26.14, 29.34, 29.44, 29.73, 32.01, 59.13, 62.98, 63.62, 64.28,

68.20, 70.66, 105.76, 115.23, 122.90, 124.87, 128.09, 138.68, 160.69 ppm. MALDI-TOF MS: Calcd. 1515.05 Found 1538.86 for  $[M^+ + Na^+]$ .

**Polymer P3:**  $^1H$  NMR (400.13 MHz,  $CDCl_3$ )  $\delta$ : 0.88(t, 12H,  $J=8Hz$ ), 1.27-1.47(m, 72H), 1.82(m, 8H), 3.38(s, 3H), 3.65(bs, 172H), 4.03(t, 8H,  $J=8Hz$ ), 4.54(m, 4H), 4.67(s, 2H), 4.99(s, 4H), 5.11(s, 8H, -ArCH<sub>2</sub>), 6.52-6.70(m, 9H), 6.98(d, 8H,  $J=8Hz$ ), 7.52(d, 8H,  $J=8Hz$ ), 7.73(s, 1H, Triazole), 7.86-7.89(m, 16H, Ar-H) ppm.  $^{13}C$  NMR ( $CDCl_3$ , 125.76 MHz): 14.22, 22.79, 26.12, 29.32, 29.45, 29.76, 32.02, 50.35, 59.12, 63.77, 68.51, 69.83, 70.68, 72.06, 72.40, 101.87, 106.61, 114.83, 122.87, 123.91, 124.89, 128.08, 139.13, 139.64, 146.97, 152.57, 160.15, 161.90 ppm.

### 3.2.4 Preparation of polymer aqueous solution and Nile red encapsulation

Aqueous solutions of the polymer were prepared by dialysis method. Polymer was first dissolved in tetrahydrofuran which is good solvent for both dendron as well as linear polymer and stirred for 2h at room temperature. Then water was added drop by drop to reach 0.1 wt% of the final polymer concentration. The final solution was transferred to dialysis tubing (MWCO = 3500) and dialyzing against water for 3 days to remove THF completely. For determination of cmc, Nile red ( $5 \times 10^{-6}$  M) was encapsulated in a micellar solution by hydrating a film of the dye using 0.1 wt% polymer solution. This solution was diluted to obtain a series of concentrations and fluorescence emission spectra of Nile red were recorded. cmc was determined by extrapolating the tangents to the emission intensity versus log (conc.) curve.

### 3.2.5 Nile red encapsulation capacity experiment

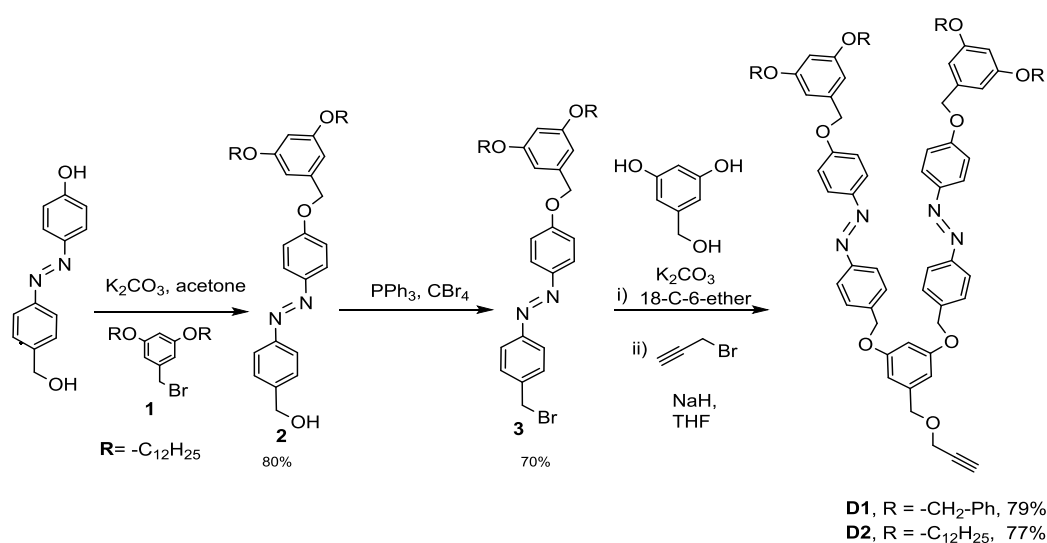
A thin film of the dye (0.5 mg) was prepared in each vial by solvent evaporation and vials were dried under vacuum for 5h. Then 0.5 wt% of aqueous solution of the polymer was added and stirred at room temperature for 12h. The insoluble dye was filtered through 0.45 $\mu$ m PVDF filter. From these solutions a known volume (0.5 mL) was taken into vials and lyophilized. The lyophilized samples were dissolved in methanol (4 mL) and absorption spectrum was recorded. The concentration of the dye was found by using reported value for molar extinction coefficient of the dye in methanol.



### 3.3 Results and discussion

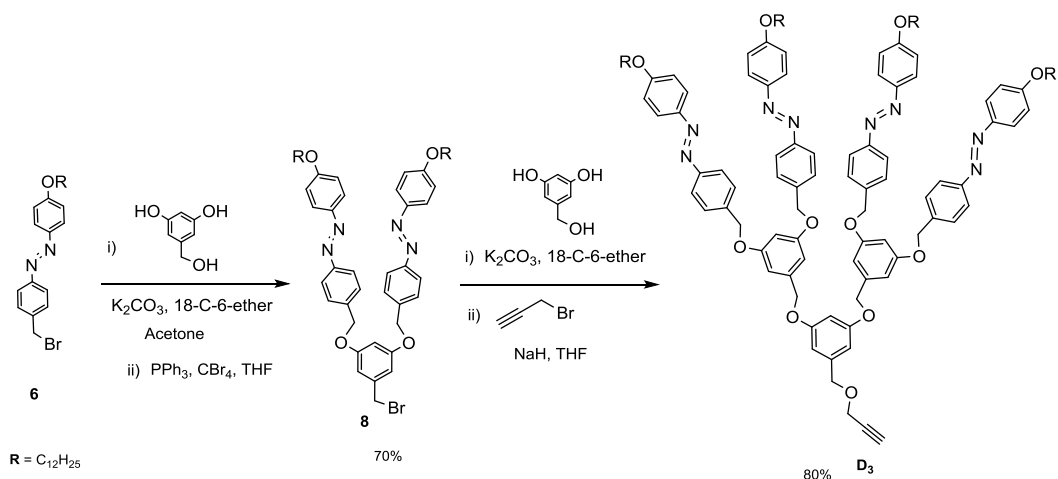
#### 3.3.1 Synthesis

Second-generation hydrophobic dendrons with azobenzene units in the dendritic backbone were synthesized by convergent approach for benzyl ether dendrons. Two dendrons comprising two azobenzene units in the interior and either benzyl group (**D1**) or dodecyl chains (**D2**) on the periphery were synthesized as shown in Scheme 3.1.



**Scheme 3.1** Synthesis of dendrons containing two azobenzene units.

To achieve variation in number of azobenzenes but with similar periphery, another dendron containing four azobenzene units and dodecyl chains on the periphery (**D3**) was also synthesized as shown in Scheme 3.2. Alkyne functionality was installed at the focal point of dendrons in the last step. Monomethoxy PEG functionalized with azide at one end was attached to alkyne-functionalized azo-dendrons by using CuAAC, an efficient coupling method for polymers. The obtained polymers **P1**, **P2** and **P3**, chemical structures of which are shown in Chart 3.1, were purified by precipitation in cold diethyl ether.



**Scheme 3.2** Synthesis of dendrons containing four azobenzene units.

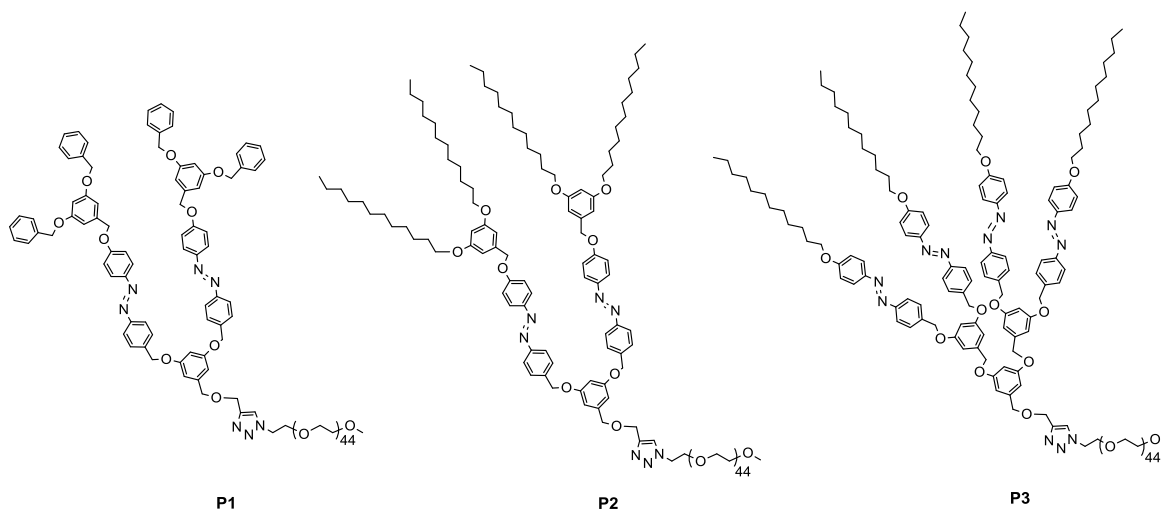


**Chart 3.1** Chemical structures of synthesized polymers.

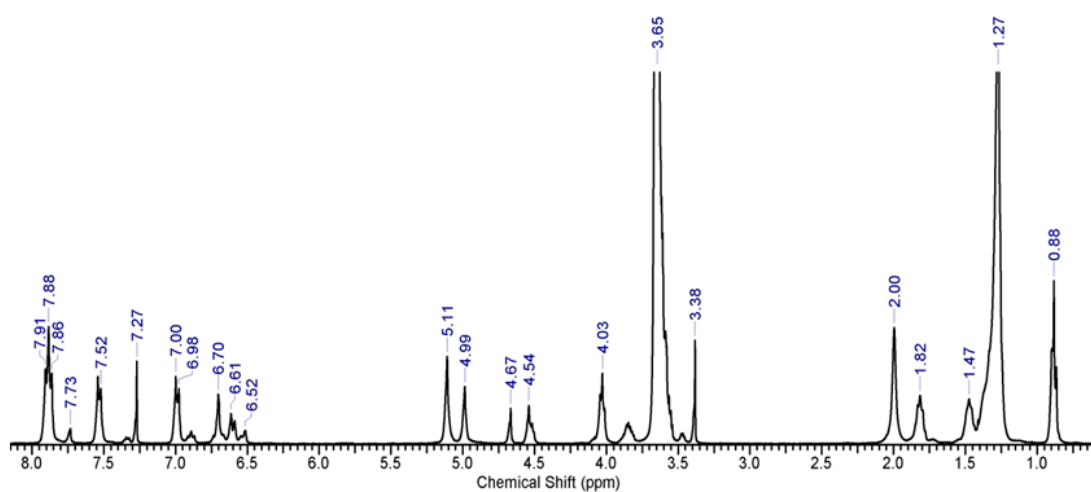


**Figure 3.1:** 200 MHz  $^1\text{H}$  NMR spectrum of **P3** in  $\text{CDCl}_3$ .

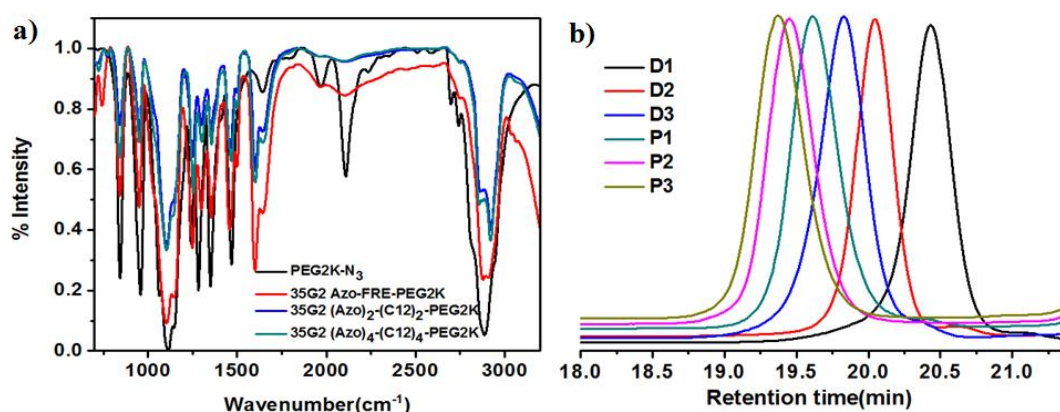


**Figure 3.2** (a) FT-IR spectra for the click reaction. (b) Overlay of GPC chromatograms of **P1-P3** and corresponding dendrons **D1-D3**.

The polymers were characterized by <sup>1</sup>H NMR, <sup>13</sup>C NMR, and MALDI-TOF techniques to ascertain their structural integrity (see Appendix II). <sup>1</sup>H NMR spectra revealed signals for protons of dendron and PEG as well as for the triazole ring proton (7.73 ppm) formed during the click reaction (Figure 3.1). Absence of azide group was confirmed from FT-IR spectra (Figure 3.2a) that showed complete disappearance of the band at 2100 cm<sup>-1</sup>. GPC analysis revealed monomodal peaks that confirmed the purity of polymers (Figure 3.2b).

### 3.3.2 Self-assembly in water

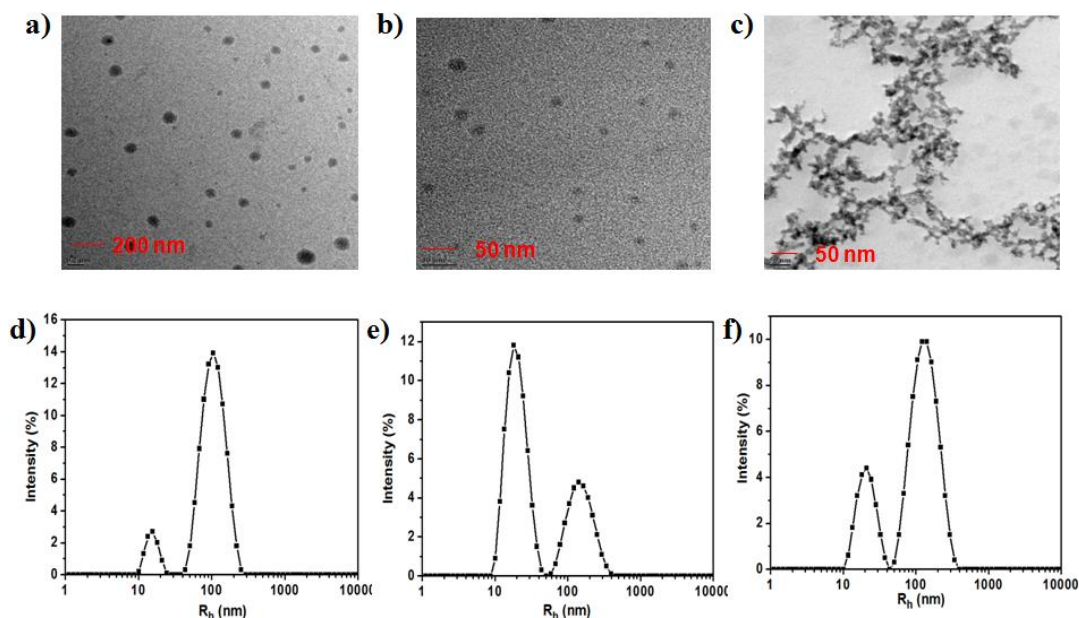


**Figure 3.3** TEM images (a) (b) (c) and DLS size distribution curves (d) (e) (f) of 0.1 wt% aqueous solution of **P1**, **P2** and **P3**, respectively.

Aqueous solutions of the amphiphilic block copolymers were prepared by the dialysis method at a concentration of 0.1 wt%. Water was slowly added to a solution in THF to induce aggregation and the mixture was dialyzed against water to remove THF completely. The micellar aggregates are expected to comprise hydrophobic azo-dendrons in the micellar core and PEG chains in the corona in water. DLS technique was used to check the presence of aggregates and the analysis showed that average hydrodynamic size ( $D_h$ ) of **P1** and **P3** micelles was similar however, **P2** micelles were much smaller while the polydispersity of aggregates increased from **P1** to **P3**, respectively (Table 3.1). Size distribution curves based on intensity average for all polymers were bimodal, however in case of **P2** the peak at lower size (10-40 nm) was the major component (Figure 3.3d) while the peak at larger size (70-300 nm) was major for **P1** (Figure 3.3b) even though both **P1** and **P2** have same position and number of azobenzene units. The smaller size of **P2** micelles among all three polymers is probably due to higher hydrophobicity of dodecyl chains and compact nature of the dendron.

**Table 3.1** Characterization data for micellar assemblies of polymers

Polymer	$W_{\text{philic}}$	$D_h$ (nm)	PDI	cmc (M) $\times 10^{-5}$
<b>P1</b>	62.8	77	0.30	2.50
<b>P2</b>	57.3	26	0.41	1.25
<b>P3</b>	51.5	70	0.54	0.89

The morphology of the aggregates was then investigated by TEM analysis that revealed spherical aggregates for **P1** and **P2**. Aqueous solution of **P1** showed aggregates of size 137 nm (Figure 3.3a) while solution of **P2** showed similar aggregates with size of 22 nm (average of 40 particles as measured from TEM images) (Figure 3.3c). Polymer **P3** showed network-like aggregates in the TEM analysis.

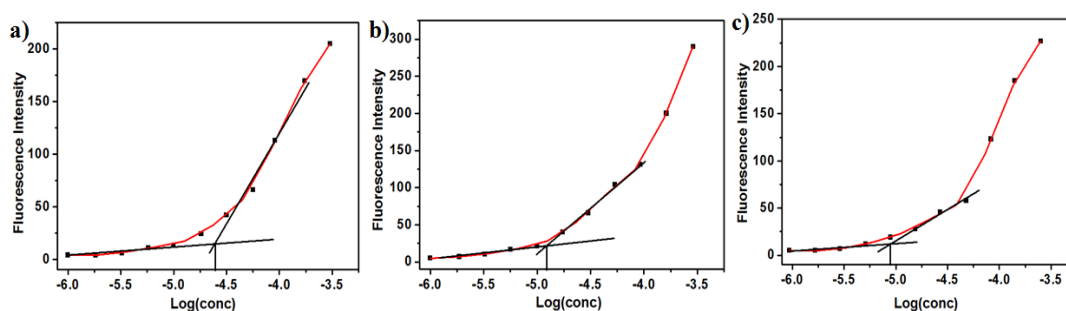


**Figure 3.4** Plots of fluorescence intensity vs. log (conc.) for (a) **P1** (b) **P2** and (c) **P3**.

The cmc of polymer assemblies was determined by using Nile red as hydrophobic solvatochromic probe. Absorption and emission maxima of Nile red are well separated from the azobenzene absorption spectra therefore it could be used for determination of cmc. The values for cmc were in the range of  $10^{-5}$  M as determined from the intensity vs.  $\log(\text{conc.})$  plot that are typical for amphiphilic macromolecules and decrease from **P1** to **P3** with increasing hydrophobicity (Table 3.1).

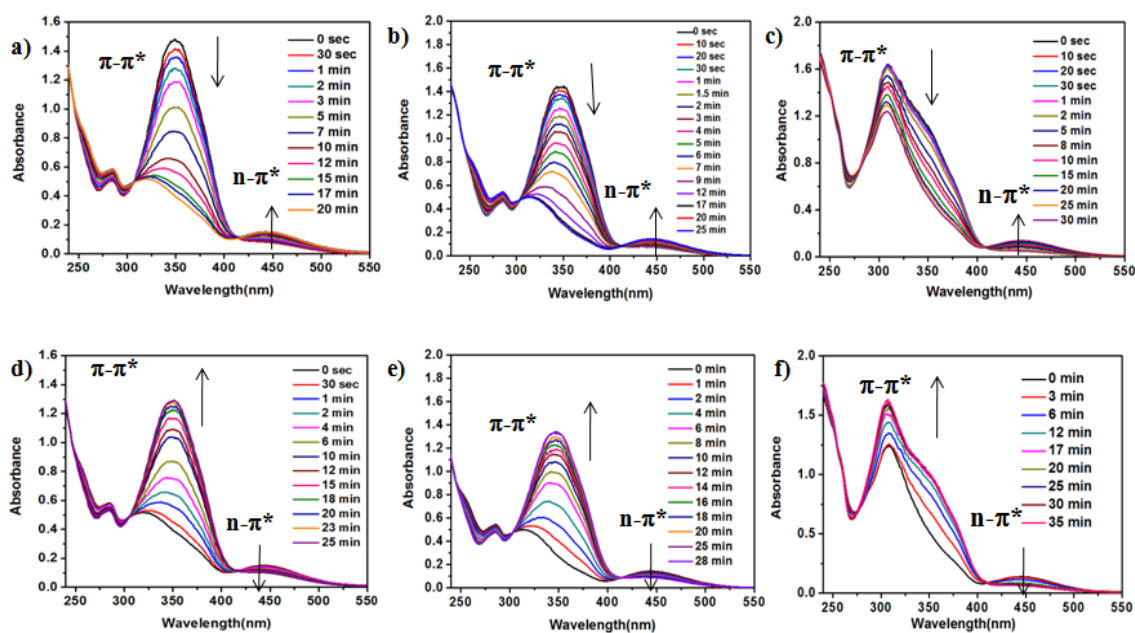


**Figure 3.5** UV-vis spectra for irradiation of 0.02 wt% aqueous solution of (a) **P1** (b) **P2** (c) **P3** with 365 nm light (8W lamp) and of (d) **P1** (e) **P2** (f) **P3** with 450 nm light (6W lamp).

### 3.3.3 Azobenzene isomerization in micelles

Light-responsive behaviour of the aggregates was investigated by irradiating the aqueous solution (0.02 wt%) with UV and visible light. For *trans* to *cis* photoisomerization of azobenzene the solution was irradiated with 365 nm light (8W lamp) and UV-vis spectra were recorded at different irradiation times. For **P1** and **P2** with increasing irradiation time absorption at the  $\pi$ - $\pi^*$  transition peak at 350 nm decreased and the weak  $n$ - $\pi^*$  transition peak at 450 nm increased indicating the isomerization of azobenzene from *trans* to *cis* form (Figures 3.4a and b). UV-vis spectra of **P3** revealed presence of H-type aggregates of azobenzene in the micellar core by the presence of blue-shifted  $\pi$ - $\pi^*$  transition peak with  $\lambda_{\text{max}}$  at 308 nm.<sup>21</sup> This peak had a shoulder at 350 nm suggesting the presence of free azobenzene, that is, azobenzene units that were not part of H-type aggregates. Irradiation of **P3** solution with 365 nm light resulted in decrease of absorbance

of 308 nm peak and increase in the absorbance at 450 nm peak indicating *trans-cis* isomerization of free as well as bound (H-aggregate) azobenzene chromophores (Figure 3.4c). The extent of *trans* to *cis* isomerization (photostationary state, PSS) of azobenzene was calculated using Fisher method<sup>22</sup> to be 73%, 79% and 25% for **P1**, **P2** and **P3**, respectively. The higher value of PSS for **P2** may be due to smaller size of the aggregate that allows greater ability to isomerize due to smaller aggregation number.<sup>23</sup>

Next, the reverse process, that is, *cis* to *trans* isomerisation of azobenzene was studied by irradiating with visible light (450 nm, 6W) and changes in the UV-vis spectra were monitored at different irradiation times. The absorption at  $\pi$ - $\pi^*$  transition peak increased and that at  $n$ - $\pi^*$  transition peak decreased, which indicated *cis-trans* isomerization azobenzene. The photoisomerisation ratio as calculated using Fisher method was found to be 70%, 79% and 25% for **P1**, **P2** and **P3**, respectively. For *cis-trans* isomerization also the %PSS was higher for **P2** than for **P1** and **P3**. Thus, it was demonstrated that the assemblies are photoresponsive and azobenzene unit in the hydrophobic core does undergo photoisomerization although the process is hindered due to the aggregation in micellar core. Azobenzene units in H-aggregate form in **P3** also underwent photoisomerization without disrupting the aggregate.<sup>21</sup>

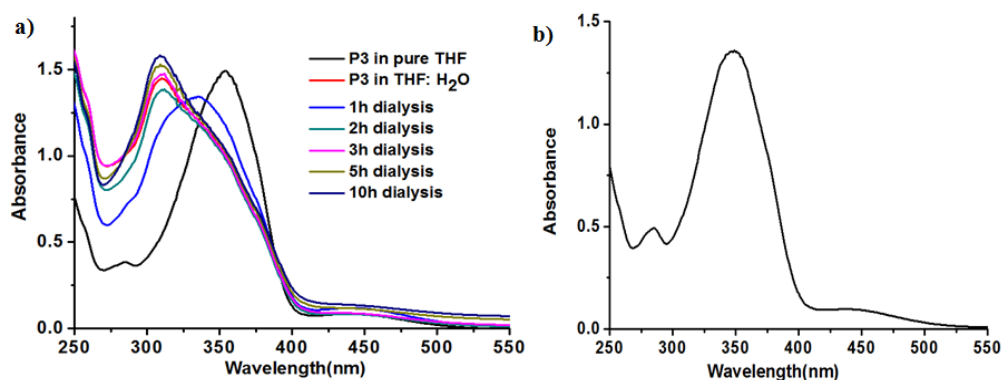


**Figure 3.6** UV-vis spectra of 0.02 wt% solution in THF/H<sub>2</sub>O of (a) **P3** during dialysis against water and (b) **P2** in THF:water (1:3 v/v).

H-type aggregates of azobenzene were present in the micellar assemblies of **P3**. Such aggregates may form during micellization as the hydrophobic dendrons in the polymer undergo self-assembly. To understand this process, UV-vis spectra of the solutions were recorded during the preparation of aqueous solution from solution of **P3** in THF via dialysis. Figure 3.6a shows that no H-type aggregates were present in THF solution. Upon addition of water to THF solution of **P3** in THF:water at 1:3 (v/v) composition the peak at

350 nm shifted with broadening to 325 nm (Figure 3.6a). Concentration of the polymer was 0.02 wt% same as that used for all photoisomerization experiments. This solution was then dialyzed against deionized water and UV-vis spectra were recorded with time. The peak at 325 nm further shifted to 308 nm after only 1h of dialysis. Continuation of dialysis resulted in increase in absorbance of the peak that reached saturation after 25h. In a control experiment UV-vis spectra of **P2** in THF:water (1:3 v/v) were recorded and no shift in the peak at 350 nm was observed (Figure 3.6b). Thus, it was ascertained that the formation of H-aggregates takes place during micellization when water content is significantly higher than THF content.

Due to higher polarity of *cis* isomer of azobenzene, micellar size or even morphology is likely to undergo significant change upon photoirradiation.<sup>24</sup> This possibility was checked using DLS analysis, however noticeable change in size of the aggregates was not observed after irradiation with 365 nm (Figure 3.7); average size ( $D_h$ ) was found to be 75 nm, 25 nm, and 68 nm for **P1**, **P2**, and **P3**, respectively, that is, very similar to size before irradiation hence TEM analysis was not carried out after irradiation.

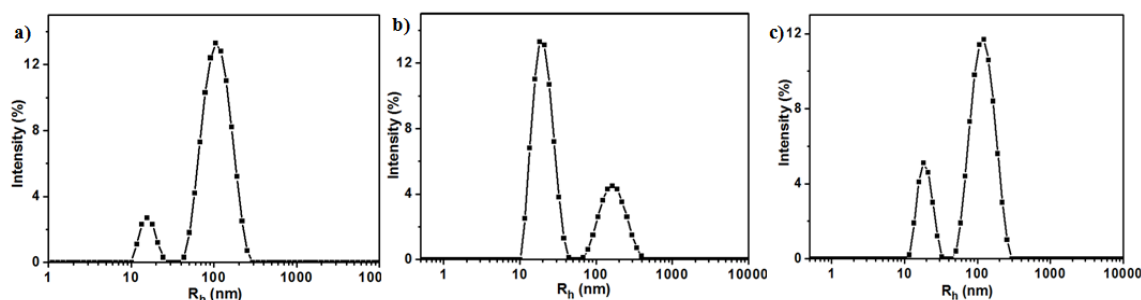


**Figure 3.7** Size distribution curves for aqueous solutions of (a) **P1**, (b) **P2**, (c) **P3** after *trans-cis* isomerization by 365 nm irradiation.

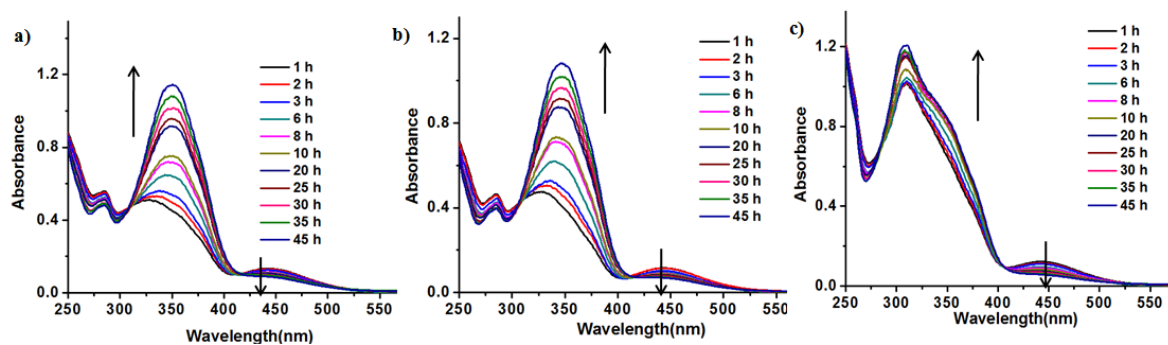


**Figure 3.8** UV-vis spectra for *cis-trans* thermal isomerization of azobenzene at different time intervals for 0.02 wt% aqueous solution of (a) **P1** (b) **P2** and (c) **P3**.



Thermal *cis-trans* isomerization process of azobenzene is much slower than under visible light irradiation and hence allows the study of kinetics of this process. Hence, to understand effect of dendron structure on the kinetics of photoisomerization, first-order rate constants were calculated for *cis-trans* thermal isomerization. The aqueous solution of polymer was stored in dark for 24h after reaching the photostationary state upon irradiation at 365 nm. Absorption spectra were recorded at different time intervals during irradiation as well as during the storage in dark (Figure 3.8). The rate constant was calculated by fitting the experimental data to the following equation<sup>25</sup>

$$\ln(A_{\infty}-A_t)/(A_{\infty}-A_0) = -kt$$

where  $k$  is thermal rate constant in  $s^{-1}$  and  $t$  is the time in seconds;  $A_t$ ,  $A_0$  and  $A_{\infty}$  are the absorbance values at 350 nm at time  $t$ , time zero and infinite time, respectively. Rate constant  $k$  was obtained as the slope of the linear plots shown in Figure 3.9.

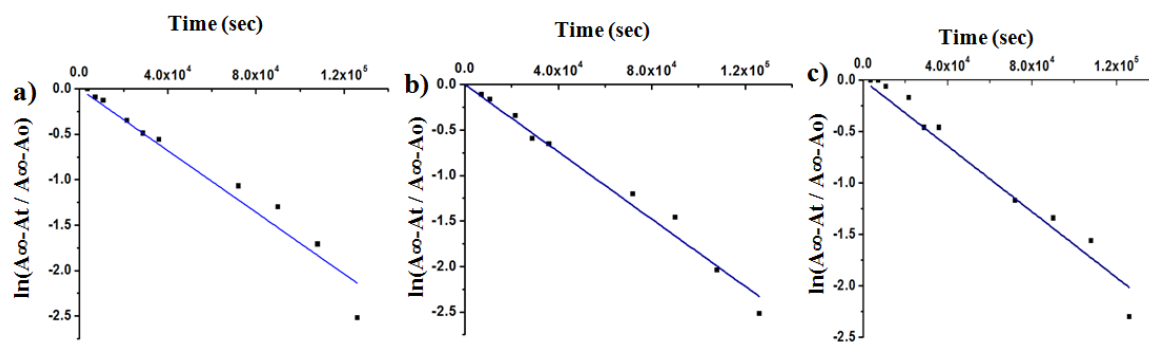


**Figure 3.9** First order rate constant plots for *cis-trans* thermal isomerization of azobenzene in 0.02 wt% aqueous solution of (a) **P1** (b) **P2** and (c) **P3**.

**Table 3.2** Data for azobenzene isomerization of polymer micelles

Polymer	% photo isomerization (trans-cis)	% photo isomerization (cis-trans)	% thermal isomerization (cis-trans)	$k$ ( $s^{-1}$ ) $\times 10^{-5}$
<b>P1</b>	73	70	62	1.69
<b>P2</b>	79	79	63	1.84
<b>P3</b>	25	25	25	1.59

As given in Table 3.2, the first order rate constant for thermal isomerization for **P1** and **P2** was found to be almost similar, however for **P3** it was found to be lower possibly owing to steric hindrance due to higher number of azobenzene units.<sup>26</sup> Also, the



photoisomerization rates as expressed in terms of rate constants are comparable with those seen in azobenzene containing amphiphilic molecules where the movement of azobenzenes in the micellar core is limited.<sup>15, 27</sup>

### 3.3.4 Dye encapsulation and release

Encapsulation and light-responsive controlled release of a hydrophobic dye from the polymer micelles was investigated as a function of dendron structure. Extent of encapsulation of the dye in polymer micelles was determined using Nile red as guest molecule by solid phase extraction method<sup>28</sup> and corresponding UV-vis spectra are shown in Figure 3.10. For calculations, the reported value of molar extinction coefficient of Nile red in methanol ( $45,000 \text{ M}^{-1}\text{cm}^{-1}$ )<sup>29</sup> was used and the values are shown in Table 3.3. The encapsulation efficiency (mg of dye/g of polymer) for **P1** and **P3** was found to be higher than for P2 probably due to higher number of aromatic rings in these polymers that can better accommodate the heterocyclic dye through  $\pi$ - $\pi$  interactions. The trend for encapsulation capacity (defined as mmol of dye/mol of polymer) was also similar.

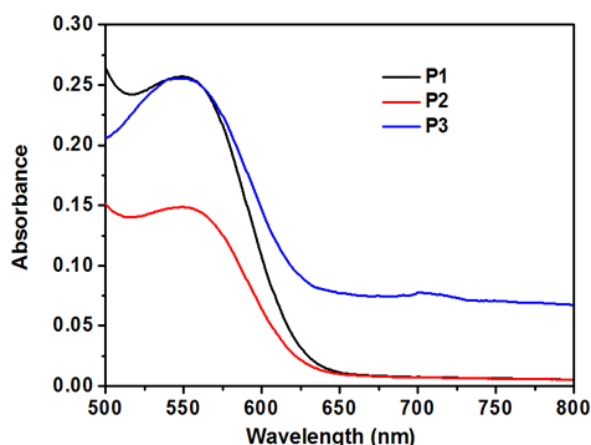


**Figure 3.10** UV-vis spectra of Nile red in aqueous solution of **P1**, **P2** and **P3** for calculation of encapsulation efficiency and encapsulation capacity.

**Table 3.3** Dye encapsulation data for the copolymers<sup>†</sup>

Polymer	Encapsulation efficiency (mg/g of polymer)	Encapsulation capacity (mmol/mol of polymer)
<b>P1</b>	0.60	17
<b>P2</b>	0.40	11
<b>P3</b>	0.60	22

<sup>†</sup> at 0.5 wt% aqueous solution.

Before studying the fate of encapsulated Nile red upon irradiation with UV and visible light, it was important to confirm the absence of its photobleaching. A solution of Nile red in methanol:water (1:1) was irradiated with 365 nm and 450 nm light separately, and fluorescence spectra were recorded at different time intervals (Figure 3.11). Fluorescence emission spectra of Nile red were found to change negligibly over 30 minutes of irradiation suggesting that any change in fluorescence emission intensity observed during dye release experiments involving multiple photoisomerization cycles will be due to change in environment of the dye and not due to photobleaching.

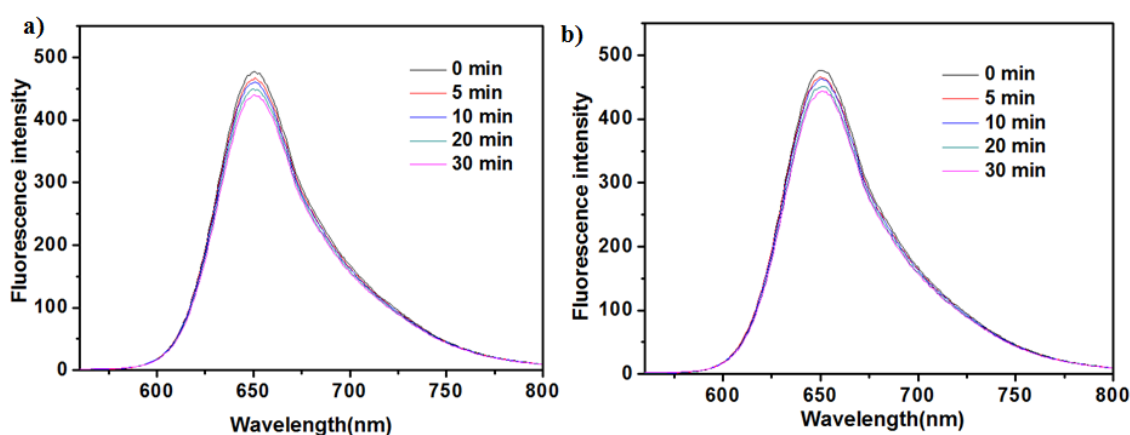


**Figure 3.11** Fluorescence emission spectra of Nile red in methanol:H<sub>2</sub>O (1:1) upon irradiation at (a) 365 nm (b) 450 nm.

When azobenzene is isomerized to *cis* form the environment of micellar core turns polar and may lead to release of the encapsulated hydrophobic dye whereas when it reverts back to *trans* form the micellar environment regains hydrophobicity and some of the dye may re-enter the core affecting the net release. This is possible only if the micellar assembly is intact after *trans-cis* isomerization. *Cis-trans* isomerization can be carried out in two different ways - either by irradiation with 450 nm light or by storing the sample in dark, that is, *via* the thermal pathway, as mentioned above. Though the percentage of photoisomerization is similar in both the pathways the rates are very different. It is worthwhile to study whether the pathway followed for *cis-trans* isomerization influences the net dye release. To investigate this possibility, Nile red loaded polymer solution was irradiated with 365 nm UV light for 30 minutes and fluorescence emission spectra of Nile red were recorded by exciting at 550 nm. It was observed that emission intensity at 630 nm decreased for all the polymers indicating that the polarity of microenvironment of the dye

increased. This change in polarity could be due to either disruption of the micelle and release of the dye from the micellar core into the aqueous solution or change in the polarity of the core due to presence of more polar *cis* isomer of azobenzene without release of the dye. *Cis-trans* isomerization was then carried out independently by irradiation with visible light as well as by storing the sample in dark and fluorescence spectra of Nile red were monitored. Emission intensity did not reach the initial value in both pathways suggesting leakage of dye from micellar core. A comparison of net decrease in intensity of Nile red emission for visible and thermal pathways is shown in Figure 3.12a. Since dye release cannot be directly quantified from fluorescence spectra due to several factors, the decrease in intensity may be considered as an approximate measure of dye release.

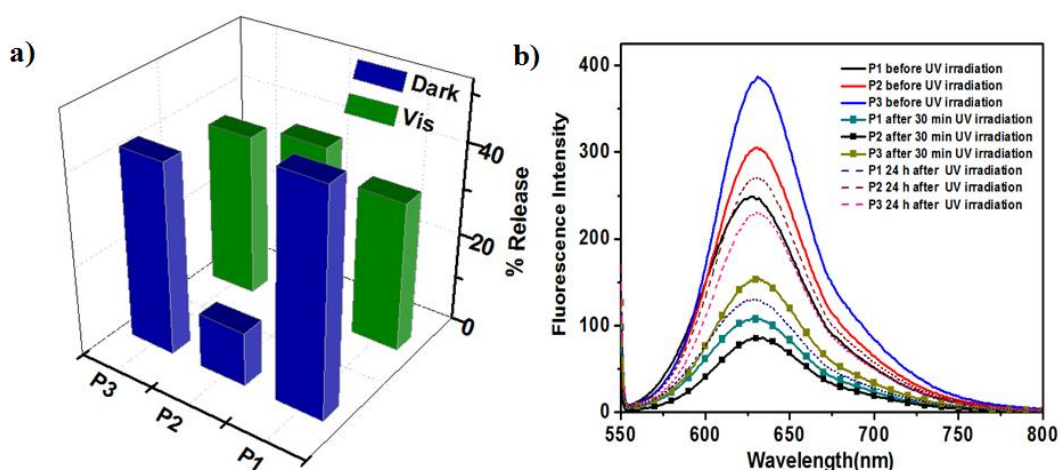


**Figure 3.12** (a) Nile red release from aqueous solution of polymers following different pathways for *cis-trans* photoisomerization. (b) Emission spectra of Nile red at different time intervals during UV-thermal *trans-cis-trans* isomerization cycle.

Decrease in intensity for thermal isomerization pathway was found to be higher than after visible light isomerization for **P1** and **P3**, however the trend was reversed in case of **P2**. In fact, decrease in Nile red intensity for thermal isomerization for **P2** was significantly lower, 12% (Table 3.4). This may be attributed to the difference in the dendron structure that is, different peripheral groups and number of azobenzene units, which in turn directs the size and nature of micellar assembly. Fluorescence emission spectra of Nile red for the photo-thermal *trans-cis-trans* isomerization pathway are shown in Figure 3.12b. Thus, it seems feasible to exert control over dye release by selecting desired pathway for *cis-trans* isomerization of azobenzene.

**Table 3.4** Data for dye release during photoisomerisation by two pathways.

Polymer	% decrease in fluorescence intensity (UV-dark)	% decrease in fluorescence intensity (UV-Vis)
<b>P1</b>	49	33
<b>P2</b>	12	39
<b>P3</b>	42	36

To study another approach for controlled release of dye, multiple photoisomerization cycles were performed with thermal restoration gap between two cycles. A *trans-cis-trans* isomerization carried out by irradiation of 365 nm light followed by 450 nm light is considered as one photocycle and the time allowed for dye to equilibrate between micellar core and aqueous environment when the sample is stored in dark is called thermal restoration period.<sup>15</sup> After the first photocycle there was a net decrease in Nile red intensity for all polymers (Figure 3.13). However, after second consecutive photocycle, that is, without any thermal restoration, no net decrease in intensity of Nile red was observed (Figure 3.14).

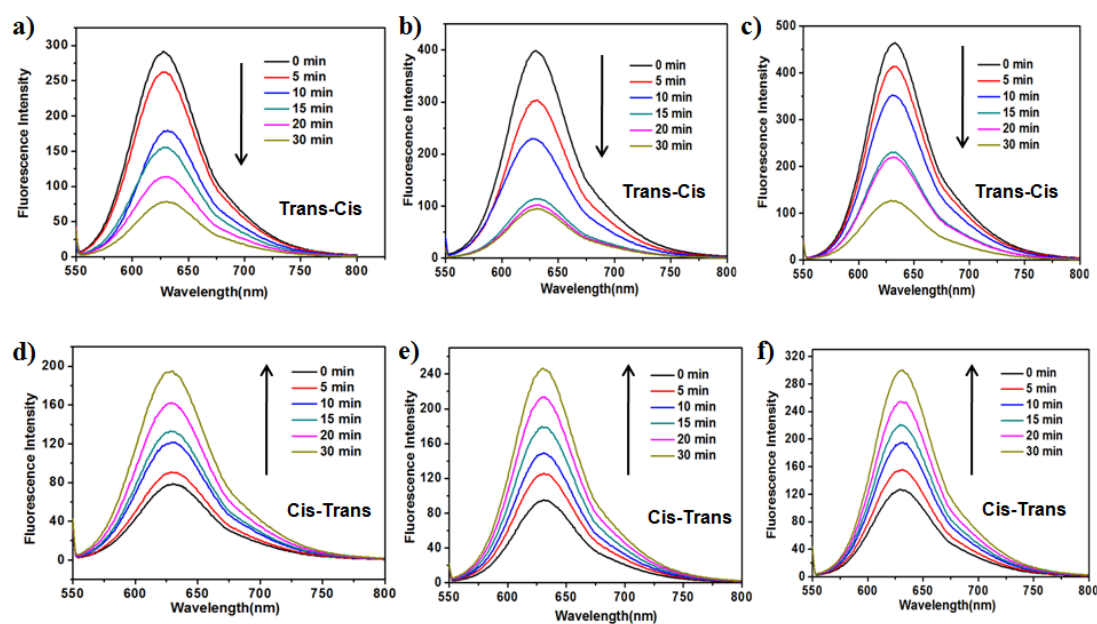


**Figure 3.13** Fluorescence emission spectra after irradiation at 365 nm for (a) **P1** (b) **P2** and (c) **P3** followed by irradiation at 450 nm for (d) **P1** (e) **P2** and (f) **P3** (first photocycle).

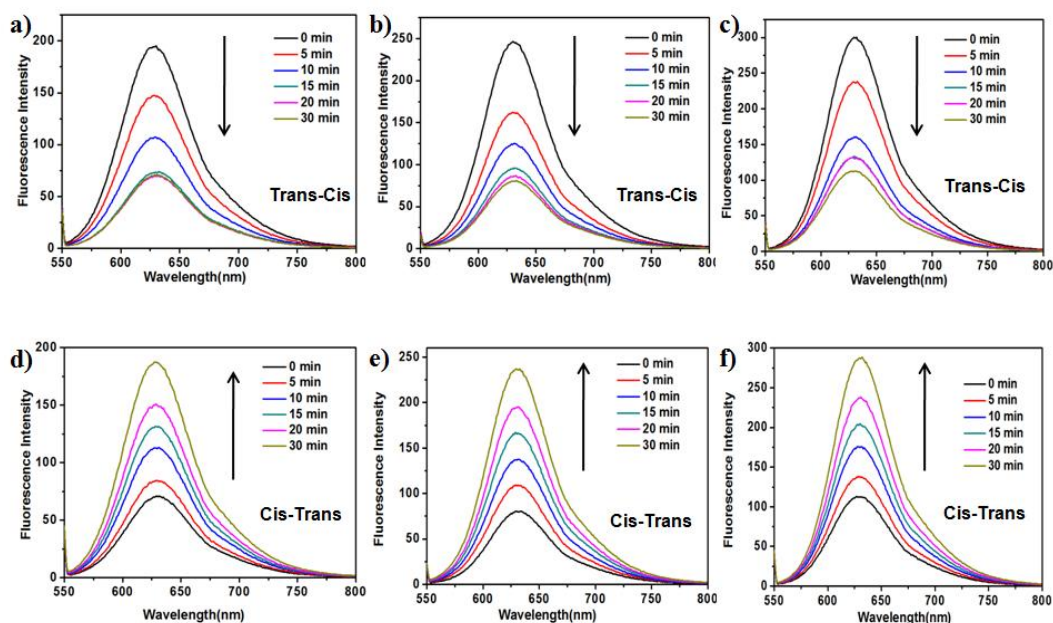


**Figure 3.14** Fluorescence emission spectra after irradiation at 365 nm for (a) **P1** (b) **P2** and (c) **P3** followed by irradiation at 450 nm for (d) **P1** (e) **P2** and (f) **P3** (second consecutive photocycle).

The sample was then kept for thermal restoration for 12 h, during which period, some of the dye had re-entered the micellar core as seen from emission spectra at the beginning of next photocycle. After the photocycle, net decrease in intensity was less than that after the first two photocycles (Figure 3.15). In fact, there was a net re-encapsulation of Nile red by micellar assemblies and the effect was more prominent for **P3**.

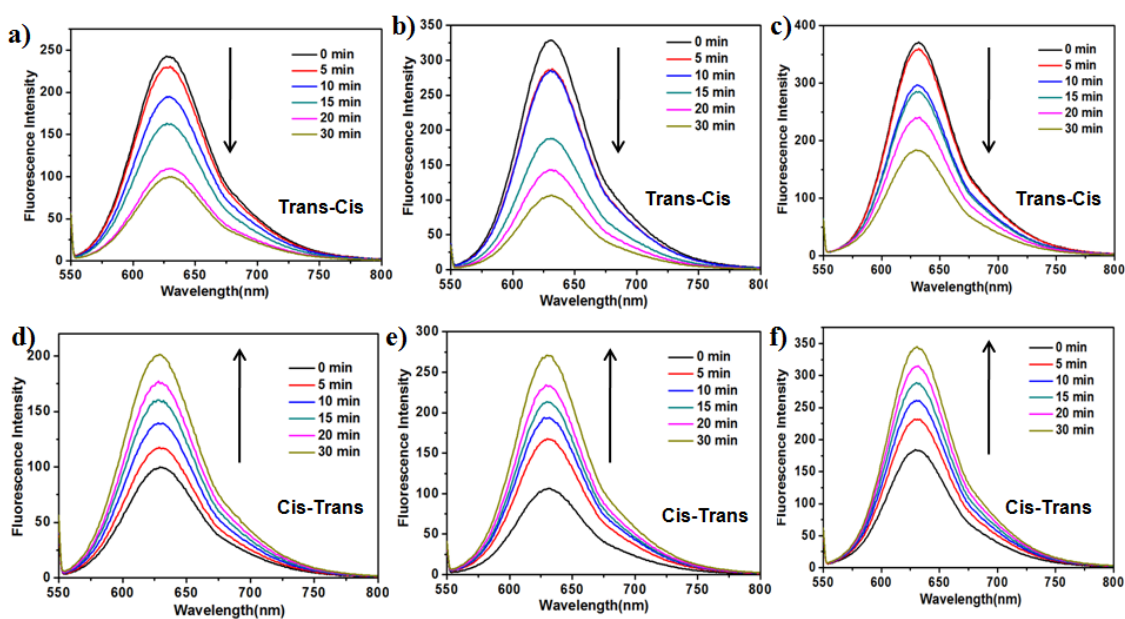


**Figure 3.15** Fluorescence emission spectra of Nile red after irradiation at (a)(b)(c) 365 nm and (d)(e)(f) 450 nm of aq. solution of **P1**, **P2**, **P3**, respectively after 12 h thermal restoration (third photocycle).

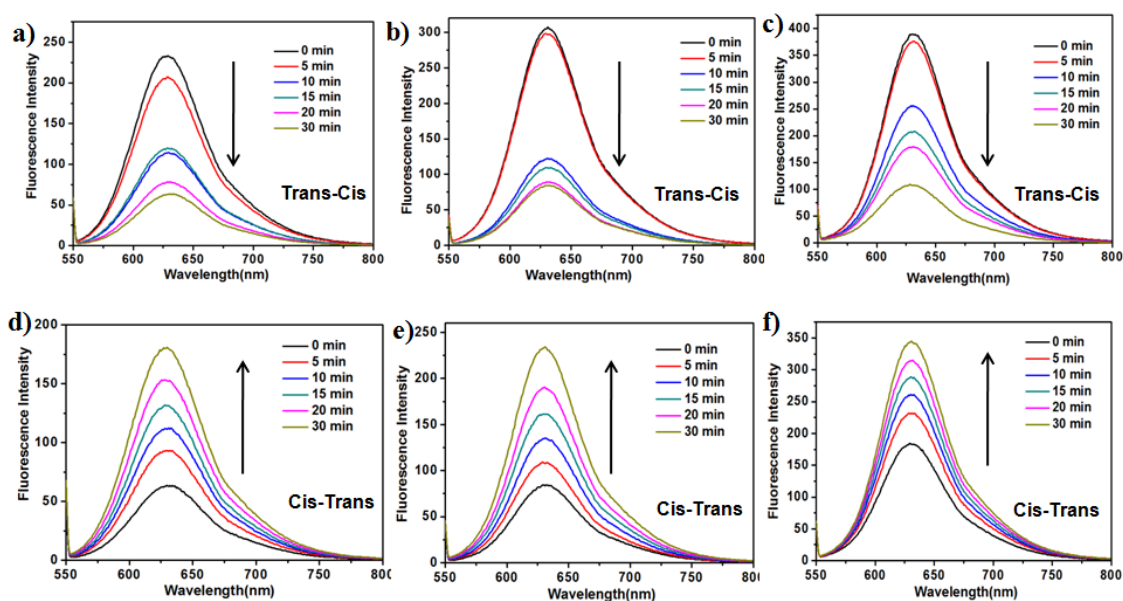


**Figure 3.16** Fluorescence emission spectra of Nile red after irradiation at (a)(b)(c) 365 nm and (d)(e)(f) 450 nm of aqueous solution of **P1**, **P2**, **P3**, respectively after 4h thermal restoration (fourth photocycle).

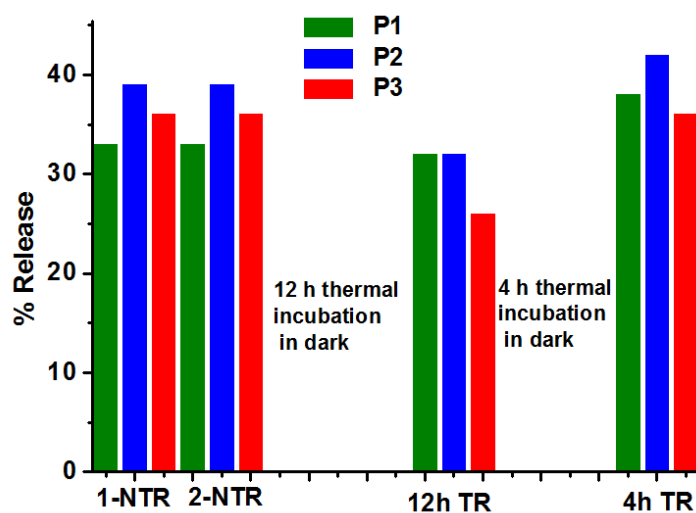


**Figure 3.17** Release of Nile red from aqueous solution of **P1**, **P2** and **P3** during photocycles with different thermal restoration intervals.

After another 4 h of thermal restoration similar effect was observed but to a lesser extent and after the fourth photocycle there was a net decrease in intensity that was only slightly higher than that after the first photocycle (Figure 3.16). Overall, after four photocycles and two thermal restoration periods only about 40% decrease in emission intensity of the dye was observed revealing a strong tendency of the LDBC micelles to retain the dye molecules. The control over Nile red release as indicated by % decrease in intensity is



shown in Figure 3.17 for all polymer micelles by tuning number of photoisomerization cycles with different thermal restoration times.

### 3.4 Summary

LDBCs with azobenzene in the dendron interior with different hydrophobic groups at the periphery were synthesized. Photo and thermal *trans-cis-trans* isomerization of azobenzene was investigated in the self-assembled polymers in aqueous solution. Higher number of azobenzene containing polymer showed H-type aggregation that remained stable during photoisomerization. Formation of H-aggregates during micellization was confirmed by following the dialysis of THF:water mixture by UV-vis spectroscopy. The assemblies did not show photo-induced change in the size. Effect of photoisomerization of azobenzene on polarity of micellar core was studied using fluorescence spectroscopy of Nile red. Decrease in fluorescence emission intensity was taken as indication of release of Nile red from micellar core. Dye release clearly depended on the pathway used for *cis-trans* isomerization. This is the first time that a comparison of different isomerization pathways for dye release from amphiphilic copolymer assemblies has been made.

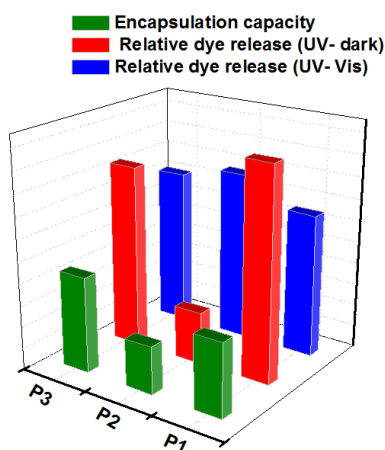


**Figure 3.17** Plot showing relative encapsulation capacity and dye release from two pathways for the three LDBC.

Dye release studied over multiple photocycles interspersed with thermal restoration time revealed excellent encapsulation capacity of the LDBC. Both the dye release experiments, clearly demonstrated the effect of dendron structure with **P1** and **P3** showing similar behaviour while **P2** - polymer with less aromatic rings, showing a different behaviour. **P2**

micelles displayed a higher release during a UV-vis photo-cycle but lower release during a UV-thermal isomerization cycle compared to the other two polymers.

### 3.5 References

- 1) Bai, S.; Zhao, Y. *Macromolecules* **2001**, *34*, 9032.
- 2) Sévigny, S.; Bouchard, L.; Motallebi, S.; Zhao, Y. *Macromolecules* **2003**, *36*, 9033.
- 3) Zhao, Y.; Tong, X. *Adv. Mater.* **2003**, *15*, 1431.
- 4) Wu, Y.; Kanazawa, A.; Shiono, T.; Ikeda, T.; Zhang, Q. *Polymer* **1999**, *40*, 4787.
- 5) Breiner, T.; Kreger, K.; Hagen, R.; Häckel, M.; Kador, L.; Müller, A. H. E.; Krammer, E. J.; Schmidt, H. W. *Macromolecules* **2007**, *40*, 2100.
- 6) Blasco, E.; Schmidt, B. V. K. J.; Kowollik, C. B.; Pinol, M.; Oriol, L. *Polym. Chem.* **2013**, *4*, 4506
- 7) Mynar, J. L.; Goodwin, A. P.; Cohen, J. A.; Ma, Y.; Fleming, G. R.; Fréchet, J. M. J. *Chem. Commun.* **2007**, 2081.
- 8) Wang, D.; Wang, X. *Prog. Polym. Sci.* **2013**, *38*, 271.
- 9) Wang, G.; Tong, X.; Zhao, Y. *Macromolecules* **2004**, *37*, 8911.
- 10 a) Chen, Z.; He, Y.; Yang, Y.; Wang, X. *Macromol. Rapid Commun.* **2011**, *32*, 977.  
b) Lee, H.; Wu, W.; Oh, J.; Mueller, L.; Sherwood, G.; Peteanu, L.; Kowalewski, T.; Matyjaszewski, K. *Angew. Chem. Int. Ed.* **2007**, *46*, 2453.
- 11) Wang, D.; Wang, X. *Prog. Polym. Sci.* **2013**, *38*, 271.
- 12) a) Schumers, J. M.; Fustin, C. A.; Gohy, J.-F. *Macromol. Rapid Commun.* **2010**, *31*, 1588. b) Gohy, J. F.; Zhao, Y. *Chem. Soc. Rev.* **2013**, *42*, 7117. c) Wang, X.; Yang, Y.; Gao, P.; Yang, F.; Shen, H.; Guo, H.; Wu, D. *ACS Macro Lett.* **2015**, *4*, 1321.
- 13) Feng, Z.; Lin, L.; Yan, Z.; Yu, Y. *Macromol. Rapid Commun.* **2010**, *31*, 640–644. b) Wang, G.; Tong, X.; Zhao, Y. *Macromolecules.* **2004**, *37*, 8911. c) Wang, S.; Shen, Q.; Nawaz, M. H.; Zhang, W. *Polym. Chem.* **2013**, *4*, 2151.
- 14) Cordel, C.; Popeney, C. S.; Haag, R. *Chem. Commun.* **2011**, *47*, 6584.
- 15) Kumari, M.; Billamboz, M.; Leonard, E.; Len, C.; Böttcher, C.; Prasad, A. K.; Haag, R.; Sharma, S. K. *RSC Adv.* **2015**, *5*, 48301.
- 16) del Barrio, J.; Oriol, L.; Sánchez, C.; Serrano, J. L.; Cicco, A. D.; Keller, P.; Li, M. H. *J. Am. Chem. Soc.* **2010**, *132*, 3762.



- 17) Blasco, E.; del Barrio, J.; Sánchez-Somolinos, C.; Piñol, M.; Oriol, L. *Polym. Chem.* **2013**, *4*, 2246.
- 18) Blasco, E.; Serrano, J. L.; Piñol, M.; Oriol, L. *Macromolecules* **2013**, *46*, 5951.
- 19) Liao, L. X.; Junge, D.M.; McGrath, D.V. *Macromolecules* **2002**, *35*, 319.
- 20) Kalva, N.; Aswal, V. K.; Ambade, A. V. *Macromol. Chem. Phys.* **2014**, *215*, 1456.
- 21) Feng, Z.; Lin, L.; Yan, Z.; Yu, Y. *Macromol. Rapid Commun.*, **2010**, *31*, 640.
- 22) Fisher, E. *J. Phys. Chem.* **1967**, *71*, 3704.
- 23) Cördel, C.; Popeney, C. S.; Haag, R. *Chem. Commun.* **2011**, *47*, 6584.
- 24) Su, W.; Kuo, Han, Kuo.; Luo, Y.; Wang, Z.; Li, Y.; Zhang, Q. *Macromol. Chem. Phys.* **2007**, *208*, 955.
- 25) Sierocki, P.; Maas, H.; Dragut, P.; Richardt, G.; Vögtle, F.; Cola, L. D.; Brouwer, F.; Zink, J. I. *J. Phys. Chem. B.* **2006**, *110*, 24390.
- 26) Nithyanandhan, J.; Jayaraman, N.; Davis, R.; Das, S. *Chem. Eur. J.* **2004**, *10*, 689.
- 27) Wang, G.; Yuan, D.; Yuan, T.; Dong, J.; Feng, N.; Han, G. *J. Polym. Sci., Part A: Polym. Chem.* **2015**, *53*, 2768.
- 28) Wyszogrodzka, M.; Haag, R. *Chem. Eur. J.* **2008**, *14*, 9202.
- 29) Adeli, M.; Nazami, H.; Du, F.; Hönzke, S.; Headtrich, S.; Keilitz, J.; Haag, R. *RSC Adv.* **2015**, *5*, 14958.

## **Chapter 4**

### **Controlled Micellar Disassembly of Photo- and pH-cleavable Linear-Dendritic Block Copolymers**

This chapter is adapted from "Kalva, N.; Parekh, N.; Ambade A. V. *Polym. Chem.* **2015**, *6*, 6826-6835. DOI: 10.1039/C5PY00792E".

## 4.1 Introduction

Self-assembly of amphiphilic linear-dendritic block copolymers has attracted attention in the area of drug delivery because the unusual architecture allows for tuning the micellar parameters either through dendron generation or linear polymer chain length and for incorporation of stimuli-responsive moieties at specific location thus augmenting their efficacy in targeted delivery.<sup>1,2</sup> As discussed in Chapter 1, LDBC responsive to the external stimuli such as pH, temperature, redox, light, and enzyme have been studied for their stimuli-responsive disassembly in aqueous solution.<sup>3-10</sup>

Cleavable stimuli-responsive linkages are of particular interest because the nanocarrier can possibly be disassembled in complete and controlled manner. Such linkages can be introduced in the side chain or at the junction of the two blocks in a block copolymer. Cleavable linkages at the junction are also explored for generation of nanoporous membranes where one of the blocks can be removed under mild conditions leaving the functionalized pores behind.<sup>11</sup> Moreover, it is desirable to incorporate multiple stimuli-responsive cleavable groups because the presence of more than one stimuli-responsive group makes it possible to tune the response and precisely control the drug release of micelles due to the cumulative effect of stimuli.<sup>12,13</sup> Thus, stimuli-responsive cleavable linkages such as disulfide, acid-labile bonds, and photo-cleavable groups have been incorporated in combination with each other into a single amphiphilic copolymer.<sup>14-17</sup> Among the drug delivery nanocarriers, pH-degradable micelles have generated lot of interest because a pH gradient exists between the intra and extracellular environment of cancer tissue. Many types of acid-cleavable bonds, such as acetal, ketal, hydrazone, and  $\beta$ -thioester that can break under mild acidic conditions have been employed.<sup>18-23</sup> Photo-cleavable groups are also promising candidates because of their ability to afford control over time and location of release.<sup>15,24-27.</sup>

There are several reports on linear block copolymers where multiple cleavable linkages are introduced at the block junction or in the main chain.<sup>28-31</sup> However, in stimuli-responsive LDBCs, the cleavable linkages have been incorporated on the periphery of dendron only. For example, aggregates of a linear-dendritic block copolymer composed of a dendron with acetal at the periphery and attached to hydrophilic PEG linear polymer at focal point could be disassembled under mild acidic conditions.<sup>3</sup> Recently, doxorubicin was conjugated to dendron periphery through acid-labile hydrazone linkage in a LDBC

towards pH-induced drug release.<sup>4</sup> However, there are no reports on incorporation of stimuli-cleavable groups at the junction of linear and dendritic segments. It is hypothesized that introduction of such groups at the junction between dendron and linear polymer could augment the advantages offered by this class of polymers. In this direction, a dual-stimuli-cleavable biocompatible LDBC with both photo- and pH-cleavable units at the junction of the two blocks was designed. The polymer was modularly synthesized by coupling hydrophobic dendron containing photo-cleavable group at focal point to a hydrophilic linear polymer carrying acid-cleavable group at one end using click chemistry. The photo and pH-responsive behaviour of the copolymer aggregates in aqueous solution was investigated and based on synergistic effect of the two stimuli for cargo release was shown.

## 4.2 Experimental section

### 4.2.1 Materials

5-hydroxy-2-nitrobenzaldehyde, PEG monomethyl ether ( $M_n = 2000$ g/mol), sodium borohydride, chloroethyl vinyl ether, 2,2-bis-methylolpropionic acid (bis-MPA), were purchased from Aldrich Chemicals. Decanoyl chloride was purchased from Acros Chemical Co. Propargyl alcohol, DMAP, pyridine, p-toluene sulfonyl chloride, potassium carbonate and triethylamine were purchased from Avra chemicals, Spectrochem and Merck Chemicals, India. Pyridine p-toluenesulfonate (PPTS)<sup>32</sup> and bis-MPA anhydride<sup>33</sup> were synthesized by following reported procedures. Dichloromethane was dried over  $\text{CaH}_2$  and acetone was dried over  $\text{K}_2\text{CO}_3$ , distilled and stored in Schlenk flask. THF was passed through alumina, dried on sodium wire and freshly distilled when required.

### 4.2.2 Instrumentation

GPC analysis was performed on Viscotek PL-GPC-220 with  $\text{CHCl}_3$  as eluent. DLS experiments were performed on 90 Plus particle size analyser by Brookhaven Instruments Corporation at an angle of  $90^\circ$  equipped with laser beam of 633 nm wavelength. Fluorescence emission spectra were recorded on a PCI photon counting spectrometer or CARY Eclipse spectrometer. For photoirradiation, a 100W UV lamp equipped with 365 nm filter (intensity  $21000 \mu\text{W cm}^{-2}$ ) was used.

### 4.2.3 Synthetic procedures and characterization data

**ONB-acetonide-bisMPAG1-alkyne (1):** 5-propargylether-2-nitrobenzyl alcohol (0.2 g, 0.96 mmol), bis-MPA anhydride (0.382 g, 1.15 mmol), DMAP (0.017 g, 0.013 mmol) and pyridine (155  $\mu$ L, 1.9 mmol) were added to dry  $\text{CH}_2\text{Cl}_2$  in a reaction flask under argon flow and reaction mixture was stirred at room temperature for 15h. After completion of the reaction excess anhydride was quenched with addition of 2 mL of water under vigorous stirring, followed of dilution with 300 ml of DCM and the solution was washed with 10 % of  $\text{NaHSO}_4$  (3 $\times$ 500 mL), and 10 % of  $\text{Na}_2\text{CO}_3$  (3 $\times$ 500 mL). The organic phase was dried over  $\text{Na}_2\text{SO}_4$ , concentrated and purified by column chromatography on silica gel, eluting with hexane and gradually increasing the polarity to ethyl acetate and pet ether (30:70) to give white colour solid. Yield: 92%.  $^1\text{H}$  NMR ( $\text{CDCl}_3$ , 200 MHz):  $\delta$  1.22(s, 3H), 1.41(s, 3H), 1.48 (s, 3H), 2.57(t, 1H, J=2Hz), 3.71(d, 2H, J=12Hz), 4.29(d, 2H, J=12Hz), 4.80(d, 2H, J=4Hz), 5.67(s, 2H), 6.98(dd, 4Hz, 1H), 7.29(s, 1H), 8.20(d, 1H, J=8Hz) ppm.  $^{13}\text{C}$  NMR ( $\text{CDCl}_3$ , 50MHz)  $\delta$  18.40, 21.07, 26.22, 29.66, 42.33, 56.23, 61.65, 63.40, 66.19, 79.15, 98.29, 114.18, 127.81, 135.78, 140.57, 161.75, 173.56 ppm.

**ONB-bisMPAG1-alkyne (2):** Compound **1** (3.5 g, 9.6 mmol) was dissolved in 200 mL MeOH and 30 mL DCM. Concentrated sulphuric acid (1.7 mL) was added drop-wise at room temperature and then stirred the reaction mixture additional 2 h in the dark. The reaction was monitored using TLC after completion of the reaction the reaction mixture was concentrated to one-third of its initial volume. Ethyl acetate was added to the reaction mixture and washed with 1M  $\text{Na}_2\text{CO}_3$  and brine solution. The organic layer was dried over  $\text{Na}_2\text{SO}_4$  and evaporated the ethyl acetate to get yellow colour solid without any further purification. Yield 85%.  $^1\text{H}$  NMR ( $\text{CDCl}_3$ , 200 MHz)  $\delta$  1.15(s, 3H), 2.58(t, 1H, J=2Hz), 3.78(d, 2H, J=10Hz), 4.03(d, 2H, J=10Hz), 4.84 (d, 2H, J=2Hz), 5.69(s, 2H), 6.98(dd, 1H, J=2Hz), 7.29(s, 1H), 8.19(d, 1H, J=8Hz) ppm.  $^{13}\text{C}$  NMR ( $\text{CDCl}_3$ , 50MHz)  $\delta$  17.25, 49.53, 56.34, 61.56, 63.72, 64.80, 68.96, 105.25, 113.40, 114.87, 127.86, 135.57, 161.87 ppm.

**ONB-acetonide-bisMPAG2-alkyne (3):** Compound **2** (2.7 g, 8.3 mmol), bis-MPA anhydride (6.8 g, 20.8 mmol), DMAP (0.305 g, 2.5 mmol) and pyridine (1.68 mL, 20.8 mmol) were added to dry DCM in a reaction flask and procedure same as compound **1** was followed to give yellow-coloured solid (4.9 g). Yield 92%.  $^1\text{H}$  NMR ( $\text{CDCl}_3$ , 200 MHz):  $\delta$

1.13(s, 6H), 1.33(s, 6H), 1.39 (s, 3H), 1.41(s, 6H), 2.64(t, 1H, J=2Hz), 3.59(d, 4H, J=12Hz), 4.12(d, 4H, J=12Hz), 4.41(s, 4H), 4.82(d, 2H, J=2Hz), 5.59(s, 2H), 7.00(dd, 1H, J=4Hz), 7.17(d, 1H, J=4Hz), 8.20(d, 1H, J=8Hz) ppm.  $^{13}\text{C}$  NMR ( $\text{CDCl}_3$ , 50MHz):  $\delta$  18.39, 19.05, 22.37, 26.02, 42.72, 47.73, 56.92, 64.65, 65.91, 66.62, 98.75, 114.72, 115.22, 128.55, 135.36, 141.41, 162.21, 172.47, 174.27 ppm.

**ONB-bisMPAG2-alkyne (4):** Compound **3** (4.4 g, 6.92 mmol) was dissolved in 300 mL of methanol and 30 mL of DCM and procedure same as compound **2** was followed to get yellow-coloured solid that was used without any further purification. Yield 85%.  $^1\text{H}$  NMR ( $\text{CD}_3\text{OD}$ , 200 MHz) 1.12(s, 6H), 1.37(s, 3H), 3.09(t, 1H, J=2Hz), 3.55-3.69(m, 8H), 4.35(m, 4H), 4.93 (d, 2H, J=2Hz), 5.55(s, 2H), 7.09(dd, 1H, J=2Hz), 7.27(s, 1H), 8.18(d, 1H, J=8Hz) ppm.

**ONB-C9-bisMPAG2-alkyne (5):** Compound **4** (1g, 1.8mmol), DMAP (0.021 g, 0.17 mmol) was dissolved in dry DCM and added triethylamine (1.5 mL, 10.7 mmol) at 0 °C. Decanoyl chloride (2.06 mL, 10.7 mmol) was added drop by drop for 15 min and allowed to stir for 12h. After completion, reaction mixture was washed with sodium bicarbonate and brine solution. Crude product was purified by column chromatography eluting with 20% ethyl acetate and pet ether to obtain yellow-coloured liquid. Yield 75%.  $^1\text{H}$  NMR ( $\text{CDCl}_3$ , 200 MHz)  $\delta$  0.88(t, J=6Hz, 12H), 1.12-1.44(m, 54H), 1.48-1.75(m, 11H), 2.28(t, 8H, J=6Hz), 2.62(t, 1H, J=2Hz), 4.14-4.40(m, 12H), 4.84(d, 2H, J=2Hz), 5.56(s, 2H), 7.02(dd, 1H, J=2Hz), 7.15(d, 1H, J=2Hz), 8.19(d, 1H, J=10Hz) ppm.  $^{13}\text{C}$  NMR ( $\text{CDCl}_3$ , 50MHz)  $\delta$  14.13, 17.77, 22.68, 24.87, 29.29, 31.88, 34.04, 46.44, 62.76, 65.01, 65.65, 114.14, 115.28, 127.99, 134.34, 161.50, 172.14, 173.25 ppm. MALDI-TOF MS: Calcd. 1171.74, Found 1194.77 for  $[\text{M}+\text{Na}]^+$ .

**PEG<sub>2K</sub>-Acetal-Cl (6):** Polyethylene glycol monomethylether ( $M_n = 2000$  g/mol) (5 g, 2.5 mmol) and pyridine p-toluenesulfonate (PPTS) (0.125 g, 0.49 mmol) were dried by azeotropic distillation with toluene just before start of the reaction. Then the reaction mixture was dissolved in the 50 mL dry DCM and chloroethyl vinyl ether (CEVE) (2.56 g, 25 mmol) was added by dissolving in 10 mL dry DCM drop-wise over 15 min under argon atmosphere at 0 °C. After one hour 20 mL of 5wt%  $\text{Na}_2\text{CO}_3$  solution was added to quench

the reaction and to avoid the cleavage of the acetal linkage. Then the reaction mixture was diluted with 100 mL DCM and washed with brine solution. Crude product was precipitated into cold hexane and the filtrate was dried under vacuum.  $^1\text{H}$  NMR ( $\text{CDCl}_3$ , 200 MHz)  $\delta$  1.31(d, J=6Hz, 3H), 3.36(s, 3H), 3.63(m, 174H), 4.80(q, J=6Hz, 1H) ppm.

**PEG<sub>2K</sub>-Acetal-N<sub>3</sub> (7):** PEG<sub>2K</sub>-Ace-Cl (8) (5 g, 2.3 mmol), NaN<sub>3</sub> (1.54 g, 23.6 mmol) were dissolved in DMF and stirred at 60 °C for 24 h. After completion of the reaction DMF was removed under reduced pressure. The crude product was precipitated in cold diethyl ether; the obtained white product was dried under vacuum. Yield 90%.  $^1\text{H}$  NMR ( $\text{CDCl}_3$ , 200 MHz)  $\delta$  1.31(d, J=6Hz, 3H), 3.36(s, 3H), 3.48-3.77(m, 178H), 4.79(q, 1H, J=6Hz) ppm.  $^{13}\text{C}$  NMR ( $\text{CDCl}_3$ , 100MHz)  $\delta$  19.37, 43.23, 64.03, 64.96, 70.49, 99.73, 125.21, 128.14, 128.94 ppm. FT-IR (KBr,  $\text{cm}^{-1}$ ): 845, 958, 1114, 1240, 1274, 1353, 1474, 1633, 1966, 2105, 2884. MALDI-TOF MS: Calcd. 2106.35 Found 2106.2 for  $[\text{M}^+]$ .

#### ***CuAAC reaction between ONB-C9-bisMPAG2-alkyne dendron and PEG<sub>2K</sub>-Acetal-N<sub>3</sub>***

Alkyne-functionalized dendron (5) (0.7 g, 0.4 mmol) and PEG<sub>2K</sub>-Ace-N<sub>3</sub> (0.7 g 0.33 mmol) were dissolved in dry THF, and resultant mixture was degassed for 15 min. CuBr (0.048 g, 0.033 mmol), and PMDETA (69  $\mu\text{L}$ , 0.33 mmol) were then added and stirred for 24h under argon atmosphere. After completion, the reaction mixture was passed through neutral alumina to remove copper salts and finally precipitated in cold hexane to remove the excess dendron. Finally, product was dried under vacuum. Yield 75%.  $^1\text{H}$  NMR ( $\text{CDCl}_3$ , 200 MHz)  $\delta$  0.88(t, 12H, J=8Hz), 1.14-1.37(m, 60H), 1.48-1.67(m, 8H), 2.28(t, 8H, J=8Hz), 3.38(s, 3H), 3.49-3.70(m, 174H), 3.99(t, 2H, J=4Hz), 4.18(m, 8H), 4.32(m, 4H), 4.57(t, 2H, J=4Hz), 4.72(q, 1H, J=6Hz), 5.33(s, 2H), 5.52(s, 2H), 7.07(dd, 1H, J=2Hz), 7.17(d, 1H, J=2Hz), 7.85(s, 1H), 8.16(d, 1H, J=8Hz) ppm.  $^{13}\text{C}$  NMR ( $\text{CDCl}_3$ , 50MHz)  $\delta$  14.06, 17.70, 19.35, 22.61, 24.78, 29.21, 31.80, 33.95, 46.33, 46.84, 58.99, 63.05, 64.91, 70.50, 99.93, 108.59, 120.58, 124.50, 142.23, 162.28, 172.06, 173.18 ppm. MALDI-TOF MS: Calcd. 3277.99, Found 3277.76 for  $[\text{M}^+]$ .

#### **4.2.4 Preparation and characterisation of aqueous solution of polymer**

A suspension of polymer in deionized water was stirred for 5 h to obtain a clear 0.1 wt% aqueous solution. For determination of cmc, Nile red ( $5 \times 10^{-6}$  M) was encapsulated in

micellar solution by hydrating a film of the dye by 0.1 wt% polymer solution. This solution was diluted to obtain series of concentrations and fluorescence emission spectra were recorded. The cmc was determined as the point of intersection of tangents to the emission intensity versus log (conc.) curve. For size analysis the solutions were filtered through 0.45 $\mu$  PVDF filters. To monitor the cleavage of acetal linkage 0.1wt% of the polymer was dissolved in 5 mL PBS (10 mM) solution and pH was adjusted by addition of 1M HCl. The solution was then placed at 37 °C with gentle shaking. At fixed time intervals the solution was lyophilized, dissolved in chloroform and analysed by GPC.

#### 4.2.5 Encapsulation of DOX in micelles

Doxorubicin (DOX)-loaded micelles were prepared by film hydration method. DOX hydrochloride (0.5mg) was dispersed in THF, triethyl amine (2 equiv) was added and stirred overnight to neutralise the drug. After filtration to remove the triethyl amine hydrochloride, 5 mg of polymer was dissolved in the filtrate (DOX solution in THF). Organic solvent was removed on rotary evaporator to obtain thin film of DOX/polymer mixture. PBS solution (pH 7) was poured onto the film and stirred for 5h at room temperature to obtain DOX-loaded micelles. The unloaded DOX was removed by filtering the micellar solution through 0.22 $\mu$ m filter. The solution was analysed by UV-Vis spectroscopy measuring the absorption at 505 nm and drug loading efficiency (DLE) and drug loading content (DLC) were calculated using the following equations.

$$\text{DLE (\%)} = (\text{Weight of DOX loaded in micelles} / \text{Weight of DOX in feed}) \times 100$$

$$\text{DLC (\%)} = (\text{Weight of DOX loaded in micelles} / \text{Weight of polymer}) \times 100$$

#### 4.2.6 Cell viability assay

**a) *With the polymer.*** The cell viability assay was analysed using colorimetric method which is based on MTT (3-(4,5-dimethylthiazol-2-yl)-2,5-diphenyltetrazolium bromide) (purchased from Invitrogen, India). MDA-MB-231, triple negative breast cancer cell line (purchased from National Centre for Cell Science, Pune, India), were seeded in a flat-bottomed 96-well plate at a density of 1 x10<sup>4</sup> cells/well in DMEM (Dulbecco's Modified Eagle Medium, purchased from Invitrogen, India) containing 10% FBS (Fetal Bovine Serum, purchased from Invitrogen, India). The plate was incubated at 37 °C with 5% CO<sub>2</sub> for 24 h. After incubation media was replaced with filter, sterile polymer (1 mg/mL in



DMEM containing 10% FBS) was added. Different concentrations of sample (0, 100, 150, 200, 300, 400, 500  $\mu\text{g/mL}$ ) were added to make final volume 100  $\mu\text{L/well}$  and incubated for 40h at 37 °C with 5%  $\text{CO}_2$ . Media was replaced with filter sterilized MTT (0.45 mg/mL) prepared in DMEM containing 10% FBS and further incubated for 4h at 37 °C with 5%  $\text{CO}_2$ . MTT reagent was replaced by DMSO 100  $\mu\text{L/well}$ . Addition of DMSO dissolves the formazan crystals formed by reaction of sample with MTT and developed colour was measured at 550 nm using a microtitre plate reader (Veroscan, Thermo Scientific). The relative % cell viability was calculated from the following equation: Relative percent cell viability =  $A_{\text{test}}/A_{\text{control}} \times 100\%$  ( $A_{\text{test}}$  is the absorbance of the sample treated cells and  $A_{\text{control}}$  is the absorbance of the untreated cells. Each absorbance was taken to be the mean of triplicate measurements. The cell viability was represented as a percentage relative to untreated cells as control.

**b) With drug-loaded polymer micelles.** The cytotoxicity of free DOX and DOX-loaded polymer micelles with or without UV irradiation was determined by MTT assay. MDA-MB-231, triple negative breast cancer cell line were seeded in a flat-bottomed 96-well plate at a density of  $1 \times 10^4$  cells/well in DMEM containing 10% FBS. The plate was incubated at 37 °C with 5%  $\text{CO}_2$  for 24 h. Media was replaced with filter sterile free DOX or DOX-loaded micelle solution and incubated for 2 h at 37 °C with 5%  $\text{CO}_2$ . Then for photo-induced drug release the cells were irradiated by UV light (365 nm) for 30 minutes. After UV treatment the media was replaced by fresh growth media and the cells were allowed to grow for further 24h under the same culture condition.

#### 4.2.7 Cellular uptake and intra-cellular release of DOX

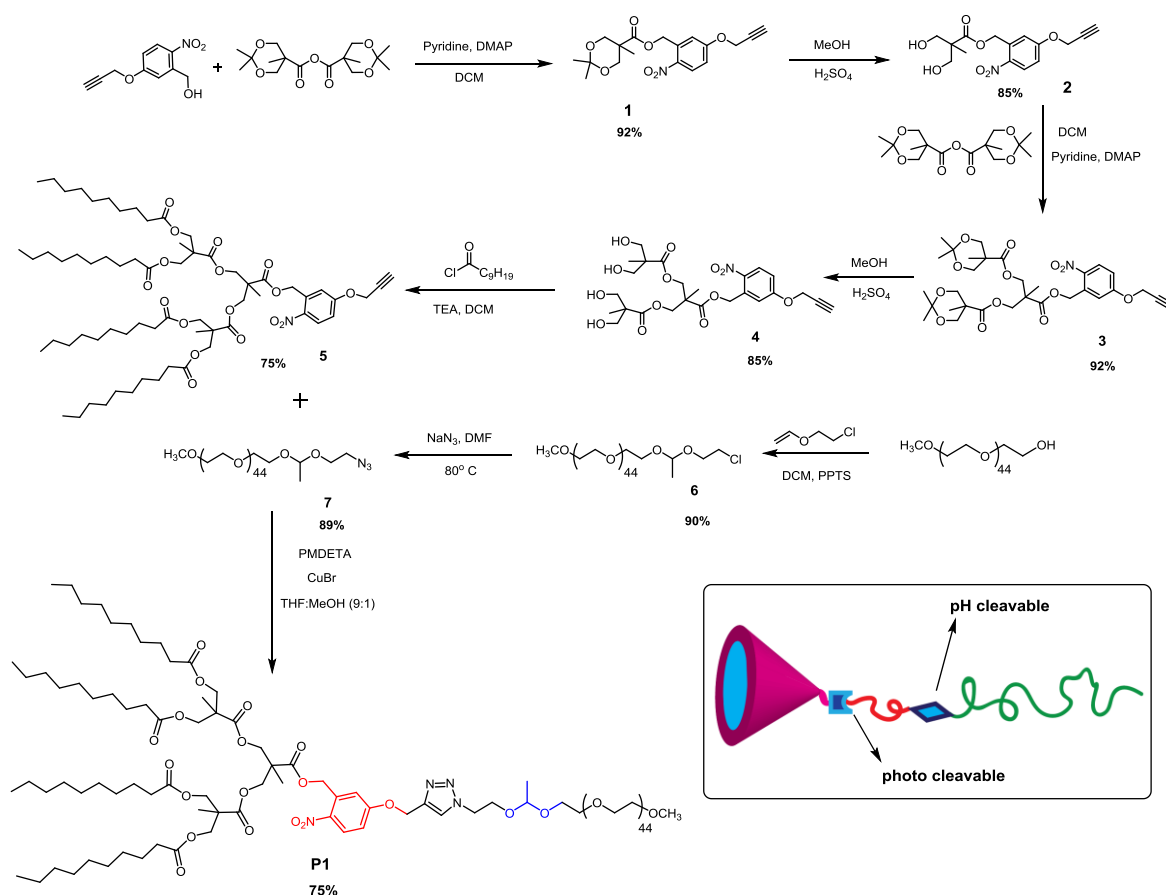
MDA-MB-231 cells were seeded in 24 well plate at a density of 50,000 cells/well in DMEM containing 10% FBS. The plate was incubated at 37 °C with 5%  $\text{CO}_2$  for 24h. After incubation the media was replaced with DOX-loaded micelles, incubated for 2h and irradiated under UV light (365nm) for 30 minutes. At the end, cells were washed 3 times with PBS and fixed with 4% paraformaldehyde. Nucleus was stained with DAPI (4',6-diamidino-2-phenylindole). Images were acquired using epifluorescence microscope by Carl Zeiss (Model: Axio Observer.Z1, Oil emersion objective, 63X). (Filters set 49 DAPI

shift free EX G 365, BS FT 395, EM BP 445/50, Filter set 20 Rhodamine shift free EX BP 54.6112, BS FT 560, EM BP 575-640).

### 4.3 Results and Discussion

#### 4.3.1 Synthesis

Bis-MPA-based polyester dendron was selected as hydrophobic block and PEG was selected as hydrophilic component of the LDBC. Bis-MPA-based dendrons are known to be biocompatible<sup>34-36</sup> and hence the targeted copolymer was expected to be biocompatible. The ONB group cleaves under UV irradiation and also by two photon absorption in the NIR region.<sup>25,37</sup> Acetal linkage is known to rupture under mild acidic conditions.<sup>19,38</sup> It was hypothesized that due to the large difference in the rates of cleavage of the two linkages it may be possible to fine tune the drug release by controlling the time of exposure.



**Scheme 4.1** Synthesis of polymer **P1**.

Bis-MPA-based polyester dendron with dodecyl chains on the periphery and alkyne-functionalized *o*-nitrobenzyl group at the focal point was synthesized in stepwise manner.

Synthesis started from alkyne-functionalized *o*-nitrobenzyl alcohol that was prepared from 5-hydroxy-2-nitrobenzaldehyde in two steps following reported procedure.<sup>39</sup> This compound was then utilized to build the second-generation bis-MPA dendron (**4**) following the reported protection-deprotection strategy involving bis-MPA anhydride (Scheme 4.1). Finally, hydroxyl groups on the dendron periphery were reacted with decanoyl chloride in esterification reaction to obtain dendron **5**. PEG functionalized with acetal and azide groups (**7**) at the same chain end was synthesized by reaction of PEG monomethyl ether with chloroethyl vinyl ether followed by substitution of the chloride with azide.<sup>40</sup> PEG **7** was coupled with the alkyne-functionalized dendron (**5**) using CuAAC, a well-known member of the ‘click’ group of reactions.<sup>41,42</sup>

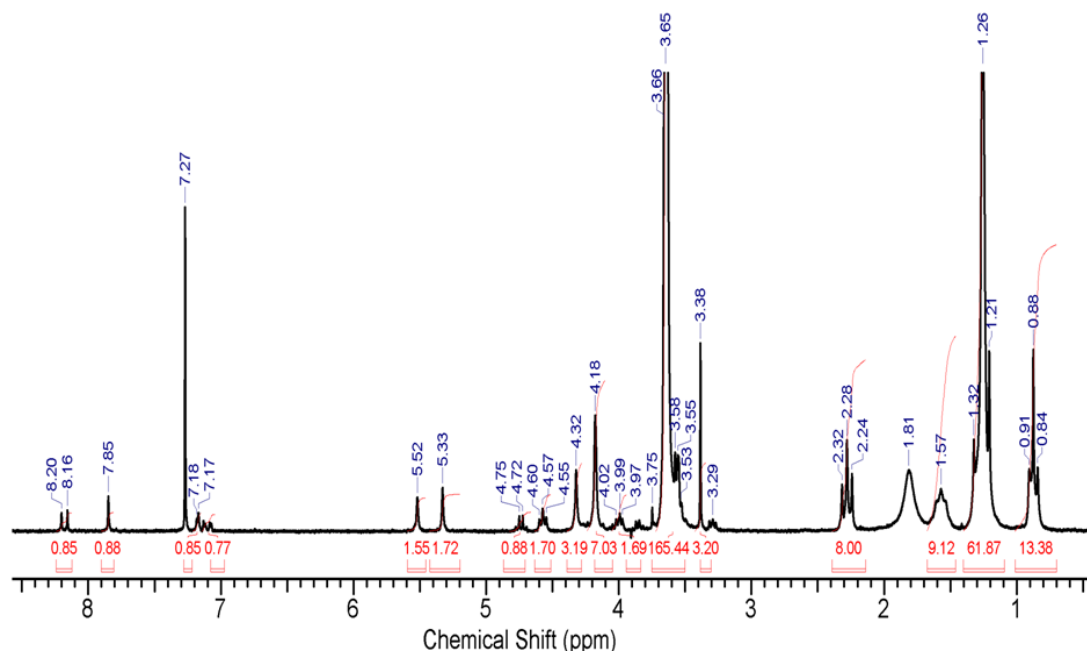


**Figure 4.1** 200 MHz  $^1\text{H}$  NMR spectrum of **P1** in  $\text{CDCl}_3$ .

Purification of the obtained LDBC **P1** was achieved by repeated precipitations and its molecular structure was confirmed by using  $^1\text{H}$  NMR and FT-IR spectroscopy. A new peak at 7.85 ppm in  $^1\text{H}$  NMR spectrum (Figure 4.1) was attributed to the proton of triazole ring and complete disappearance of peak at 2.62 ppm, characteristic of the alkyne proton was noted. Disappearance of the  $2109\text{ cm}^{-1}$  band for the azide stretching frequency was observed in FT-IR spectra (Figure 4.2a). **P1** was also characterized by  $^{13}\text{C}$  NMR spectroscopy and MALDI-TOF technique (see Appendix III). Purity of the polymer was ascertained by GPC analysis (Figure 4.2b).

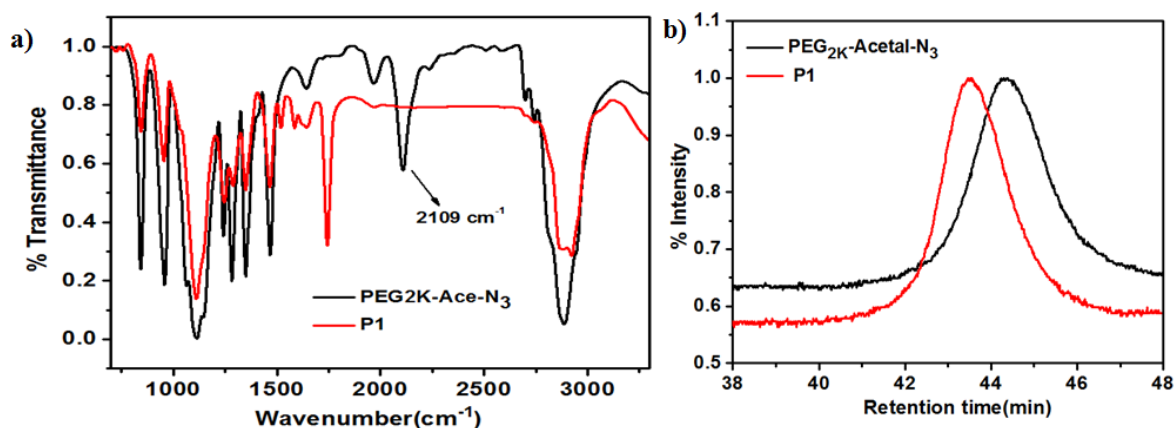


**Figure 4.2** (a) FT-IR spectrum of **P1** overlaid with that of starting polymer. (b) GPC chromatograms of PEG<sub>2K</sub>-acetal-N<sub>3</sub> (**7**) and **P1** (eluant: CHCl<sub>3</sub>; PS standards).

### 4.3.2 Self-assembly

The LDBC **P1** can self-assemble in water into aggregates, the core of which is made up of hydrophobic dendrons and corona contains PEG chains. To prepare aqueous solution of **P1** for self-assembly studies at pH 7 a suspension of the polymer was stirred in water for 5h, after which a clear solution was obtained. Use of organic co-solvent and dialysis was not found to be necessary for preparing aqueous solution. DLS analysis indicated the presence of aggregates with an average size of 90 nm (size PDI = 0.28). TEM analysis did not show well-defined morphology, possibly due to dynamic nature of the assembly (Figure 4.3).

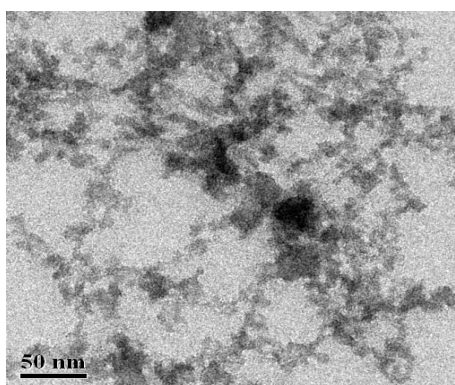


**Figure 3.3** TEM image 0.1wt % aqueous solution of **P1** at pH 7.

Dye encapsulation experiment was used to further support the formation of aggregates. Nile red, a poorly water-soluble dye, was taken up by the micellar solution as evident by change in colour suggesting its encapsulation in the aggregates. Decrease in fluorescence intensity of Nile red with dilution was used to determine cmc of the aggregates; the value

was found to be  $1.34 \times 10^{-5}$  M (Figure 4.4). The shape of the plot of intensity versus  $\log(\text{conc.})$  was typical of cmc curves.

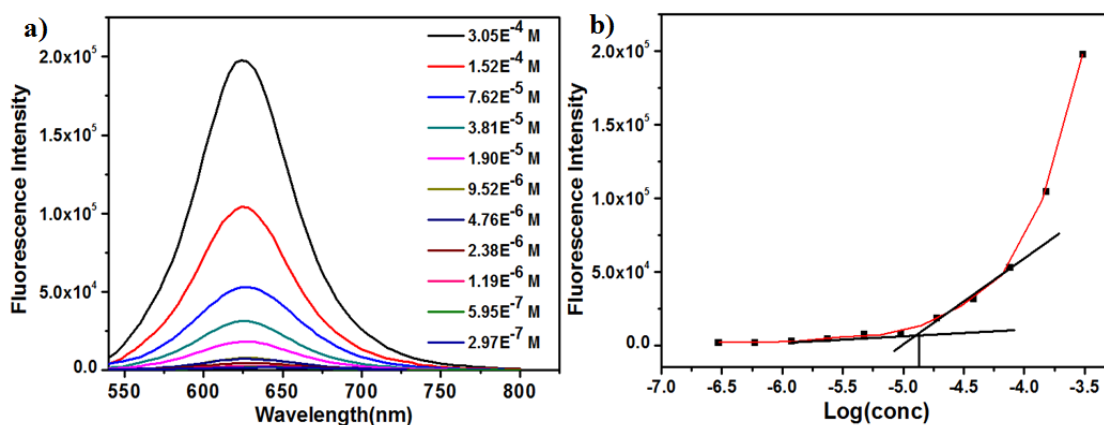
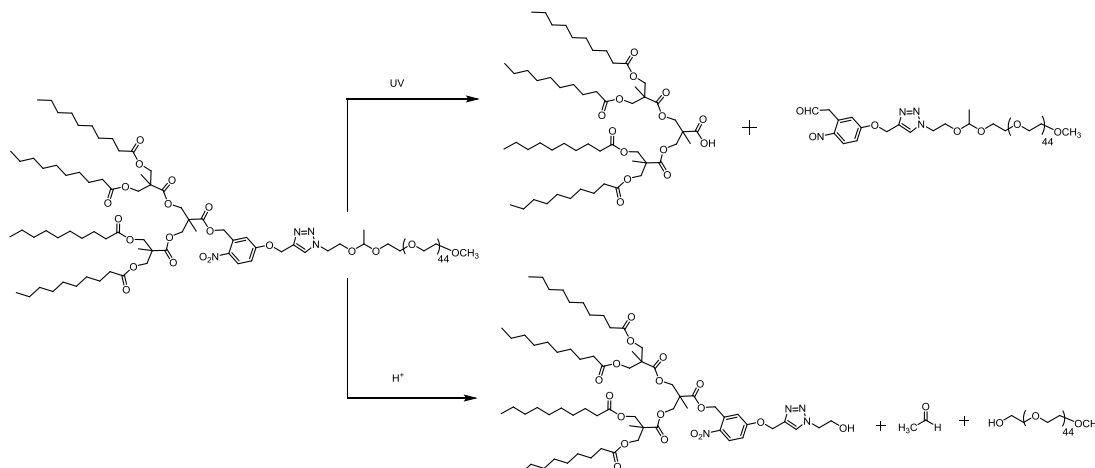


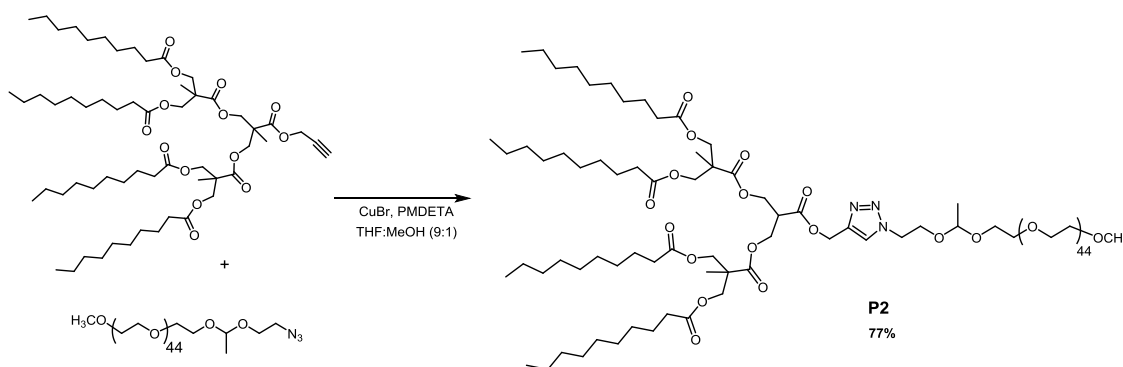
**Figure 4.4** (a) Fluorescence emission spectra of Nile red with varying concentration of **P1** in water. (b) Plot of emission intensity versus  $\log(\text{conc.})$  for cmc determination of **P1**.



**Scheme 4.2** Proposed photo- and pH-induced cleavage pathways for **P1**.

The micellar disassembly can be achieved in two ways owing to the two stimuli-responsive groups in **P1** as shown in Scheme 4.2. Responsiveness of the photo-cleavable group in the polymer was investigated first. Aqueous solution of **P1** (0.1 wt%) was irradiated at 365 nm using a 100W UV lamp and absorption spectrum was monitored at different time intervals for change in signature peaks of ONB group. The characteristic absorption band for ONB group at 306 nm decreased with irradiation time accompanied by increase in the absorption peak at 350 nm due to the resulting nitroso compound (Figure 4.5a). After 1 h of irradiation no further change was observed. A clear visible change occurred in the solution that changed from colourless to pale brown (inset, Figure 4.5a) confirming the cleavage of ONB group. DLS analysis of the irradiated solution was used

to monitor disassembly of the micelle caused by photocleavage. The  $D_h$  of micelles decreased to 30 nm from 90 nm before irradiation as shown in Figure 4.5b. To confirm that this decrease in size is indeed due to photocleavage of the polymer, a control polymer **P2** was synthesized. This polymer was without the *o*-nitrobenzyl group but had acetal group at the junction (Scheme 4.3); the required alkyne-functionalized dendron was synthesized following reported procedure.<sup>43</sup>



**Scheme 4.3** Synthesis of polymer **P2**.

An aqueous solution of **P2** (0.1 wt%) was prepared by direct dissolution in water and it showed an average size of 30 nm (size PDI = 0.188) in DLS analysis. The size remained unchanged after irradiation at 365 nm as expected (Figure 4.5b).

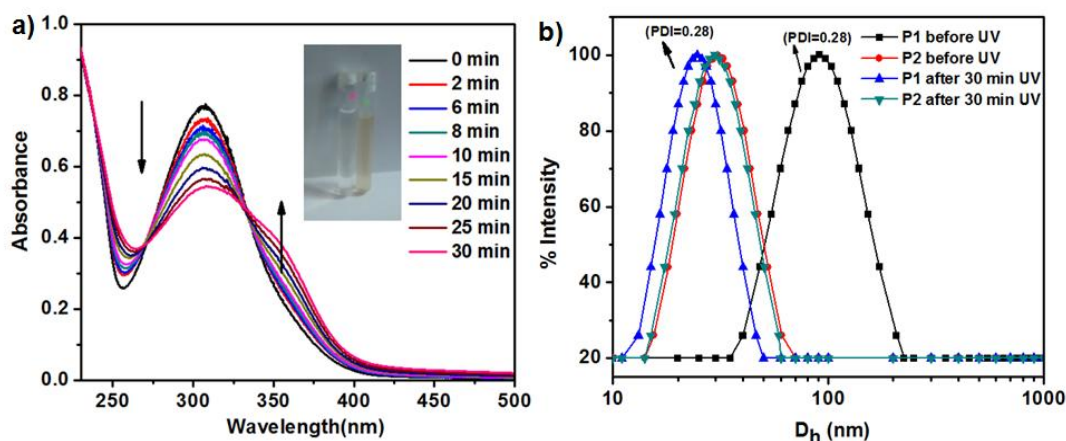


**Figure 4.5** (a) UV-Vis spectra of 0.1 wt% aqueous solution of **P1** recorded at various time intervals after irradiation with 365 nm light. (Inset: photograph of the solution before and after irradiation). (b) DLS size distribution curves for 0.1 wt% aqueous solution of **P1** and **P2** before and after the UV irradiation.

Next, the disassembly under acidic conditions due to cleavage of acetal linkage in **P1** was studied. Initially, studies were carried out at pH 5. Micellar solutions were prepared in pH 7 buffer and 1M HCl was added to arrive at pH 5. The solution was stirred for 7 days

at 37 °C - the physiological temperature. The mixture of products was isolated by lyophilization. GPC analysis showed a new peak, which corresponded to that of the dendron (Figure 4.6a). However, concentration of the cleaved dendron was much less even after 7 days, which indicated that polymer degradation at pH 5 occurred at very slow rate. It is proposed that presence of compound micelle-like morphology, wherein acetal groups are not easily accessible, is probably responsible for this slow degradation.

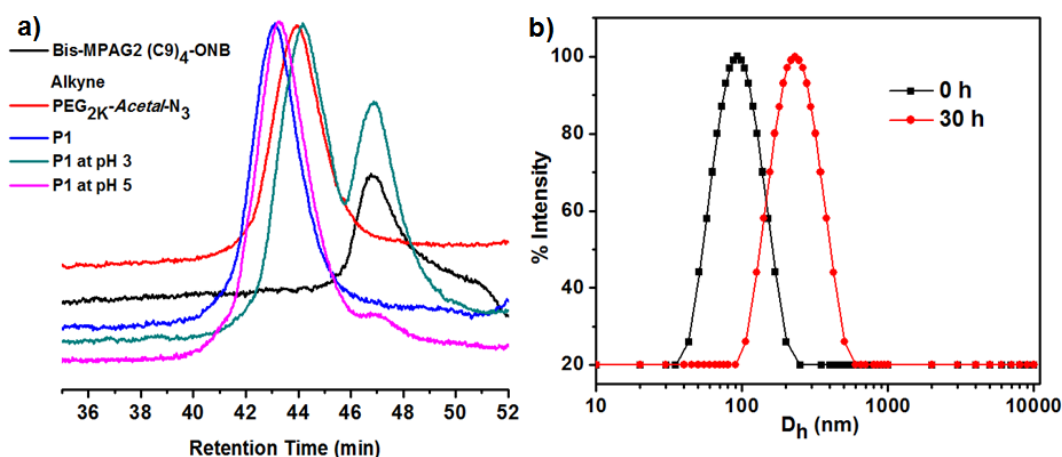


**Figure 4.6** (a) GPC chromatogram overlay for **P1** after stirring at pH 3/37 °C/48 h; data at pH 5 is for 7d/37 °C. (b) DLS size distribution curves for 0.1 wt% aq. solution of **P1** stirred at pH 3/37 °C.

Acetal cleavage was then studied at pH 3 by stirring at 37 °C for 48 h and the mixture was analyzed by GPC. The chromatogram showed a bimodal distribution wherein the two peaks closely matched those of the dendron and PEG, confirming cleavage of **P1** into dendron and PEG fragments (Figure 4.6a). After stirring the solution at pH 3 for 30h the average size in DLS analysis increased to 200 nm in comparison to the size of 90 nm observed at pH 7 (Figure 4.6b). This could be attributed to the suspension of particles of aggregated hydrophobic dendron in the solution formed after degradation of the polymer.

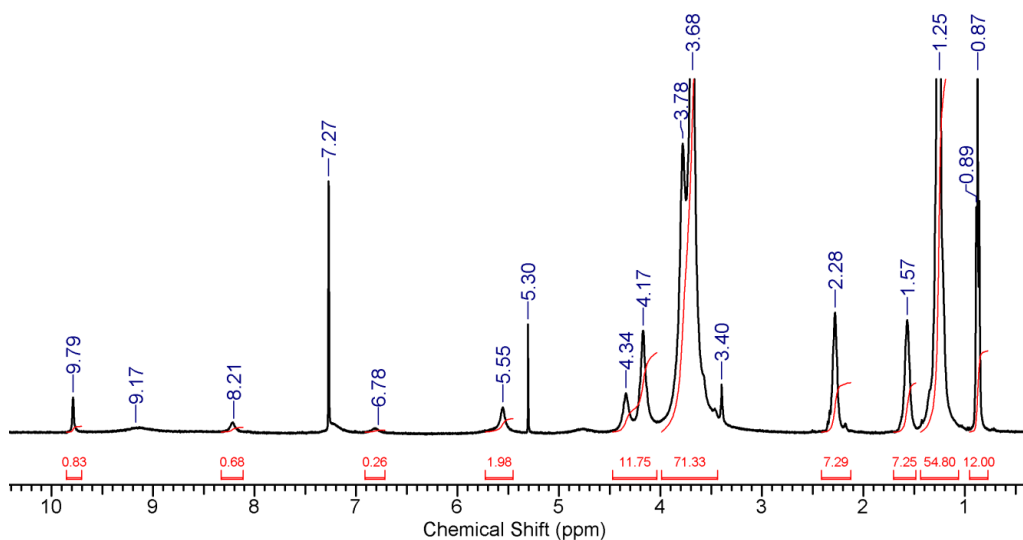


**Figure 4.7**  $^1\text{H}$  NMR spectrum of **P1** in  $\text{CDCl}_3$  with addition of 20  $\mu\text{L}$  DCl.

$^1\text{H}$  NMR spectroscopy was also used to confirm degradation of **P1** under acidic conditions. A drop of deuterated HCl was added to the polymer solution in  $\text{CDCl}_3$ . A new peak at 9.79 ppm attributable to the aldehydic proton of acetaldehyde, which is the side product after acetal cleavage (Scheme 4.2), appeared in the  $^1\text{H}$  NMR spectrum and the signal at 4.72 ppm for acetal proton reduced significantly (Figure 4.7).

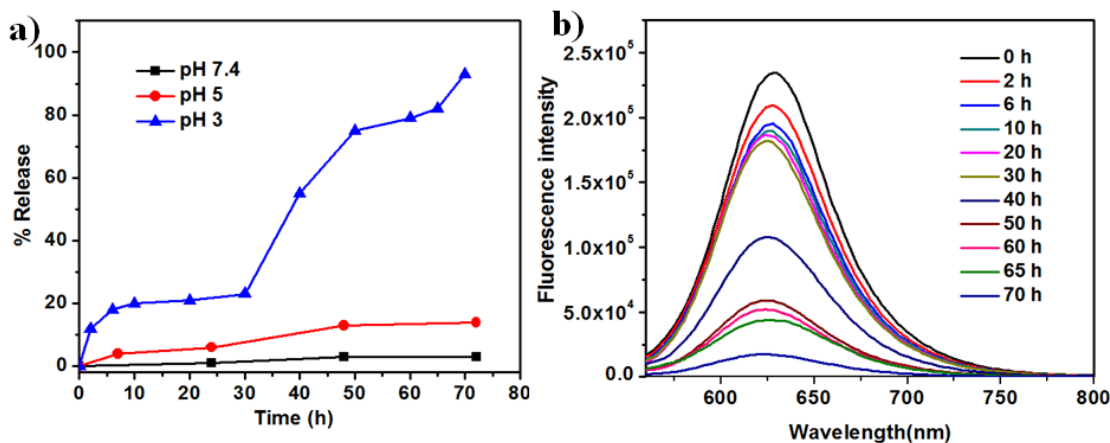


**Figure 4.8** (a) Nile red release profiles at pH 7.4, 5.0 and pH 3.0 for 0.1wt% of aqueous solution of **P1** at 37°C. (b) Fluorescence emission spectra of Nile red encapsulated in 0.1wt% of aqueous solution of **P1** at different intervals at pH 3 and 37°C.

Nile red release from micellar aggregates at pH 7.4, 5 and 3 was also studied by monitoring its emission spectra at different time intervals. At pH 5 only 14% of the encapsulated dye was released after 72h, however around 90% of the dye escaped at pH 3



during the same period (Figure 4.8a). The release at pH 7.4 was negligible as expected. Corresponding decrease in emission intensity of the dye with time was observed in fluorescence spectra (Figures 4.8b and 4.9). Release profile at pH 3 shown in Figure 3.8a has an interesting pattern. In the first 10h only 20% release occurred that remained constant up to 30h and in the next 20h, the total release reached up to almost 80%, suggesting that the micellar degradation as well as dye release take place in multiple stages.

After studying the dye release in response to both photo and pH stimuli separately, the synergistic effect of the two stimuli was explored. Simultaneous application of two stimuli can help increase guest release under acidic environment whenever desired by ‘turning on’ the light stimulus.

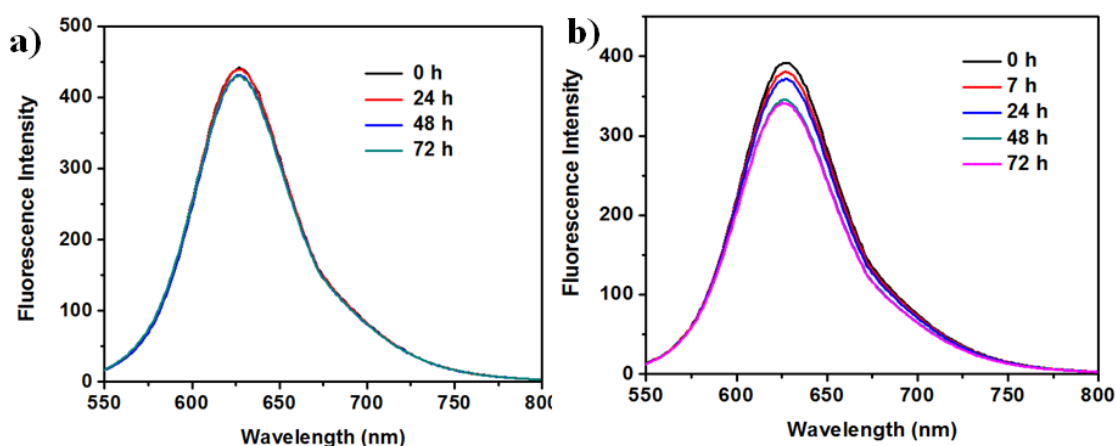


**Figure 4.9** Fluorescence emission spectra of Nile red in **P1** (0.1wt% aqueous solution) at (a) pH 7.4. (b) pH 5.0.

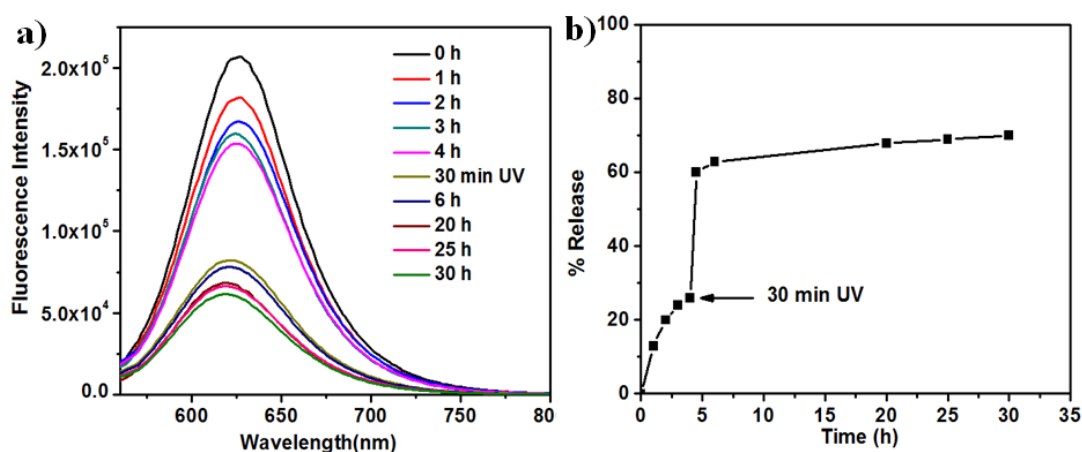


**Figure 4.10** (a) Fluorescence emission spectra of Nile red at different intervals when 0.1 wt% aqueous solution of **P1** was stirred at pH 3 and exposed to UV light. (b) Nile red release profile from aqueous solution of **P1** for the simultaneous application of pH and light.

Micellar solution was stirred at pH 3 for 4 h and then irradiated for 30 min with 365 nm light so that both the stimuli were applied simultaneously. Emission intensity of encapsulated Nile red was monitored during the entire period at regular time intervals. A sharp decrease in fluorescence intensity was seen upon photoirradiation indicating sudden increase in degradation of micelles and consequent dye release (Figure 4.10a). About 60% of dye was released after 5h compared to 20% when only pH stimulus was applied for the same period of time (Figure 4.10b). Thus, percentage of dye release could be increased by simultaneous application of photo and pH stimuli as desired.

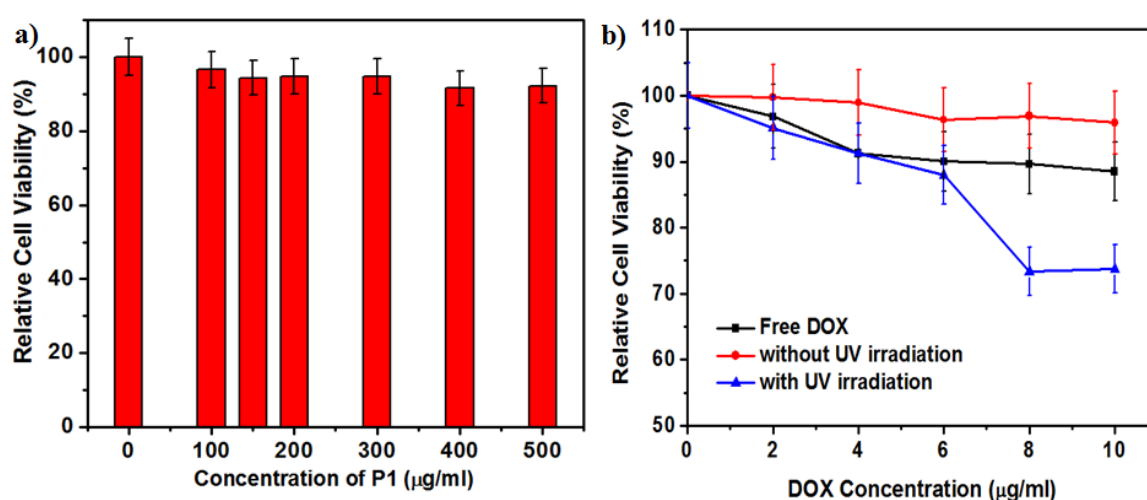


**Figure 4.11** (a) Cell viability of MDA-MB-231 cells incubated with different concentrations of **P1** for 40h. (b) Cell viability of MDA-MB-231 cells with free DOX and DOX loaded **P1** micelles with different DOX concentrations for 2h of incubation before and after UV irradiation.

Biocompatibility of the copolymer was evaluated by carrying out *in vitro* cytotoxicity assay (MTT assay). Figure 4.11a shows relative percent cell viability in the presence of different concentrations of the polymer. Excellent biocompatibility of the synthesized LDBC was suggested by more than 90% cell viability observed up to 500 µg/mL of polymer. The polymeric micelles were then tested for the ability to transport an encapsulated drug into tumor cells and its stimuli-responsive release. DOX, an anticancer drug, was encapsulated in **P1** micelles in the same manner as described for Nile red. Free DOX (up to 10 µg) showed no cytotoxic effect (>85% cell viability) after 2h of incubation as expected. This is because MDA-MB-231 cells are known for resistance to DOX.<sup>44</sup> The DOX-loaded micelles were then incubated with the cells. Good cell viability (>90%) was observed without UV irradiation. However, after UV irradiation the viability decreased by

about 30% suggesting cellular uptake and controlled release of the drug (Figure 4.11b). UV-vis spectroscopy was used to calculate drug loading efficiency (DLE) and drug loading content (DLC) of the micelles as 20% and 2%, respectively (Figure 4.12).

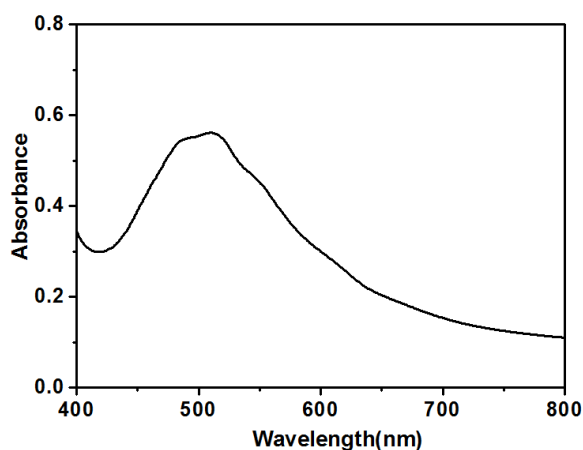


**Figure 4.12** UV-vis spectrum of DOX in aqueous solution of **P1**.

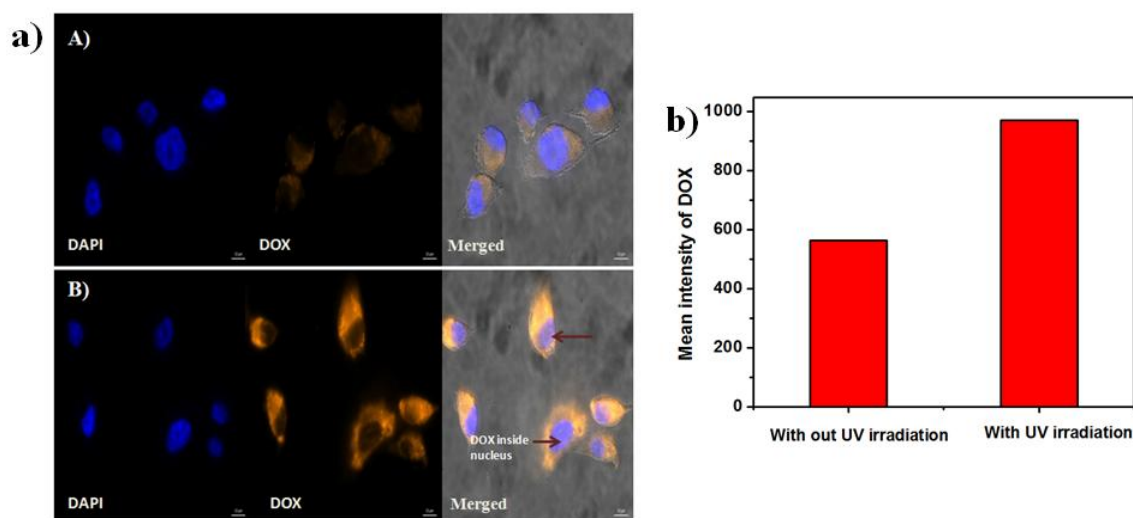


**Figure 4.13** (a) Epifluorescence images of MDA-MB-231 cells incubated for 2h with DOX-loaded **P1** micelles without UV irradiation (panel A) and after UV irradiation (panel B). For each panel, the images from left to right show cell nuclei stained by DAPI (blue), fluorescence of DOX (red), and overlay of the two images. All images were taken at same exposure time for DOX and scale bar is 10 $\mu$ m. (b) Mean fluorescence intensity of DOX quantified by Imaging Software ZEN PRO 2012 (From Carl ZEISS). Total number of cells counted =10.

The uptake and release of DOX into cells was confirmed by epifluorescence microscopy. The images revealed internalization of DOX through micellar carrier (Figure 4.13, panel A) and its release upon photoirradiation (panel B). About 40% increase in

mean fluorescence intensity of DOX was observed after exposure to UV light (Figure 4.13b). Thus, uptake of DOX-loaded micelles by tumor cells and significant release of the drug took place after photocleavage of the polymer upon UV irradiation.

#### 4.4 Summary

A novel biocompatible amphiphilic LDBC containing photo- and pH-cleavable units at the junction of two blocks was synthesized. Photo-cleavable *o*-nitrobenzyl group and acid-labile acetal linkage were installed between the hydrophobic and hydrophilic blocks using click chemistry. The design is such that upon application of either stimulus the two blocks can be separated from each other. Self-assembly of the polymer was established using DLS analysis and determination of cmc. Photo and pH stimuli were applied separately to polymeric aggregates in aqueous solution to establish their effectiveness and the dye release rates. A polymer without the photo-cleavable group was synthesized for control experiments. Both the stimuli were also used simultaneously to achieve tunable release profile with rapid disassembly to study synergistic effect of light and pH. The percentage release of dye was higher when both stimuli were in force than when only pH was used as stimulus. Biocompatibility of the polymer was ascertained using MTT assay. The polymer micelles were shown to be able to transport DOX into the cells and release it in a controlled manner after photoirradiation. This was evident by higher cytotoxicity of drug-loaded micelles than that of free drug.

#### 4.5 References

- 1) Gheybi, H.; Adili, M. *Polym. Chem.* **2015**, *6*, 2580.
- 2) Fox, M. E.; Szoka, F. C.; Fréchet, J. M. J. *Acc. Chem. Res.* **2009**, *42*, 1141.
- 3) Gillies, E. R.; Jonsson, T. B.; Fréchet, J. M. J. *J. Am. Chem. Soc.* **2004**, *126*, 11936.
- 4) Zhang, Y.; Xiao, C.; Li, M.; Chen, J.; Ding, J.; He, C.; Zhuang X.; Chen, X. *Macromol. Biosci.* **2013**, *13*, 584.
- 5) Tian L.; Hammond, P. T. *Chem. Mater.* **2006**, *18*, 3976.
- 6) Kim, J. H.; Lee, E.; Park, J. S.; Kataoka, K.; Jang, W. D. *Chem. Commun.* **2012**, *48*, 3662.
- 7) Zhou, Z.; Ma, X.; Jin, E.; Tang, J.; Sui, M.; Shen, Y.; van Kirk, E. A.; Murdoch, W. J.; Radosz, M. *Biomaterials* **2013**, *34*, 5722.

- 8) Mynar, J. L.; Goodwin, A. P.; Cohen, J. A.; Ma, Y.; Fleming, G. R.; Fréchet, J. M. J. *Chem. Commun.* **2007**, 2081.
- 9) Blasco, E.; Pinol, M.; Oriol, L. *Macromol. Rapid Commun.* **2014**, *35*, 1090.
- 10) Harnoy, A. J.; Rosenbaum, I.; Tirosh, E.; Ebenstein, Y.; Shaharabani, R.; Beck, R.; Amir, R. J. *J. Am. Chem. Soc.* **2014**, *136*, 7531.
- 11) Ryu, J. H.; Park, S.; Kim, B.; Klaikherd, A.; Russell, T. P.; Thayumanavan, S. *J. Am. Chem. Soc.* **2009**, *131*, 9870.
- 12) Schattling, P.; Jochum, F. D.; Theato, P. *Polym. Chem.* **2014**, *5*, 25.
- 13) Zhuang, J.; Gordon, M. R.; Ventura, J.; Li, L.; Thayumanavan, S. *Chem. Soc. Rev.* **2013**, *42*, 7421.
- 14) Dong, J.; Wang, Y.; Zhang, J.; Zhan, X.; Zhu, S.; Yang, H.; Wang, G. *Soft Matter* **2013**, *9*, 370.
- 15) Jin, Q.; Cai, T.; Han, H.; Wang, H.; Wang Y; Ji, J. *Macromol. Rapid Commun.* **2014**, *35*, 1372.
- 16) Cao, Z.; Wu, H.; Dong, J.; Wang, G. *Macromolecules* **2014**, *47*, 8777.
- 17) Han, D.; Tong, X.; Zhao, Y. *Langmuir* **2012**, *28*, 2327.
- 18) Wu, W. X.; Wang, N.; Liu, B. Y.; Deng Q. F.; Yu, X. Q. *Soft Matter* **2014**, *10*, 1199.
- 19) Hu, J.; He, J.; Zhang, M.; Ni, P. *Polym. Chem.* **2015**, *6*, 1553.
- 20) Wang, H.; He, J.; Zhang, M.; Tao, Y.; Li, F.; Tam, K. C.; Ni, P. *J. Mater. Chem. B.* **2013**, *1*, 6596.
- 21) Petrova, S.; Jager, E.; Konefat, R.; Jager, A.; Venturini, C. G.; Spevacek, J.; Pavlova, E.; Stepanek, P. *Polym. Chem.* **2014**, *5*, 3884.
- 22) Bae, Y.; Fukushima, S.; Harada, A.; Kataoka, K. *Angew. Chem. Int. Ed.* **2003**, *42*, 4640.
- 23) Du, J. Z.; Du, X. J.; Mao, Q.; Wang, J. *J. Am. Chem. Soc.* **2011**, *133*, 17560.
- 24) Huang, Y.; Dong, R.; Zhu, X.; Yan, D. *Soft Matter* **2014**, *10*, 6121.
- 25) Gohy, J. F.; Zhao, Y. *Chem. Soc. Rev.* **2013**, *42*, 7117.
- 26) Zhao, H.; Sterner, E. S.; Coughlin, E. B.; Theato, P. *Macromolecules* **2012**, *45*, 1723.
- 27) Cabane, E.; Malinova, V.; Meier, W. *Macromol. Chem. Phys.* **2010**, *211*, 1847.
- 28) Klaikherd, A.; Nagamani, C.; Thayumanavan, S. *J. Am. Chem. Soc.* **2009**, *131*, 4830.
- 29) Dan, K.; Ghosh, S. *Angew. Chem. Int. Ed.* **2013**, *52*, 7300.
- 30) Xuan, J.; Han, D.; Xia, H.; Zhao, Y. *Langmuir* **2014**, *30*, 410.

- 31) Zhuang, J.; Gordon, M. R.; Ventura, J.; Li, L.; Thayumanavan, S. *Chem. Soc. Rev.* **2013**, *42*, 7421.
- 32) Moore, J. S.; Stupp, S. I. *Macromolecules* **1990**, *23*, 65.
- 33) Ihre, H.; Padilla de Jesus, O. L.; Fréchet, J. M. J. *J. Am. Chem. Soc.* **2001**, *123*, 5908.
- 34) Gillies, E. R.; Dy, E. E.; Fréchet, J. M. J.; Szoka, F. C. *Mol. Pharmaceutics* **2005**, *2*, 129.
- 35) Zhang, W.; Jiang, W.; Zhang, D.; Bai, G.; Lou, P.; Hu, Z. *Polym. Chem.* **2015**, *6*, 2274.
- 36) Hed, Y.; Zhang, Y.; Andren, O. C. J.; Zeng, X.; Nystrom, A. M.; Malkoch, M. *J. Polym. Sci., Part A: Polym. Chem.* **2013**, *51*, 3992.
- 37) Yan, Q.; Han, D.; Zhao, Y. *Polym. Chem.* **2013**, *4*, 5026.
- 38) Gillies, E. R.; Goodwin, A. P.; Fréchet, J. M. J. *Bioconjugate Chem.* **2004**, *15*, 1254.
- 39) Schumers, J. M.; Gohy, J.-F.; Fustin, C. A. *Polym. Chem.* **2010**, *1*, 161.
- 40) Satoh, K.; Poelma, J. E.; Campos, L. M.; Stahl, B.; Hawker, C. J. *Polym. Chem.* **2012**, *3*, 1890.
- 41) Meldal, M.; Tornøe, C. W. *Chem. Rev.* **2008**, *108*, 2952.
- 42) Kolb, H. C.; Finn, M. G.; Sharpless, K. B. *Angew. Chem., Int. Ed.* **2001**, *40*, 2004.
- 43) Wu, P.; Malkoch, M.; Hunt, J. N.; Vestberg, R.; Kaltgrad, E.; Finn, M. G.; Fokin, V. V.; Sharpless, K. B.; Hawker, C. J. *Chem. Commun.* **2005**, 5775.
- 44) Aroui, S.; Brahim, S.; De Waard, M.; Kenani, A. *Biochem. Biophys. Res. Commun.* **2010**, *391*, 419.

## **Chapter 5**

### **Effect of Dendron Periphery on Thermoresponsive Properties of bis-MPA Dendron-Azobenzene-PNIPAM Copolymer Assemblies**

## 5.1 Introduction

The importance of stimuli-responsive amphiphilic polymer micelles for drug delivery applications<sup>1,2</sup> was highlighted in Chapter 1. These assemblies are designed in order to overcome problems such as overstability and lack of control over releasing payloads at specific sites. Initially, majority of the polymers dealt with single stimulus however, a combination of different stimuli is likely to afford better control over release of the drug as discussed and demonstrated in Chapter 4 with dual-stimuli-responsive LDBC. Towards this goal, multi-stimuli-responsive linear amphiphilic polymers, particularly those with more than two groups, have been investigated recently. Thayumanavan and co-workers reported the triple stimuli-sensitive linear polymer comprising pH-sensitive hydrophobic block, temperature-sensitive hydrophilic block and redox-sensitive disulfide moiety in between the two blocks.<sup>3</sup> Degradation of the aggregates with different stimuli and controlled release of encapsulated dye was shown. Yuan and co-workers reported the linear polymer exhibiting light-, pH- and temperature-response comprising pH- and temperature-responsive PDMAEMA as the hydrophilic block and poly{6-[4-(4-pyridyazo)phenoxy]]hexyl methacrylate} as the photo-responsive hydrophobic block.<sup>4</sup> Cao, et al. reported<sup>5</sup> synthesis of quadruple stimuli-responsive linear polymer poly(2-nitrobenzyl methacrylate)-SS-poly(dimethylaminoethyl methacrylate) (PNBM-SS-PDMAEMA) that is responsive to pH, photo, temperature and reducing agent. The polymer was self-assembled into micelles in aqueous solution with light-responsive hydrophobic core, pH- and temperature-responsive hydrophilic PDMAEMA corona and the redox-sensitive disulphide linker.

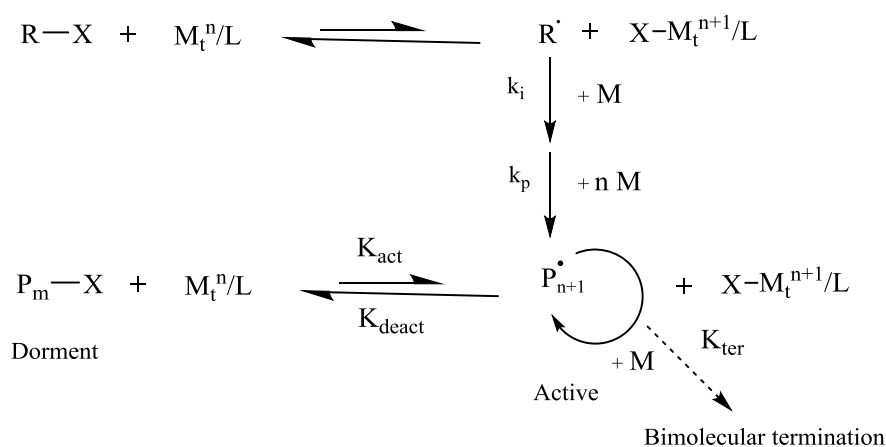
In contrast to linear polymers, there are few reports on LDBCs with different stimuli such as pH, temperature, redox and light in the same polymer as discussed in Chapter 1. For example, Zou et al.<sup>6</sup> reported a dual-stimuli responsive PNIPAM-poly(benzyl ether) dendron copolymer *via* complexation between  $\beta$ -cyclodextrin ( $\beta$ -CD) and azobenzene and reversible change in morphology with photoirradiation was shown. Later, double hydrophilic LDBC comprising temperature-responsive poly(2-(2'-methoxy ethoxy)ethyl methacrylate) linear polymer was reported<sup>7</sup> and were shown to undergo reversible transition between double hydrophilic and amphiphilic form upon heating ( $>$  LCST) and cooling ( $<$  LCST). Recently, pH-responsive poly(benzyl ether) dendrons with carboxylic acid groups at the periphery attached to temperature-responsive poly(2-isopropyl 2-



oxazoline) (PiPrOx) were reported<sup>8</sup>. These LDBC's showed change in the morphology over a wide range of pH and temperatures. Recently, pH- and redox-responsive PEG-PAMAM LDBC's were synthesized.<sup>9</sup> Lipoic acid and DOX were attached to PAMAM periphery *via* hydrazone linkage and the polymer micelles were cross-linked using dithiothreitol (DTT) and controlled release of the drug from micelles at acidic pH and by adding glutathione was shown.

PNIPAM is one of the most studied temperature-responsive polymer and displays LCST around 32 °C.<sup>10</sup> The phase separation is energetically favourable considering the Gibbs free energy of the system given by  $\Delta G = \Delta H - T\Delta S$ . With increase in temperature the entropy of the system increases because the water associated with polymer chains goes from order to disorder state as the polymer crashes out of the solution. Examples of temperature-responsive LDBC's are known in literature. PNIPAM was synthesized from the focal point of the second generation poly(benzyl ether) dendron using ATRP and the resulting linear-dendritic copolymer exhibited change in morphology from micelles to nanotubes above the LCST.<sup>11</sup> Liu et.al synthesized<sup>12</sup> dendritic-linear-dendritic triblock copolymers by polymerizing N-isopropylacrylamide in the presence of G3 poly(benzyl ether) dendron chain-transfer agent. The triblock copolymers self-assembled in water into spherical micelles with dendron in the core and PNIPAM loops surrounding the core. Later, poly(benzylether) dendron-b-PNIPAM diblock copolymers were reported<sup>13</sup> using the same strategy. Two stage collapse of PNIPAM chains well before LCST temperature was shown by using pyrene as fluorescence probe. Kim et al. reported<sup>14</sup> the synthesis of biodegradable LDBC's with third generation poly(L-lysine) dendron and PNIPAM grafted with poly(L-lactide) chains on periphery. The temperature-responsiveness of these polymers was found to be concentration dependent. This aspect of change in morphology of polymer assemblies upon increasing temperature due to presence of PNIPAM as one of the blocks has been explored in detail in amphiphilic polymers.<sup>15-17</sup> Such dynamic change in a self-assembly caused by external stimulus is a way to generate smart materials and biomimetic systems. The morphological transformation also alters the encapsulation and release behaviour of the assembly. Hence, study of change in morphology with temperature, particularly by varying the polarity of dendron periphery, is of interest in this chapter since such a study on assemblies of PNIPAM has not been reported.

In this chapter, PNIPAM with different chain lengths was synthesized using ATRP, which is one of the most widely used controlled radical polymerization (CRP) techniques that afford good control over chain length and molecular weight distribution. It was developed independently by Matyjaszewski<sup>18</sup> and Sawamoto<sup>19</sup> in 1995. The mechanism involved in ATRP is derived from redox-catalyzed telomerisation reaction and atom transfer radical addition. In conventional radical polymerization, high concentration of propagating radicals leads to termination and chain transfer that causes broadening of molecular weight distribution. Fast initiation is necessary to ensure that all the propagating chains grow simultaneously in a controlled manner. In ATRP, this problem of controlling propagating radicals was overcome by achieving dynamic equilibrium between active radical species and dormant species. The lowered concentration of active radicals results in less termination reactions and chain ends remain active.<sup>20</sup> In ATRP, alkyl halide is used as the initiator and R radicals are generated in a controlled manner from the alkyl halides *via* a reversible process mediated by complex of a transition metal, mainly copper, as shown below.



**Scheme 5.1** Mechanism of ATRP

In this chapter, dual-stimuli-responsive LDBC s made up of bis-MPA dendron attached to PNIPAM through azobenzene linker were designed and synthesized. Polarity of dendron was varied by installing two different groups - acetamide and hydroxyl on the periphery and its effect on temperature-responsive morphologies was studied. Dye release behaviour in response to light and temperature was also investigated.

## 5.2 Experimental Section

### 5.2.1 Materials

2,2-bismethylolpropionic acid (bis-MPA), Dowex H<sup>+</sup> resin, 2-bromoisobutyryl bromide, copper(I)chloride, 4-aminobenzyl alcohol and anhydrous DMF were purchased from Aldrich chemicals. N-isopropyl acrylamide was purchased from Acros chemicals and purified by recrystallization in hexane and benzene mixture. Propargyl alcohol, dicyclohexyl carbodiimide (DCC), phenol, 2-chloroethanol, p-toluenesulphonyl chloride, potassium carbonate and triethylamine were purchased from Avra chemicals, Spectrochem and Merck Chemicals, India. 4-(N,N-dimethylamino)pyridine p-toluenesulfonate (DPTS) and Me<sub>6</sub>TREN were synthesized by the reported procedures.<sup>21,22</sup> Dichloromethane was dried over CaH<sub>2</sub> and acetone was dried over K<sub>2</sub>CO<sub>3</sub>, distilled and stored in a Schlenk flask.

### 5.2.2 Instrumentation

Transmittance with variable temperature was recorded on Unisoku Coolspek UV USP-203-A spectrophotometer. Fluorescence emission spectra were recorded on CARY Eclipse spectrometer or Horiba Jobin Yvon Fluorolog 3 spectrometer. For photoisomerization, a 100W UV lamp equipped with 365 nm filter (intensity 21000 μW cm<sup>-2</sup>) and Naava LT 6W T5 lamp (450 nm) were used. DLS measurements were performed on Zetasizer Nano ZS, Malvern instrument equipped with a 633nm He-Ne laser at 90° scattering angle.

### 5.2.3 Synthesis

**Acetonide-protected bis-MPA-G3-alkyne:** It was synthesized following the same procedure as described in Chapter 4.

**Compound 1:** The compound was synthesized by reacting 4-aminobenzyl alcohol (5 g, 0.04 mmol) in NaNO<sub>2</sub>/HCl solution with phenol (4.58 g, 0.048 mmol) and KOH (4.47 g, 0.07 mmol) following reported procedure.<sup>23</sup> Yield 55%. <sup>1</sup>H NMR (CDCl<sub>3</sub> 200MHz) δ: 4.62 (d, J=4Hz, 2H), 5.40 (t, J=6Hz, 1H), 6.96 (d, J=10Hz, 2H), 7.51(d, J=10Hz, 2H), 7.82(d, J=8Hz, 4H), 10.34(s, 1H) ppm.

**Compound 2:** Compound 1 (1 g, 0.0043 mmol) and 2-azidoethyl tosylate (1.26 g, 0.0052

mmol) were dissolved in dry DMF and  $K_2CO_3$  (2.43 g, 0.0175 mmol) was added. Reaction mixture was stirred at 70 °C for 12 h. Product was purified by column chromatography eluting with 20% ethyl acetate in DCM to give compound 8 as orange coloured powder. Yield 85%.  $^1H$  NMR ( $CDCl_3$  200MHz)  $\delta$ : 3.66 (t, J=4Hz, 2H), 4.25(t, J=4Hz, 2H), 4.79(s, 2H), 7.03(d, J=8Hz, 2H), 7.49(d, J=8Hz, 2H), 7.92(t, J=8Hz, 4H) ppm.  $^{13}C$  NMR ( $CDCl_3$ , 50MHz): 50.13, 64.94, 67.22, 114.84, 122.86, 124.8, 127.47, 143.33, 147.42, 152.2, 160.62 ppm.

**Compound 3:** Compound 2 (0.3 g, 0.001 mmol) was dissolved in dichloromethane and triethylamine (0.212 mL, 0.0015 mmol) was added followed by drop wise addition of 2-bromoisobutyryl bromide (0.187 mL, 0.0015 mmol) and stirred at room temperature for 2h. Product was purified by column chromatography by eluting with dichloromethane. Yield 90%.  $^1H$  NMR ( $CDCl_3$  200MHz)  $\delta$ : 1.98(s, 6H), 3.66(t, J=4Hz, 2H), 4.25(t, J=4Hz, 2H), 5.29(s, 2H), 7.03(d, J=8Hz, 2H), 7.50(d, J=8Hz, 2H), 7.92(t, J=10Hz, 4H).  $^{13}C$  NMR ( $CDCl_3$ , 50MHz): 30.88, 50.21, 55.69, 67.17, 114.94, 122.93, 124.97, 128.63, 137.77, 147.47, 152.56, 160.84, 171.54 ppm.

#### *General procedure for the $N_3$ -Azo-PNIPAM synthesis*

Schlenk tube was charged with ATRP initiator 3 (0.15g, 0.33 mmol), NIPAM (3.45g, 30.5 mmol) and tris(2-dimethylaminoethyl)amine ( $Me_6$ -TREN) (0.1 mL, 0.34 mmol) followed by DMF and water (4:1 v/v) and purged for 30 min with  $N_2$  to remove the dissolved oxygen. Then three freeze-pump-thaw cycles were applied and CuBr (0.048 g, 0.33 mmol) was added under  $N_2$  flow. Solvents were removed under high vacuum and reaction mixture was passed through neutral alumina to remove copper salts. The residue was precipitated into cold hexane to remove the monomer.

**$N_3$ -Azo-PNIPAM<sub>48</sub>:**  $^1H$  NMR ( $CDCl_3$  200MHz)  $\delta$ : 1.14 (s, 6H,  $-N(CH_3)_2$ ), 1.64-2.15 (m, 3H, polymer backbone), 3.66(t, 2H, J=4Hz,  $-CH_2$ ), 4.00 (s, 1H,  $-NH(CH_3)$ ), 4.25(t, 2H, J=4Hz,  $-CH_2$ ), 5.15(s, 2H,  $-CH_2$ ), 7.04(d, 2H, J=8Hz, (ArH)), 7.47(d, 2H, J=8Hz ArH), 7.88(m, 4H, (ArH)) ppm. GPC (eluent: DMF, PMMA stds).  $M_n=6400$ ,  $M_w=7800$ , PDI=1.21.

**N<sub>3</sub>-Azo-PNIPAM<sub>79</sub>:** <sup>1</sup>H NMR (CDCl<sub>3</sub> 200MHz) δ: 1.14 (s, 6H, -N(CH<sub>3</sub>)<sub>2</sub>), 1.63-2.11 (m, 3H, polymer backbone), 3.67(t, 2H, J=4Hz, -CH<sub>2</sub>), 4.01 (s, 1H, -NH(CH<sub>3</sub>)), 4.24(t, 2H, J=4Hz, -CH<sub>2</sub>), 5.16(s, 2H, -CH<sub>2</sub>), 7.04(d, 2H, J=8Hz, (ArH)), 7.47(d, 2H, J=8Hz, (ArH)), 7.88(m, 4H, (ArH)) ppm. GPC (eluent: DMF, PMMA stds). M<sub>n</sub>=12600, M<sub>w</sub>=14500, PDI=1.15.

***Click reaction between acetonide-bis-MPAG3-alkyne and N<sub>3</sub>-Azo-PNIPAM:***

Bis-MPAG3-alkyne (0.2 g, 0.1 mmol) and N<sub>3</sub>-azo-PNIPAM (0.91 g, 0.09 mmol) were dissolved in mixture of THF and MeOH (9:1) and CuBr (0.014 g, 0.09 mmol) and PMDETA (20 μL, 0.09 mmol) were added under N<sub>2</sub> atmosphere. Reaction mixture was stirred at room temperature for 24 h. Solvents were removed under reduced pressure and precipitated in cold diethyl ether to get the LDBC as yellow-coloured powder.

**Polymer P1:** <sup>1</sup>H NMR (CDCl<sub>3</sub> 400MHz) δ: 1.13 (s, 6H, -N(CH<sub>3</sub>)<sub>2</sub>), 1.34(s,12H, acetonide group), 1.40(s, 12H, acetonide group), 1.63-2.14 (m, 3H, polymer backbone), 3.60(s, 4H-CH<sub>2</sub>,bis-MPA), 3.63(s, 4H, -CH<sub>2</sub> of bis-MPA), 4.00(s, 1H, -NH(CH<sub>3</sub>)), 4.13 (s, 4H, -CH<sub>2</sub>,bis-MPA), 4.16 (s, 4H, -CH<sub>2</sub> of bis-MPA), 4.22-4.27 (m, 12H, -CH<sub>2</sub>, bis-MPA), 4.47(t, 2H, -CH<sub>2</sub> (Azo)), 4.86(s, 2H, -CH<sub>2</sub> of bis-MPA), 5.14(s, 2H, -CH<sub>2</sub> (azo)), 7.01(d, 2H, ArH), 7.43(d, 2H, -CH<sub>2</sub>, ArH), 7.85-7.95(m, 5H, triazole and ArH) ppm. Yield 75%.

**Polymer P2:** <sup>1</sup>H NMR (CDCl<sub>3</sub>, 400MHz) δ: 1.13 (s, 6H, -N(CH<sub>3</sub>)<sub>2</sub>), 1.33(s, 12H, acetonide group), 1.40(s, 12H, acetonide group), 1.63-2.11 (m, 3H, polymer backbone), 3.60(s, 4H, -CH<sub>2</sub>,bis-MPA), 3.63(s, 4H, -CH<sub>2</sub>,bis-MPA), 4.00(s, 1H, -NH(CH<sub>3</sub>)), 4.12 (s, 4H, -CH<sub>2</sub>,bis-MPA), 4.15 (s, 4H, -CH<sub>2</sub>,bis-MPA), 4.22-4.26 (m, 12H, -CH<sub>2</sub>, bis-MPA), 4.48(t, 2H, -CH<sub>2</sub> (Azo)), 4.84(s, 2H, -CH<sub>2</sub>, bis-MPA), 5.13(s, 2H, -CH<sub>2</sub> (azo)), 7.01(d, 2H, ArH), 7.46(d, 2H, -CH<sub>2</sub>, ArH), 7.85-7.95(m, 5H, triazole and ArH) ppm. Yield 77%.

***Synthetic procedure for deprotected polymers P3 and P4:***

Polymers **P1** and **P2** were dissolved in 0.1N HCl at 20 °C and stirred for 48h. The reaction mixture was lyophilized to obtain yellow-coloured powder. Yield 88%.

**Polymer P3:** <sup>1</sup>H NMR (CD<sub>3</sub>OD, 400MHz) δ: 1.14 (s, 6H, -N(CH<sub>3</sub>)<sub>2</sub>), 1.41-2.09(m, 3H, polymer backbone), 3.57-3.68(m, 16H, (bis-MPA)), 3.96(s, 1H, -NH(CH<sub>3</sub>)), 4.22(m, 12H, bis-MPA), 4.55(t, 2H, J=4Hz -CH<sub>2</sub>(Azo)), 5.18(s, 1H, -CH<sub>2</sub> (Bis-MPA)), 7.09(d, 2H,

$J=12\text{Hz}$ , ArH), 7.54(d, 2H,  $J=8\text{Hz}$ , (ArH)), 7.86-7.92(m, 4H, (ArH)), 8.22(s, 1H, triazole) ppm.

**Polymer P4:**  $^1\text{H}$  NMR ( $\text{CD}_3\text{OD}$ , 400MHz)  $\delta$ : 1.16 (s, 6H,  $-\text{N}(\text{CH}_3)_2$ ), 1.43-2.09(m, 3H, polymer backbone), 3.58-3.68(m, 16H, (bis-MPA)), 3.96(s, 1H,  $-\text{NH}(\text{CH}_3)$ ), 4.23(m, 12H, (bis-MPA)), 4.54(t, 2H,  $J=4\text{Hz}$   $-\text{CH}_2(\text{ArH})$ ), 5.18(s, 1H,  $-\text{CH}_2(\text{bis-MPA})$ ), 7.12(d, 2H,  $J=8\text{Hz}$ , (ArH)), 7.52(d, 2H,  $J=8\text{Hz}$ , (ArH)), 7.86-7.92(m, 5H, (ArH)) 8.22(s, 1H, triazole) ppm.

#### 5.2.4 Preparation of aqueous solution of polymer and Nile red encapsulation

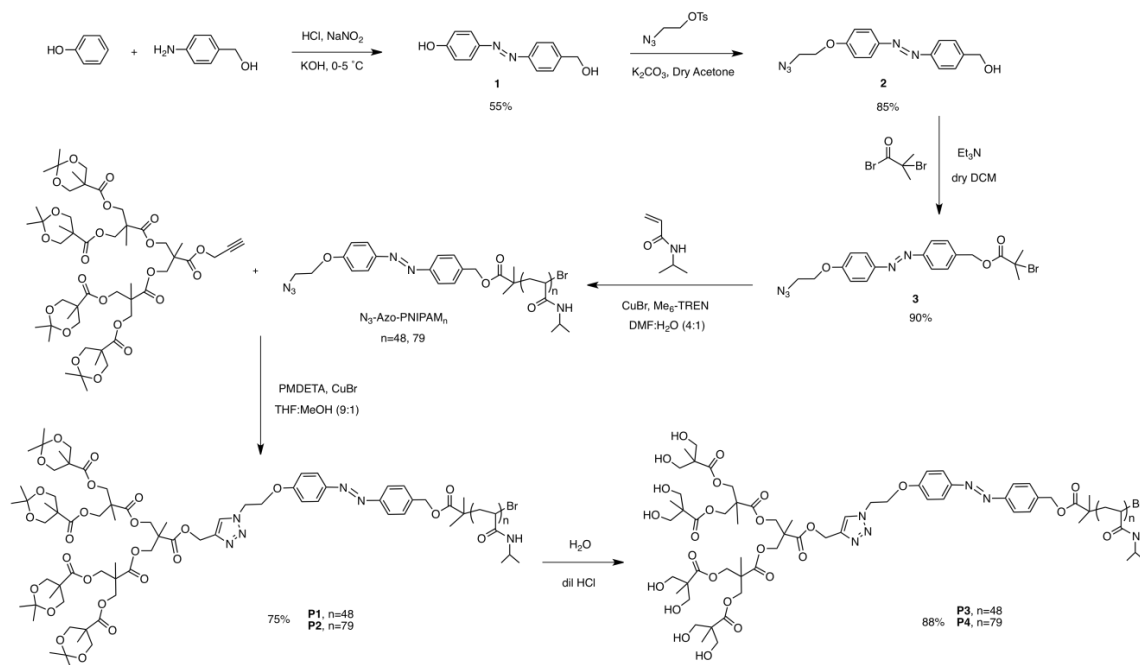
Aqueous solutions of the polymer were obtained by stirring the polymer in water at room temperature for 2 h. For determination of cmc, Nile red ( $5 \times 10^{-6}$  M) was encapsulated in a micellar solution by hydrating a film of the dye using 0.1 wt% polymer solution. This solution was diluted to obtain a series of concentrations and fluorescence emission spectra of Nile red were recorded. The cmc was determined by extrapolating the tangents to the emission intensity versus log (conc.) curve.

### 5.3 Results and discussion

#### 5.3.1 Synthesis

Second generation bis-MPA dendron with acid-cleavable acetonide groups on periphery and alkyne functionality at the focal point was synthesized by following the procedure given in Chapter 4. Photo and temperature-responsive linear polymer was synthesized by ATRP. Azobenzene was selected as photo-responsive linker between the dendron and linear part. Hence it was decided to install azide functionality for click reaction and ATRP initiator moiety for polymerization of NIPAM on 4 and 4' positions of azobenzene. This molecule, **3**, was synthesized from 4-hydroxy-4'-hydroxymethyl azobenzene (**1**) by reacting it with 2-azidoethyl tosylate under Williamson etherification conditions (**2**) followed by 2-bromoisobutyryl bromide in the presence of triethylamine (Scheme 5.2). Subsequently, NIPAM was polymerized from the ATRP initiator site in **3** to obtain PNIPAM with azide and azobenzene at the same chain end. Two different chain lengths, 48 and 79, as determined from  $^1\text{H}$  NMR spectra were obtained (Figure 5.1a). Finally, both the segments were coupled by using CuAAC reaction. The final polymers **P1** and **P2** were

purified by precipitating in cold diethyl ether. In order to obtain a set of polymers with different polarity of the dendron periphery, acetonide (hydrophobic) groups were deprotected to yield polymers **P3** and **P4** with hydroxyl groups at the dendron periphery.



**Scheme 5.2** Synthesis of the targeted copolymers.

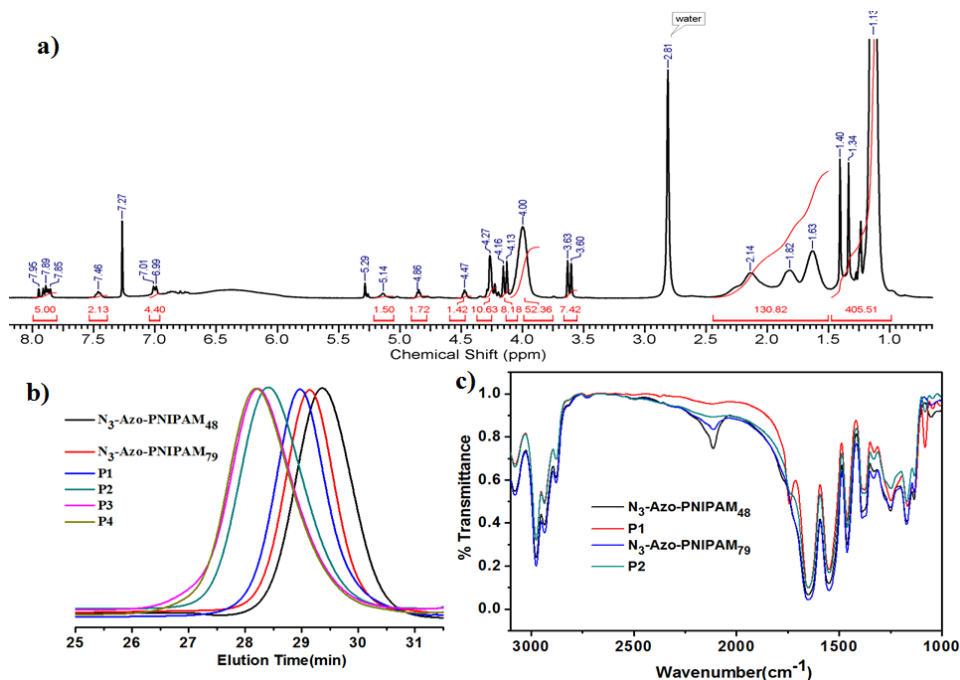


**Figure 5.1** (a)  $^1\text{H}$  NMR spectrum of **P1**. (b) Overlay of GPC chromatograms of **P1–P4** and their precursor linear polymers. (c) FT-IR spectra of final polymers before and after CuAAC reaction.

All four polymers were characterized by using  $^1\text{H}$  NMR and  $^{13}\text{C}$  NMR spectroscopy. Disappearance of azide stretching frequency band at  $2100\text{ cm}^{-1}$  after the click reaction was confirmed from FT-IR spectra (Figure 5.1c). Purity of the polymers was analyzed by GPC, which showed monomodal chromatograms for all polymers (Figure 5.1b). Molecular attributes of all synthesized LDBC's are given in Table 5.1.

### 5.3.2 Temperature-responsive self-assembly

It is well known that PNIPAM chains exhibit LCST around  $32\text{ }^\circ\text{C}$  in water that is characterized by reversible coil-globule transition. However, when NIPAM units are part of a random or a block copolymer, the LCST varies depending upon the relative hydrophobicity/hydrophilicity of the final copolymer.<sup>24</sup> LCST of PNIPAM chain can also be tuned by attachment of a substituent, such as azobenzene, at one end.<sup>25</sup> Since the synthesized PNIPAM containing an azide-functionalized azobenzene at one end are not reported before, their LCST was determined using turbidity measurements carried out on variable temperature UV-vis spectrometer.

**Table 5.1** Molecular parameters of synthesized polymers and LCST values.

Polymer	$M_n$ (NMR)	$M_n$ (GPC) <sup>†</sup>	PDI	LCST ( $^\circ\text{C}$ )
<b>N<sub>3</sub>-Azo-PNIPAM<sub>48</sub>*</b>	5900	6400	1.21	28
<b>N<sub>3</sub>-Azo-PNIPAM<sub>79</sub>*</b>	9400	12600	1.15	32
<b>P1</b>	6900	7800	1.14	29
<b>P2</b>	10400	15000	1.26	32
<b>P3</b>	6700	11600	1.03	28
<b>P4</b>	10200	13800	1.12	32

<sup>†</sup>GPC: Eluent - DMF/0.1 M LiBr,  $60\text{ }^\circ\text{C}$ , RI detector and calibrated with PMMA standards.

\* Degree of polymerization calculated from  $^1\text{H}$  NMR.

Aqueous solution of the polymer at 0.2 wt% concentration was used and measurements were performed at a fixed wavelength (600 nm), which is far from azobenzene absorption. LCST was defined as the temperature corresponding to 10% decrease in the optical



transmittance based on literature reports.<sup>26</sup> Precursor polymers N<sub>3</sub>-Azo-PNIPAM<sub>48</sub> and N<sub>3</sub>-Azo-PNIPAM<sub>79</sub> exhibited a sharp decrease in the transmittance at 28 °C and 32 °C, respectively and the values were taken as LCST of the two polymers (Figure 5.2). LCST increased with increase in molecular weight of the polymers due to concomitant increase in hydrophilicity. It is well known that with increasing hydrophilicity LCST temperature increases.<sup>27</sup> LCST behaviour of the LDBC's comprising acetonide-protected dendron was also studied. LCST values of 29 °C and 32 °C were observed for **P1** and **P2**, respectively, as evidenced from the transmittance vs. temperature curve (Figure 5.2).

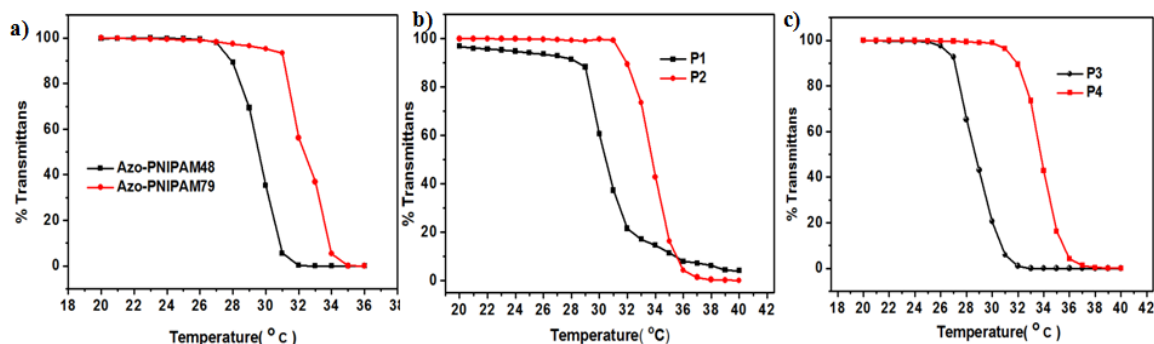


**Figure 5.2** LCST curves for (a) N<sub>3</sub>-Azo-PNIPAM<sub>48</sub>, N<sub>3</sub>-Azo-PNIPAM<sub>79</sub> (b) **P1**, **P2** and (c) **P3**, **P4**.

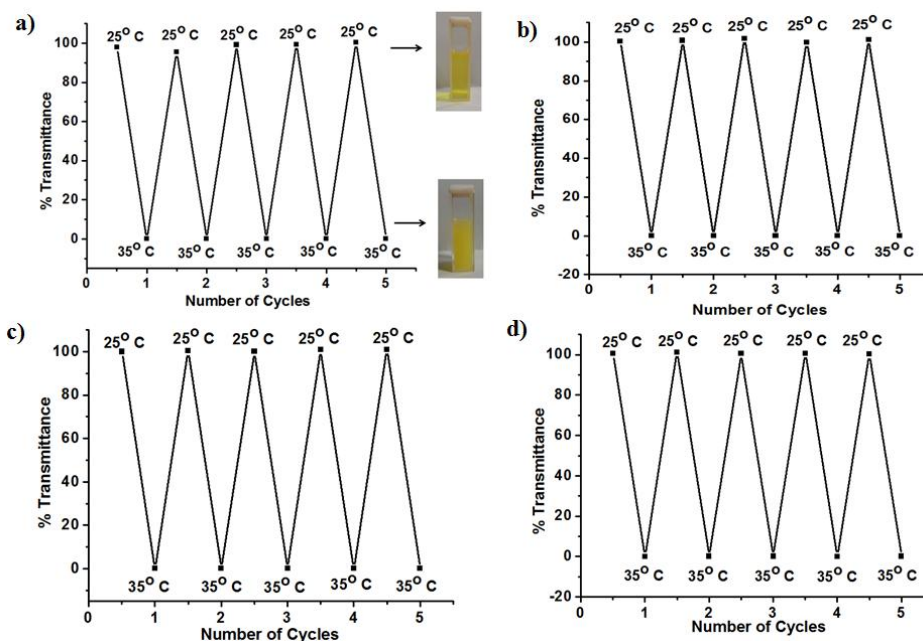


**Figure 5.3** Change in transmittance above and below LCST transition for polymers (a) **P1**, (b) **P2**, (c) **P3** and (d) **P4**.

A slight increase of 1 °C was seen for **P1** suggesting that attachment of mildly hydrophobic dendron did not affect the LCST. The deprotected polymers **P3** and **P4** with

hydroxyl groups at the periphery of dendron showed LCST of 28 °C and 32 °C, respectively. For these polymers with hydrophilic dendron no change in LCST was observed. It is possible that the dendron is only mildly hydrophobic or hydrophilic and does not cause significant change in overall hydrophilicity of the polymer. Reversibility of LCST behaviour of the polymers was demonstrated by recording transmittance with temperature cycling below and above the LCST. All the polymer solutions showed reversible behaviour up to five cycles as shown in Figure 5.3. The solutions turned from clear to turbid and back to clear during the cycles as shown by a representative example of **P1** (pictures in 5.3a).

LDBC **P1** and **P2** were directly soluble in water below LCST and dialysis was not necessary to obtain self-assembled structures. The aggregates would comprise a hydrophobic dendron in the core and hydrophilic PNIPAM chains in the corona below the LCST temperature. DLS was used to detect the presence of aggregates in aqueous solution at 0.1 wt%. Polymers **P1** and **P2** revealed average size ( $D_h$ ) of 42 and 88 nm, respectively. Even though **P3** and **P4** possess polar dendron periphery and only a hydrophobic azobenzene linker is present between the dendron and hydrophilic PNIPAM, DLS analysis revealed average size of 181 and 77 nm for **P3** and **P4**, respectively (Table 5.2).

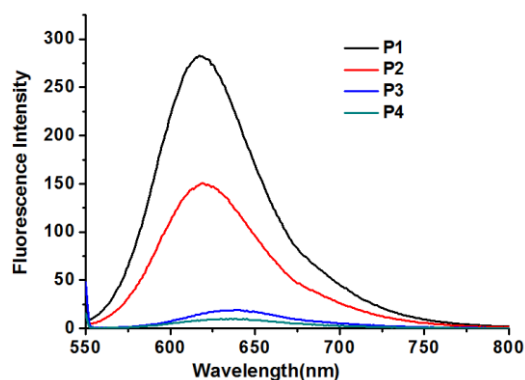


**Figure 5.4** Fluorescence emission spectra of Nile red encapsulated in 0.1 wt% aqueous solutions of **P1–P4**.

However, these aggregates were thought to be loose ensembles of polymer chains and hence TEM analysis was not performed. To support this assumption, dye encapsulation experiment for aqueous solutions of these two polymers and that of **P2** was carried out using Nile red. Fluorescence emission spectra of Nile red encapsulated in aqueous

solutions of **P3** and **P4** was very weak and shifted towards 650 nm suggesting lack of defined hydrophobic core in the aggregates (Figure 5.4). Solution of **P2** showed appreciable dye encapsulation indicating presence of micellar aggregates.

Change in aggregate size in response to temperature was investigated by DLS measurements above LCST that showed large increase in average size to 300–500 nm for all polymers (Table 5.2). Size distribution curves of intensity average for all polymers were monomodal below and above LCST except for **P2** at room temperature (Figure 5.5). Polydispersity in aggregate size also decreased significantly above LCST.

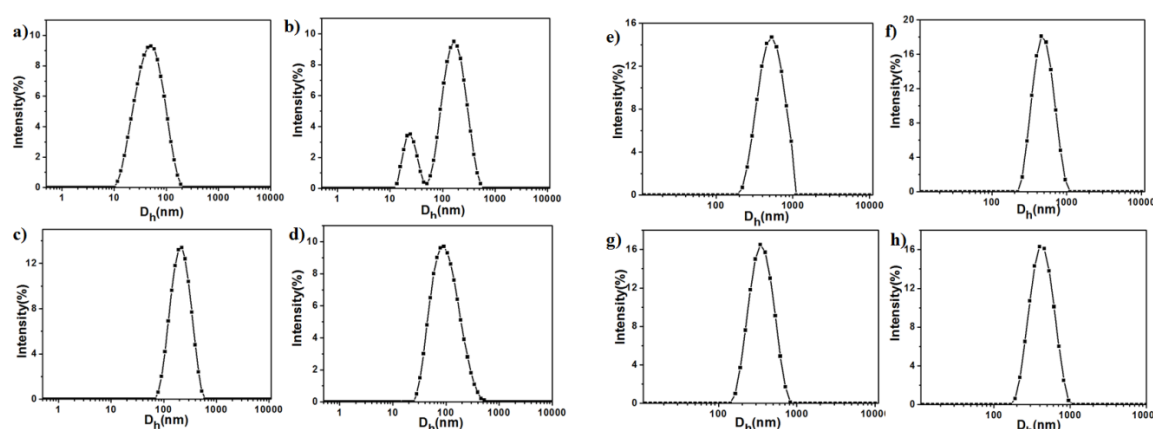


**Figure 5.5** Size distribution curves below (a–d) and above (e–h) LCST for aqueous solutions of **P1–P4**, respectively.

**Table 5.2** DLS data for **P1–P4** below and above the LCST.

Polymer	$D_h$ (nm)	PDI	$D_h$ (nm)	PDI
	at RT		above LCST	
<b>P1</b>	42	0.28	476	0.13
<b>P2</b>	88	0.62	324	0.11
<b>P3</b>	181	0.23	465	0.07
<b>P4</b>	77	0.28	391	0.11

Self-assembly of these polymers was also analyzed using TEM. Aqueous solutions of the polymer prepared in water at 25 °C were spotted on carbon-coated grid and negatively stained by uranyl acetate. **P1** showed cylindrical micelle-like aggregates (Figure 5.6a) whereas **P2** did not show well defined structures at room temperature (Figure 5.6d). To

study the temperature-responsiveness of aggregates temperature of the solutions was increased above the LCST ( $> 40\text{ }^{\circ}\text{C}$ ) and the turbid solution was spotted. A complete change in the morphology was observed for **P1** that showed large vesicle-like aggregates (Figure 5.6b).

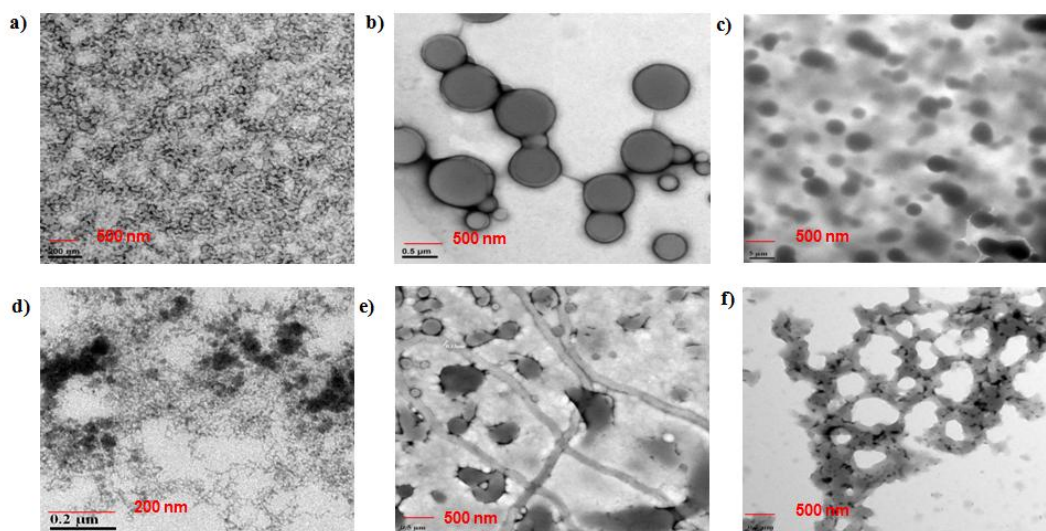


**Figure 5.6** TEM images for **P1** and **P2** (a) (d) at RT and (b) (e) above LCST and for **P3** and **P4** (c), (f) above LCST, respectively.

The average size of the larger aggregates was 275nm measured from TEM images as average of 40 aggregates. Above LCST, **P2** showed spherical micelles co-existing with hundreds of nanometres long tubular micelles (Figure 5.6e). Similarly, self-assembly of deprotected polymers **P3**, **P4** was studied above the LCST. **P3** revealed large spherical micellar aggregates (Figure 5.6c) while **P4** showed ill-defined network-like structures (Figure 5.6f). To check the reversibility in morphology of these polymer aggregates TEM analysis of **P1** was carried out after cooling the solution from above LCST since only **P1** formed well-defined structures at room temperature. Same morphology as the one before heating was not observed upon returning to room temperature, instead network-like aggregates were observed as shown in Figure 5.7.

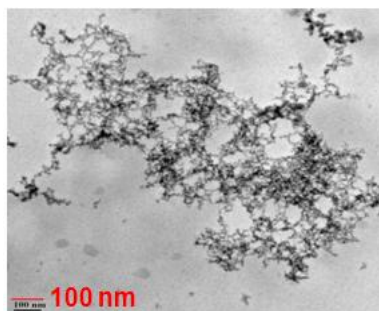


**Figure 5.7** TEM image of 0.1 wt% aqueous solution of **P1** after complete heating and cooling cycle.

Critical micelle concentration of polymers **P1** and **P2** were determined by Nile red solvatochromic hydrophobic dye. The values for polymers **P1** and **P2** are determined as  $5.37 \times 10^{-5}$  M and  $3.71 \times 10^{-5}$  M, respectively from the plots of fluorescence intensity versus log (conc.) shown in Figure 5.8.

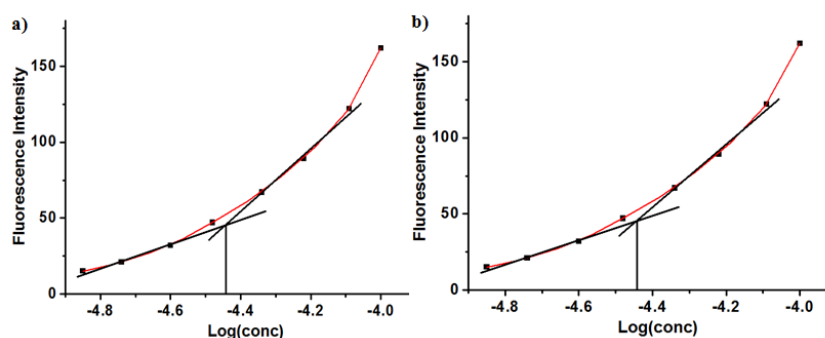


**Figure 5.8** Plots of fluorescence intensity vs. log (conc.) for (a) **P1** and (b) **P2**.

PNIPAM with only one azobenzene unit at the chain end have been studied for photoresponsive behaviour where photoisomerization of azobenzene is shown to affect the LCST as well as micellar assembly.<sup>25,28,29</sup> The polymers synthesized here have a single azobenzene unit in the main chain that is attached to a dendron and PNIPAM on either side and hence the isomerization of azobenzene may be restricted. To investigate light-responsive behaviour of aggregates, solutions of **P1** and **P2** were irradiated with UV and visible light. During photoisomerization of azobenzene two absorption peaks are observed. The peak at 350 nm is ascribed to the  $\pi$ - $\pi^*$  transition of the trans form and the peak at 450 nm is ascribed to n-  $\pi^*$  transition of cis form of azobenzene. Aqueous solution of the aggregates at 0.05wt% concentration was exposed to UV light (365 nm, 100W lamp) with different irradiation times and UV spectra were recorded. With increasing time of



irradiation the  $\pi$ - $\pi^*$  transition peak decreased and n- $\pi^*$  transition peak increased, which indicated transition of azobenzene from *trans*-to-*cis* form (Figure 5.9a and 5.9d). The *trans-cis* photoisomerization was calculated according to Fisher method as 71% and 82% for **P1** and **P2**, respectively. Lower percentage of isomerization in **P1** suggests restricted movement of azobenzene due to well defined morphology. The reverse *cis-trans* isomerization of azobenzene was studied by irradiating with visible light (450 nm, 6W) and absorbance was monitored at different irradiation times. The  $\pi$ - $\pi^*$  transition peak increased and n- $\pi^*$  transition peak decreased, which indicated transition of azobenzene from *cis* to *trans* form (Figure 5.9b and 5.9e). The photoisomerization ratio was calculated to be 60% and 68% for **P1** and **P2**, respectively. Lower values than for *trans-cis* process suggest incomplete reversal of the *cis* isomer to *trans* form. Effect of photoisomerization on morphology of the aggregates was checked by TEM analysis that did not show noticeable change (Figure 5.9c and 5.9f). This is understandable since azobenzene with restricted movement due to its location between dendron and linear polymer may not be able to influence the morphology.

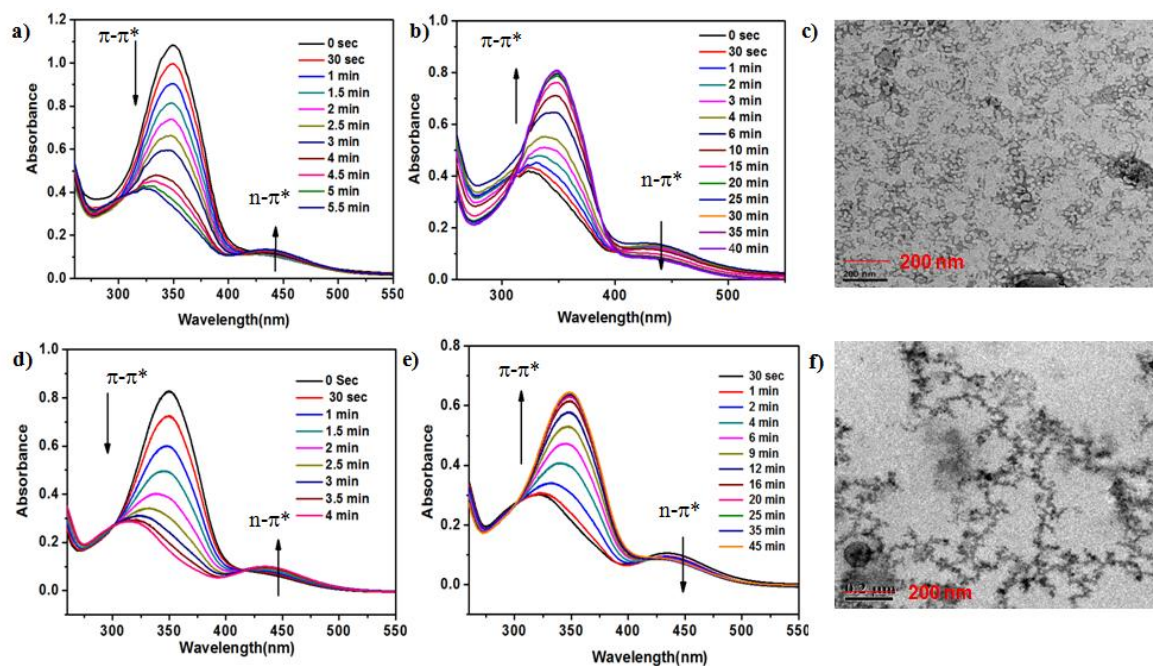


**Figure 5.9** UV-Vis spectra for irradiation of 0.05 wt% aqueous solutions of (a) **P1** (d) **P2** with 365 nm light irradiation and of (b) **P1** (e) **P2** using 450 nm visible light irradiation. TEM images of (c) **P1** and (f) **P2** after UV light irradiation.

### 5.3.3 Photo-responsive behaviour

As studied in Chapter 4, photoinduced release of hydrophobic dye upon *trans-cis* photoisomerization of azobenzene was also investigated for assemblies of **P1**. Since there is only one azobenzene unit per polymer chain and is attached to macromolecular units on both sides, its isomerization may not be sufficient for release of the dye. Nile red was encapsulated in the micellar core by stirring the dye with 0.1 wt% aqueous solution of the polymer. Dye loaded solution was irradiated with 365 nm UV light for 15 minutes to reach photo-stationary state and fluorescence emission spectra of Nile red were recorded by exciting at 550 nm. Peak at 630 nm for Nile red emission decreased to less than 50% of initial intensity (Figure 5.10a). Decrease in the emission intensity could be due to either release of the dye into the aqueous solution or change in the polarity of micellar environment due to presence of more polar *cis* isomer without release of the dye. This possibility was checked by irradiating sample with visible light and monitoring Nile red fluorescence spectra. If the dye has escaped the micelle, fluorescence intensity will not be regained upon *cis-trans* isomerization of azobenzene. Figure 5.10b shows that fluorescence intensity was recovered to the initial value, suggesting that the dye had remained encapsulated and the change in intensity was only due to change in polarity of its environment. This supports one of the assumptions that after UV irradiation the micellar core becomes more polar and causes the decrease in the fluorescence intensity but not the release of dye.

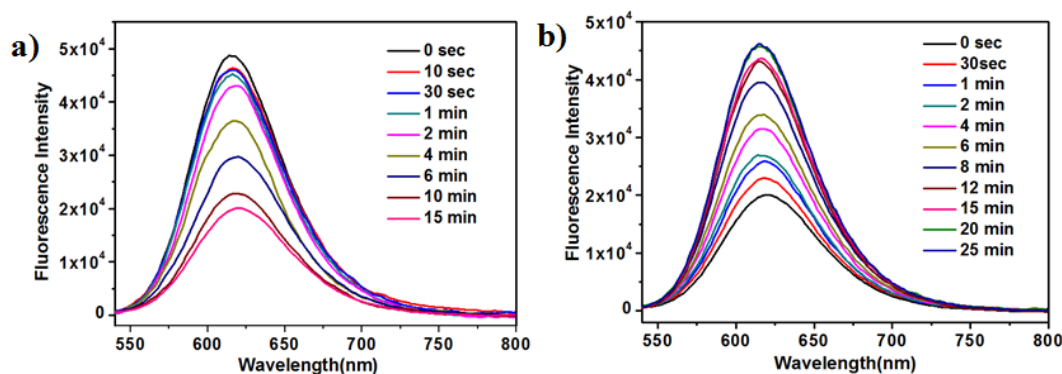


**Figure 5.10** Fluorescence emission spectra of Nile red encapsulated in 0.1 wt% aqueous solution of **P1** upon (a) irradiation with UV light and (b) irradiation with visible light.

### 5.3.4 Temperature-induced dye release

Temperature-responsive property of PNIPAM was also exploited to investigate whether temperature-induced release of Nile red from micellar assemblies was possible. A

significant change in the micelle size and morphology had been observed for **P1** from DLS and TEM analysis, respectively. Nile red was encapsulated into the micelles by stirring with 0.05 wt% polymer solutions at room temperature. Then temperature was increased from 27 °C to 60 °C and the fluorescence intensity of Nile red emission was monitored. Figure 5.11a shows gradual increase in the fluorescence intensity with increasing temperature, which indicates that the dye is now in more hydrophobic environment due to collapse of PNIPAM chains. Temperature was then decreased from 60 °C to 27 °C. Decrease in the emission intensity to a value lower than initial value at 27 °C was observed (Figure 5.11b), which indicates release of the dye from polymer assemblies due to expanded hydrophilic PNIPAM chains.

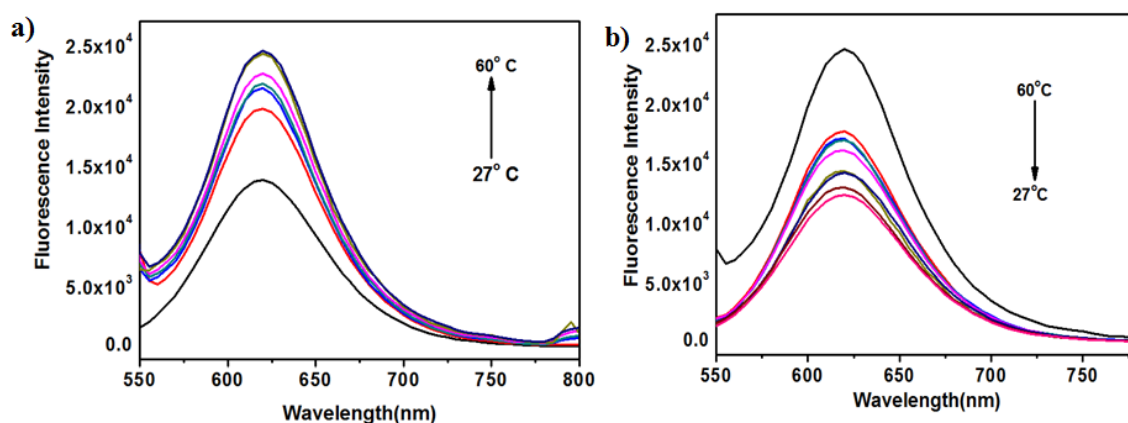


**Figure 5.11** Fluorescence emission spectra of 0.05 wt% aqueous solution of **P1** encapsulated with Nile red (a) heating cycle from 27 °C to 60 °C. (b) cooling cycle from 60 °C to 27 °C.

Heating and cooling cycles were repeated and small decrease in the fluorescence intensity was observed for every cycle (Figure 5.12a). Plot of final emission intensity versus number of cycles shows a total of 9% release of Nile red over four cycles (Figure 5.12b).



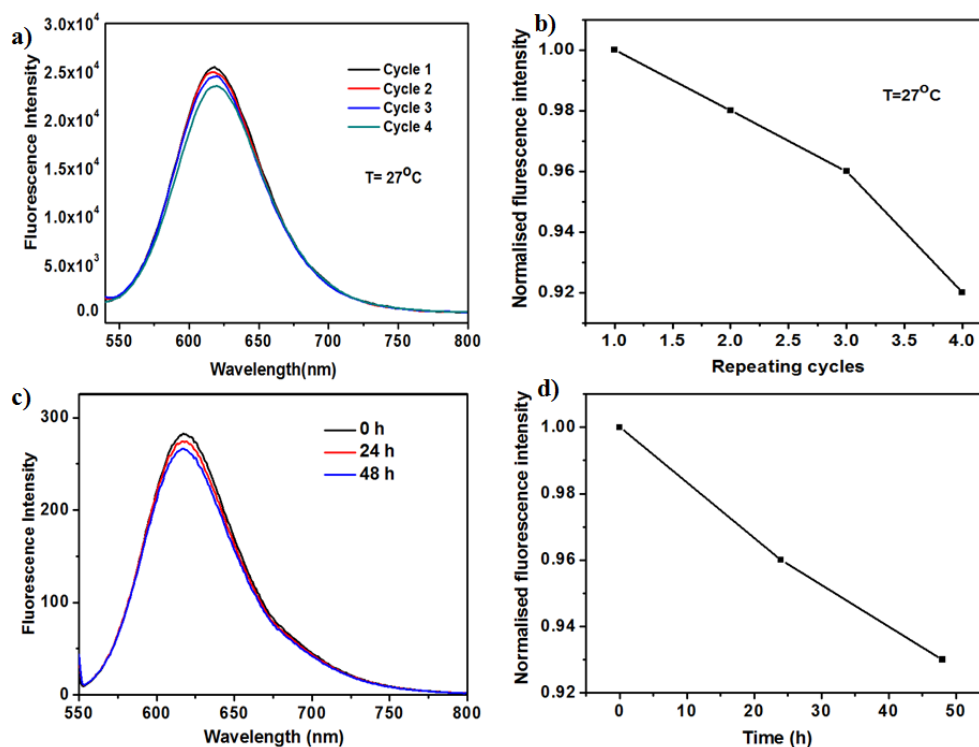


**Figure 5.12** Fluorescence emission spectra of Nile red encapsulated in 0.05 wt% aqueous solution of **P1** during (a) heating-cooling cycling process and (c) at room temperature. Normalized fluorescence intensity profile at (b)  $27^\circ\text{C}$  after 4 cycles and (d) at room temperature.

In a control experiment, fluorescence intensity of Nile red encapsulated in aqueous solution of **P1** was monitored with time at room temperature. About 7% decrease in fluorescence intensity was observed after 48 h suggesting control over dye release during temperature cycling (Figure 5.12c and d).

Polymer **P3** formed loose aggregates without defined hydrophobic core and showed negligible dye encapsulation ability at room temperature as discussed earlier. However, it was expected that when PNIPAM chains collapse above LCST, micelles with hydrophobic pockets may form and dye encapsulation would increase. DLS had also shown large increase in size above LCST. Therefore, similar experiment as above that is monitoring dye fluorescence with temperature cycling was carried out with **P3** as well.

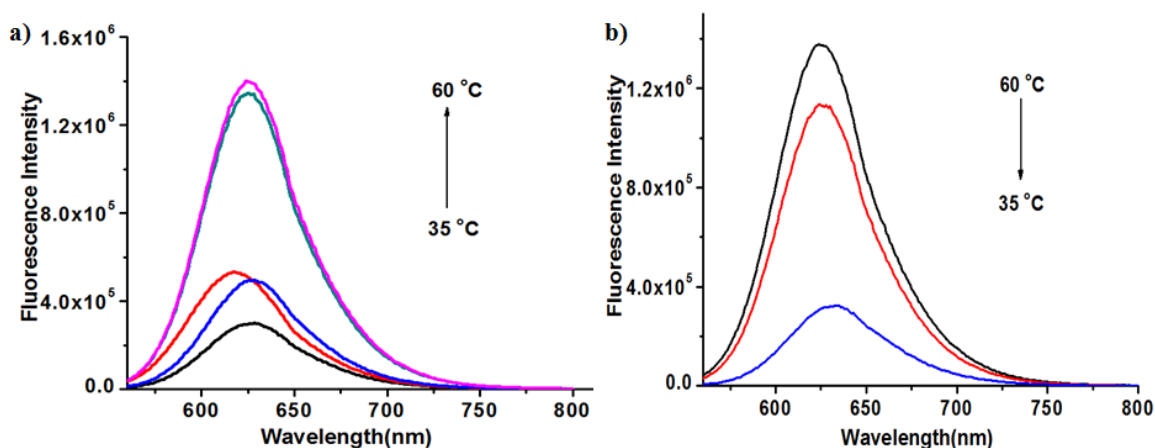


**Figure 5.13** Fluorescence emission spectra of 0.05 wt% aqueous solution of **P3** encapsulated with Nile red (a) heating cycle from 35 °C to 60 °C. (b) cooling cycle from 60 °C to 35 °C.

Fluorescence intensity of Nile red in aqueous solution of **P3** (0.05 wt%) increased upon increasing temperature of the solution from 35 °C to 60 °C with a small hypsochromic shift (Figure 5.13a) suggesting that environment of the dye had become more hydrophobic that is, defined micelles had formed. When temperature was decreased to 35 °C again the fluorescence intensity decreased to earlier value and the peak was red-shifted that is, the dye returned to environment of higher polarity (Figure 5.13b). Thus, dye encapsulation could be effected in a reversible manner in LDBC assemblies using temperature-responsive property of PNIPAM.

#### 5.4 Summary

Two sets of dual-stimuli responsive LDBC with PNIPAM as linear part, azobenzene as linker and either acetonide (**P1**, **P2**) or hydroxyl (**P3**, **P4**) groups at the dendron periphery were synthesized. PNIPAM was synthesized from a novel azobenzene-containing ATRP initiator. In all, four polymers were obtained with varied PNIPAM chain length and dendron periphery. Dendron polarity seemed to affect LCST only slightly. Only **P1** showed well defined morphology at room temperature however, **P2** and **P3** also showed morphologies above LCST as seen in TEM analysis. Polymer **P1** exhibited complete change in morphology above LCST however, the change was not reversible. Change in aggregate size with temperature was also monitored by DLS analysis. Encapsulated Nile red was not released upon photoisomerization, however it showed reversible change in

fluorescence intensity due to change in microenvironment polarity. A small amount of dye release was observed in temperature-variation cycles involving heating above LCST and cooling to room temperature for **P1**. Dye release from micellar aggregates was negligible at room temperature. Polymer **P3** showed dye encapsulation above LCST and release with decrease in temperature. Thus, PNIPAM block copolymers with polar and non-polar groups on periphery of attached dendron displayed completely different morphology and dye encapsulation behaviour in response to temperature variation in aqueous solution.

## 5.5 References

- 1) a) Dong, C. M.; Liu, G. *Polym. Chem.* **2013**, *4*, 46. b) Whitton, G.; Gillies, E. R. *Polym. Chem.* **2015**, *53*, 148. c) Gheybi, H.; Adeli, M. *Polym. Chem.* **2015**, *6*, 2580.
- 2) a) Zhou, Z.; Ma, X.; Jin, E.; Tang, J.; Sui, M.; Shen, Y.; Kirk, E. A. V.; Murdoch, W. J.; Radosz, M. *Biomaterials* **2013**, *34*, 5722. b) Hed, Y.; Zhang, Y.; Andrén, O. C. J.; Zeng, X.; Nyström, A. M.; Malkoch, M. *J. Polym. Sci., Part A: Polym. Chem.* **2013**, *51*, 3992.
- 3) Aathimanikandan, S. V.; Savariar, E. N.; Thayumanavan, S. *J. Am. Chem. Soc.* **2005**, *127*, 14922.
- 4) Yuan, W.; Guo, W.; Ren, G. *Polym. Chem.* **2013**, *4*, 3934.
- 5) Cao, Z.; Wu, H.; Dong, J.; Wang, G. *Macromolecules* **2014**, *47*, 8777.
- 6) Zou, J.; Guan, B.; Liao, X.; Jiang, M.; Tao, F. *Macromolecules* **2009**, *42*, 7465.
- 7) Lee, H.; Lee, J. A.; Poon, Z.; Hammond, P. T. *Chem. Commun.* **2008**, *32*, 3726.
- 8) Kim, J. H.; Lee, E.; Park, J. S.; Jang, Kotaoka, K.; W. D. *Chem. Commun.* **2012**, *48*, 3662.
- 9) Zhang, Y.; Xiao, C.; Li, M.; Ding, J.; He, C.; Zhuang, X.; Chen, X. *Polym. Chem.* **2014**, *5*, 2801.
- 10) Ward, M. A.; Georgiou, T. K. *Polymers* **2011**, *3*, 1215.
- 11) Zhu, L.; Zhu, G.; Li, M.; Wang, E.; Zhu, R.; Qi, X. *Eur. Polym. J.* **2002**, *38*, 2503.
- 12) Ge, Z.; Chen, D.; Zhang, J.; Rao, J.; Yin, J.; Wang, D.; Wan, X.; Shi, W.; Liu, S. *J. Polym. Sci. Part A: Polym. Chem.* **2007**, *45*, 1432.
- 13) Ge, Z.; Luo, S.; Liu, S. *J. Polym. Sci. Part A: Polym. Chem.* **2006**, *44*, 1357.
- 14) Kim, Y. S.; Gil, E. S.; Lowe, T. L. *Macromolecules* **2006**, *39*, 7805.
- 15) Cai, Y.; Aubrecht, K. B.; Grubbs, R. B. *J. Am. Chem. Soc.* **2011**, *133*, 1058.

- 16) Kessel, S.; Urbani, C. N.; Monteiro, M. J. *Angew. Chem., Int. Ed.* **2011**, *50*, 8082.
- 17) Moughton, A. O.; Patterson, J. P.; O'Reilly, R. K. *Chem. Commun.* **2011**, *47*, 355.
- 18) Wang, J. S.; Matyjaszewski, K. *J. Am. Chem. Soc.* **1995**, *117*, 5614.
- 19) Kato, M.; Kamigaito, M.; Sawamoto, M.; Higashimura, T. *Macromolecules* **1995**, *28*, 1721.
- 20) a) Matyjaszewski, K. *Macromolecules* **2012**, *45*, 4015. b) Matyjaszewski, K.; Xia, J. *Chem. Rev.* **2001**, *101*, 2921. c) Matyjaszewski, K. *Isr. J. Chem.* **2012**, *52*, 206
- 21) Ciampolini, M.; Nardi, N. *Inorg. Chem.* **1996**, *5*, 41.
- 22) Moore, J. S.; Stupp, S. *Macromolecules* **1990**, *23*, 65.
- 23) Liu, Z. X.; Feng, Y.; Yan, Z. C.; He, Y. M.; Liu, C. Y.; Fan, Q. H. *Chem. Mater.* **2012**, *24*, 3751.
- 24) Schild, H. G.; Tirrel, D. A. *J. Phys. Chem.* **1990**, *94*, 4352.
- 25) Akiyama, H.; Tamaoki, N. *Macromolecules* **2007**, *40*, 5129.
- 26) Zhang, N.; Salzinger, S.; Rieger, B. *Macromolecules* **2012**, *45*, 9751.
- 27) Fujishige, S.; Kubota, K.; Ando, I. *J. Phys. Chem.* **1989**, *93*, 3311.
- 28) Ishii, N.; Mamiya, J.; Ikeda T.; Winnik, F. M. *Chem. Commun.* **2011**, *47*, 1267.
- 29) Jochum, F. D.; Borg, L. Z.; Roth, P. J.; Theato, P. *Macromolecules* **2009**, *42*, 7854.

## **Chapter 6**

### **Summary and Future Directions**

## 6.1 Summary

Amphiphilic LDBC's have emerged as important building blocks for advanced materials particularly upon introduction of stimuli-responsive groups into the backbone. In this work, a detailed structure-property relationship study was attempted in order to understand the stimuli-responsive behaviour of the self-assembly of LDBC's in solution. The goal of the research work presented in this thesis was two-fold. One of the goals was to understand the influence of structural variations in the dendron upon micellar behaviour of LDBC's and the other was to develop materials that could be used as nanocarriers for drug delivery. Hence, non-biocompatible but easier to synthesize building blocks were used in the first half of the work (Chapters 2 and 3) while biocompatible building blocks were used in the second half (Chapters 4 and 5). Towards synthesis of all LDBC's described here, CuAAC reaction was used for coupling of dendron to linear polymer. As a pre-requisite, dendrons with alkyne at the focal point and linear polymer with azide at one chain end were synthesized in multiple steps from commercially available starting materials. In all of the polymers studied here, the dendron is hydrophobic while the linear part is hydrophilic. Self-assembly of all polymers was studied in aqueous solutions; in the first chapter THF/water mixture (10:90) was used for easy preparation of samples for neutron scattering experiments. The major results obtained from the self-assembly studies are discussed below.

A series of dendrons based on two building blocks with different substitution pattern on phenyl ring was synthesized so that they possessed slight structural variation across the series. This variation in dendron structure allowed incremental variation in hydrophobicity of the polymer unlike the large variation seen across generations in literature reports. PEG of constant chain length was used as the hydrophilic linear polymer. Effect of hydrophobicity of dendron on micellar behaviour was clearly laid out in the SANS studies. Micellar core size increased gradually with dendron generation, however the aggregation number and number of THF molecules in the micellar core were influenced by the branching pattern (building block) that determined hydrophobic density. The difference in micellar properties was strongly marked at higher generations due to different shapes of the hydrophobic dendrons. This effect could also be observed when SANS analysis was carried out by varying solvent ratio and temperature.

Photoresponsive azobenzene units have been installed on dendron periphery in all of the reports in literature on LDBC. In this work, polymers containing dendrons with azobenzene along the dendritic backbone were synthesized. PEG of constant chain length was used as the linear part. Self-assembly in aqueous solution studied using photoirradiation showed a clear dependence of dye encapsulation and photo-induced release properties on the dendron structure, that is, position and number of azobenzene units as well as different groups (dodecyl or benzyl) on the dendron periphery. Dye release was also shown to be influenced by the pathway used for *cis-trans* isomerization that is, using visible light or under thermal conditions. Thus, fine-tuning of dye encapsulation and release could be achieved by varying the position of photoresponsive groups along the dendritic structure.

The second half of the work was focused on LDBC-based biocompatible nanomaterials for drug delivery. Hence, aliphatic polyester dendron built from bis-MPA and PEG or PNIPAM as hydrophilic linear polymer were employed. In one of the designs, pH-cleavable linear acetal and photo-cleavable ONB groups were installed at the junction of two blocks. The dual-stimuli responsive polymer assembled into micelles upon direct dissolution in water. Encapsulated hydrophobic dye was released upon photoirradiation at 365 nm due to photo-induced cleavage of ONB group as well as under acidic conditions. Acetal group showed variation in rate of cleavage depending on the pH, which helped to control the dye release with pH - dye was released much faster at pH 3 than at pH 5. Synergy between the two stimuli was observed when a solution of dye-encapsulated micelles at pH 5 was irradiated by 365 nm wavelength of light. Dye release was significantly enhanced during photoirradiation and returned to slower rate when light was turned off. This polymer was also shown to be non-cytotoxic. Cellular uptake of DOX and its release upon photoirradiation into MDA-MB-231 cells was also seen using epifluorescence microscopy.

In another design, pH-cleavable acetonide units (cyclic acetal) were installed onto bis-MPA dendron periphery and the dendron was connected to PNIPAM of varied chain lengths via azobenzene linker, thus making the polymer triple stimuli-responsive. Acetonide groups were cleaved to obtain double hydrophilic polymers with a polar dendron periphery. Interestingly, no effect of dendron periphery was seen on the LCST values. Polymers with acetonide dendron showed complete change in morphology at

temperature higher than LCST while polymers with polar dendron showed morphology only above LCST. The morphology change was found to be irreversible. Different morphologies were observed for different PNIPAM chain lengths. Small amount of dye release was observed from polymeric micelles containing acetamide dendron after multiple heating-cooling cycles whereas only change in microenvironment of the dye was observed upon photoisomerization without any release. On the other hand, polymeric micelles containing polar dendron showed encapsulation of dye with increasing temperature and its release with decreasing temperature. Thus, control over morphology and dye encapsulation property of temperature-responsive micelles was shown by varying the polarity of dendron periphery. To summarize, four different designs of amphiphilic LDBC's based on position and nature of stimuli-responsive group were studied for their stimuli-responsive behaviour in aqueous solution and control over dye encapsulation and release from the micelles was demonstrated.

## 6.2 Future directions

Based on the results obtained in this work, a discussion on possible future directions is presented here. In Chapters 2, 3 and 4 PEG has been used as the hydrophilic linear part and dendron structure was varied. In these polymers, well-defined morphology was not observed for solution assemblies. In Chapter 5 where PNIPAM was used defined structures were observed for the polymer with highest hydrophobic fraction. It was surmised that for the dendrons used in this work the difference in polarity of dendron and PEG was not sufficient to drive the assembly towards well defined nanostructure. To confirm this hypothesis, poly(N,N-dimethylamino) ethyl methacrylate (PDMAEMA) was used as the hydrophilic linear polymer. With pendent tertiary amine groups, this polymer is more polar and strongly hydrophilic compared to PEG.

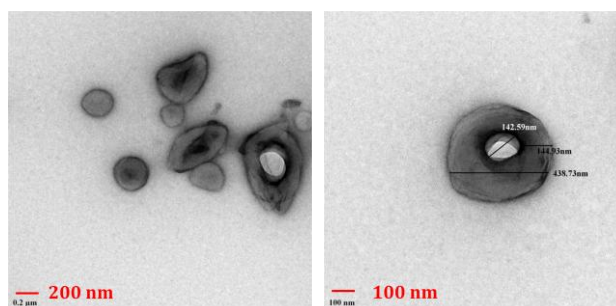


**Figure 6.1** TEM images of 0.1 wt% aqueous solution of 3,4,5G2-PDMAEMA



A LDBC containing the 3,4,5G2 dendron used in Chapter 1 attached to PDMAEMA was synthesized using CuAAC. This polymer in aqueous solution (0.1 wt%) displayed toroid-type (doughnut shaped) morphology in TEM analysis (Figure 6.1). This is an uncommon nanostructure and is possibly formed in this case due to the presence of a strongly hydrophobic dendron and strongly hydrophilic polymer. It will be interesting to explore different morphologies by attaching PDMAEMA to the different dendrons used in this thesis.

LDBCs with azobenzene in the interior have shown interesting dye encapsulation and release properties although only second generation dendrons were used. If higher generation dendrons are synthesized, more variation in the position of azobenzene units in the dendritic backbone can be introduced and furthermore attaching such dendrons to PDMAEMA chains may yield well-defined and unusual photoresponsive morphologies.

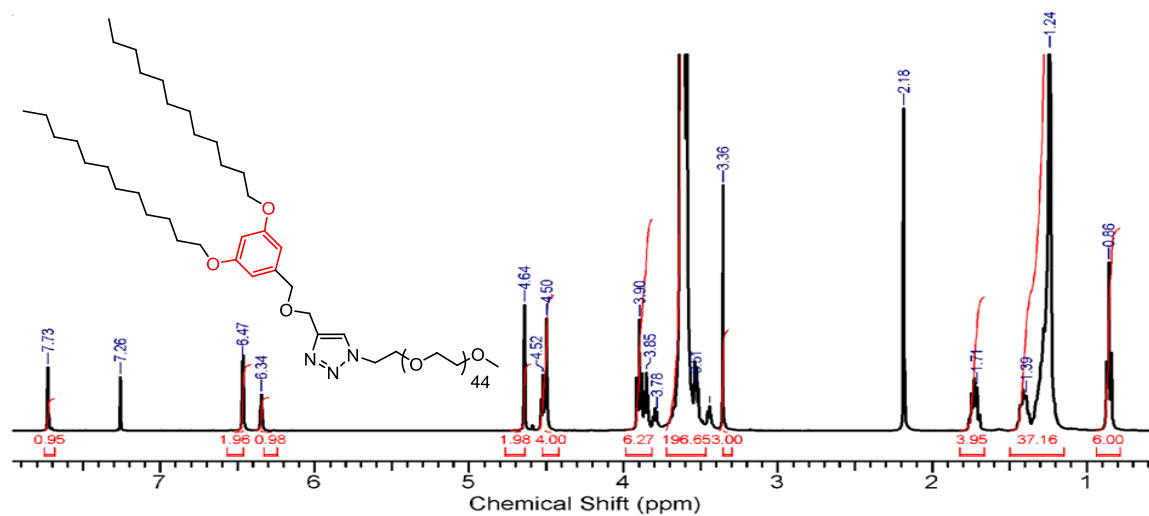
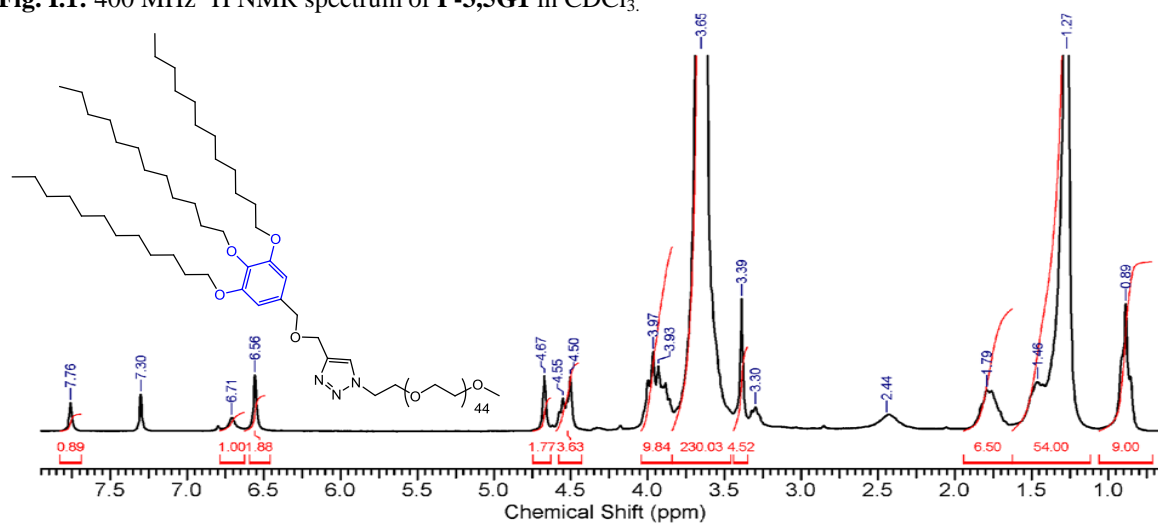
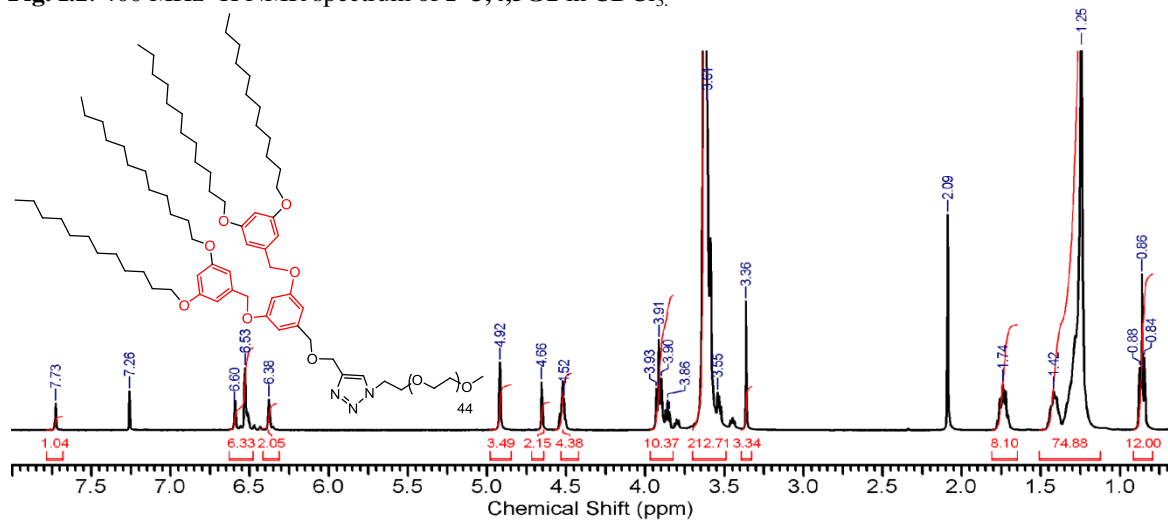
Although the field of LDBCs is now well established and many designs have been explored for efficacy in drug delivery as well as applications requiring solid-state morphologies, more research is still needed to elucidate parameters of the assemblies in real life applications. For example, studies on factors such as bio- distribution, pharmacokinetics, and side effects would lead to better understanding of the design of LDBC-based drug delivery systems.<sup>1</sup> This may help to achieve better targeting properties, higher anticancer efficacy and less side effects thereby arriving at optimized clinical protocols for nanocarriers based on this class of copolymers. Higher, tunable functionality and anisotropic architecture may prove more significant than the shortcomings inherent in the tedious dendrimer synthesis.<sup>2</sup> Multiple groups for targeting, imaging and more than one drug can be introduced in the same dendron in a controlled manner thus making the drug carrier more efficient.<sup>3</sup> It may be worthwhile to expect that development of functional LDBC assemblies for high end applications in catalysis, biomedicine, and drug delivery will take place in the coming years.

### 6.3 References

1. Gheybi, H.; Adeli, M. *Polym. Chem.* **2015**, *6*, 2580.
2. Whitton, G.; Gillies, E. R. *J. Polym. Sci. Part A: Polym. Chem.* **2015**, *53*, 148.
3. Pathak, R. K.; Dhar, S. *J. Am. Chem. Soc.* **2015**, *137*, 8324.

## Appendix I

## NMR, GPC and MALDI-TOF spectra for Chapter 2

Fig. I.1: 400 MHz  $^1\text{H}$  NMR spectrum of **P-3,5G1** in  $\text{CDCl}_3$ .Fig. I.2: 400 MHz  $^1\text{H}$  NMR spectrum of **P-3,4,5G1** in  $\text{CDCl}_3$ .Fig. I.3: 400 MHz  $^1\text{H}$  NMR spectrum of **P-3,5G2** in  $\text{CDCl}_3$ .

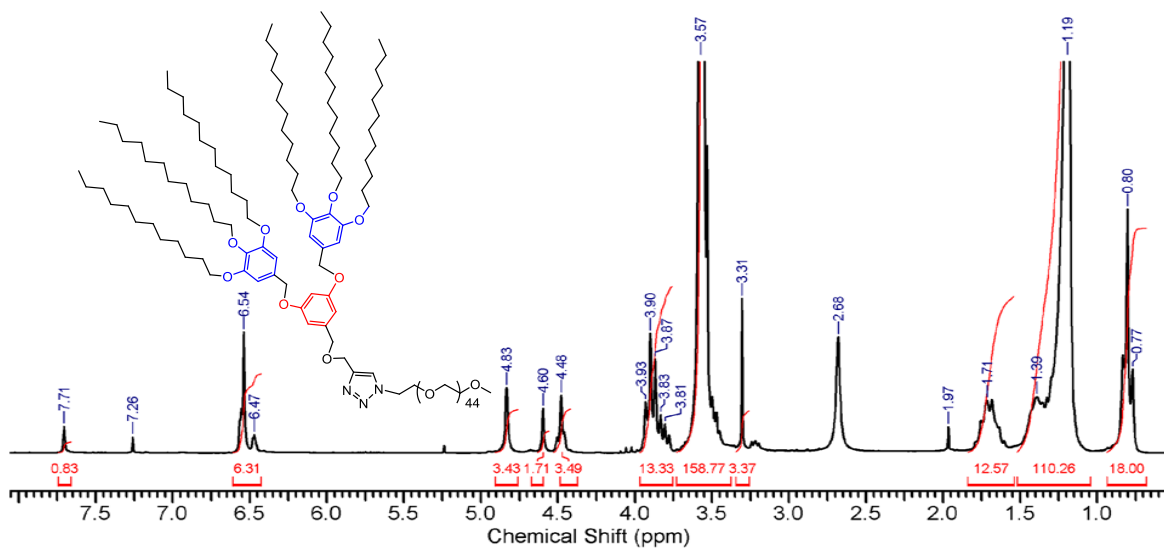


Fig. I.4: 400 MHz  $^1\text{H}$  NMR spectrum of P-(3,4,5)3,5G2 in  $\text{CDCl}_3$ .

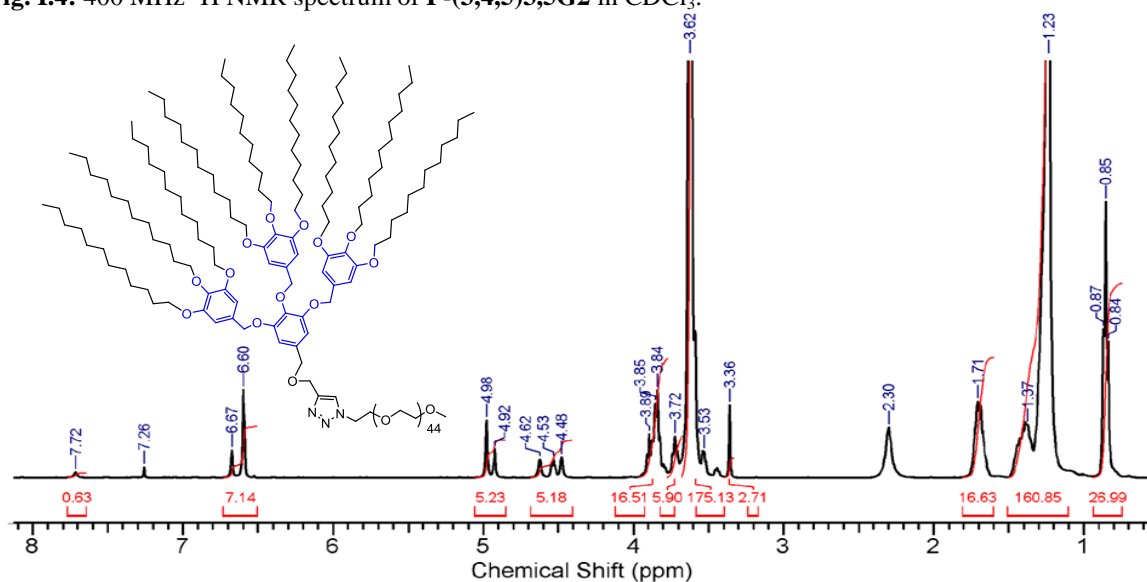


Fig. I.5: 400 MHz  $^1\text{H}$  NMR spectrum of P-3,4,5G2 in  $\text{CDCl}_3$ .

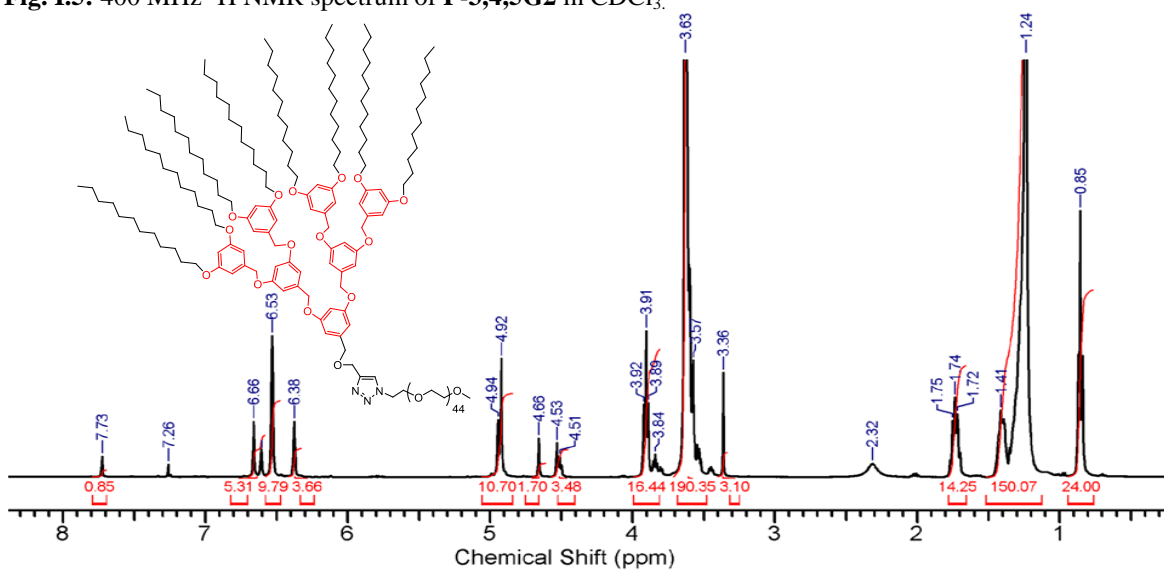


Fig. I.6: 400 MHz  $^1\text{H}$  NMR spectrum of P-3,5G3 in  $\text{CDCl}_3$ .

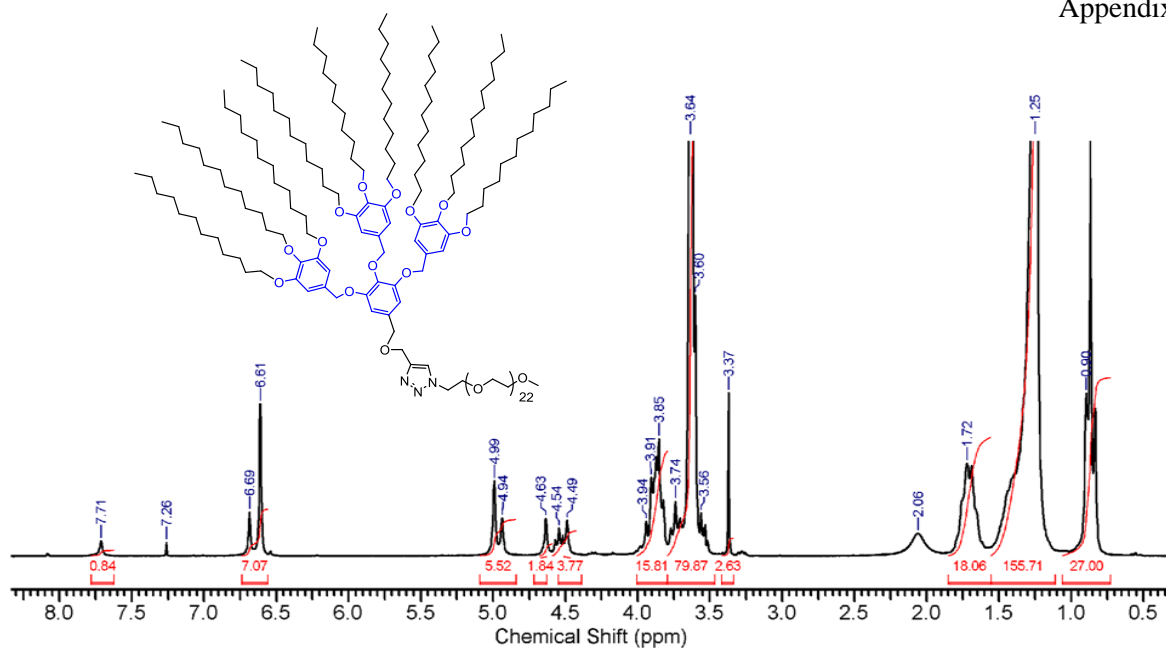


Fig. I.7: 400 MHz  $^1\text{H}$  NMR spectrum of P-(3,4,5)G2-1000 in  $\text{CDCl}_3$ .

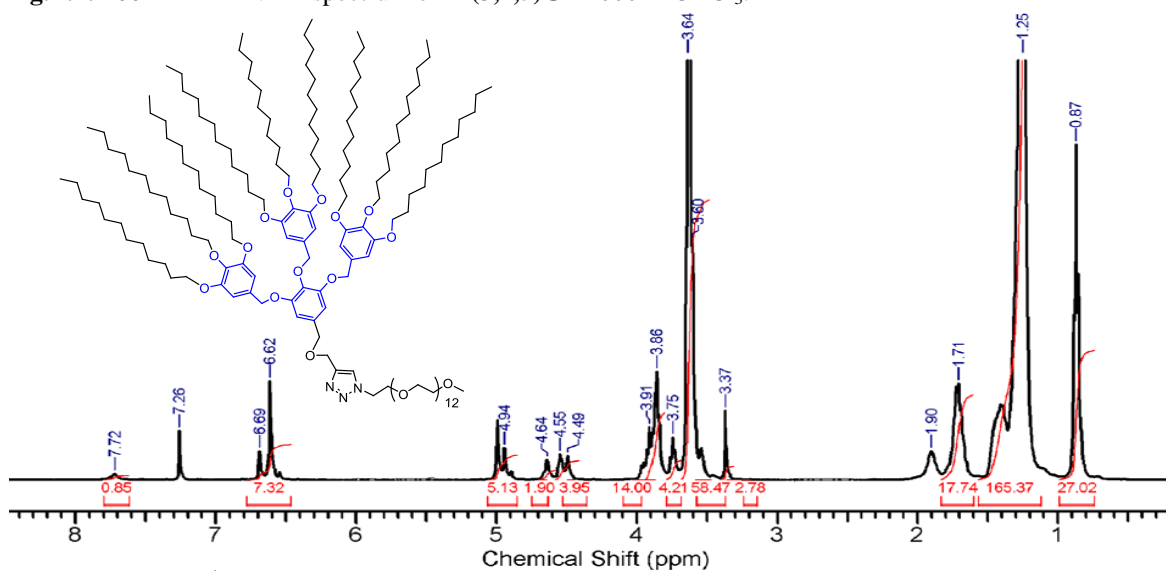


Fig. I.8: 400 MHz  $^1\text{H}$  NMR spectrum of P-(3,4,5)G2-550 in  $\text{CDCl}_3$ .

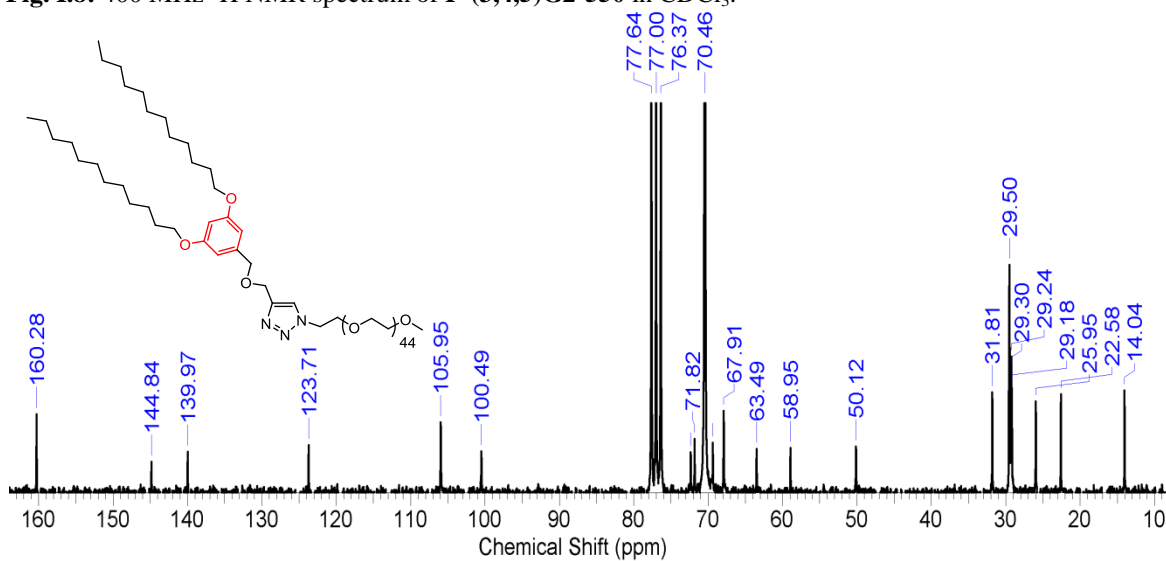


Fig. I.9: 50 MHz  $^{13}\text{C}$  NMR spectrum of P-3,5G1.

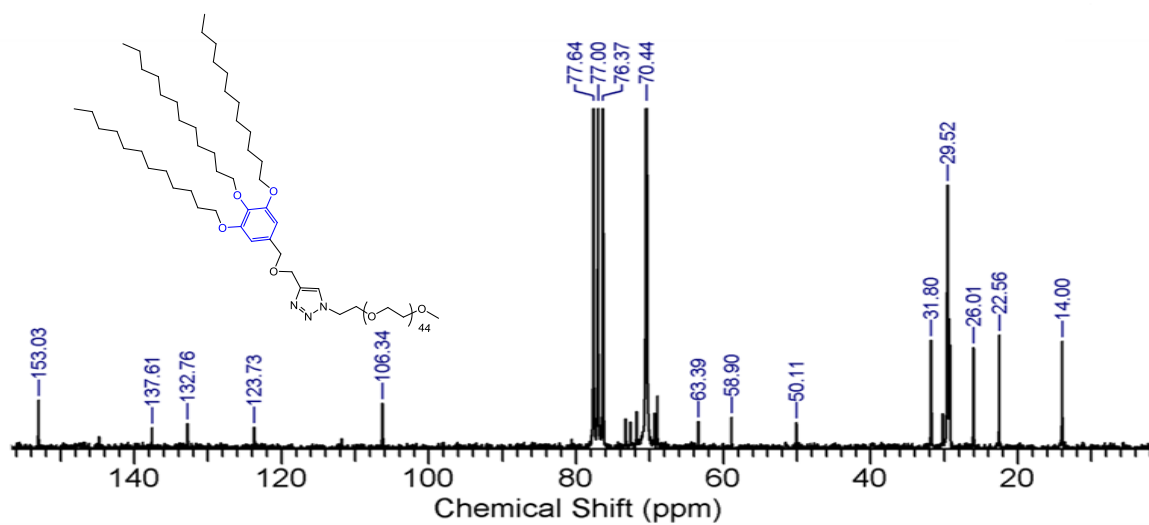


Fig. I.10: 50 MHz  $^{13}\text{C}$  NMR spectrum of P-3,4,5G1.

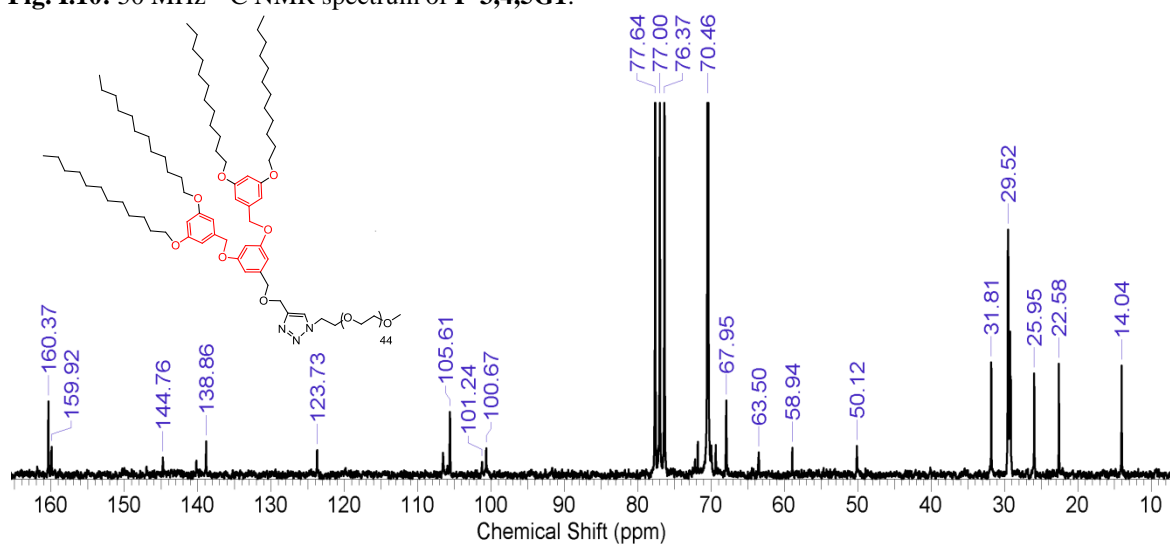


Fig. I.11: 50 MHz  $^{13}\text{C}$  NMR spectrum of P-3,5G2

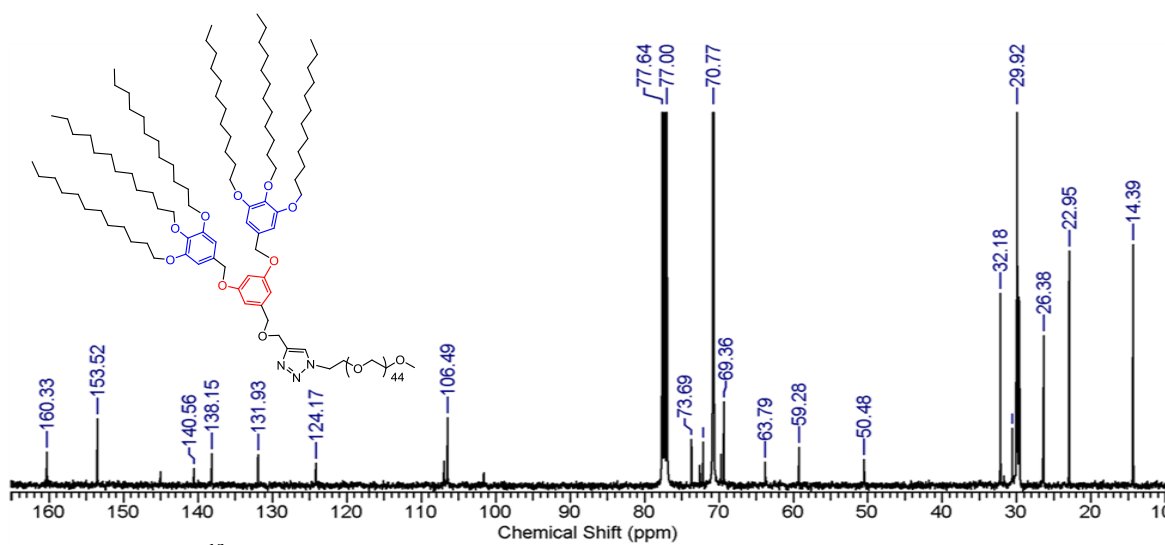


Fig. I.12: 50 MHz  $^{13}\text{C}$  NMR spectrum of P-(3,4,5)3,5G2.





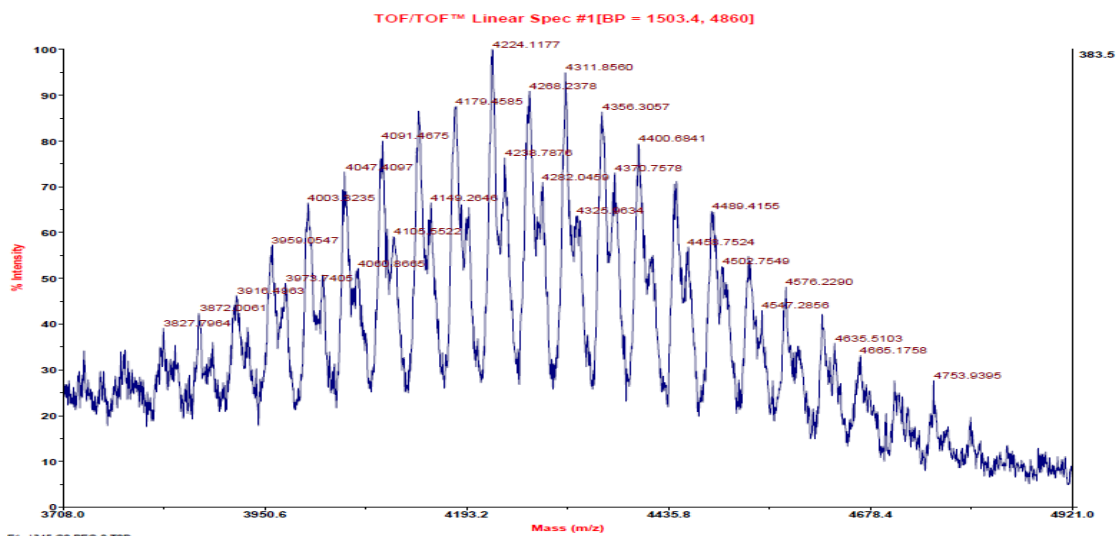


Fig. I.19: MALDI-TOF spectrum of P-3,4,5G2.

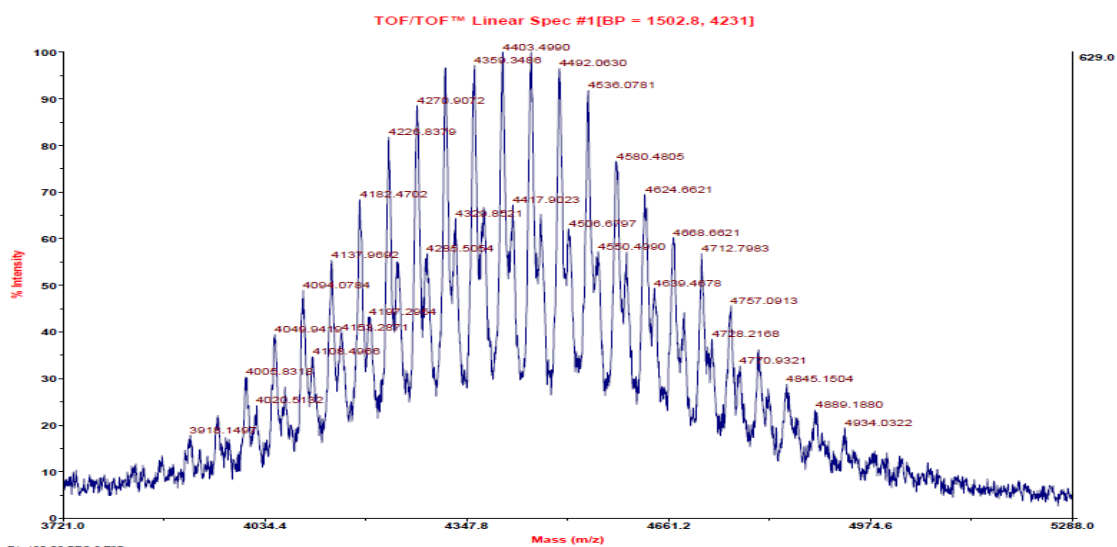
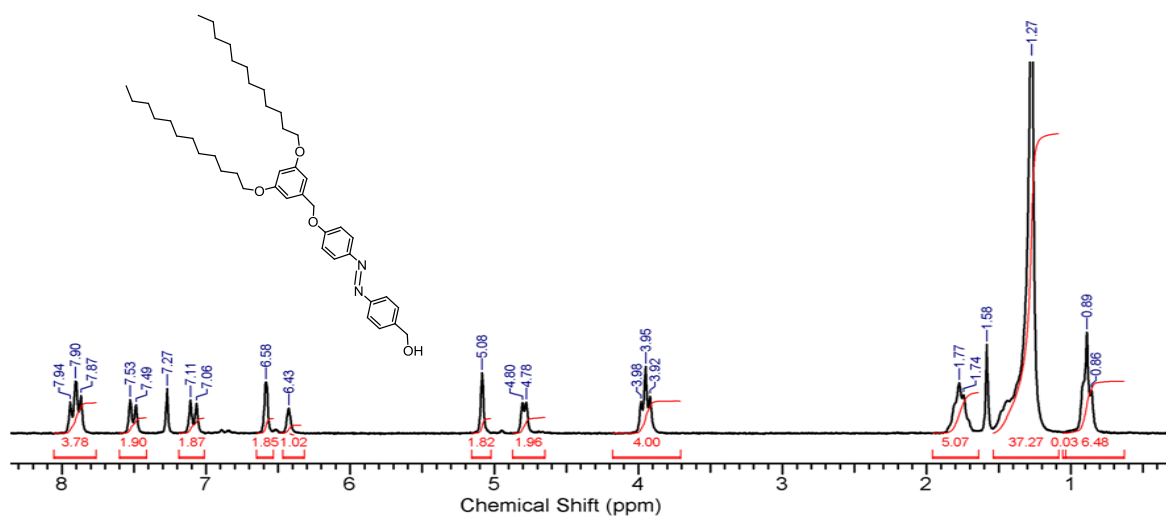
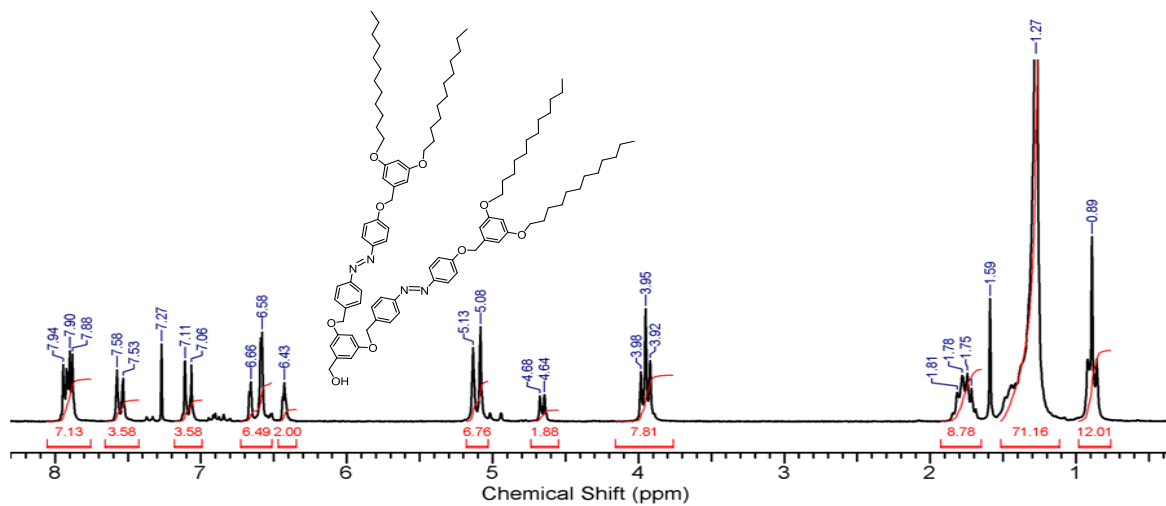
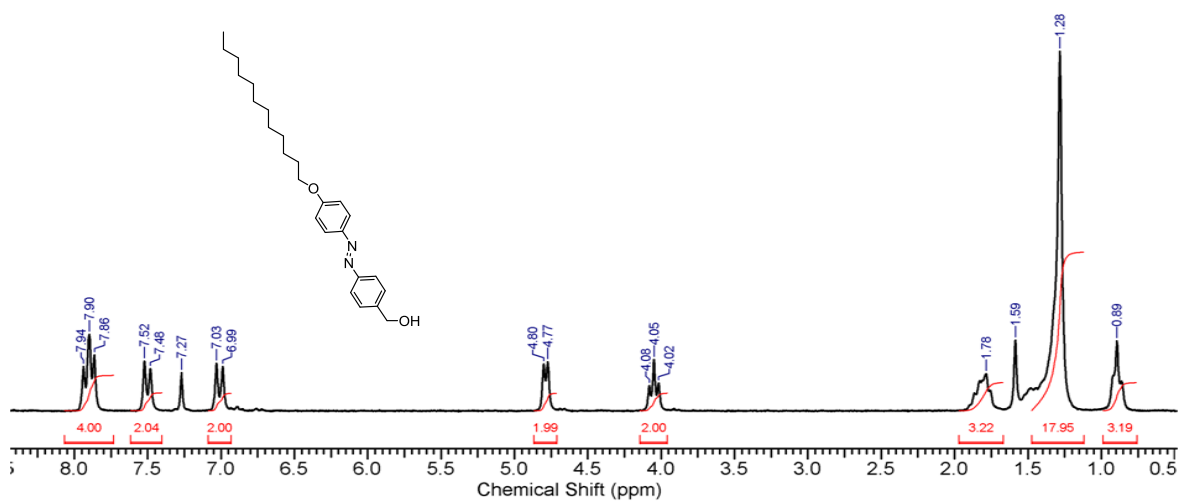


Fig. I.20: MALDI-TOF spectrum of P-3,5G3.



## Appendix II

## NMR and MALDI-TOF spectra for Chapter 3

Fig. II.1: 200 MHz  $^1\text{H}$  NMR spectrum of compound 2  $\text{CDCl}_3$ .Fig. II.2: 200 MHz  $^1\text{H}$  NMR spectrum of compound 4 in  $\text{CDCl}_3$ .Fig. II.3: 200 MHz  $^1\text{H}$  NMR spectrum of AzO-C<sub>12</sub>-OH in  $\text{CDCl}_3$ .

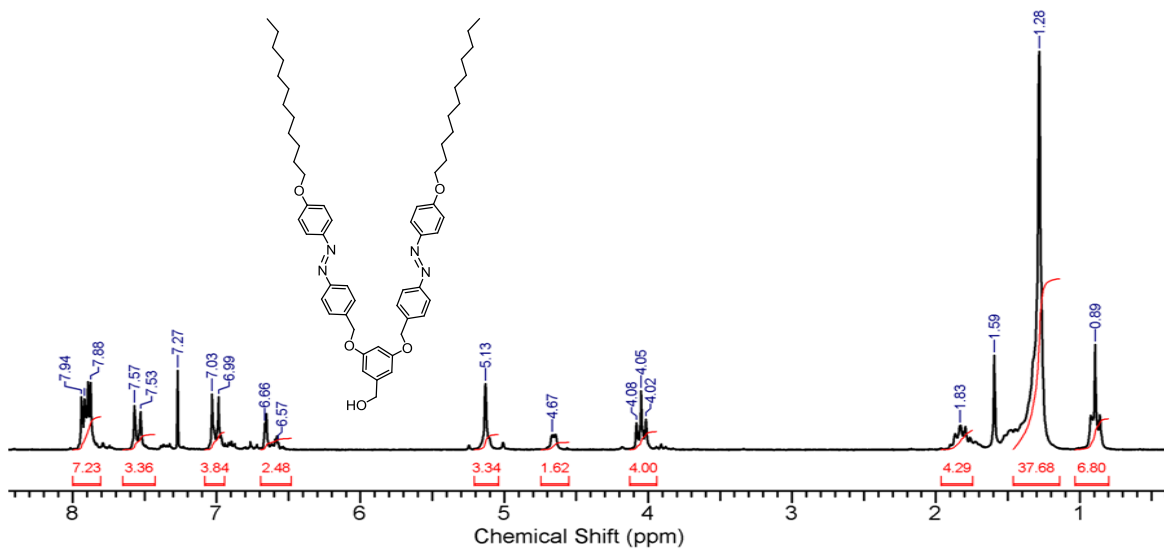


**Fig. II.4:** 200 MHz  $^1\text{H}$  NMR spectrum of compound **7** in  $\text{CDCl}_3$ .

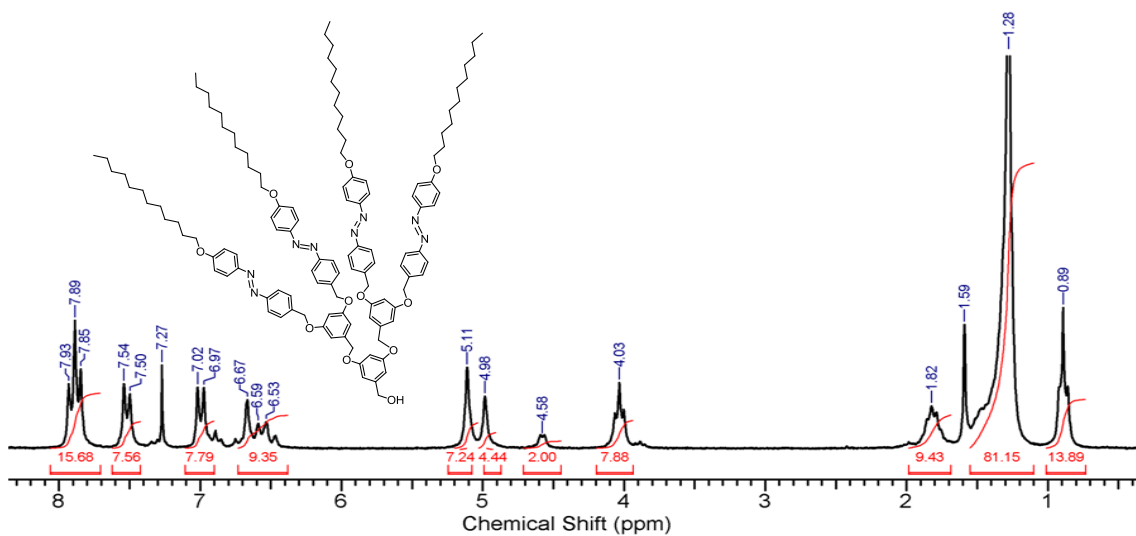


**Fig. II.5:** 200 MHz  $^1\text{H}$  NMR spectrum of compound **9** in  $\text{CDCl}_3$ .

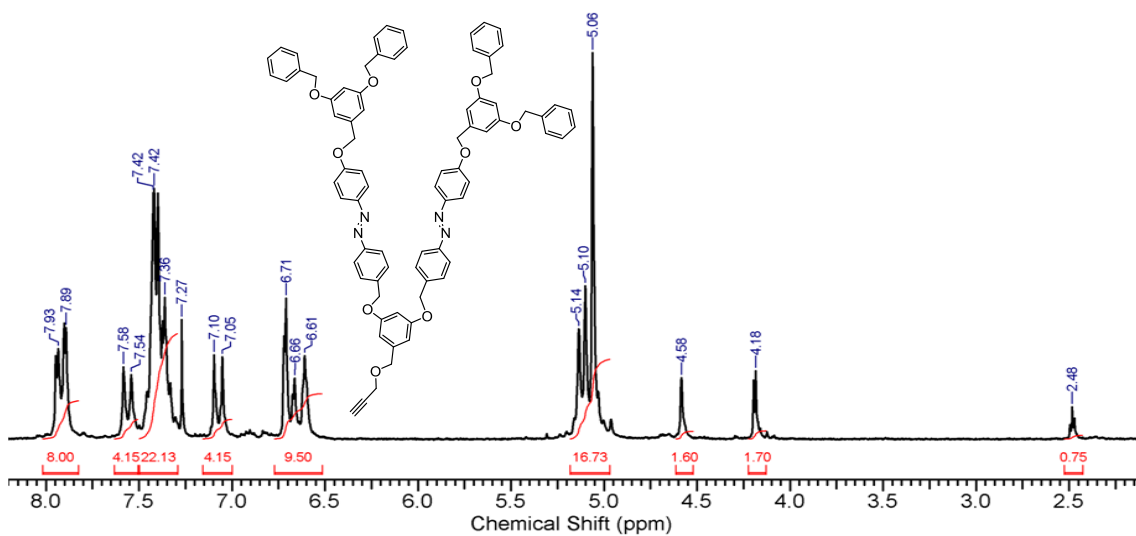


**Fig. II.6:** 200 MHz  $^1\text{H}$  NMR spectrum of **D1** in  $\text{CDCl}_3$ .

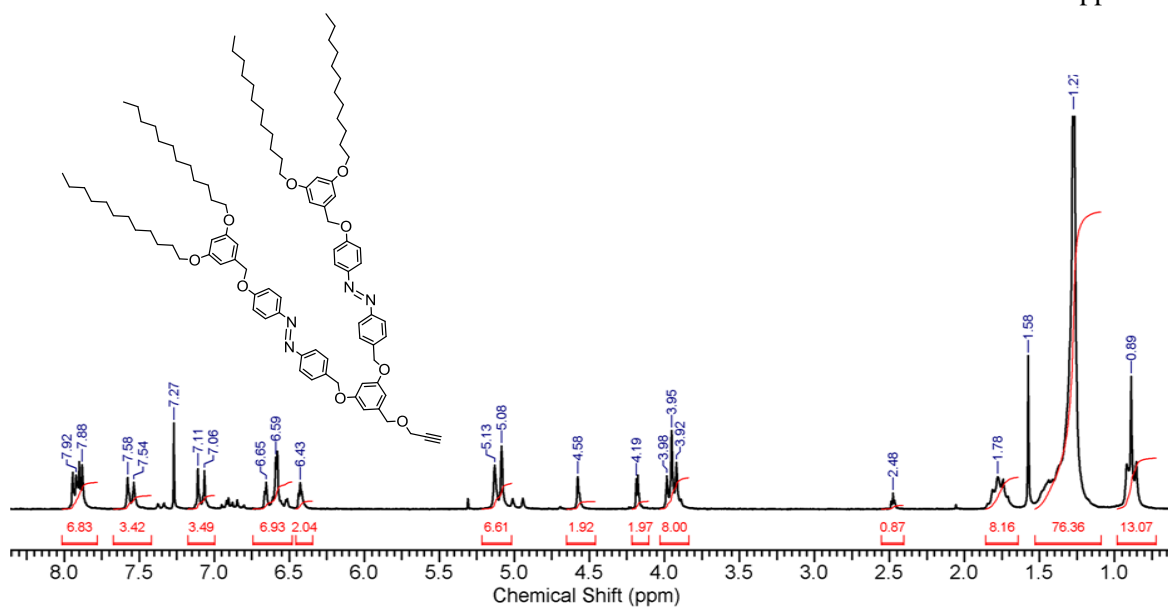


**Fig. II.7:** 200 MHz  $^1\text{H}$  NMR spectrum of **D2** in  $\text{CDCl}_3$ .

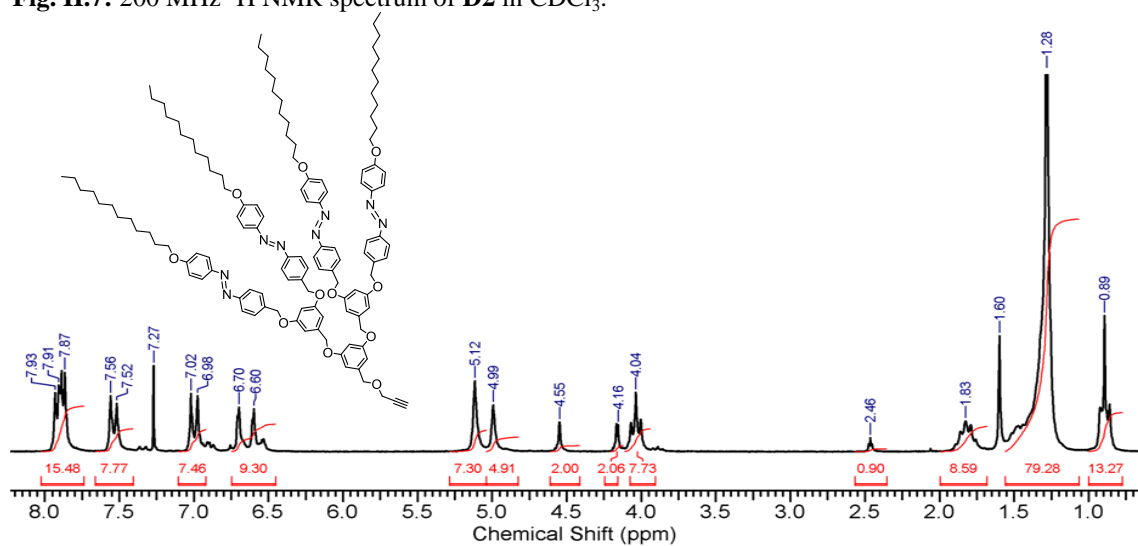


**Fig. II.8:** 200 MHz  $^1\text{H}$  NMR spectrum of **D3** in  $\text{CDCl}_3$ .

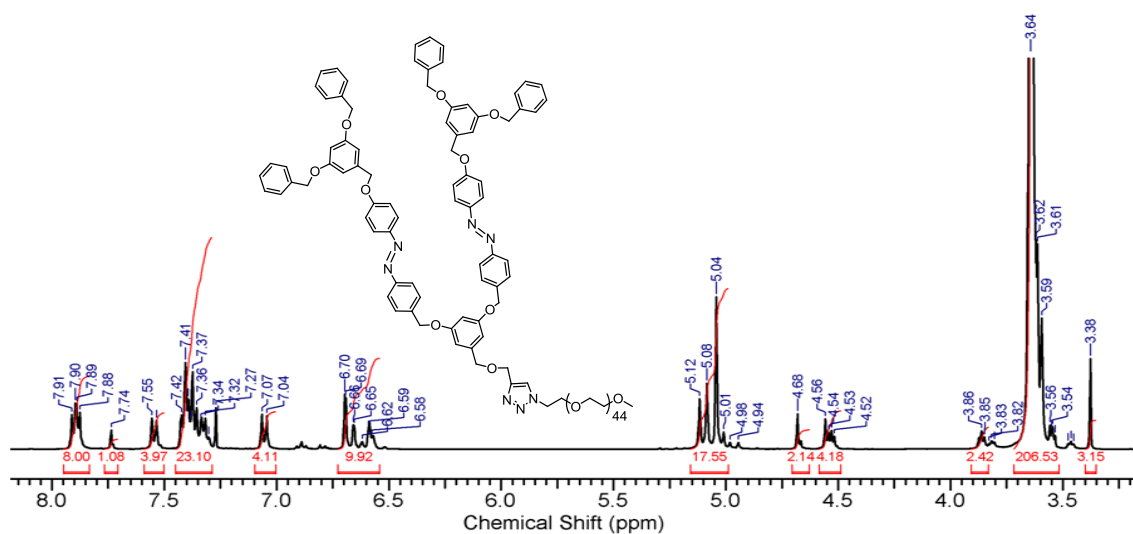


**Fig. II.9:** 400 MHz  $^1\text{H}$  NMR spectrum of **P1** in  $\text{CDCl}_3$ .

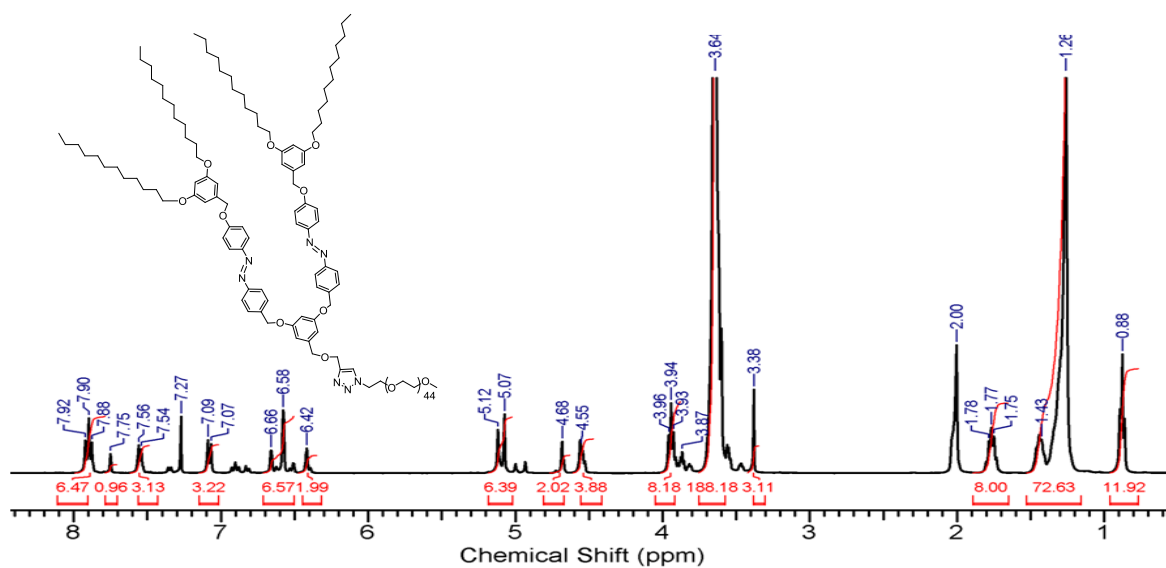


**Fig. II.10:** 400 MHz  $^1\text{H}$  NMR spectrum of **P2** in  $\text{CDCl}_3$ .

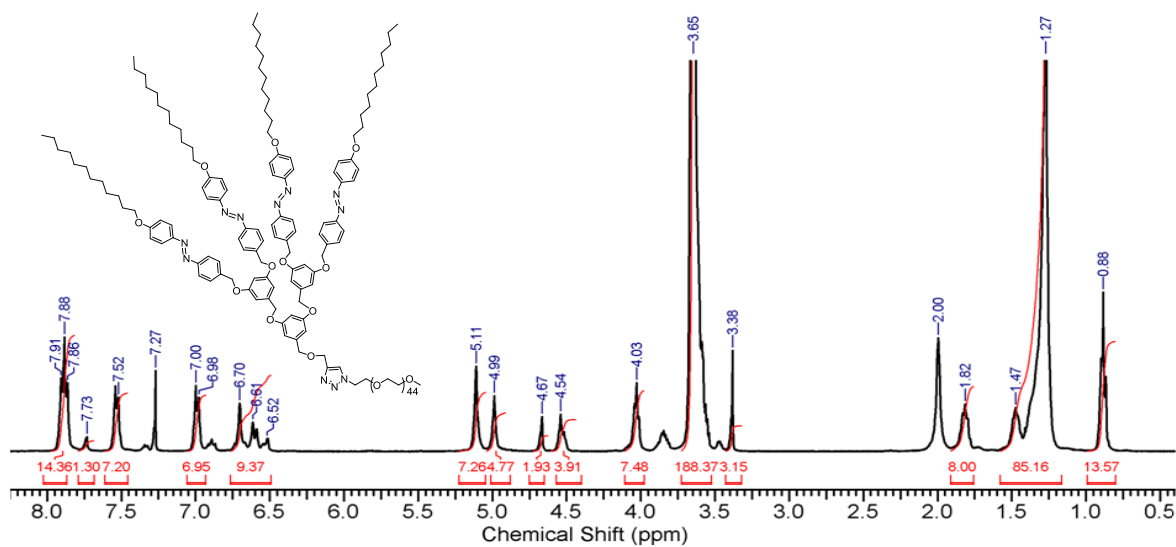


**Fig. II.11:** 400 MHz  $^1\text{H}$  NMR spectrum of **P3** in  $\text{CDCl}_3$ .

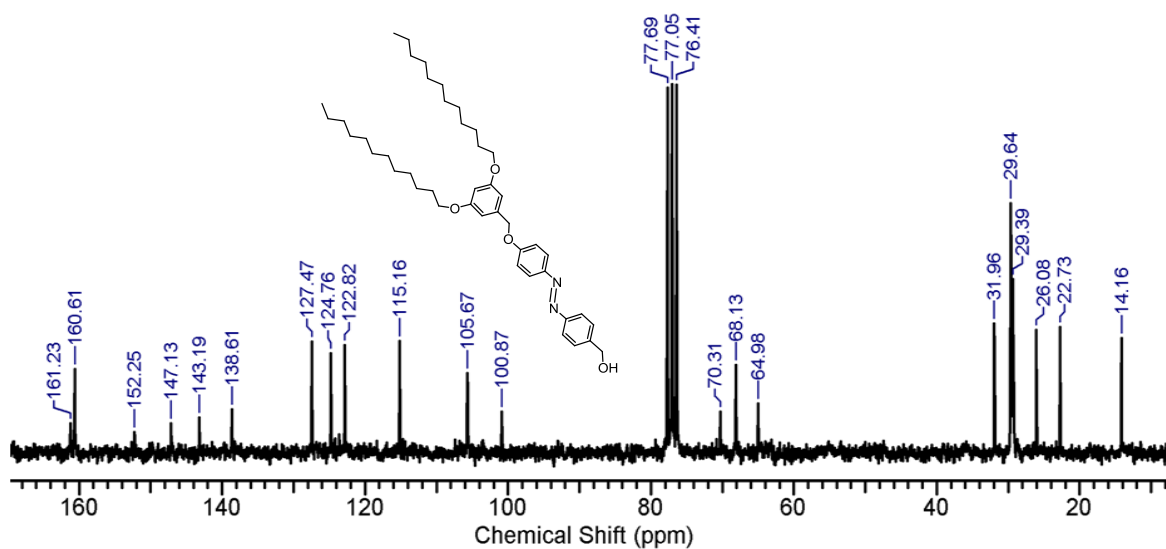


**Fig. II.12:** 50 MHz  $^{13}\text{C}$  NMR spectrum of compound **2** in  $\text{CDCl}_3$ .

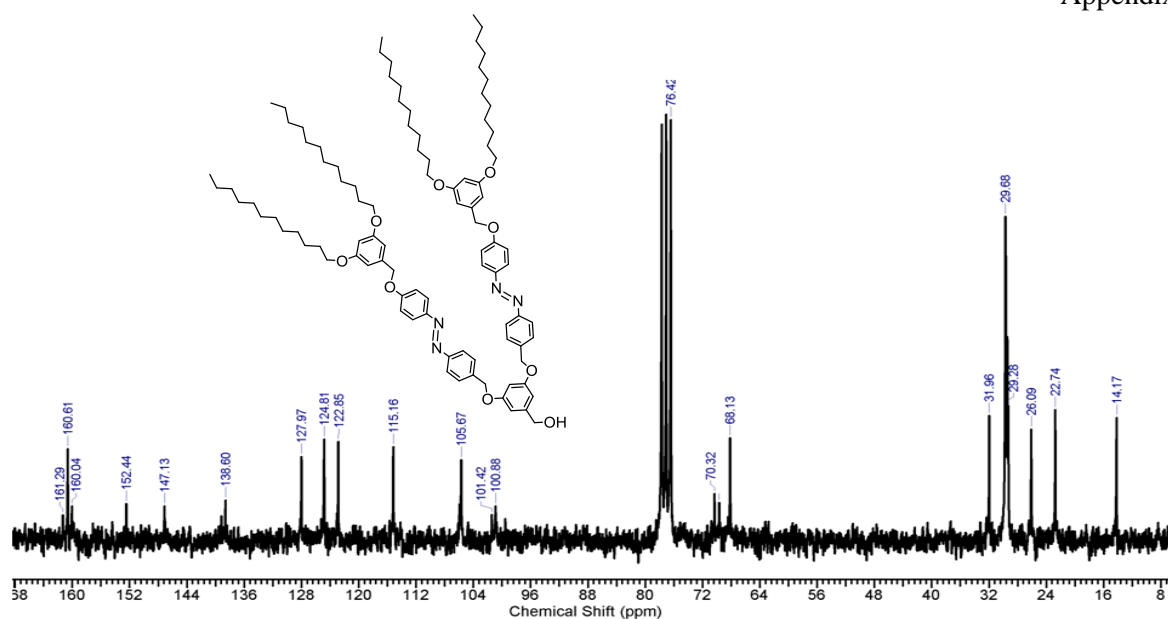


Fig. II.13: 50 MHz  $^{13}\text{C}$  NMR spectrum of Compound **4** in  $\text{CDCl}_3$ .

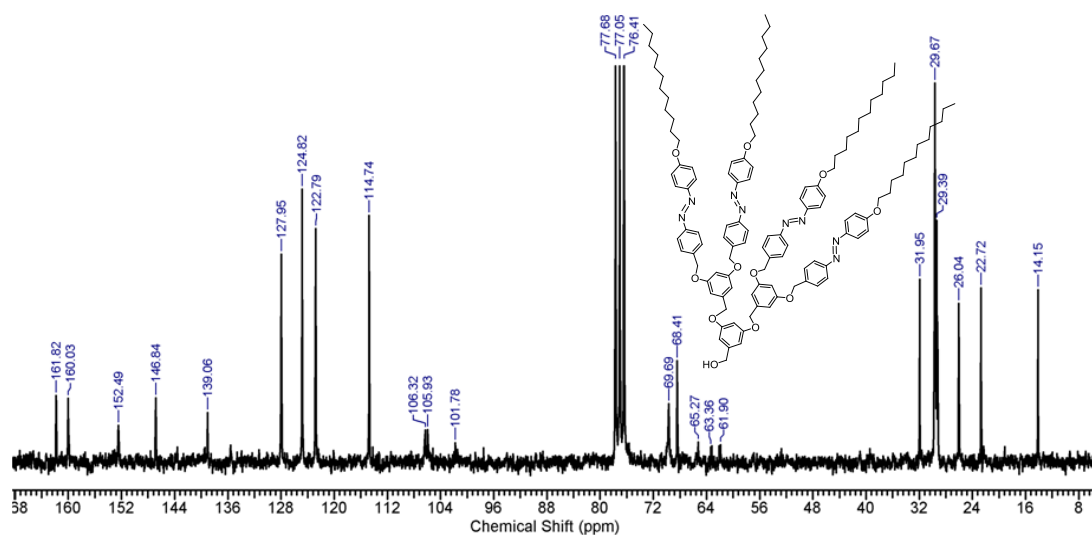


Fig. II.14: 50 MHz  $^{13}\text{C}$  NMR spectrum of compound **9** in  $\text{CDCl}_3$ .

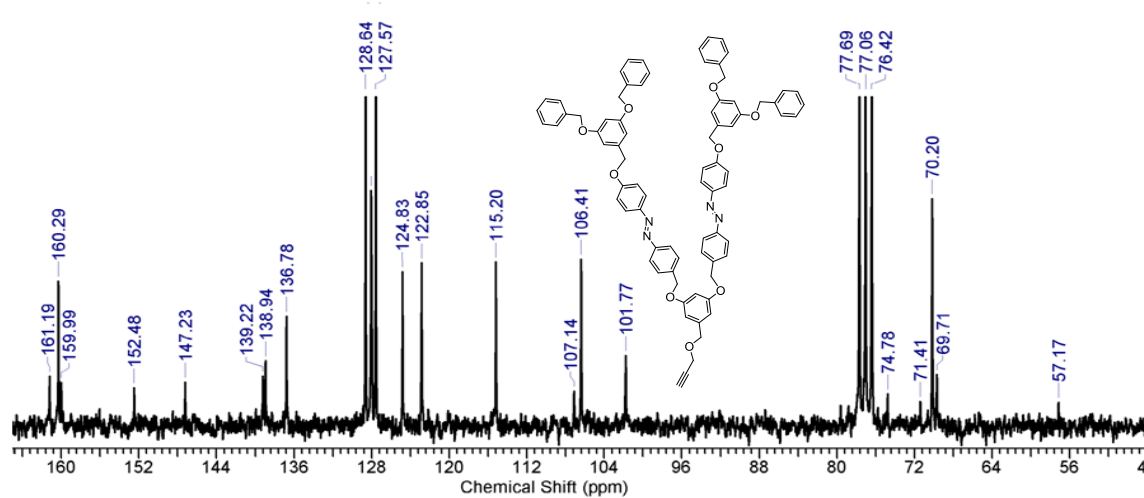


Fig. II.15: 50 MHz  $^{13}\text{C}$  NMR spectrum of **D1** in  $\text{CDCl}_3$ .

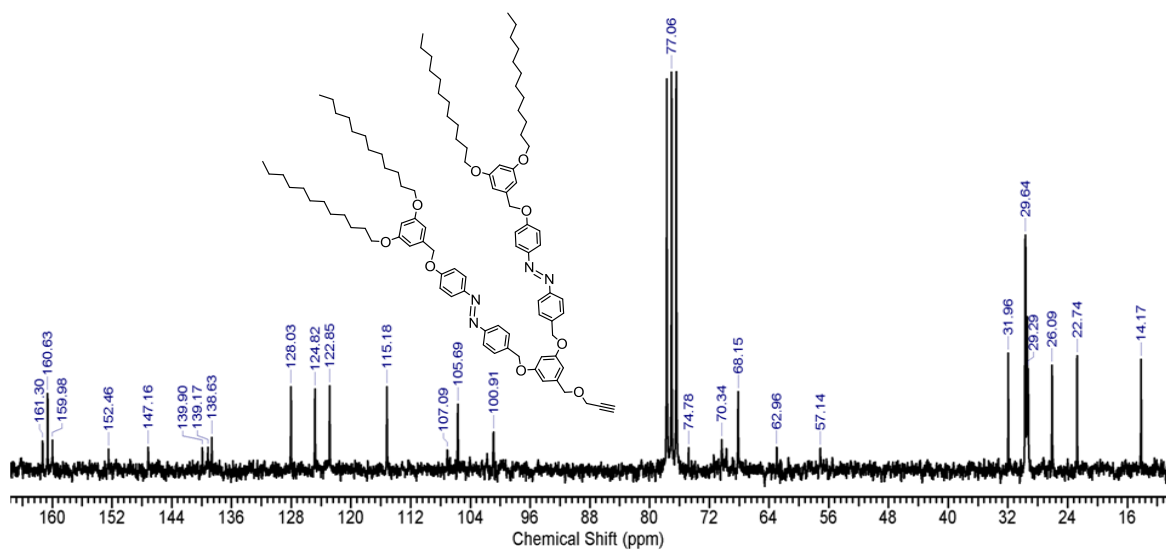


Fig. II.16: 50 MHz  $^{13}\text{C}$  NMR spectrum of D2 in  $\text{CDCl}_3$ .

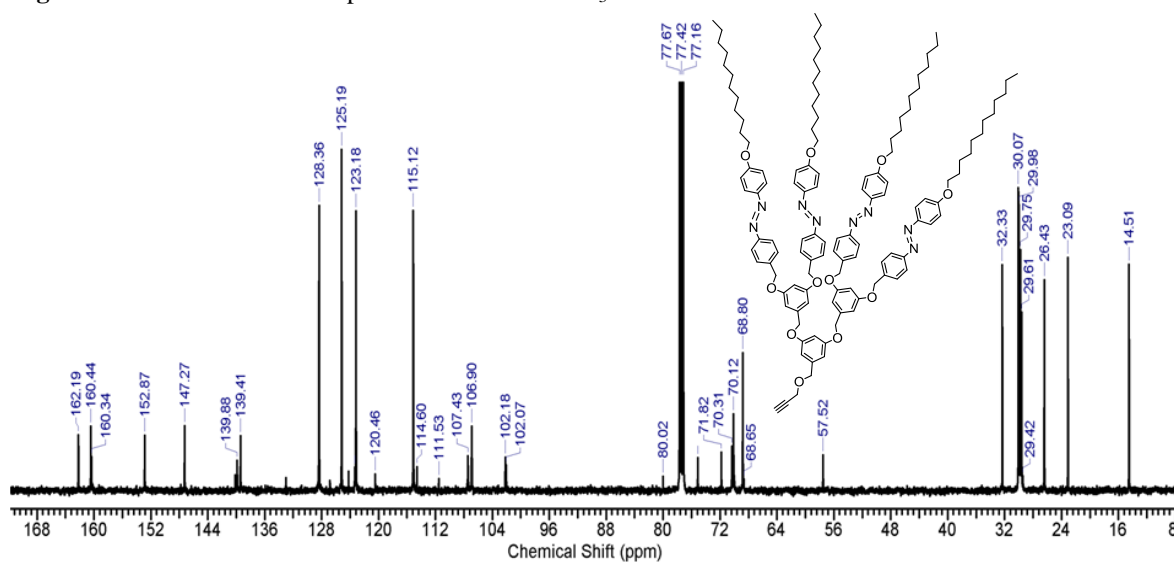


Fig. II.17: 125 MHz  $^{13}\text{C}$  NMR spectrum of D3 in  $\text{CDCl}_3$ .

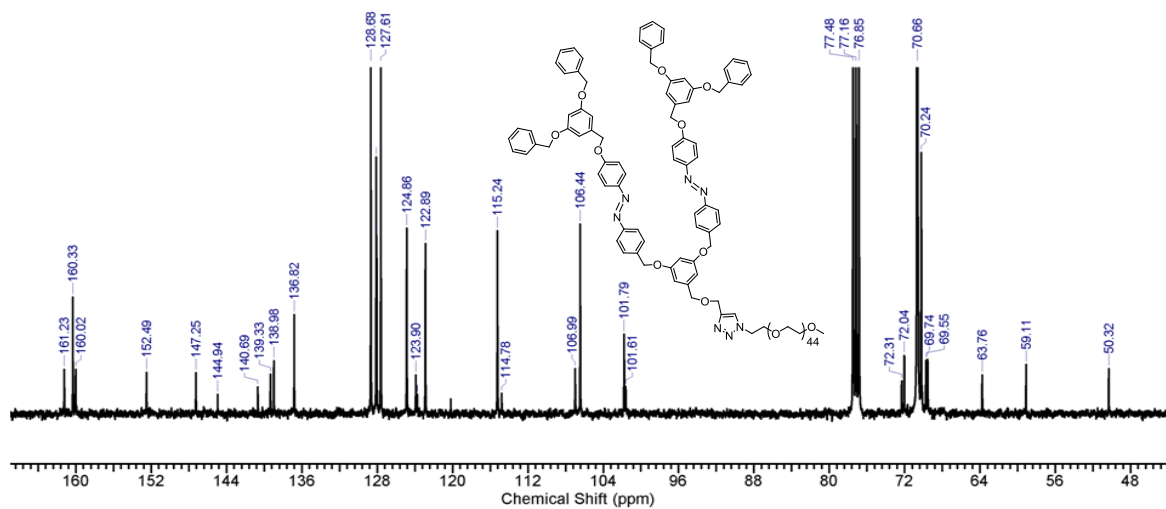


Fig. II.18: 100 MHz  $^{13}\text{C}$  NMR spectrum of P1 in  $\text{CDCl}_3$ .

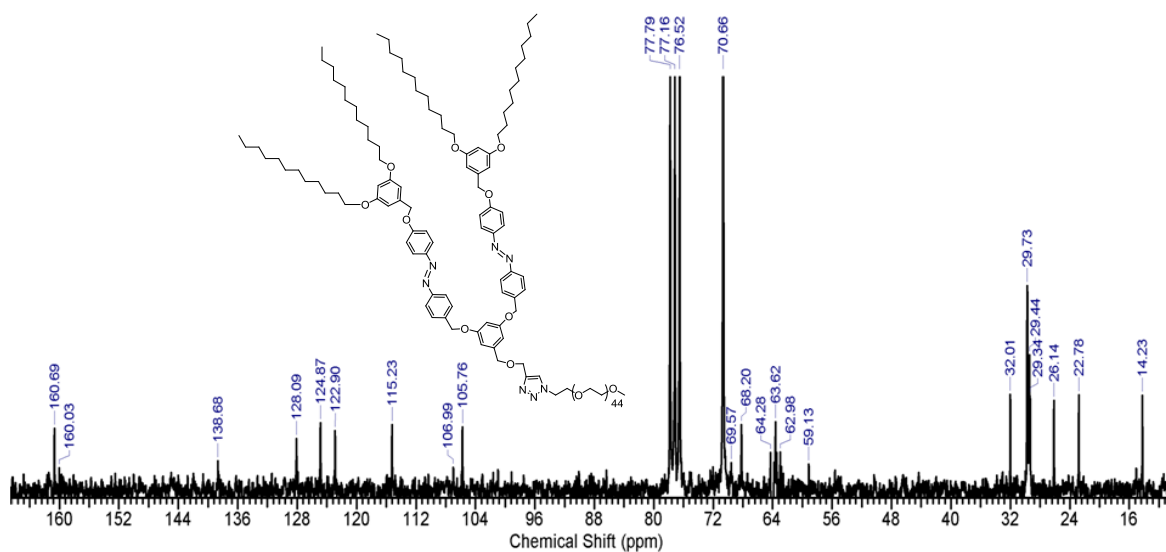


Fig. II.19: 50 MHz  $^{13}\text{C}$  NMR spectrum of P2 in  $\text{CDCl}_3$ .

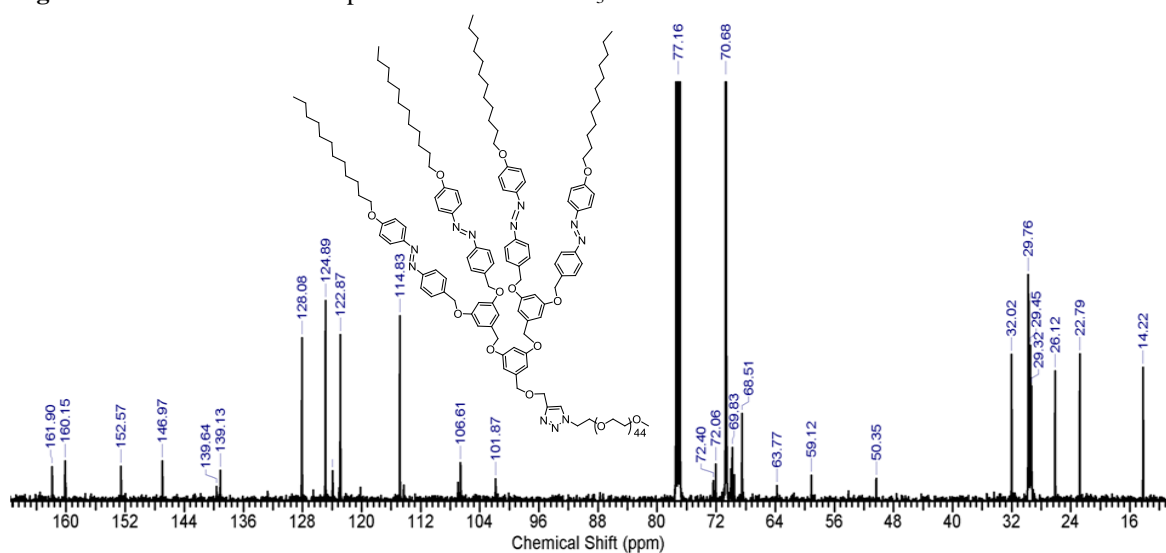


Fig. II.20: 125 MHz  $^{13}\text{C}$  NMR spectrum of P3 in  $\text{CDCl}_3$ .

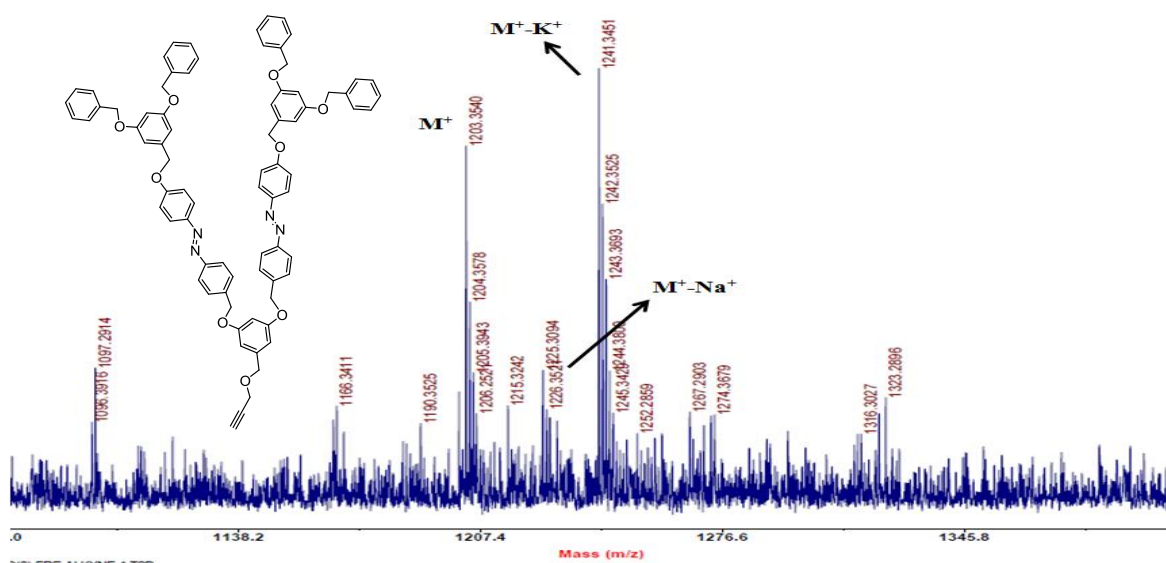


Fig. II.21: MALDI-TOF spectrum of D1.



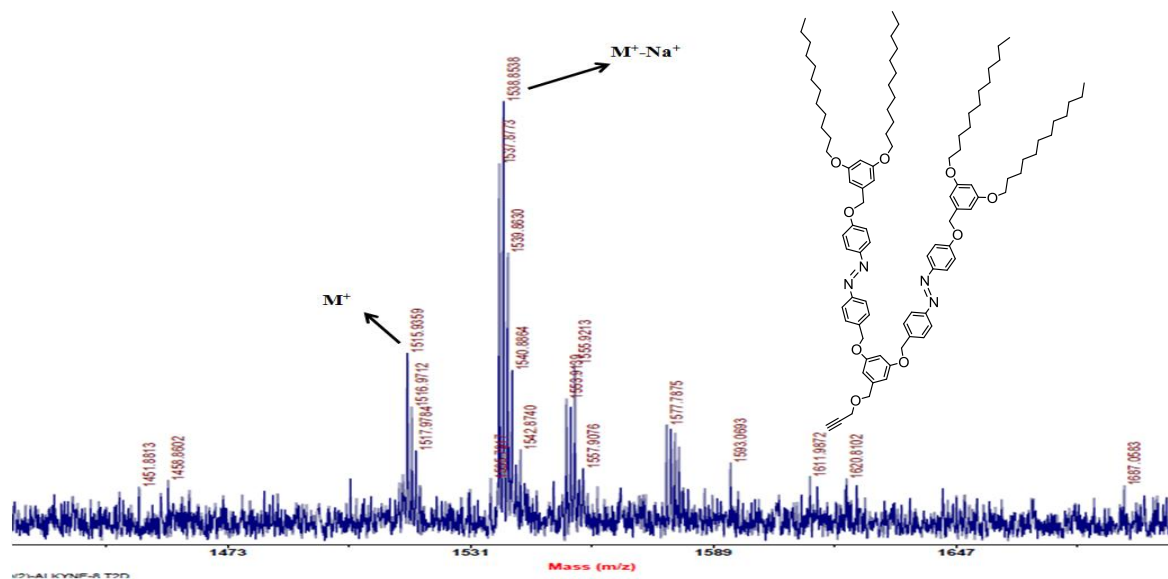


Fig. II.22: MALDI-TOF spectrum of **D2** in  $\text{CDCl}_3$ .

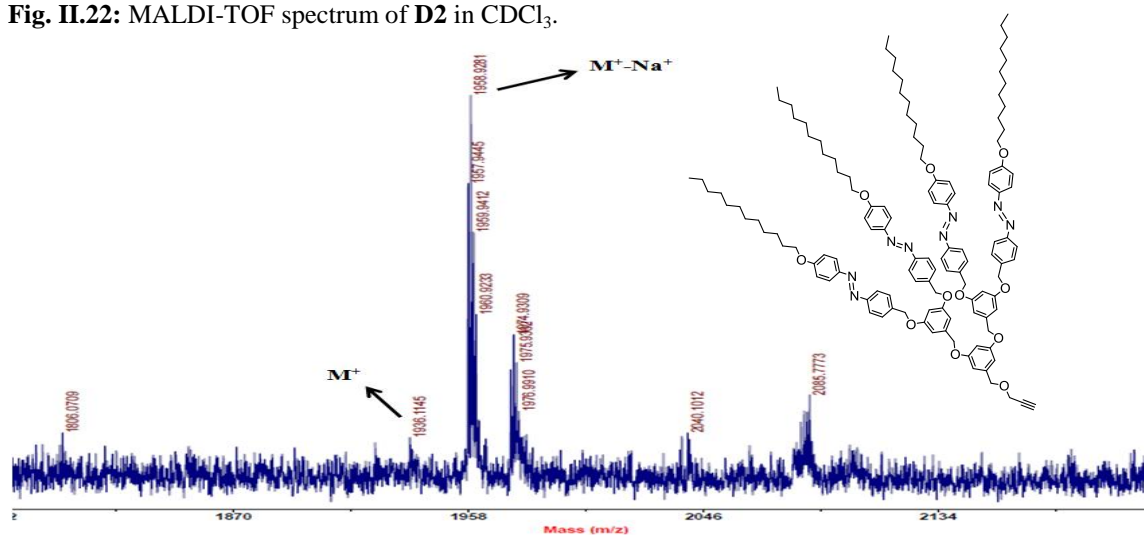


Fig. II.23: MALDI-TOF spectrum of **D3** in  $\text{CDCl}_3$ .

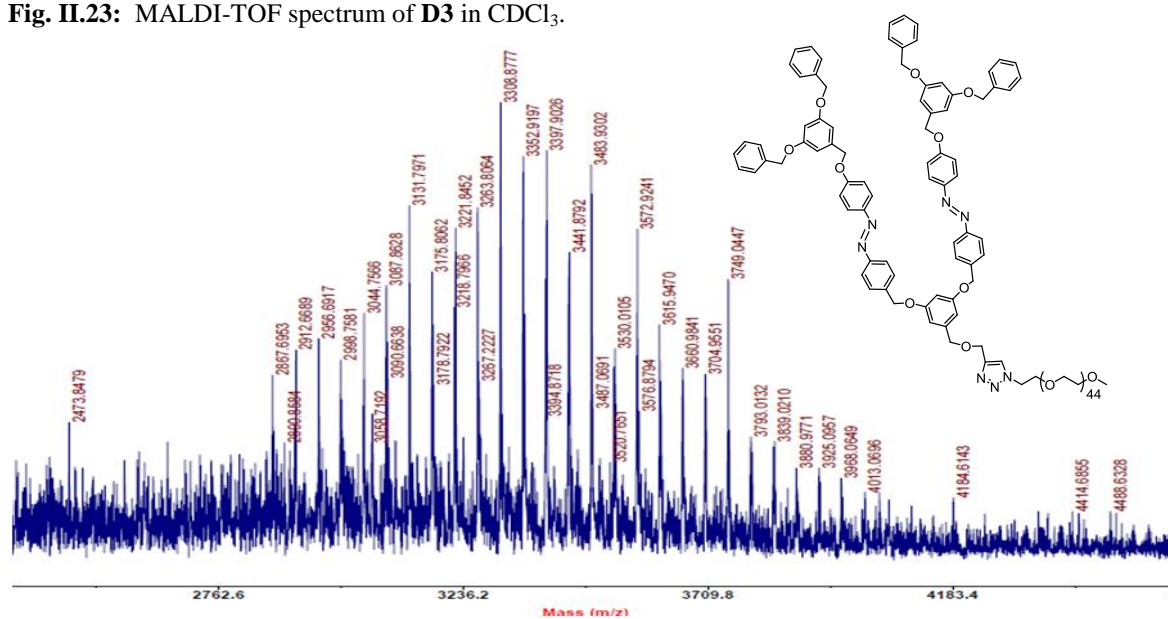


Fig. II.24: MALDI-TOF spectrum of **P1**.



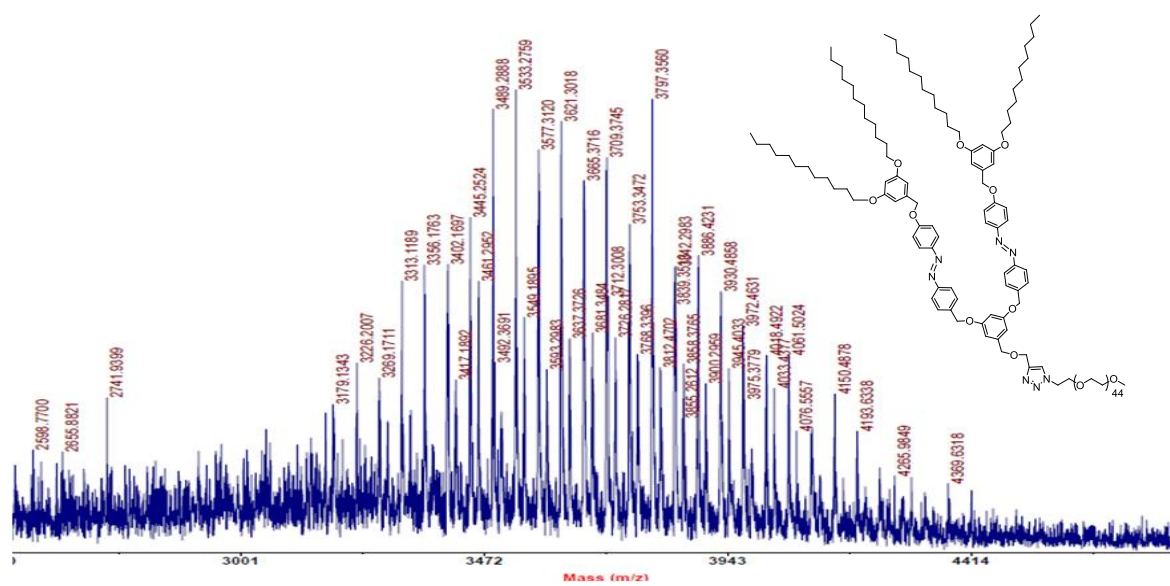
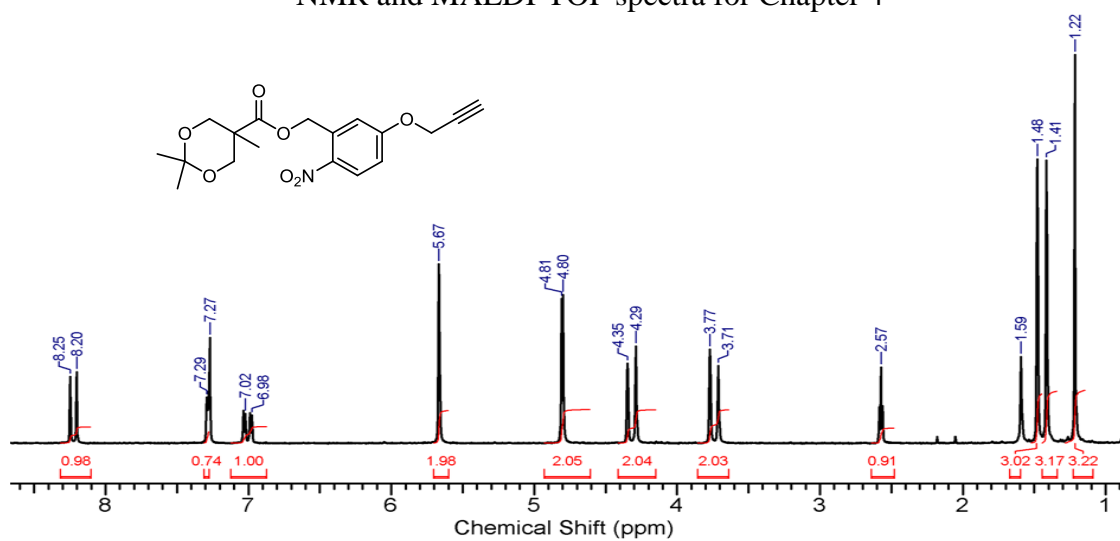
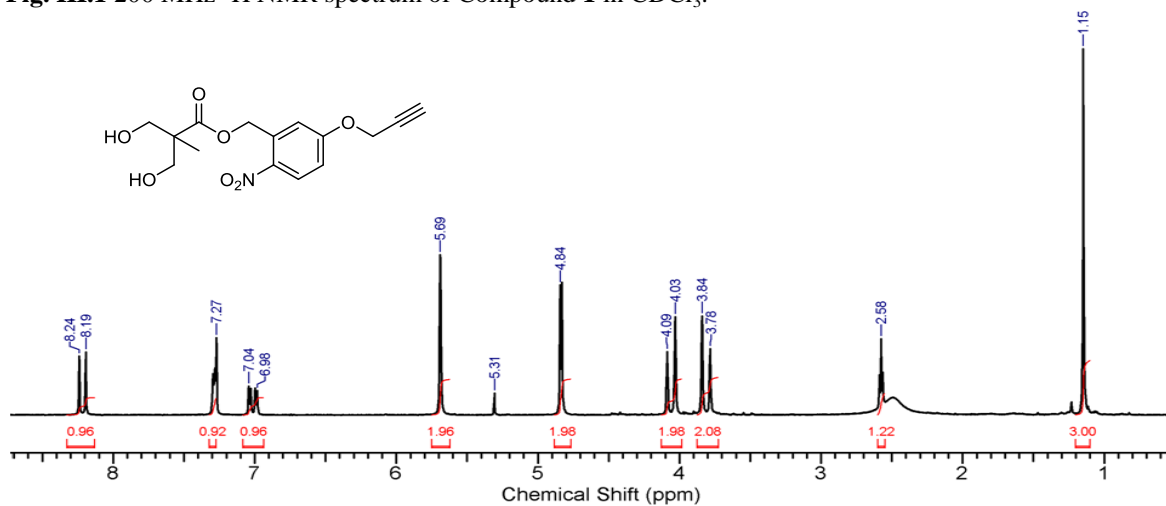
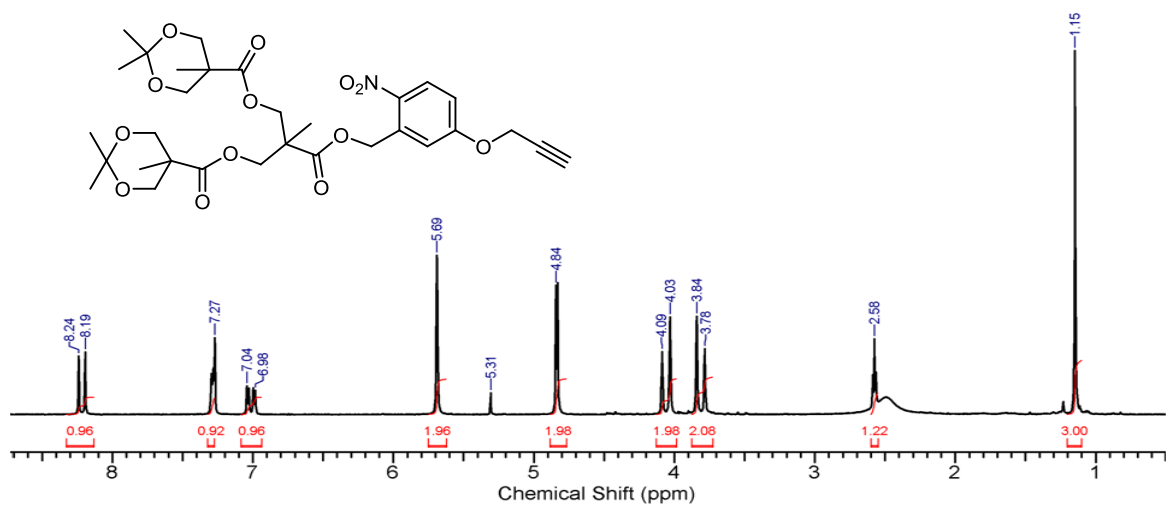


Fig. II.25. MALDI-TOF spectrum of P2.

## Appendix III

## NMR and MALDI-TOF spectra for Chapter 4

Fig. III.1 200 MHz  $^1\text{H}$  NMR spectrum of Compound **1** in  $\text{CDCl}_3$ .Fig. III.2. 200 MHz  $^1\text{H}$  NMR spectrum of Compound **2** in  $\text{CDCl}_3$ .Fig. III.3. 200 MHz  $^1\text{H}$  NMR spectrum of Compound **3** alkyne in  $\text{CDCl}_3$ .

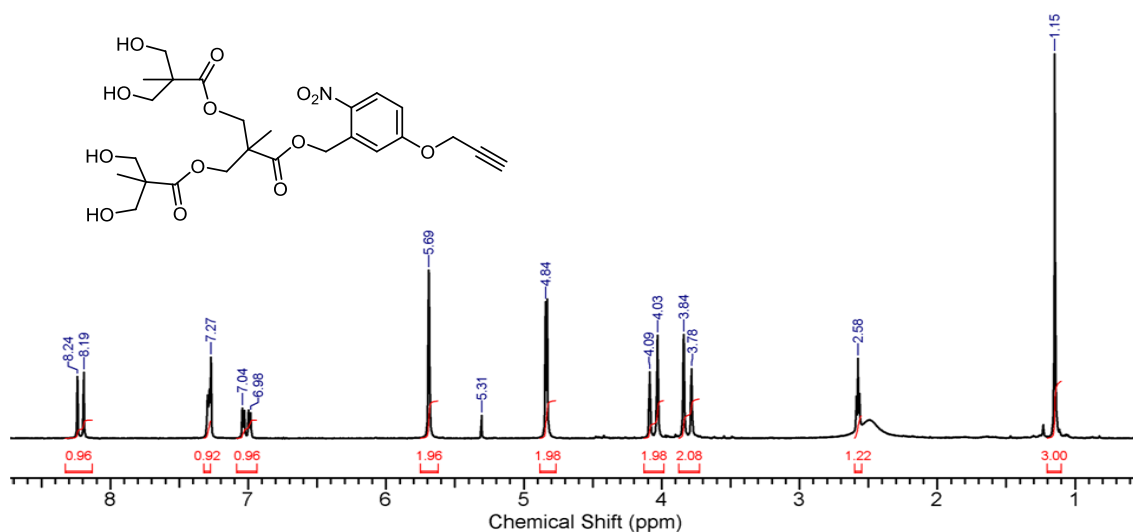


Fig. III.4. 200 MHz  $^1\text{H}$  NMR spectrum of Compound 4 in  $\text{CDCl}_3$ .

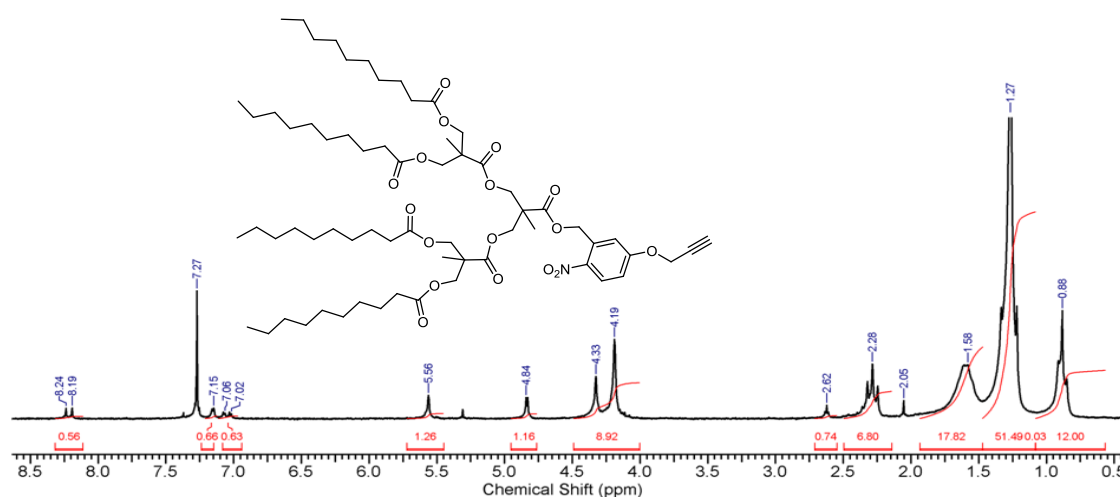


Fig. III.5. 200 MHz  $^1\text{H}$  NMR spectrum of Compound 5 in  $\text{CDCl}_3$ .

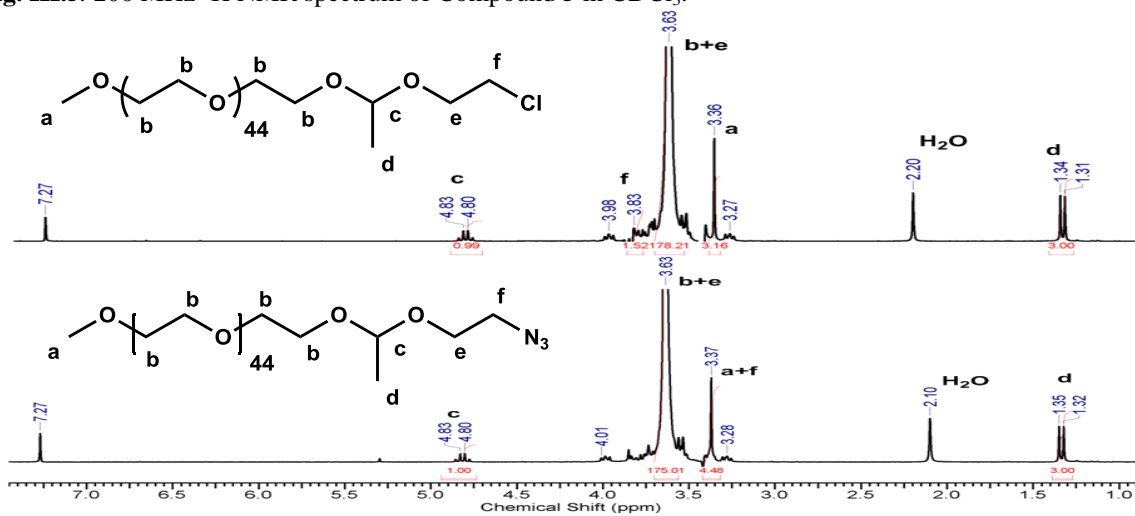


Fig. III.6. 200 MHz  $^1\text{H}$  NMR spectrum of Compound 6 (upper) and Compound 7 in  $\text{CDCl}_3$ .

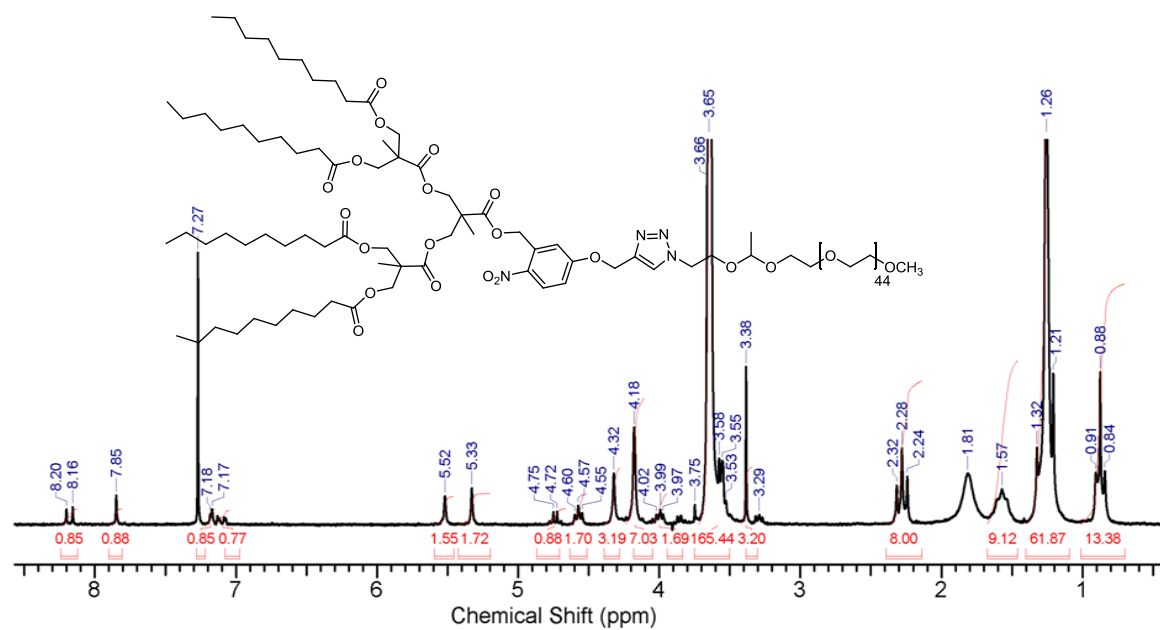


Fig. III.7. 200 MHz  $^1\text{H}$  NMR spectrum of **P1** in  $\text{CDCl}_3$ .

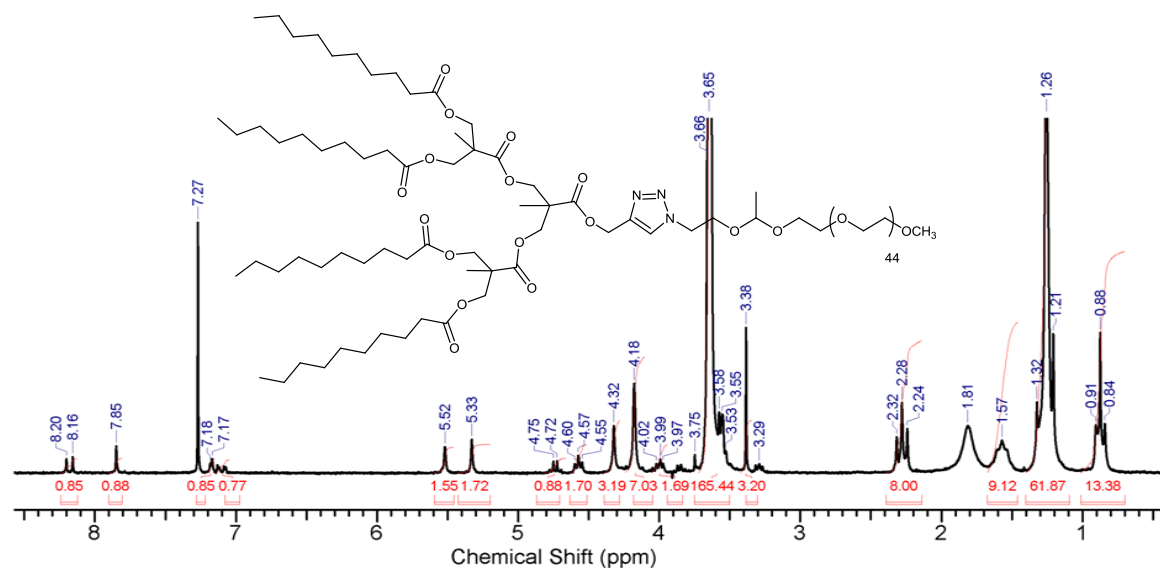


Fig. III.8. 200 MHz  $^1\text{H}$  NMR spectrum of **P2** in  $\text{CDCl}_3$ .

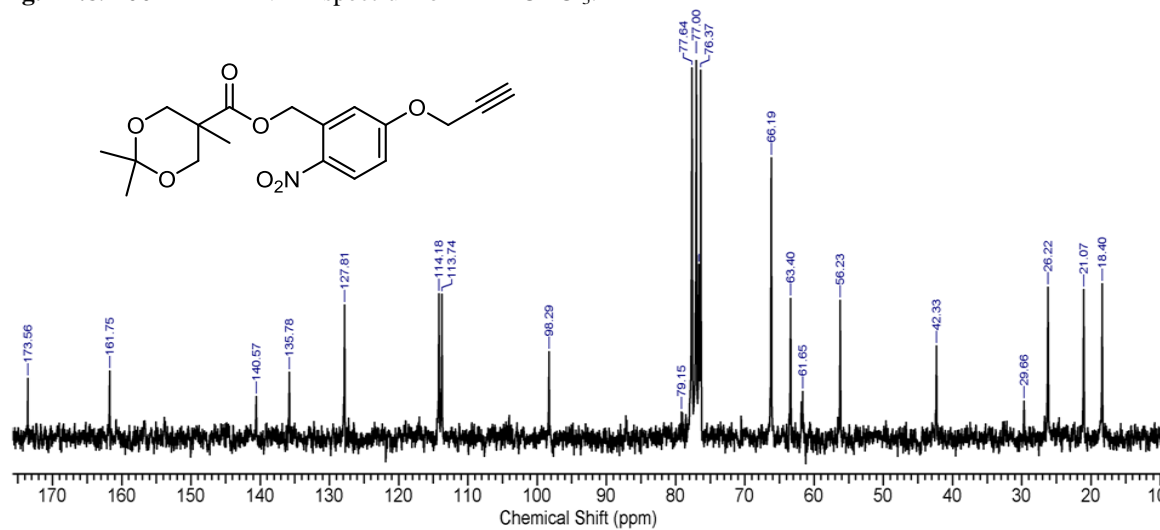


Fig. III.9: 50 MHz  $^{13}\text{C}$  NMR spectrum of Compound **1** in  $\text{CDCl}_3$ .

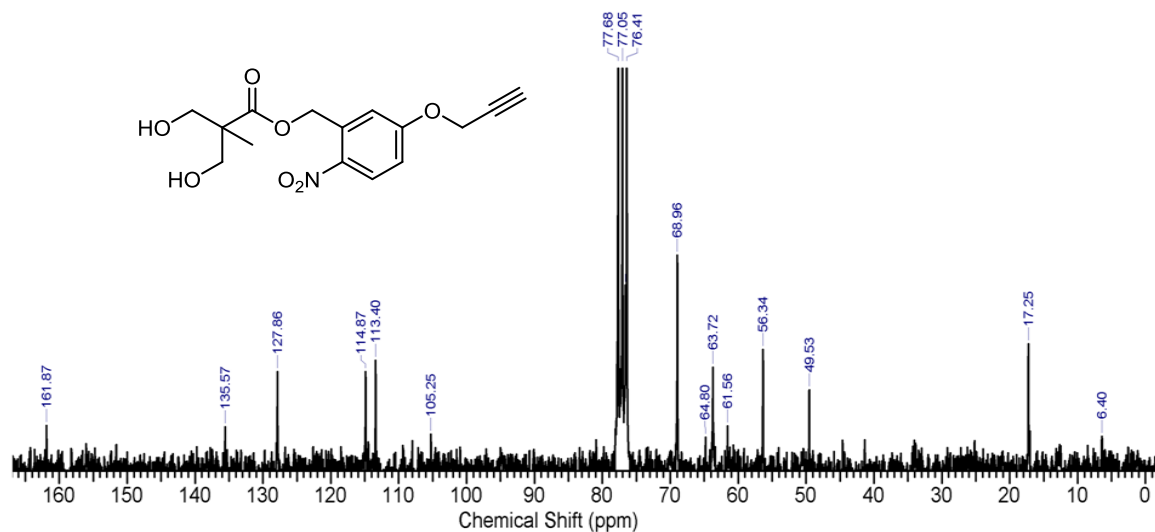


Fig. III.10: 50 MHz  $^{13}\text{C}$  NMR spectrum of Compound 2 in  $\text{CDCl}_3$ .

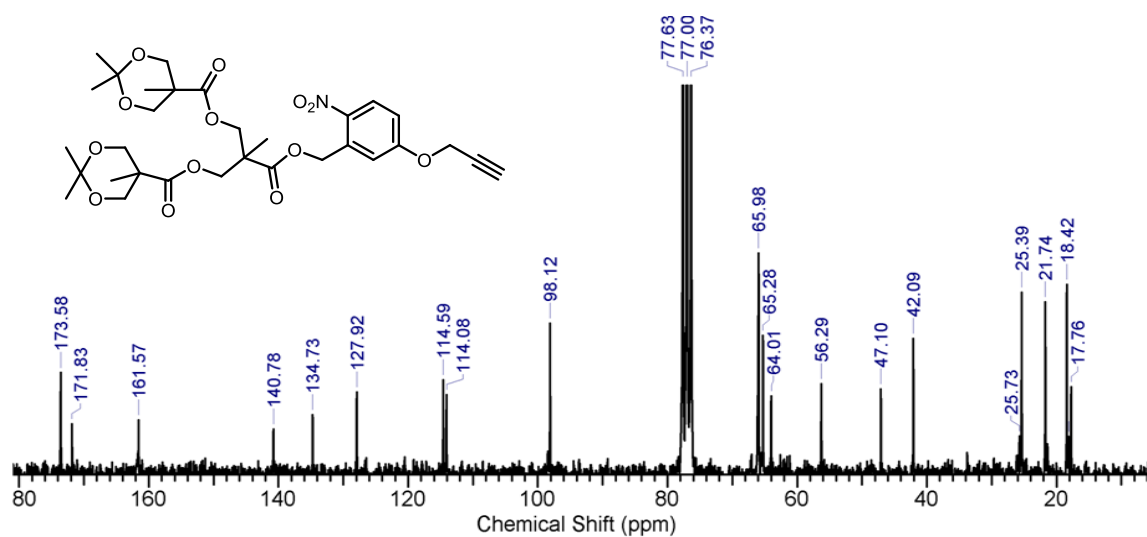


Fig. III.11: 50 MHz  $^{13}\text{C}$  NMR spectrum of Compound 3 in  $\text{CDCl}_3$ .

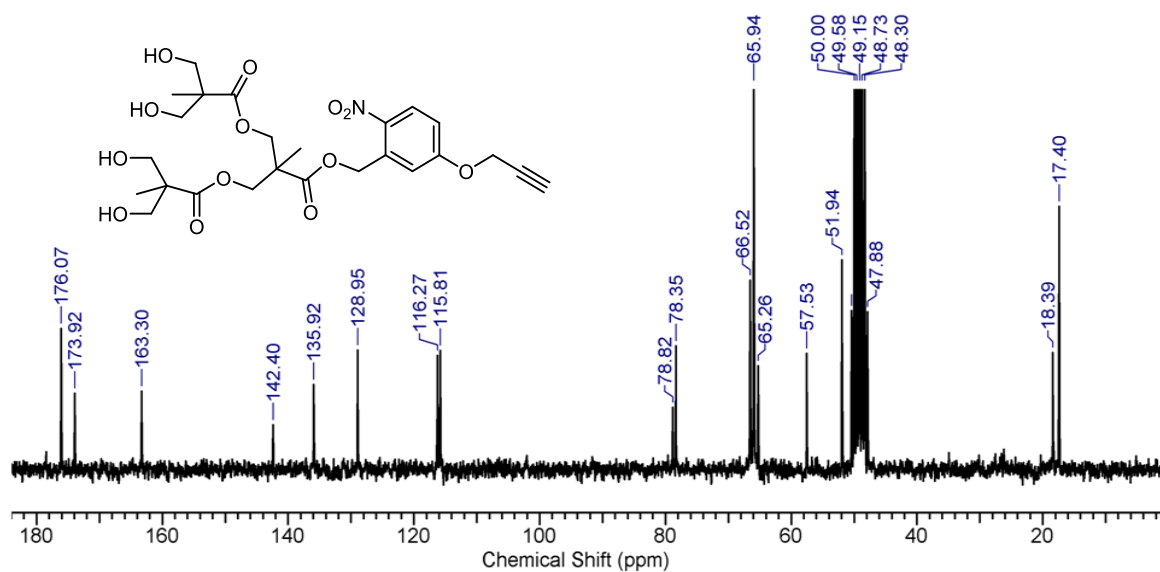
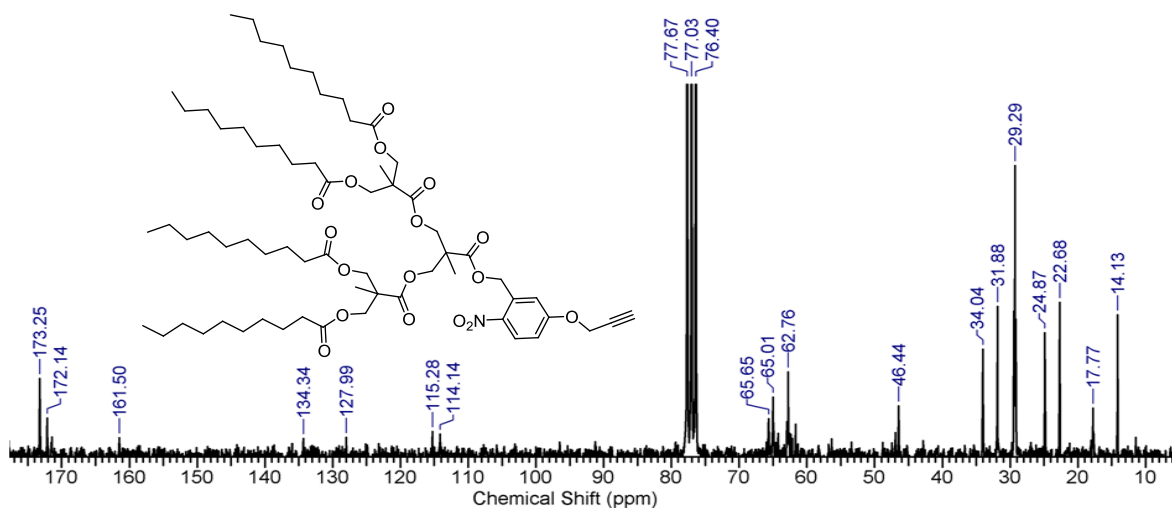
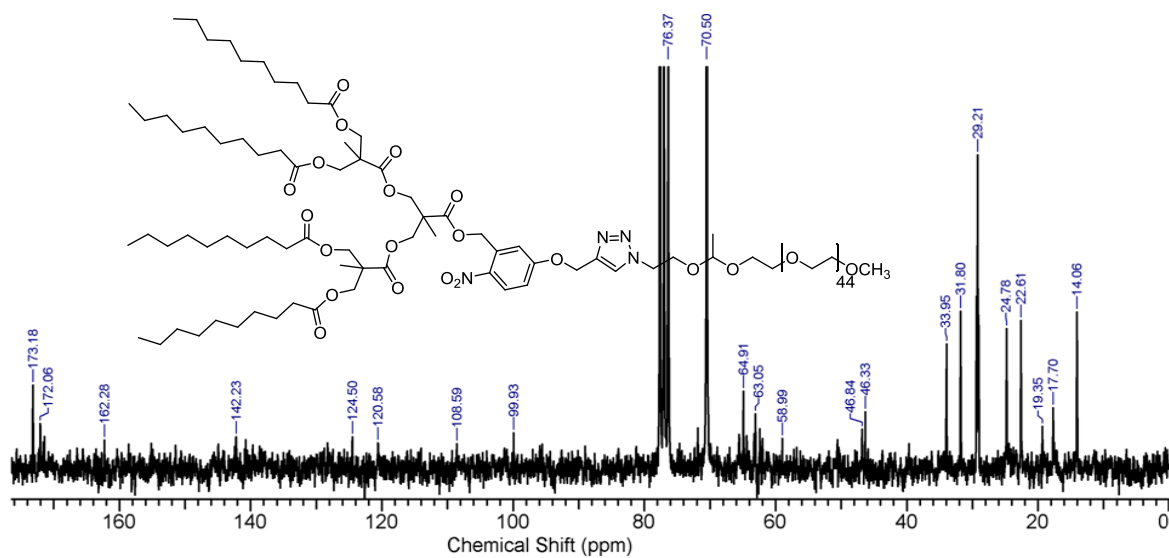


Fig. III.12: 50 MHz  $^{13}\text{C}$  NMR spectrum of Compound 4 in  $\text{CDCl}_3$ .



**Fig. III.13:** 50 MHz  $^{13}\text{C}$  NMR spectrum of Compound **5** in  $\text{CDCl}_3$ .



**Fig. III.14:** 50 MHz  $^{13}\text{C}$  NMR spectrum **P1** in  $\text{CDCl}_3$ .

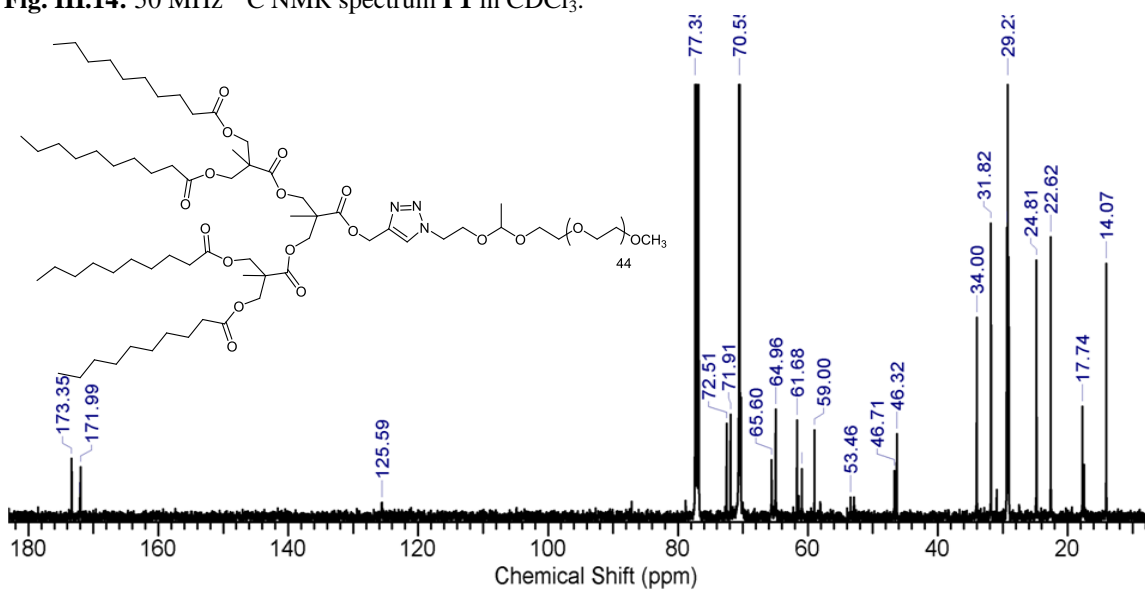


**Fig. III.15:** 100 MHz  $^{13}\text{C}$  NMR spectrum of **P2** in  $\text{CDCl}_3$ .

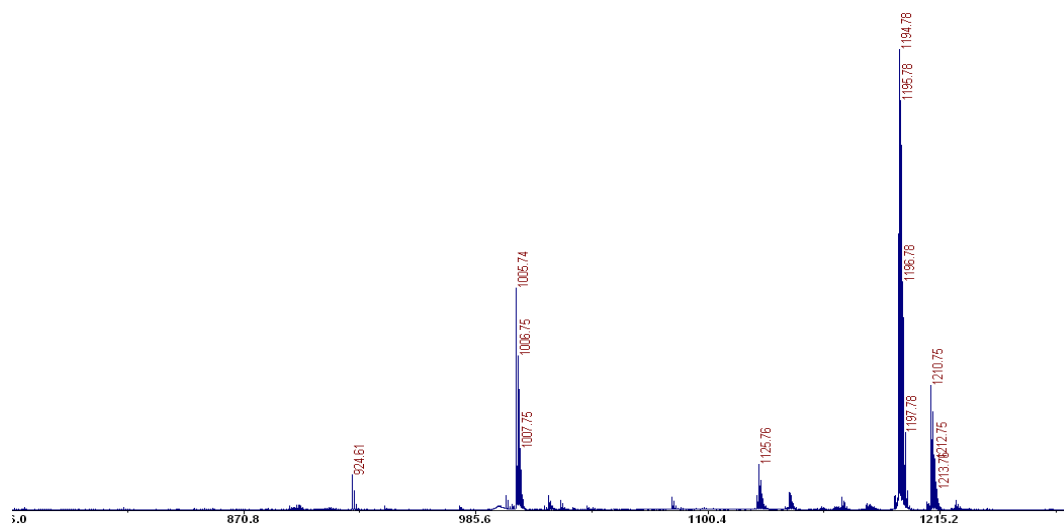


Fig. III.16: MALDI-TOF spectrum of Compound 5.

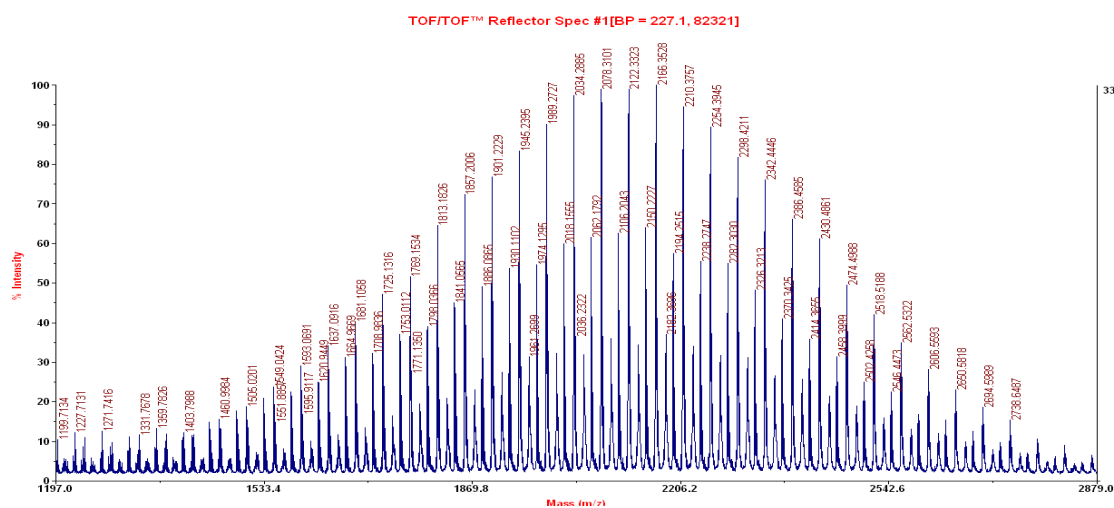


Fig. III.17: MALDI-TOF spectrum of Compound 7.

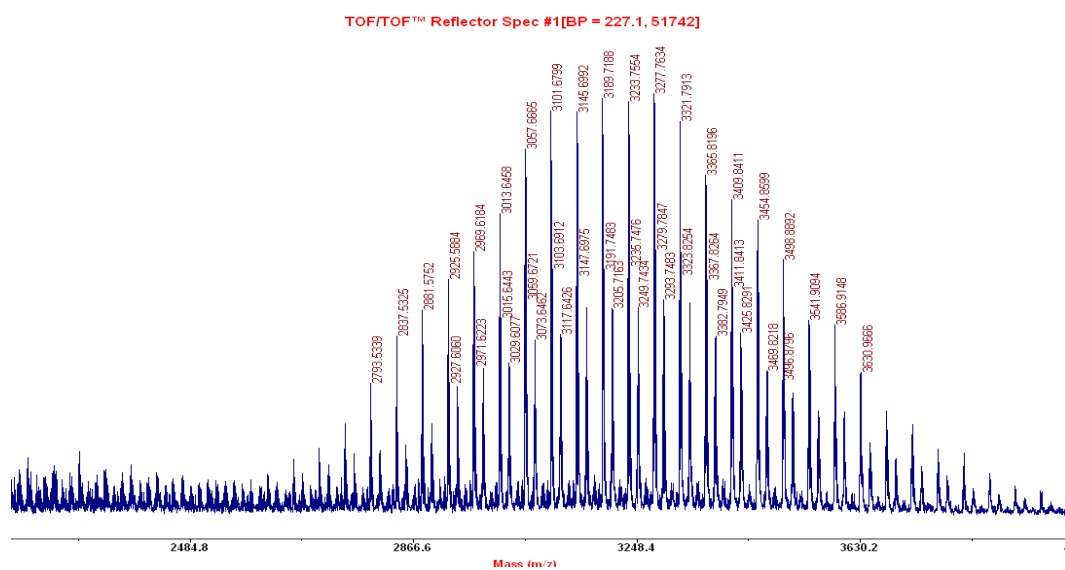
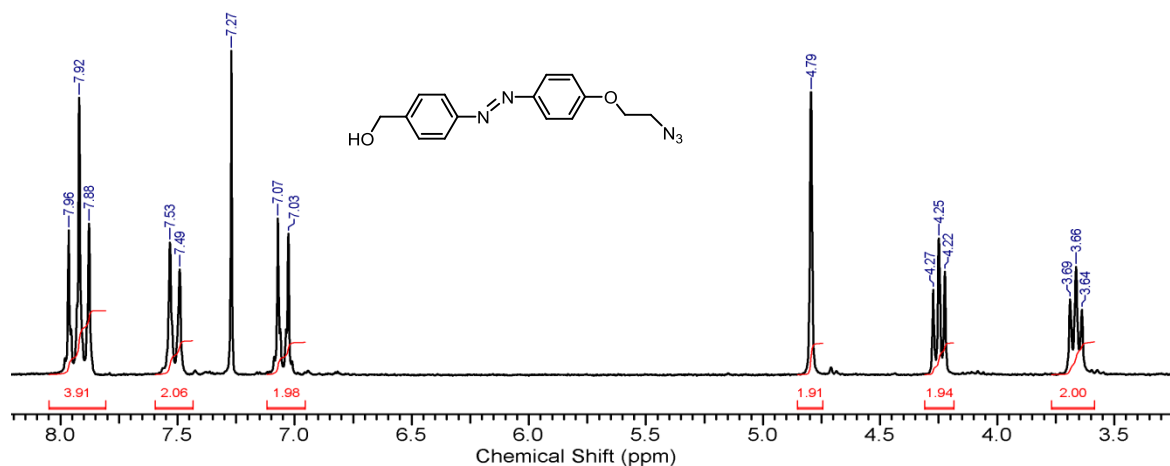
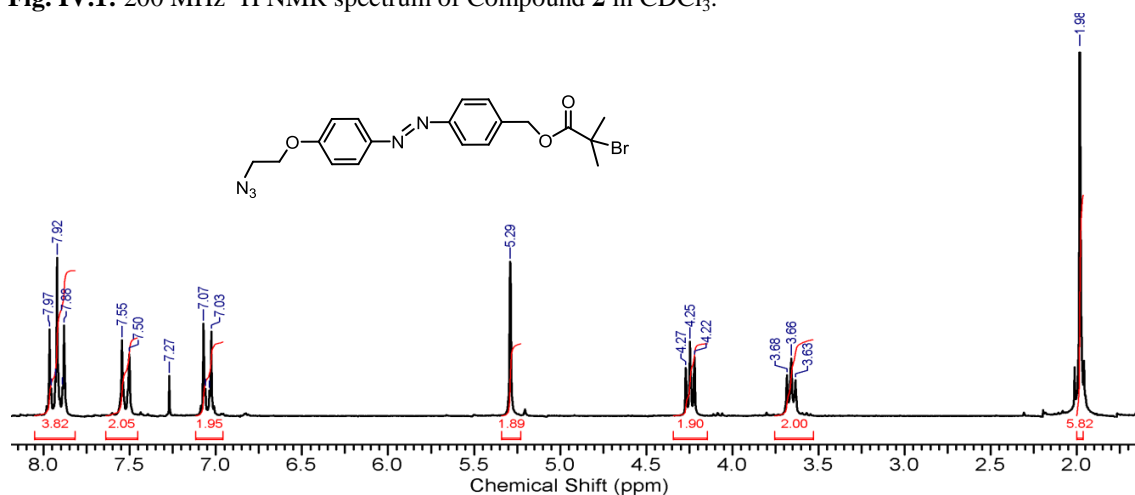
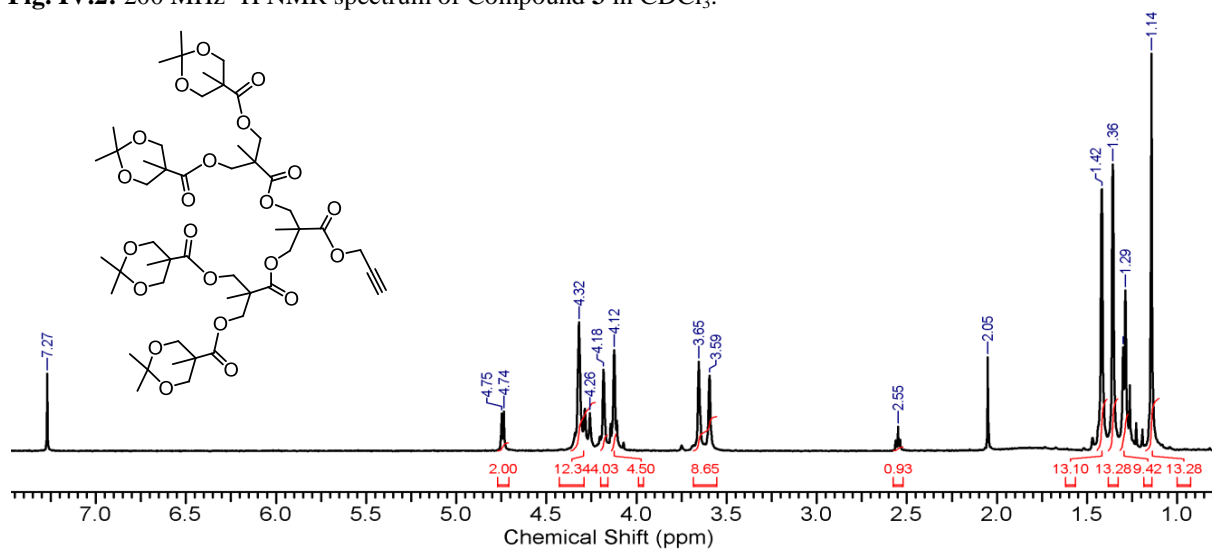


Fig. III.18: MALDI-TOF spectrum of P1.

## Appendix IV

## NMR spectra for Chapter 5

Fig. IV.1: 200 MHz  $^1\text{H}$  NMR spectrum of Compound 2 in  $\text{CDCl}_3$ .Fig. IV.2: 200 MHz  $^1\text{H}$  NMR spectrum of Compound 3 in  $\text{CDCl}_3$ .Fig. IV.3: 200 MHz  $^1\text{H}$  NMR spectrum of bis-MPAG3-alkyne in  $\text{CDCl}_3$ .



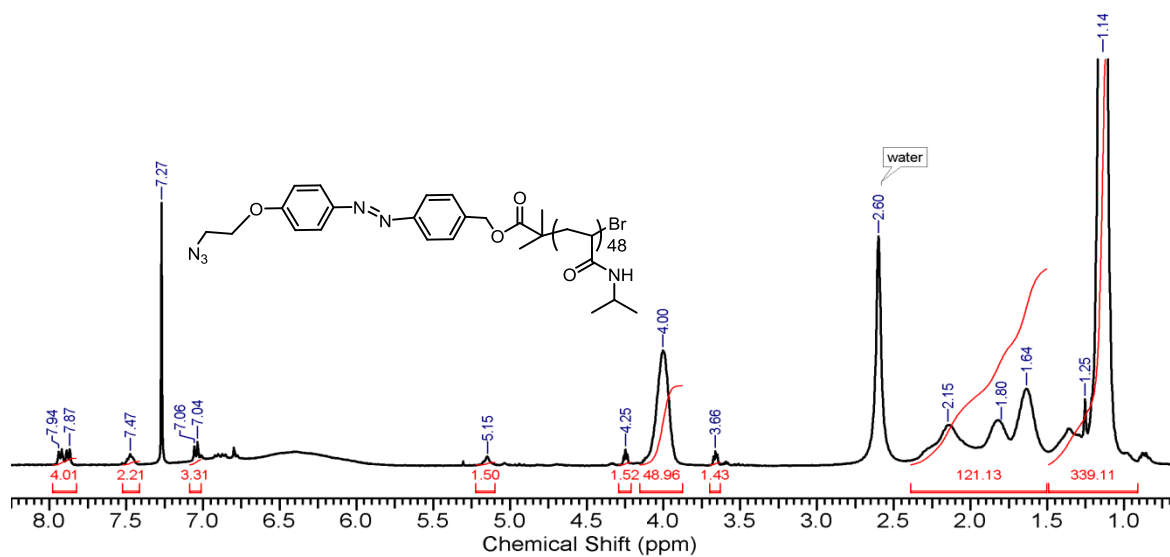


Fig. IV.4: 400 MHz  $^1\text{H}$  NMR spectrum of  $N_3$ -Azo-PNIPAM<sub>48</sub> in  $\text{CDCl}_3$ .

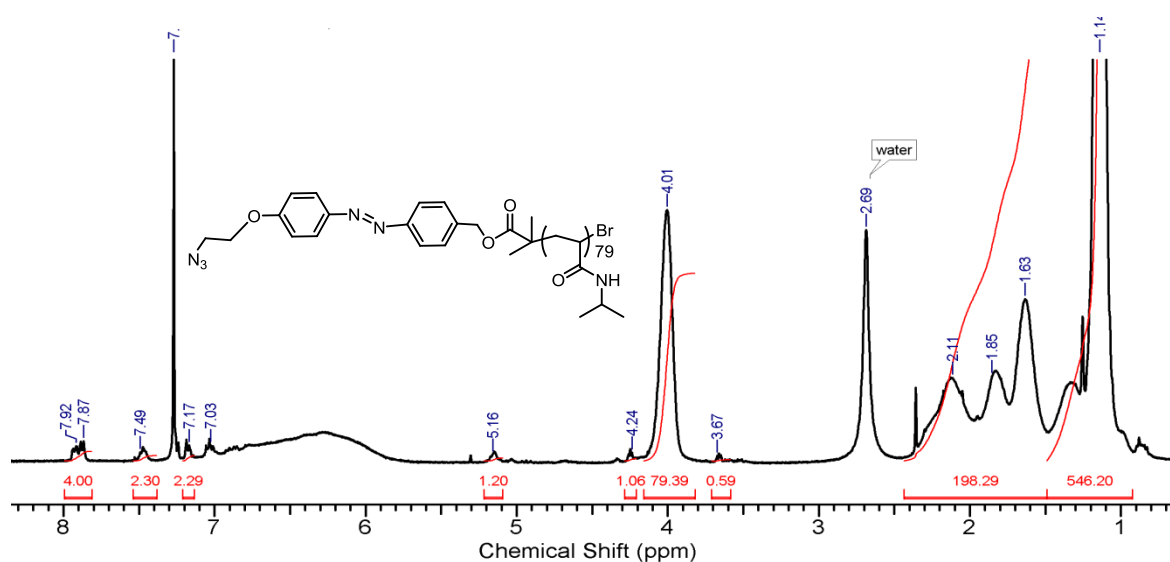


Fig. IV.5: 400 MHz  $^1\text{H}$  NMR spectrum of  $N_3$ -Azo-PNIPAM<sub>79</sub> in  $\text{CDCl}_3$ .

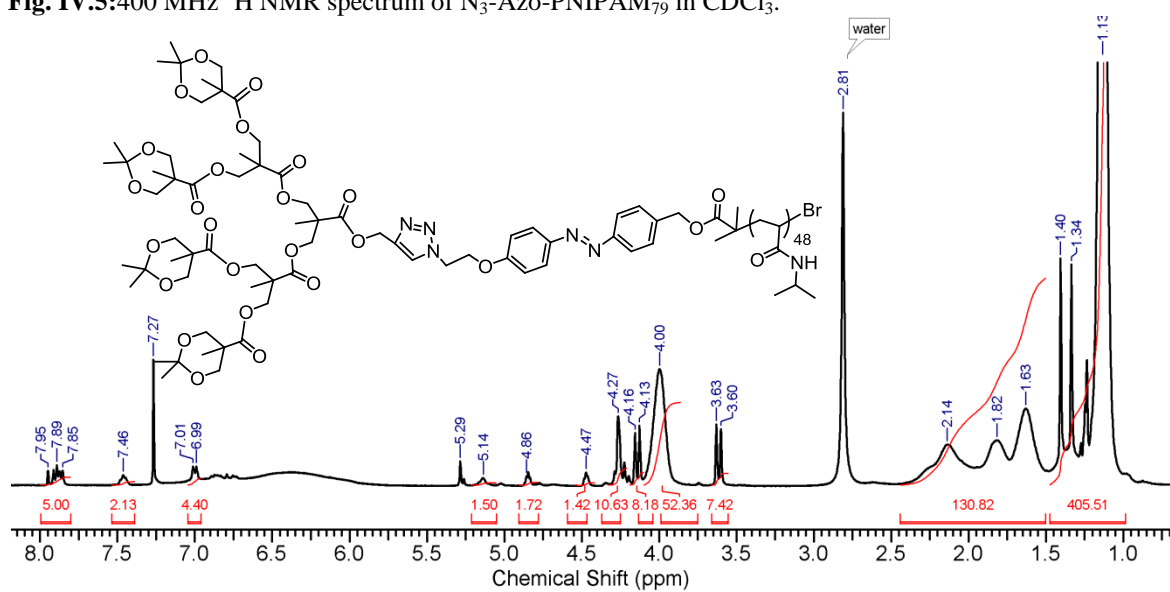


Fig. IV.6: 400 MHz  $^1\text{H}$  NMR spectrum of **P1** in  $\text{CDCl}_3$ .

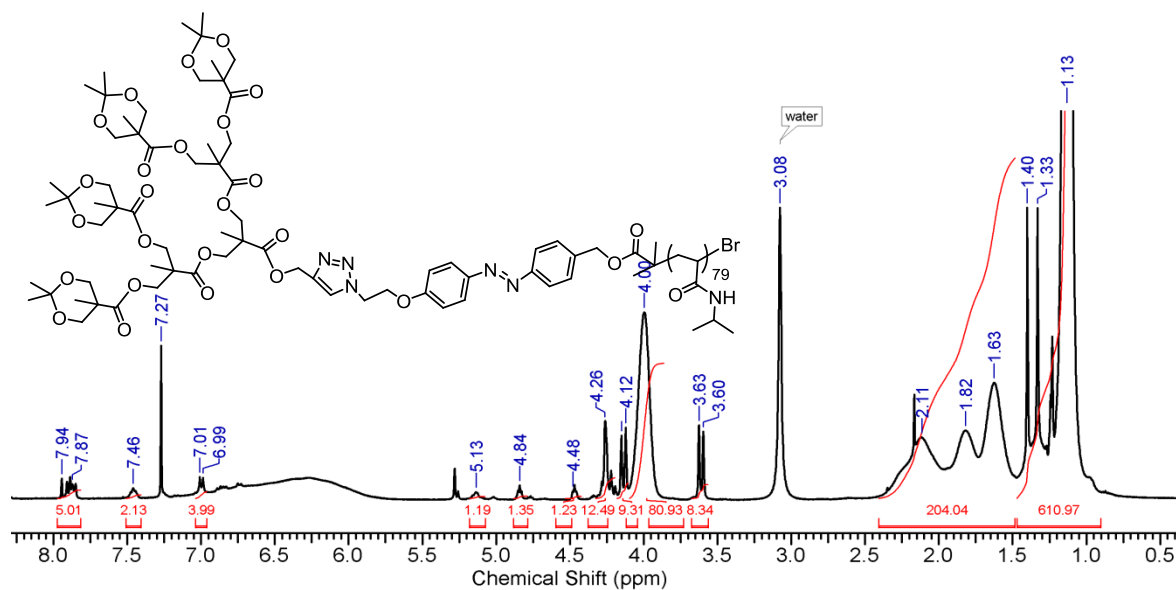


Fig. IV.7: 400 MHz  $^1\text{H}$  NMR spectrum of **P2** in  $\text{CDCl}_3$ .

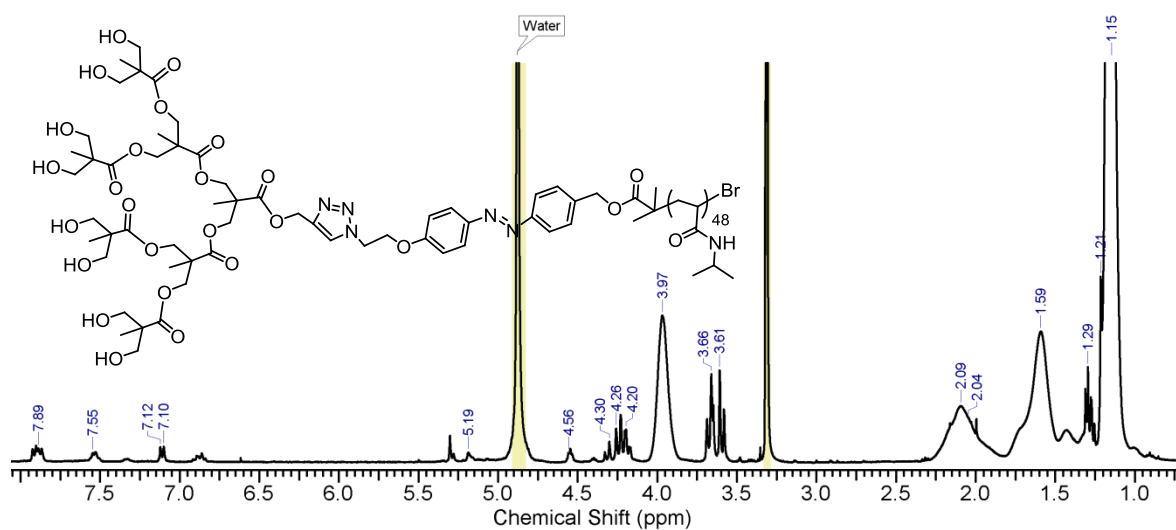


Fig. IV.8: 400 MHz  $^1\text{H}$  NMR spectrum of **P3** in  $\text{CDCl}_3$ .

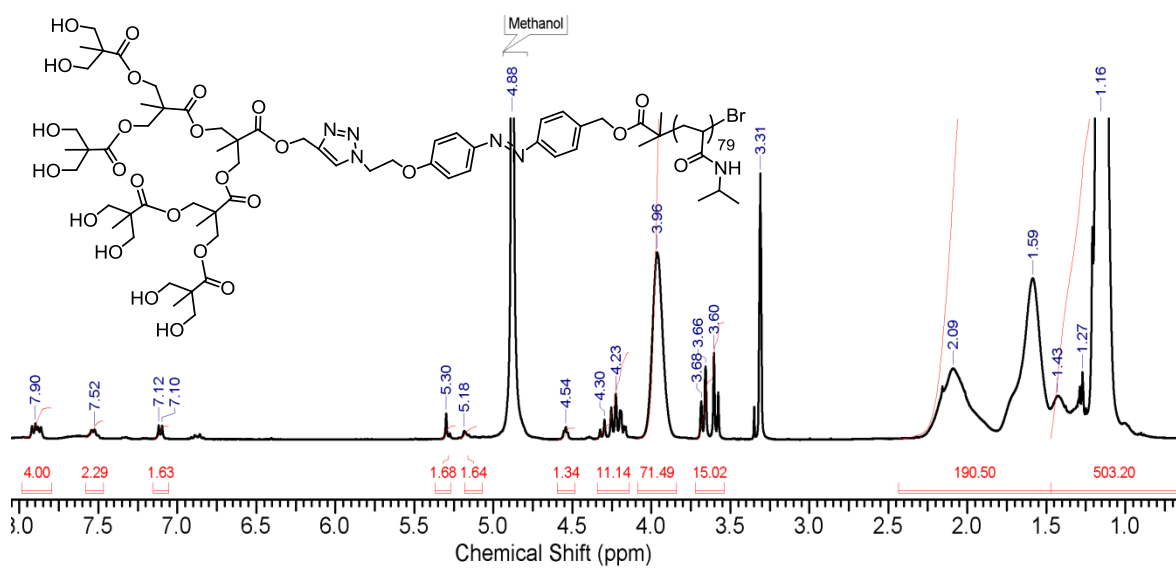


Fig. IV.9: 400 MHz  $^1\text{H}$  NMR spectrum of **P4** in  $\text{CDCl}_3$ .

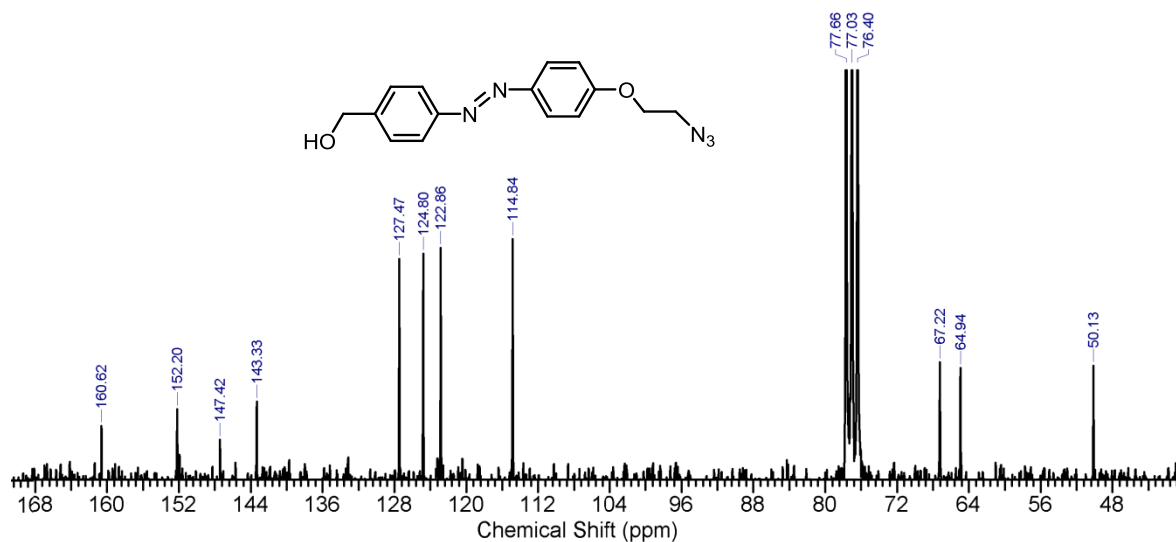


Fig. IV.10: 50 MHz  $^{13}\text{C}$  NMR spectrum of compound 3 in  $\text{CDCl}_3$ .

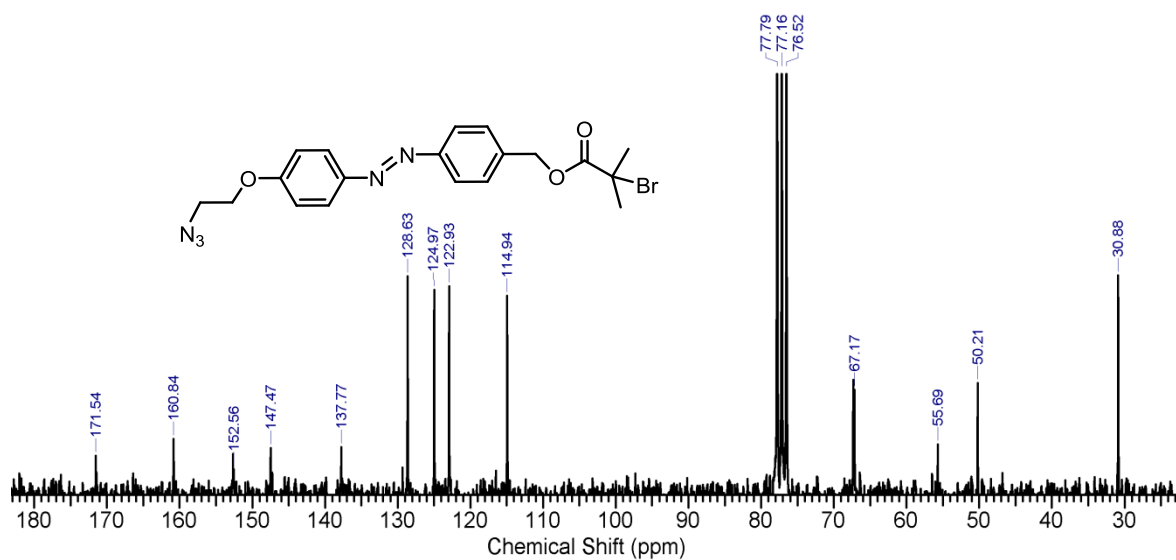


Fig. IV.11: 50 MHz  $^{13}\text{C}$  NMR spectrum of compound 4 in  $\text{CDCl}_3$ .

## List of Publications

- 1) **Nagendra Kalva**, Nitin Basutkar and Ashootosh V. Ambade, “Photoresponsive assemblies of linear-dendritic copolymers containing azobenzene in the dendron interior: Effect of dendron structure on dye encapsulation and release” *Rsc Adv.*, **2016**, *6*, 43163–43170.
- 2) **Nagendra Kalva**, Nimisha Parekh and Ashootosh. V. Ambade, “Controlled Micellar Disassembly of Photo- and pH-cleavable Linear-Dendritic Block Copolymers” *Polym. Chem.* **2015**, *6*, 6826-6835.
- 3) **Nagendra Kalva**, Vinod. K. Aswal and Ashootosh. V. Ambade, “Effect of the Branching Pattern of Hydrophobic Dendrons on the Core Structure of Linear-Dendritic Copolymer Micelles” *Macromol. Chem. Phys.* **2014**, *215*, 1456 -1465.
- 4) Debasis Pati, **Nagendra Kalva**, Soumen Das, Guruswamy Kumaraswamy, Sayam Sen Gupta and Ashootosh. V. Ambade, “Multiple Topologies from Glycopolypeptide–Dendron Conjugate Self-Assembly: Nanorods, Micelles, and Organogels” *J. Am.Chem.Soc.* **2012**, *134*, 7796 -7802.
- 5) **Nagendra Kalva** and Asootosh. V. Ambade, “Effect of Dendron Periphery on Thermoresponsive Properties of bis-MPA Dendron-Azobenzene-PNIPAM Copolymer Assemblies” (*Manuscript Under preparation*)